UNIVERSITY OF STRATHCLYDE

DEPARTMENT OF ELECTRICAL AND ELECTRONIC ENGINEERING

MACHINE ANALYSIS

Being a study of the application of the finite element method for solving the two-dimensional field of the single-phase shaded-pole induction motor.

Thesis presented for the degree of
Doctor of Philosophy in Electrical
Engineering of the University of Strathclyde.

by

Mohamad Najjar, M.Sc.

July, 1985

PAGE NUMBERING AS ORIGINAL

CONTENTS

SUMMARY

This thesis contains eight chapters, dealing with machine analysis and representation. A definition and a brief survey of previous investigation devoted to shaded-pole motors and the application of finite element method for solving the two-dimensional electromagnetic field is given in Chapter 1. An outline of the present investigation is also given. In Chapter 2, the experimental requirements and details of the equipment are given. This includes the techniques of recording the transient torque patterns and the method of measuring the complete torque-speed characteristics. The experimental methods for parameters determination are also mentioned.

The finite element method is outlined in Chapter 3. This chapter deals also with the assumptions made, the formulation of the non-linear energy function, the solution of Poisson's equation and an example of a simple shape contianing 16 elements for illustrating the method.

In Chapter 4, the computer program for the finite element is outlined. The iteration process and the numerical representation of the magnetization curve are mentioned. Application of the finite element method to the shaded-pole motor is also given. Calculation of parameters by finite element technique is given in Chapter 5. Self inductance is calculated using the concept of stored energy and the results of self and mutual inductances are tabulated. Basic performance equations of an electrical machine are derived in Chapter 6. Solution of the basic performance equations, by a step-by-step numerical method, is also given.

In Chapter 7, the steady state performance equations are

established in terms of harmonic currents and inductance coefficients. The flux linkages are evaluated by the approximated functions of mutual inductances. The electromagnetic torque is calculated from the stored energy in the magentic field.

General conclusions and suggestion for further work are mentioned in Chapter 8.

LIST OF PRINCIPAL SYMBOLS

A	Magnetic vector potential
B	flux density
D	diameter of stator bore
f	frequency
F	magnetomotive force
h	order of space harmonic
i	time varying current
I	r.m.s. current
J	rotor inertia
l	self inductance
$\bar{M}$	inductance coefficient, phasor quantity
N	total number of turns
P	$\frac{d}{dt}$
P_o	number of pole pairs
R	resistance
S	slip
t	time
T	torque
v	time varying voltage
W_s	stored magnetic energy
W_s'	co-energy
X	reactance
μ_o	magnetic space constant
Ψ	flux linkage

θ	angular position
$\dot{\theta}$	angular speed
$\ddot{\theta}$	angular acceleration
ω	constant angular velocity
α	fundamental rotor slot angle

Subscripts

s	stator
r	rotor
d	stator main winding
q	shading coils
b	rotor bar
e	rotor end ring

CHAPTER 1

INTRODUCTION

A shaded-pole motor may be defined as a single-phase induction motor provided with an auxiliary short-circuited winding displaced in space from the main winding and carrying current which has a phase displacement from the main winding current. Because of its simple construction, low cost and reliability, the shaded-pole motor is one of the most popular motors for a large variety of applications requiring power of 300 watts or less. The main disadvantage is the low effeciency, 30% or less. The analysis of a shaded pole motor is highly complex despite its simple construction. The complexities are due mainly, to the unsymmetrical stator windings and the abundance of space harmonics. Additional difficulties arise in the analysis of the 'reluctance-augmented' shaded-pole motor where saliency is introduced on the stator pole face by increasing the air gap length under the leading pole tips.

As any other induction motor the shaded-pole motor runs due to the action of revolving magnetic field. The shading coil causes the flux in that portion of the pole surrounding it to lag behind the flux in the rest of the pole. The resultant rotating field which is produced by the main winding and the shading coil (two componant fields displaced in space and phase) is enough to produce considerable torque to make the motor rotate. The direction of rotation is always from the unshaded to the shaded portion of the pole.

The starting torque is low. It varies from 20 to 50 percent of peak load torque. The direction of rotation depends upon the position of the shaded portion of the pole relative to the main portion of the pole, so to reverse the direction of rotation it is necessary to change the position of the shading portion of the pole.

To produce an accurate prediction of electrical machine performance requires an accurate analytical model and correct parameters. The present investigation will employ the finite element method for the purpose of calculating accurate parameters to produce a simple representation of the shaded-pole motor.

1.1 Review of Previous Work

The earliest theoretical analysis of shaded-pole motors was published by Trickey (1,2). Performance equations under locked-rotor conditions were derived in his first paper.

Kron (3) used both cross-field and revolving-field theories to derive general performance equations and equivalent circuits, the effects of saliency and space harmonics were considered. An equivalent circuit, by separating the stator windings into a main winding and an auxiliary winding, based on the flux divisions between the shaded and unshaded portions of the pole, was developed by Chang (4). Though the effects of space harmonics were taken into consideration, the analysis assumes 90 degrees displacement between the shaded and unshaded portions, and neglecting the effect of saliency. Sherer and Hertzog (5) employed Chang's equivalent circuit to study the effect of parameters variations on the performance of the motor. Surk (6) developed an equivalent circuit

based on the resolution of the exciting winding and auxiliary winding magnetomotive forces into quadrature components and then applying symmetrical component theory. Performance equations in terms of the two actual stator circuits and two equivant rotor circuit, for the squirrel cage were developed by Desai and Mathew (7). Transient performance, under locked-rotor and dynamic starting conditions, was obtained numerically by solving the performance differential equations. The equations are also used to obtain the steady state performance of the motor. Butler and Wallace (8, 9, 10) developed equivalent circuits applicable to shaded-pole motors using transformation of the asymmetrical primary windings to their equivalent tapped-quadrature windings and then applying 2-phase rotating field theory. Poloujadoff (11) analysed the characteristics of saturated shaded-pole motors by treating the squirrel cage as a series of pseudostationary loops, and solved this numerically for the flux likages and loop currents by an iterative technique. Since a steady state solution is obtained from the transient solution, at the convergence stage, a large amount of computing time is required.

All the authors mentioned before dealt with uniform air-gap. Ooka (12, 13, 14, 15) and Williamson (16, 17, 18, 19) published anlytical and experimental results on the reluctance-augmented shaded pole motors with up to two rings per pole.

The analytical approach adopted by Williamson is based on the electromegnetic model of the induction motor which was developed by Cullen and Barton (20). Chin (21) made the first attempt in this department to develop machine representation based on circuit

equations which incorporate an analysis of the flux distribution in the air-gap. By numerical solution of the basic performance differential equations, Chin analysed the performance of a uniform air-gap shaded pole motor with removed shading rings. Lock (22) established a mathematical model for performance analysis of the shaded-pole motor based on 2-dimensionial field analysis of the air gap flux distribution in conjunction with conventional circuit theory. The effect of air gap variation, distribution of winding and skew angle were taken into consideration. Finite-element method is the new technique introduced to investigate electrical machines or part of the machine. The versatility of the finite-element method is, by now, well known, and its use grew rapidly. The application of finite element for solving the magnetic field problems in the electrical machines was first proposed by Silvester and Chari (23). Rather than dealing with Poisson's partial differential equation.

Finite element work on machines divides broadly into two categories. The first is the use of finite element analysis to study a specific part of the machine in order to determine a parameter or coefficient for use in a standard equivalent circuit. In such studies, the current distribution is known, and the field is determined for this known distribution. Chari and Sharma (24) used this category to solve the magnetic field in the end region of a turbine generators. The second category is to model the machine as a whole, for predicting performance under specified operating conditions. In this case some of the electrical variables are unknown and must be determined.

Brandl et al. (25) showed how the governing nonlinear circuit

equations could be solved in parallel with the nonlinear field equations using a single iterative process. Williamson and Ralph (26, 27) analysed the magnetic field of shaded-pole motors by the finite element approach using complex current sources in the first paper. In the second paper a constant voltage source was used, some of the parameters were calculated and steady state characteristics were obtained and there is a close agreement between experiment and computed results.

1.2 Object and Scope of Present Work

The first main object of the present investigation is to establish a new approach for solving field problems of electrical machines using Finite-Element technique incorporating field equations. The approach is based on a 2-dimensional field analysis of flux distirbution through the machine. The second object is to calculate the parameters of the machine and then derive simple mathematical expressions for basic performance equations. Distribution of windings is considered. The cage rotor is treated as a number of cascaded coils, each coil is formed by two adjacent bars and the section of end ring joining the two bars. The first category of finite element is used to investiage the magnetic field of the machine where the currents are calculated, using the steady state program developed by Lock (22), at different speeds and different times for each speed. Self induCtance of each coil in the machine and mutual inductance between any coil and the rest of the coils are calculated for three values of speed and two times. Flux maps are plotted for each particular coil in addition to flux

maps of all the coils at a time. The results which are obtained by by the finite element technique are employed to study the machine performance. Step-by-step numerical method is used to solve the basic differential performance equations. Figure 1.1 shows a practical reluctance-augmented shaded pole motor used in the investigation.

CHAPTER 2

Experiemental Requirements and Determination of Parameters

Experiemental results are required from the test motor to verify the validity and accuracy of the method of analysis. For the steady state characteristics the main requirements for the experimental work are:

1. A system for loading the test motor over its complete speed range. This means that a closed loop control system is required to operate the test motor at the unstable speed region.
2. A means for measuring the torque and speed and input quantitites.

To obtain the transient characteristics of the test motor, the requirements are:

1. A device which can switch on the supply at a selected point on the supply wave.
2. A method of recording the transient torque-time pattern.

2.1 Test Rig

In the theoretical analysis, a concentric air gap is assumed. To compare theoretical and experimental results on the same basis, it is desirable that the test motor also has a concentric air gap. However, this is seldom achieved with mass production of small electrical machines because it is not economically feasible to keep such close mechanical tolerance. The air gap of a typical shaded-pole motor is 0.5 mm. A small eccentricity in the rotor alignment can cause a large peripheral air gap variation. It was

found that a small eccentricity in the air gap did not significantly affect the experimental results. Another reason for requiring a test motor with a concentric air gap is for the measurement of machine parameters using a search coil in the air gap. If there is a large variation in the air gap under different poles the search coil induced emf will also change from one pole to another.

A test rig was constructed for holding the stator and rotor such that the air gap can be adjusted. Figure 2.1 shows the structure of the test rig. The stator which is held in a V-block can be moved in both the vertical and horizontal direction. The rotor shaft is mounted on two well lubricated bearings, each bearing is held by three finely threaded adjustable screws. Fine adjustment of the air gap is achieved by using these six screws.

2.2 Measurement of Steady State Characteristics

The torque/speed characteristics of a shaded-pole motor, as shown in Figure 2.2, is very sensitive to winding temperature variations. It is therefore imperative to measure the characteristic as rapidly as possible. This will ensure that the high losses that occur in the motor, particularly over the unstable region, do not produce a significant temperature rise. Ideally, the characteristics should be measured when the windings are hot so that the rate of temperature rise is small. From the experimental point of view, it is rather difficult to maintain the same temperature whenever any result is taken. So the characteristics are measured immediately when the motor is switched on at room temperature. Main winding resistance, before and after each measurement was noted. As the whole characteristics were taken within very short time, the

change in winding resistance was small.

A magtrol dynamometer and speed control unit were employed for the measurement of the steady state characteristic : their features are described below.

2.2.1 Magtrol dynamometer and speed control unit

A hysteresis brake is used in the dynamometer. It consists of a permanent magnet rotor in the form of a drag-cup revolving in the field produced by the stator winding.

When the stator is energised, a torque is exerted on the rotor by hysteresis action. The torque which is a function of the existing current is independent of speed through the entire speed range from zero to full speed This is an advantage over the normal eddy current devices which depend on relative motion between stator and rotor. The braking torque is measured by the stator reaction of the dynamo-meter. The suspended stator of the brake assembly is weighted at the bottom so that it is able to rotate only as far as the brake torque is able to lift the weight. The value of this torque is indicated on a calibrated scale. Alternatively, a load cell can be attached to the stator and its output signal, which is proportional to the pressure exerted on it, can be calibrated to measure the braking torque. The linearity of the output signal of the load cell is checked by measuring the output signal corresponding to several standard weights.

The principle of speed measurement is the resolution of increments of a revolution by interrupting light on a photocell. This interruption is obtained by a segmented plastic disc attached to the rotor shaft of the brake assembly. As the light to the

photo cell is modulated, the cell changes its resistance resulting in a voltage modulation across the cell. This modulated signal is converted to an analogue signal, which is proportional to the speed, to facilitate recording of torque/speed characteristic on a X-Y plotter. The magtrol dynamometer is provided with a closed loop control system to enable the test to include the unstable speed region of the motor. A speed control damping switch is provided for varying the rate feedback in the servo amplifier. Another feature of the control unit is the inertia compensation control which allows for the effect of torque changes due to acceleration and deceleration of the rotor. Thus, an accurate torque/speed curve can be obtained quickly without appreciably heating up the machine windings.

2.2.2 Recording of torque/speed and current/speed characteristic

The torque and speed signals from the Magrol dynamometer and control unit are fed to a X-Y plotter. The complete torque/speed curve is obtained by varying the speed control switch of the Magrol unit. It is essential that this curve is not obtained too rapidly, because once the recording rate exceeds the combined response time of the feedback control system and the X-Y recorder, accuracy deteriorates rapidly. However, if the performance curve is drawn too slowly, excessive temperature rise in the motor may result. For shading-pole motor under investigation, a plotting time of approximately 15 seconds was found to be sufficient.

Since the input current is a.c. the voltage drop across the shunt due to this current cannot be fed directly to the X-Y plotter. Instead, this a.c. signal is rectified by a precision voltage rectifier, whose d.c. output is proportional to the a.c. input

voltage. Calibration of the current scale on the X-Y plotter is done by passing a known current through the shunt.

2.3 Recording of Transient Characteristics

The transient behaviour of induction motors received an active investigation in this department since early 1960 (28, 29, 30, 31). Various experimental techniques were successfully developed for the recording of the transient torque characteristic. These techniques are employed in the present investigation.

2.3.1 Switching angle selector

The transient characteristic of an electrical machine depends on the point-on-wave of the supply voltage at the instant when the supply is connected to the machine. For this reason, both singlephase and three-phase point-on-wave switches were developed in this department (32). To cater for three phase machines, 2-pole or 3-pole versions were designed so that the poles could be closed either simultaneously or non-simultaneously. Since the shaded pole motor is a single-phase machine, only the feature of a singlephase switching angle selector is being examined here. A block diagram illustrating the principle of operation of the switching angle selector is shown in Figure 2.3. The mag-slip is essentially a phase shifter. The phase of this mag-slip output voltage relative to its stator input, is controlled by its rotor position. Thus any switching angle can be selected by varying the rotor position. This output voltage is fed via a pulse-forming unit to a trigger unit. The output from the trigger unit is used to trigger the gate of the thyristor and so connect the supply to the test motor. This

switching angle selector was capable of a consistancy and accuracy for any selected switching angle of better than $\pm 1^0$.

2.3.2 Transient torque sensing system

The direct method of measuring transient torque is by measurement of the stator reaction using a force sensing device such as the load cell. However, this method was found, in previous investigations in this department (30), to be unsatisfactory because the output signal of the load cell was badly distorted by mechanical noise from the suspended stator reaction system. The natural frequency of oscillation of the mechanical system was of the same order as that of the double slip frequency torque pattern. In the present investigation an indirect method of measuring the rotor acceleration was employed for the case of free-rotor torque transients. A limitation of this indirect method is that the locked rotor transient torque cannot be obtained. In any case, since steady state performance is the main emphasis, no attempt was made to obtain the locked rotor transient torque pattern. It is thought that experimental results on free-rotor transient torque and current patterns are sufficient to check the transient analysis employed.

2.3.3 Records of free-rotor transient pattern

A 2-phase drag-cup induction generator and storage oscilloscope were used to obtain free-rotor transient torque patterns. When the drag-cup induction generator is energised with alteranting current on one phase, the output on the other phase is of the same frequency and has a magnitude proportional to the speed (33, 34). With direct current excitation, the output is proportional to the rate of

change of speed, i.e. acceleration.

The accelerometer was calibrated by exciting it with an a.c. supply and driving it at constant speed.

The acceleration constant which is the ratio of output voltage to acceleration is

$$K_s = \frac{V/W_r}{W} \qquad mV\ s^2/rad$$

where V = r.m.s. output voltage of accelerometer

W_r = angular velocity of rotor

With an excitation current of 0.2 amp the sensitivity of the accelerometer was found to be 0.272 $mV\ s^2/rad$ The acceleration records were converted to torque records by using the moment of inertia of the motor.

The acceleration pattern measures only the rotor accelerating torque. However, for an unloaded motor, with negligible mechanical loss, the developed torque is proportional to the acceleration of the shaft

$$\frac{d^2\theta m}{dt^2} = \frac{T}{J} = \frac{V}{K_s}$$

so

$$T = \frac{J}{K_s} \cdot V$$

where T = developed torque

J = moment of inertia of the rotor.

For this case the electromagnetic torque is equal to the rotor acceleration torque. This was confirmed by examining the

deceleration pattern occuring when the supply was disconnected from the rotating motor.

A plastic tube was used as the coupling between the accelerometer and the motor. This eliminates the effects of mechanical irregularities and yet provides sufficient rigid coupling to ensure a correct transmission of acceleration torque.

2.4 Determination of parameters

The accurate prediction of an electrical machine performance needs a correct set of parameters in addition to a good analytical model.

Parameters required for the solution of the steady state equations of shaded-pole motors are the winding details and the physical dimensions of both the stator and the rotor, the resistances and the inductances of the windings. Some of the parameters were calculated while the others were obtained experimentally.

2.4.1 Determination of Resistances

2.4.1.1 Resistance of Stator windings

The main winding resistance of the test motor was measured using a Kelvin Double Bridge. The resistance was measured before and after the test and the average value was taken. The shading ring resistance was calculated from its dimensions.

2.4.1.2 Rotor bar resistance

In the steady state analysis the cage rotor was represented by cascaded loops, each formed of two adjacent bars and the

interconnecting portions of the end rings, only the effective resistance of that portion of the end ring, as well as the bar resistance, were required to be evaluated. Bar resistance cannot be measured directly so it was calculated from the rotor dimensions using the resistivity for die-cast aluminium.

2.4.1.3 End ring resistance

The value of end ring resistance required is the effective resistance of that portion of the end ring which joins two adjacent bars, it is calculated from the ring dimensions. The total resistance of the ring is divided by the number of rotor bars to get the end ring resistance.

$$R_{er} = \frac{\rho \cdot \pi \cdot Dr}{S_2 \cdot a} \left(1 + \alpha(t_1 - t_o)\right) \quad \ldots\ldots 2.4.1$$

where ρ is the resistivity of the ring at t_o ^0C,

α is the temperature coefficient, and Dr is the diameter at which the bars enter the ring.

The above expression is based on the assumption that the current would distribute itself uniformly in the end ring, but it is not correct if the end ring is wide compared with the distance between two bars.

Trickey (35) determined the distribution of end ring current for different numbers of poles and different widths of rings. Figure 2.4 gives the correction factor which should be applied to the end ring resistance calculated using equation (2.4.1).

The correction factor was given as

$$K_{ring} = \frac{Po(1-C)(1+C^{2Po})}{(1-C^{2Po})} \quad \ldots \ldots \quad 2.4.2$$

where Po = pair of poles

C = ratio of inside diameter of ring to outside diameter.

The calculated end ring resistance was corrected according to equation 2.4.2.

2.4.2 Determination of Inductance Coefficients

Self and mutual inductances are required for the solution of performance equations. The values of inductance coefficients depend on the reluctance of the magnetic flux paths and the nature of the winding. The flux produced by any winding is divided whether or not it crosses the air gap. Inductance coefficients due to flux crossing the air gap are functions of the rotor position as well as the shape of the air gap.

2.4.2.1 Inductance coefficients of stator windings.

The stator has two asymmetrical windings, the main winding (d) and the shading ring (q). The total impedence for each winding per pole are termed Z_d and Z_q and are defined as

$$Z_d = (R_d + jwl_d) + jwM_{dq} + jwM_{dr}$$

$$\ldots \ldots \quad 2.4.3$$

$$Z_q = (R_q + jwl_q) + jwM_{qd} + jWM_{qr}$$

It is assumed that the impedance Z_d of the main winding is

associated only with the main winding electromagnetic circuits when it is the only one excited. l_d is the leakage inductance for the main winding. M_{dq} is the mutual inductance between the main winding and the shading ring on each pole.

M_{dr} is the mutual inductance due to the flux crossing the airgap. A similar definition can be given to Z_q, l_q, M_{qd} and M_{qr}.

Equation 2.4.3 may be written as:

$$Z_d = R_d + jw(l_d + M_d) = R_d + jwL_d \qquad \ldots\ \ldots\ 2.4.4$$

$$Z_q = R_q + jw(l_q + M_q) = R_q + jwL_q$$

where $L_d = l_d + M_d$, $M_d = M_{dq} + M_{dr}$

$$L_q = l_q + M_q \quad , \quad M_q = M_{qd} + M_{qr}$$

For the analysis of shaded-pole motors, the following inductance coefficients are required.

1. Main winding leakage inductance
2. Shading ring leakage inductance
3. The mutual couplings for the main winding and the shading ring.

2.4.2.2 Determination of main winding leakage inductance

The main winding leakage inductance consists of two major components, the slot and overhang leakage inductances. Because of the complicated shape of the slot and the effect of saturation at the pole tips, it is very difficult to calculate the slot leakage accurately. Also it is not easy to determine the overhang

leakage, so the value of the leakage inductance is determined experimentally by two separate methods, namely the rotor out test and the search coil test.

a) The rotor out test

This method was used by Desai and Mathew (7). In this test the shading rings are removed and the rotor is also removed. The stator winding is energised at different values of supply voltage, and the corresponding input current is measured. The input impedance under these conditions consists of the resitance, the leakage reactance and the magnetizing reactance due to the flux crossing the enlarged air gap. Alger (36) showed that for a stator without a rotor, the effective air gap length is equal to the ratio of the radius of the stator bore to the number of pole-pairs. The magnetizing reactance corresponding to this equvalent air gap is calculated using the normal expression,

$$X_m = \sum_h \frac{\mu_o . D . L_c . f . N_d^2 . KW_h^2}{Po^2 . lg} \quad \ldots \ldots \quad 2.4.5$$

where $l_g = \frac{D/2}{Po}$

D = diameter of stator bore

L_c = stack length

For the test motor, X_m was found to be 3 Ω. The leakage inductance of the main winding was calculated by substituting for X_m and the winding resistance in the input impedance equation

$$Z_{in} = \frac{V}{I} = R + jX = \sqrt{R_d^2 + X^2}$$

so

$$Z_{in}^2 - R_d^2 = X^2$$

$$X_l = \sqrt{Z_{in}^2 - R_d^2} - X_m \quad \ldots\ldots\ldots 2.4.6$$

The following table shows the results of the out rotor test and Figure 2.5 gives an idea how the leakage inductance varies with the input current.

V_{volts}	I_{amp}	Zin_{Ω}	X_l (Ω)	R_d (Ω)
240	12	20	15.33	
220	11.1	19.81	15.43	
150	5.8	25.8	22.8	7.3
125	4.6	27.17	24.17	
110	3.6	27.7	24.7	

the justification of the 'rotor out' method is that the leakage reactance is very much larger than the equivalent magnetizing reactance, and the error in evaluating the equivalent magnetizing reactance does not significantly affect the calculated value of leakage inductance.

b) <u>The search coil test</u>

This method can be used to evaluate the main winding leakage reactance as well as the mutual inductances. A search coil of serveral turns was wound on a dummy rotor without any bars. The coil span of the search coil should be one pole pitch. The

shading rings were removed and a search coil of the same number of turns was wound on each pole. It is assumed that all the flux produced by the main winding links with the stator search coil. The dummy rotor and the stator were set up on the test ring to allow a balanced air gap to be adjusted. The rotor search coil was adjusted to be coaxial with a stator pole to produce a maximum emf in the search coil. The difference between the stator and the rotor emf should be measured for different values of applied voltage. An average value should be taken over all four poles to allow small air gap irregularities. The total leakage inductance of the main winding was calculated from

$$l_d = \frac{e_{sc} \cdot N_d}{N_{sc} \cdot W \cdot I} \quad \ldots \ldots \quad 2.4.7$$

where N_d is the total number of the main winding turns, N_{sc} is the number of search coil turns, e_{sc} is the difference between the stator and the rotor search coil emf.

2.4.2.3 Shading ring leakage inducatance

The slot leakage inductance is the most effective component of the shading ring. This was calculated using the standard expression (37) for the side of the shading ring situated in the slot. The other side of the ring is linked by leakage flux which has a circuit in the air and through the saturated pole tips. The associated leakage inductance is comparatively small, so it was taken as 25% of the slot leakage inductance.

Hence the leakage inductance was found to be 0.122×10^{-6} H.

2.4.2.4 Mutual inductance between main winding and shading ring

This is due to the portion of the slot leakage flux of the main winding which links the shading ring, it can be calculated by using the search coil method or an approximate value may be obtained by assuming that one third of the total leakage flux of the main winding links with the shading ring.

2.4.2.5 Bar and end ring leakage inductance

Because three sides of the end ring are surrounded by air and the section of end ring between adjacent bars is short, the end ring leakage inductance is assumed to be negligible. The rotor bars are located in closed slots, with 0.5 mm below the rotor surface. The leakage inductance of the rotor bar is mainly due to the flux passing internally through the bar and the flux passing through the magnetic bridge. The inductance due to the flux passing internally is independent of the rotor diameter and it has a value of 7.83×10^{-7} H/m (35). Since the rotor current is large and the bridge is considered to be saturated, the closed slot is replaced with an open slot of opening A_o which varies proportionally with the bar current

i.e. $$\frac{B_s \cdot A_o}{\mu_o} = I_b$$

where B_s = saturation flux density, I_b = bar current.

The leakage inductance due to flux passing through the equivalent slot opening is:

$$I_b = \frac{V}{I_b}$$

so

$$I_b = \frac{B_s . h . L_c}{I_b} \quad \ldots \ldots \quad 2.4.8$$

where h = height of the bridge

L_c = core length of the rotor

Hence I_b is inversely proportional to the bar current. Apart from locked rotor condition, the bar current is a mixture of currents of different frequencies. For this reason, I_b was taken as the total r.m.s. value of all the harmonic bar currents.

2.4.2.6 Mutual inductance between a rotor loop and the main winding.

The mutual inductance between a rotor loop and the main winding was measured using a search coil. Consider the emf of a single turn of search coil wound on a dummy rotor without bars, the shading rings being removed.

The emf is given by

$$e = \frac{d}{dt} (M.i)$$

$$= M\frac{di}{dt} + i\frac{dM}{dt} \quad \ldots \ldots \quad 2.4.9$$

For stationary rotor, with a.c. excitation

$$e = M\frac{di}{dt}$$

so

$$M = \frac{E}{WI} \quad \ldots \ldots \quad 2.4.10$$

The single turn search coil was wound with a coil span of one rotor slot pitch and with the same skew as the rotor bars. Thus, the value of M calculated by equation (2.4.10) is the mututal inductance between a rotor loop and the main winding at a particular position.

Alternatively, the measurement of mutual inductance can be obtained by exciting the main winding with dc and driving the rotor at constant speed. The emf of rotor search coil is then

$$e = I_{dc} \frac{dM}{dt} \quad \ldots \ldots \quad 2.4.11$$

For constant speed

$$\theta = W_r . t$$

so

$$dt = \frac{d\theta}{W_r}$$

Substituting in equation 2.4.11

$$e = I_{dc} . W_r \frac{dM}{d\theta}$$

which shows that the search coil emf is proportional to the change of mutual inductance with rotor position. Connecting the search coil to an integrator.

$$e_i = K_i \; I_{dc} \; M \quad \ldots \ldots \quad 2.4.12$$

where e_i = integrator output

K_i = integrator constant

As current and speed are maintained constant, the integrated emf waveform of the search coil is a measure of the cyclic variation of mutual inductance with rotor position. Figure 2.6 shows an oscillogram of the integrated emf. A peak value of mutual inductance of 0.177 mH was obtained from the oscillogram.

2.4.3 Skin Effect

For a rotor bar in a slot, the flux linking the lower part of the conductor is greater than that linking the upper part, thus increasing the effective resistance and decreasing the reactance. The current density therefore falls in moving from the top to the bottom of the bar, and increases the bar impedance. This phenomenon is termed 'skin effect'. If a cage rotor has deep bars, it will be necessary to use variable rotor parameters to allow for changes in bar impedance with changes in the frequencies of the bar current. The influence of skin effect on the test motor was examined by Lock (22). He used the program written by Fultun (38) and showed for the present rotor bar, of 5.6 mm diameter, skin effect is negligible.

2.4.4 Determination of Moment of Inertia of Rotor

The inertia of the rotor was measured by means of the trifilar method. In this method a disc is suspended horizontally by means of three long parallel wires at three points equidistant from the centre of the disc and equidistant from each other. The rotor is placed vertically on the centre of the disc. The disc is then rotated a few degrees and then released. The disc and the rotor rotate. The equation of motion of the system, neglecting the damping, being

$$J\frac{d^2\theta}{dt^2} + \frac{WR^2}{L} \cdot \theta = 0 \quad \ldots \quad \ldots \quad 2.4.13$$

where J = inertia of rotor and disc ($kg.m^2$)

W = weight of rotor and disc (newtons)

L = length of suspension wires (metres)

R = distance from centre of the disc to points of suspension on the disc (metre)

Solution of equation (2.4.13) for the frequency of oscillation gives

$$F = \frac{1}{2\pi}\sqrt{\frac{WR^2}{L.J}}$$

or

$$t = 2\pi\sqrt{\frac{L.J}{W.R^2}} \quad \ldots \quad \ldots \quad 2.4.14$$

Equation 2.4.14 was applied to calculate the inertia of the disc and the rotor. The accuracy of this method was checked by applying it to find the inertia of a solid cylinder. The difference between the calculated and measured value was found to be less than 2%. The moment of inertia of the test rotor was therefore found to be $7.8x10^{-4} kg.m^2$.

2.4.5 Losses

It is a well known fact that the shaded pole motors have very low efficiency. This is mainly caused by the large amount of copper loss which occurs in the main winding shading rings and the rotor bars. Even at no load, the copper loss is high. Since copper loss is accounted for by the set of perforamnce equations, losses which

need to be determined separately are the friction and windage losses, core losses and stray losses.

2.4.5.1 Windage and friction losses

Both windage and friction losses are associated with rotation of the rotor. For the rotor without a fan, the windage loss is proportional to its surface area and the square of the peripheral velocity. The friction losses are caused by the presence of bearings and are a function of the viscosity of the lubricant, and are inversely proportional to the thickness of the oil film.

The friction and windage losses are usually determined by empirical formulas. For example, Vickers (39) used the following expressions:

The bearing loss in watts = (speed of journal in meters per second)$^{1.5}$ x d_j x l_j x 0.19

where dj = diameter of journal in cm;

lj = length of journal in cm.

The windage loss in watts = 0.17 x 10^{-3} rotor barrel surface in cm^2 x (peripheral speed in metres per second)^2

Generally, friction and windage losses constitute only a small percentage of the output power of a motor. These losses were ignored in the measured characteristics of the shaded-pole motor. Therefore the windage and friction losses are considered to be negligible.

2.4.5.2 Core and stray losses.

Core losses resulting from hysteresis and eddy currents, are usually determined by multiplying the volume of core and teeth by empirical watt loss coefficients, depending on the maximum flux density. For a normal 3-phase induction motor, they can be measured by the standard 'no load' test. However this test is not applicable to single phase motors such as the shaded-pole motor which even at synchronous speed has other losses. To estimate the magnitude of the core losses of the shaded-pole motor, its shading rings were removed. The rotor was replaced with one without bars. Subtracting copper loss of the main winding from the input power, a value of 34 watts was obtained for core losses at rated voltage of 240 volts.

Interbar losses are caused by the flow of current through the rotor iron between two adjacent bars. For a cast aluminium rotor. They are the most significant part of the stray losses. Although there was a considerable amount of investigation (40.41) on the stray losses of polyphase induction motors, the expressions derived are not suitable for shaded-pole motors.

2.4.6 Details of Motor used

A commercial produced reluctance-augmented shaded pole motor, as shown in figure (1.1), was used as the base or standard motor. The following details were obtained:

Rated output	=	80 watts
Rated voltage	=	240 volts
Frequency	=	50 Hz
Number of poles	=	4
Number of turns of stator winding per pole	=	154
Number of shading ring per pole	=	1
Number of rotor bars	=	22
Rotor skew angle	=	36^0 electrical
Rotor diameter	=	7.19 cm
Stator stack length	=	5.04 cm
Stator winding resistance	=	7.3 Ω
Rotor bar resistance	=	0.6×10^{-4} Ω
Rotor end ring resistance between adjacent bars	=	0.5×10^{-5} Ω
Stator winding leakage inductance		
Rotor bar leakage inductance	=	0.234×10^{-3} Henry
Resistance of each ring	=	0.125×10^{-3} Ω
Leakage inductance between main winding and shading ring	=	0.122×10^{-6} Henry
Span of shading ring	=	18.5^0 electrical
Width of slot of shading ring	=	12^0 electrical
Width of interpole air gap	=	12^0 electrical
Narrow air gap length	=	0.5 mm
Wide air gap length	=	1.5 mm
Width of step with wide air gap length	=	77^0 electrical
Rotor inertia	=	7.8×10^{-4} $Kg.m^2$

CHAPTER 3

Finite Element Method

3.1 Theory

The application of the finite element method for solving the magnetic field problems in Electrical Machines was first proposed by Silvester and Chari [1]. Instead of dealing with Poissson's partial differential equation.

$$\frac{\partial^2 \bar{A}}{\partial x^2} + \frac{\partial^2 \bar{A}}{\partial y^2} = \mu \bar{J} \quad \ldots.(3.1.1)$$

It exploits the fact known from variational calculus, that equation (3.1.1) is satisfied when an energy functional

$$W = \int\int_R \frac{1}{2\mu} \left[\left(\frac{\partial \bar{A}}{\partial x}\right)^2 + \left(\frac{\partial \bar{A}}{\partial y}\right)^2 - 2\mu \bar{J}\bar{A} \right] dx\, dy \ \ldots\ (3.1.2)$$

is a minimum. This function is the basis of the finite element technique which has been used to study the field problems of different type of electrical machines. The method requires a grid, usually consisting of triangles, in the region being investigated. The grid can be made fine or coarse in various parts of the machine in a very flexible way depending upon the particular requirements of the solution. Such a grid can easily be fitted to the contours of an electrical machine. It is assumed that the current density vector $\bar{J}$ has a component in the z-direction only, of magnitude J. The two dimensional magnetic vector potentional $\bar{A}z(X.Y)$, then

satisfies the non-linear Poisson's equations (3.1.1), subject to the appropriate boundary conditions, in a space of magnetic reluctivity $\nu = \frac{1}{\mu}$, which is generally both position and field dependant.

The basis of the variational finite element technique for solving equation (3.1.2), is to give an initial approximation variation to the function $\bar{A}(X,Y)$ in each element of the problem in the region R depending on the values of $\bar{A}(x,y)$ at the vertices of each triangle. This will constitute an approximate representation for $\bar{A}(x,y)$ equivalent to a linear variation within the element such as

$$\bar{A} = \alpha_1 + \alpha_2 x + \alpha_3 y \quad \ldots \quad (3.1.3)$$

The potential variation over each element is expressed in terms of the nodal potential considering the first order only.

A first order polynomial of the magnetic vector potential gives constant flux in any element. A second order polynomial gives first order variation in flux density, and so on.

The advantage of first-order interpolation is that only one value of reluctivity applies to each element. Higher-order polynomials results in flux-density variation within the elements, therefore reluctivity also must vary in saturable materials. This was catered for using the iterative solution where the flux density is variable until convergence is reached.

The three vertices values $\bar{A}_i$, $\bar{A}_j$ and $\bar{A}_m$ of each element are varied until the energy function in equation (3.1.2) reaches a minimum value. This is possible since there exist only a finite number of vertex values. When a minimum is reached, the resulting

approximation for $\bar{A}(x,y)$ solution must be the best possible one.

3.2 Formulation of the non-linear energy functional

The energy function which is given in equation 3.1.2 is formulated as follows:

$$P_d = \frac{d}{dt} W_s + \rho \bar{J}^2 \qquad , \quad \bar{E} = \rho . \bar{J}$$

$$= \frac{d}{dt} \int_o^B \bar{H} . d\bar{B} + \bar{J} . \bar{E} \qquad \ldots 3.2.1$$

considering only J as source (i.e. ρ charge = 0)

$$\bar{\nabla} \times \bar{E} = - \frac{\partial}{\partial t} \bar{B} = - \frac{\partial}{\partial t} \bar{\nabla} \times \bar{A}$$

therefore

$$\bar{E} = - \frac{\partial}{\partial t} \bar{A}$$

so

$$P_d = \frac{d}{dt} \int_o^B \bar{H} . d\bar{B} - J \frac{\partial \bar{A}}{\partial t}$$

where $\bar{H}$ is the magnetic field intensity vector, $\bar{B}$ is the flux density vector, $\bar{A}$ is the magnetic vector potential, $\bar{J}$ is the current density vector.

The energy density is

$$W_d = \int P_d . dt \quad = \int_o^B \bar{H} . d\bar{B} - \bar{J} \int_o^A d\bar{A}$$

The total energy is the volume integration of energy density.

$$W = \int_v (W_d) dV = \int_v \left[\int_o^B \bar{H} . d\bar{B} - \bar{J} \int_o^A d\bar{A} \right] dv$$

Consider the two dimensional field, the total energy will be

$$W = \iint_R \left[\int_o^B \bar{H}.dB - \bar{J}\bar{A} \right] dx\, dy \quad \ldots (3.2.2)$$

The first term of the right hand side is

$$\int_o^B \bar{H}.d\bar{B} = \frac{B^2}{2\mu} \quad , \quad \bar{H} = \frac{\bar{B}}{\mu}$$

$$\text{curl } \bar{H} = \bar{J} \quad \text{so} \quad \text{curl } \bar{B} = \mu\bar{J}$$

$$\bar{B} = \text{curl } \bar{A}$$

$$(\bar{B})^2 = (\text{curl } \bar{A})^2$$

but

$$A(x,y) = A_z(x,y)$$

so $$\bar{B}^2 = \left(\frac{\partial A}{\partial x}\right)^2 + \left(\frac{\partial A}{\partial y}\right)^2$$

Substituting in the energy expression (3.2.2)

$$W = \iint_R \frac{1}{2\mu} \left[\left(\frac{\partial \bar{A}}{\partial x}\right)^2 + \left(\frac{\partial \bar{A}}{\partial y}\right)^2 - 2\mu\bar{J}.\bar{A} \right] dxdy \quad \ldots(3.2.3)$$

$$W = \iint_R f(A_x, A_y, x, y, A)\, dxdy$$

Applying the variational calculus to the energy function gives

$$\frac{\partial W}{\partial \bar{A}} = \frac{\partial}{\partial x} \cdot \frac{\partial W}{\partial \bar{A}_x} + \frac{\partial}{\partial y} \cdot \frac{\partial W}{\partial \bar{A}y} \qquad \ldots (3.2.4)$$

where $$\bar{A}_x = \frac{\partial \bar{A}}{\partial x} \quad , \quad \bar{A}y = \frac{\partial \bar{A}}{\partial y}$$

From equation (3.2.3)

$$\frac{\partial W}{\partial \bar{A}} = -\bar{J}$$

$$\frac{\partial}{\partial x} \cdot \frac{\partial W}{\partial \bar{A}x} = \frac{1}{\mu} \frac{\partial^2 \bar{A}}{\partial x^2}$$

$$\frac{\partial}{\partial y} \cdot \frac{\partial W}{\partial \bar{A}y} = \frac{1}{\mu} \frac{\partial^2 \bar{A}}{\partial y^2}$$

Substituting in equation (3.2.4) gives:

$$\frac{\partial^2 \bar{A}}{\partial x^2} + \frac{\partial^2 \bar{A}}{\partial y^2} = -\mu J$$

which is Poisson's equation. Hence the energy function yields the differential equation of the physical system.

3.3 Solution of Poisson's equation

To solve equation (3.1.1) for linear or saturable magnetic field problems using the variational finite element method it is essential like any variational technique, to search directly for a function related to the problem $\bar{A}(x,y)$, which minimizes the energy functional, equation (3.1.2), instead of attempting to solve equation (3.1.1). Using the variational finite element method is

necessary to make the problem discrete. Discrete representation of the magnetic field problem is achieved as follows:-

Considering the two dimensional field over region R of the shaded-pole motor in the X-Y plane (Fig. 3.1), the entire region is subdivided into L triangle and N points, each triangle representing an element of the system in the region. The three vertices magnetic vector potential for each element will take the form:

$$\left.\begin{aligned} \bar{A}_i &= \alpha_1 + \alpha_2 X_i + \alpha_3 Y_i \\ \bar{A}_j &= \alpha_1 + \alpha_2 X_j + \alpha_3 Y_j \\ \bar{A}_m &= \alpha_1 + \alpha_2 X_m + \alpha_3 Y_m \end{aligned}\right\} \quad \ldots 3.3.1$$

where $\bar{A}_i$, $\bar{A}_j$ and $\bar{A}_m$ are the values of $(\bar{A})$ at the nodes i, j and m of element (k), hence equation 3.1.2 can be written as

$$W = \sum_{K=1}^{NE} W^{e_k} \quad \ldots 3.3.2$$

Where NE is number of elements

$$W^{e_k} = \iint_R \frac{1}{2\mu} \left[\left(\frac{\partial \bar{A}^{e_k}}{\partial x} \right)^2 + \left(\frac{\partial \bar{A}^{e_k}}{\partial y} \right)^2 - \mu \bar{J} \bar{A}^{e_k} \right] dxdy \quad \ldots 3.3.3$$

The system of equation 3.3.1 will yield a unique solution for the constants α_1, α_2 and α_3 provided that the determinant of the coefficient matrix does not vanish, Norrie [43], that is

$$2\Delta = \begin{vmatrix} 1 & X_i & Y_i \\ 1 & X_j & Y_j \\ 1 & X_m & Y_m \end{vmatrix} \neq 0 \quad \ldots 3.3.4$$

It is clear that the determinant equals twice the area Δ of the triangle. Since the area of the triangle never equals zero, $\Delta \neq 0$, the solution for α_1, α_2 and α_3 exists and is unique, and solving equation 3.3.1 yields

$$\left.\begin{aligned} \alpha_1 &= \frac{1}{2}(a_i\bar{A}_i + a_j\bar{A}_j + a_m\bar{A}_m) \\ \alpha_2 &= \frac{1}{2}(b_i\bar{A}_i + b_j\bar{A}_j + b_m\bar{A}_m) \\ \alpha_3 &= \frac{1}{2}(c_i\bar{A}_i + c_j\bar{A}_j + c_m\bar{A}_m) \end{aligned}\right\} \quad \ldots 3.3.5$$

where $a_i = X_jY_m - X_mY_j$, $b_i = y_i - y_m$, $c_i = x_m - x_j$ and a_j, a_m, b_j, b_m, c_j, c_m can be obtained by permutation of the indices.

Substitution of eqluation 3.3.5 into equation 3.1.2 yields the shape function representation.

$$\bar{A}^e{}_k(x,y) = \frac{1}{2\Delta}\left[(a_i + b_ix + c_iy)\bar{A}_i + (a_j + b_jx + c_jy)\bar{A}j\right.$$

$$\left. + (a_m + b_mx + c_my)\bar{A}_m\right] \quad \ldots 3.3.6$$

where $$\Delta = \frac{1}{2}(c_mb_j - c_jb_m) \quad \ldots 3.3.7$$

From equation 3.3.6

$$\frac{\partial \bar{A}}{\partial x}^{e_k} = \frac{1}{2\Delta} [b_i \bar{A}_i + b_j \bar{A}_j + b_m \bar{A}_m] \quad \ldots 3.3.8$$

$$\frac{\partial \bar{A}}{\partial y}^{e_k} = \frac{1}{2\Delta} [c_i \bar{A}_i + c_j \bar{A}_j + C_m A_m] \quad \ldots 3.3.9$$

and from $\bar{B}$ = curl $\bar{A}$ ... 3.3.10

$$\bar{B} = \frac{\partial \bar{A}}{\partial y} \bar{i} - \frac{\partial \bar{A}}{\partial x} J = \bar{B}_x \bar{i} + \bar{B}_y \bar{j}$$

$$B^2 = B_x^2 + B_y^2 = \left(\frac{\partial A}{\partial y}\right)^2 + \left(\frac{\partial A}{\partial x}\right)^2 \quad \ldots 3.3.11$$

Substituting from equation 3.3.8 and 3.3.9 into equation 3.3.11

$$B = \sqrt{B_x^2 + B_y^2} = \frac{1}{2\Delta} \sqrt{\left(\sum_q b_q A_q\right)^2 + \left(\sum_q C_q A_q\right)^2} \quad q=i, j, m \quad \ldots 3.3.12$$

Substituting from equations 3.3.8 and 3.3.9 into equation 3.3.3

$$W^{e_k} = \int_{e_k} \left[\frac{1}{8\Delta^2 \mu} (b_i \bar{A}_i + b_j \bar{A}_j + b_m \bar{A}_m)^2 \right.$$

$$\left. + \frac{1}{8\Delta^2 \mu} (c_i \bar{A}_i + C_j \bar{A}_j + C_m \bar{A}_m)^2 - \bar{J} \bar{A}^{e_k} \right] dxdy \quad \ldots 3.3.13$$

Let A^{e_k} to represent the value at the centre of the element.

This is the average of the magnetic vector potential values of the three vertices of element K, thus

$$\bar{A}^{e_k} = \frac{1}{3}(A_i + A_j + A_m) \quad \ldots\ 3.3.14$$

Assuming constant current density within each element, the integration in equation 3.3.13 is independent of the variables x and y, so

$$\int_{e_k} dxdy = \Delta \quad \ldots\ \ldots\ 3.3.15$$

Equation 3.3.13 may be written

$$W^{e_k} = \frac{1}{9\Delta\mu}\left[(b_iA_i + b_jA_j + b_mA_m)^2 + (c_iA_i + c_jA_j + c_mA_m)^2\right]$$

$$- \frac{\Delta}{3} J\,(A_i + A_j + A_m) \quad \ldots\ \ldots\ 3.3.16$$

Such an expression can be obtained for each element.

Substituting all these elements' contributions into equation 3.3.2 transforms the functional in equation 3.1.2 into a function of all the nodal values $A_1, A_2, A_3, \ldots, A_n$ so

$$W = W(A_1, A_2, A_3, \ldots, A_n) \quad \ldots\ \ldots\ 3.3.17$$

The condition for W to be minimum can therefore be written as

$$\frac{\partial W}{\partial Aa} = 0 \quad a = 1, 2, 3, \ldots, n \quad \ldots\ \ldots\ 3.3.18$$

Substituting equation 3.3.2 into equation 3.3.18 gives

$$\frac{\partial W}{\partial A_a} = \sum_{i=1}^{L} \frac{\partial W^{e_i}}{\partial A_a} = 0 \quad \ldots\ 3.3.19$$

a = 1, 2,3, ..., number of points

L = number of elements

Although the summation in equation 3.3.19 is taken over all the elements, only those elements, that have mode P in common have non-zero contribution. Differentiating equation 3.3.16 with respect to the proper $\bar{A}_p$ allows the contribution $\frac{\partial W}{\partial A_a}^{e_i}$ of element e_i in equation 3.3.19 to be determined. Thus if the node identifiers i, j and m of element e_i refer to the system node number p, q, and r respectively, differentiation of equation 3.3.16 with respect to $\bar{A}_a$ yields

$$\frac{\partial W}{\partial A_p}^{e_i} = \frac{1}{4\Delta_{e_i}\mu_{e_i}}\left[b_p(b_pA_p + b_qA_q + b_rA_r) + C_p(C_pA_p + C_qA_q + C_rA_r)\right] - \frac{\Delta_{e_i} J_{e_i}}{3}$$

$$\frac{\partial W}{\partial A_q}^{e_i} = \frac{1}{4\Delta_{e_i}\mu_{e_i}}\left[b_q(b_pA_p + b_qA_q + b_rA_r) + C_q(C_pA_p + C_qA_q + C_rA_r)\right] - \frac{\Delta J}{3}$$

$$\frac{\partial W}{\partial Ar}^{e_i} = \frac{1}{4\Delta_{e_i}\mu_{e_i}}\left[b_r(b_pA_p + b_qA_q + b_rA_r) + C_r(c_pA_p + C_qA_q + C_rA_r)\right] - \frac{\Delta_{e_i} J_{e_i}}{3} \quad \ldots 3.3.20$$

The assembly of the component element equations prescribed by equation 3.3.20 is an assembly by nodes since the assembly process

must be carried out separately for each node of the system. The system of equation 3.3.20 can be written in matrix form and considering the element e_i is the object without putting the initial e_i for each term.

$$\begin{bmatrix} \frac{\partial W}{\partial A_p} \\ \frac{\partial W}{\partial A_q} \\ \frac{\partial W}{\partial A_r} \end{bmatrix} = \frac{1}{4\Delta\mu} \begin{bmatrix} K_{pp} & K_{pq} & K_{pr} \\ K_{qp} & K_{qq} & K_{qr} \\ K_{rp} & K_{rq} & K_{rr} \end{bmatrix} \begin{bmatrix} A_p \\ A_q \\ A_r \end{bmatrix} - \begin{bmatrix} \frac{\Delta . J}{3} \\ \frac{\Delta . J}{c} \\ \frac{\Delta . J}{3} \end{bmatrix}$$

or

$$\left[\frac{\partial W}{\partial A_a}\right] = \left[K\right]\left[A_a\right] - \left[I/3\right] \quad \ldots 3.3.21$$

Where $[K]$ is the element K - matrix for element e_i

$$[K] = \frac{1}{4\Delta\mu} \begin{bmatrix} b_p^2+C_p^2 & b_p b_q+C_p c_q & b_p b_r+c_p c_r \\ b_q b_p+c_q c_p & b_q^2+c_q^2 & b_q b_r+c_q c_r \\ b_r b_p+c_r c_p & b_r b_q+c_r c_q & b_r^2+c_r^2 \end{bmatrix} \quad \ldots 3.3.22$$

and $[A]$ is the element nodal vectors matrix

$$[A_a] = \begin{bmatrix} A_p \\ A_q \\ A_r \end{bmatrix}$$

The generalisation of the contribution $\frac{\partial W}{\partial A_a}^{e_i}$ and their assembly will be illustrated further by subdividing the region of the present problem into 16 elements having a total of 15 nodes as shown in

Figure 3.2. Table 3.1 relates the nodes identifiers i, j and m for each element to the system node numbers.

Referring to figure 3.2 shows that the node identifiers are allocated counterclockwise. All elements are of the same size. The x and y coordinates of the nodes are listed in table 3.2, the parameters b_i, b_j, b_m, c_i, c_j and c_m calculated according to equation 3.3.5 are given in table 3.3. Consider now, for illustration, element 5. Table 3.1 shows that the node identifiers i, j and m for this element correspond, respectively, to the system node numbers 7, 4 and 8. Substituting this information and the appropriate parameters for element 5 from table 3.3 into equation 3.3.16 yield the element contribution as follows:

Element	Node Identifiers i	j	m	Element	Node Identifiers i	j	m
1	4	1	5	10	8	11	7
2	2	5	1	11	11	8	12
3	5	2	6	12	9	12	8
4	3	6	2	13	13	10	14
5	7	4	8	14	11	14	10
6	5	8	4	15	14	11	15
7	5	8	9	16	12	15	11
8	6	9	5				
9	10	7	11				

Table 3.1

Relationship between System Node Number and Element Node Identifiers.

Node	Coordinate x	Coordinate y	Node	Coordinate x	Coordinate y
1	0	0	9	2	1
2	1	0	10	0	1.5
3	2	0	11	1	1.5
4	0	0.5	12	2	1.5
5	1	0.5	13	0	2
6	2	0.5	14	1	2
7	0	1	15	2	2
8	1	1			

Table 3.2

Nodal coordinates

Table. 3.3

Element	PARAMETERS					
	b_i	b_j	b_m	c_i	c_j	c_m
1	-0.5	0	0.5	1	-1	0
2	0.5	0	-0.5	-1	1	0
3	-0.5	0	0.5	1	-1	0
4	0.5	0	-0.5	-1	1	0
5	-0.5	0	0.5	1	-1	0
6	0.5	0	-0.5	-1	1	0
7	-0.5	0	0.5	1	-1	0
8	0.5	0	-0.5	-1	1	0
9	-0.5	0	0.5	1	-1	0
10	0.5	0	-0.5	-1	1	0
11	-0.5	0	0.5	1	-1	0
12	0.5	0	-0.5	-1	1	0
13	-0.5	0	0.5	1	-1	0
14	0.5	0	-0.5	-1	1	0
15	-0.5	0	0.5	1	-1	0
16	0.5	0	-0.5	-1	1	0

Element Characteristic Dimensions

$$W^5 = \frac{1}{8\Delta_5\mu_5}\left[(-0.5\,\bar{A}_7 + 0\bar{A}_4 + 0.5\bar{A}_8)^2 + (1\bar{A}_7 - 1\bar{A}_4 + 0\bar{A}_8)^2\right] - \frac{\Delta_5\bar{J}_5}{3}(\bar{A}_7 + \bar{A}_4 + \bar{A}_8) \quad \ldots\ 3.3.23$$

From equation 3.3.23 it is clear that $\frac{\partial W^5}{\partial A_a}$ is nonzero only when a = 7, 4 or 8. In other words element 5 is one of the contributing elements for the system equations involving A_7, A_4 and A_8. From equation 3.3.23 the only nonzero derivatives for element 5 are:

$$\frac{\partial W^5}{\partial \bar{A}_7} = \frac{1}{4\Delta_5\mu_5}\left[-0.5(-0.5\bar{A}_7 + 0\bar{A}_4 + 0.5\,\bar{A}_8) + (1\bar{A}_7 - 1\bar{A}_4 + 0\bar{A}_8) - \frac{\Delta_5\bar{J}_5}{3}\right]$$

$$\frac{\partial W^5}{\partial \bar{A}_4} = \frac{1}{4\Delta_5\mu_5}\left[0(-0.5\bar{A}_7 + 0\bar{A}_4 + 0.5\bar{A}_8) - 1(1\bar{A}_7 - 1\bar{A}_4 + 0\bar{A}_8)\right] - \frac{\Delta_5 J_5}{3}$$

$$\frac{\partial W^5}{\partial \bar{A}_8} = \frac{1}{4\Delta_5\mu_5}\left[0.5(-0.5\bar{A}_7 + 0\bar{A}_4 + 0.5\bar{A}_8) + 0(1\bar{A}_7 - 1\bar{A}_4 + 0\bar{A}_8)\right] - \frac{\Delta_5 J_5}{3} \quad \ldots\ 3.3.24$$

In matrix form the system of equation 3.3.24 become the element matrix equation of element 5.

$$\begin{bmatrix} \frac{\partial W^5}{\partial \bar{A}_7} \\ \frac{\partial W^5}{\partial \bar{A}_4} \\ \frac{\partial W^5}{\partial \bar{A}_8} \end{bmatrix} = \frac{1}{16\Delta_5\mu_5}\begin{bmatrix} 5 & -4 & -1 \\ -4 & 4 & 0 \\ -1 & 0 & 1 \end{bmatrix}\begin{bmatrix} \bar{A}_7 \\ \bar{A}_4 \\ \bar{A}_8 \end{bmatrix} - \begin{bmatrix} \frac{I_5}{3} \\ \frac{I_5}{3} \\ \frac{I_5}{3} \end{bmatrix} \quad \ldots\ 3.3.25$$

where

$$I_5 = \Delta_5 \cdot J_5$$

Since the elements 1, 3, 5, 7, 9, 11, 13, 15 are of identical size and orientation with respect to the frame of reference oxy, it can be shown that the element K matrix is the same for these elements provided the node identifiers are replaced by their proper corresponding node numbers. Thus for element 9 the element matrix equation is:

$$\begin{bmatrix} \frac{\partial W^9}{\partial \bar{A}_{10}} \\ \frac{\partial W^9}{\partial \bar{A}_7} \\ \frac{\partial W^9}{\partial \bar{A}_{11}} \end{bmatrix} = \frac{1}{16\Delta_9\mu_9} \begin{bmatrix} 5 & -4 & -1 \\ -4 & 4 & 0 \\ -1 & 0 & 1 \end{bmatrix} \begin{bmatrix} \bar{A}_{10} \\ \bar{A}_7 \\ \bar{A}_{11} \end{bmatrix} - \begin{bmatrix} \frac{I_9}{} \\ \frac{I_9}{3} \\ \frac{I_9}{3} \end{bmatrix} \quad \ldots \; 3.3.26$$

$$\text{where } I_9 = \Delta_9 . I_9$$

The rest of the elements 2, 4, 6, 8, 10, 12, 14, 16 have also a common element K-matrix, which for this particular case is identical to that obtained above for elements 5 and 9. Thus for element 10, the element matrix equation is:

$$\begin{bmatrix} \frac{\partial W^{10}}{\partial \bar{A}_8} \\ \frac{\partial W^{10}}{\partial \bar{A}_{11}} \\ \frac{\partial W^{10}}{\partial \bar{A}_7} \end{bmatrix} = \frac{1}{16\Delta_{10}\mu_{10}} \begin{bmatrix} 5 & -4 & -1 \\ -4 & 4 & 0 \\ -1 & 0 & 1 \end{bmatrix} \begin{bmatrix} \bar{A}_8 \\ \bar{A}_{11} \\ \bar{A}_7 \end{bmatrix} - \begin{bmatrix} \frac{I_{10}}{3} \\ \frac{I_{10}}{3} \\ \frac{I_{10}}{3} \end{bmatrix} \quad \ldots \; 3.3.27$$

Having obtained the contributions $\frac{\partial W^e}{\partial A_a}$ for all the elements, the next step is to assemble these into the system matrix equation. For assembly by nodes, the basic assembly equation is equation 3.3.19.

For node 7 the relvant assembly relation is:

$$\frac{\partial W}{\partial \bar{A}_7} = \sum_{e=1}^{L} \frac{\partial W^e}{\partial \bar{A}_7} \quad , \quad L = 16 \quad \ldots \ldots \quad 3.3.28$$

From figure 3.1 it is clear that for node 7 the only contributing elements are 5, 9 and 10 so equation 3.3.28 reduces to;

$$\frac{\partial W}{\partial \bar{A}_7} = \frac{\partial W^5}{\partial \bar{A}_7} + \frac{\partial W^9}{\partial \bar{A}_7} + \frac{\partial W^{10}}{\partial \bar{A}_7} \quad \ldots \ldots \quad 3.3.29$$

Substituting from equations 3.3.25, 3.3.26 and 3.3.27 for $\frac{\partial W^5}{\partial \bar{A}_7}$, $\frac{\partial W^9}{\partial \bar{A}_7}$ and $\frac{\partial W^{10}}{\partial \bar{A}_7}$ respectively, into equation 3.3.29 gives

$$\frac{\delta W}{\delta \bar{A}_7} = \frac{1}{16\Delta_5\mu_5} [5 \quad -4 \quad -1][A_1] +$$

$$\frac{1}{16\Delta_9\mu_9} [-4 \quad 4 \quad 0][A_2] +$$

$$\frac{1}{16\Delta_{10}\mu_{10}} [-1 \quad 0 \quad 1][A_3] - \left(\frac{\Delta_5 J_5}{3} + \frac{\Delta_9 J_9}{3} + \frac{\Delta_{10} J_{10}}{3} \right) = 0$$

$$\ldots \ldots \quad 3.3.30$$

where

$$[A_1] = \begin{bmatrix} \bar{A}_7 \\ \bar{A}_4 \\ \bar{A}_8 \end{bmatrix}, \quad [A_2] = \begin{bmatrix} \bar{A}_{10} \\ \bar{A}_7 \\ \bar{A}_{11} \end{bmatrix}, \quad [A_3] = \begin{bmatrix} \bar{A}_8 \\ \bar{A}_{11} \\ \bar{A}_7 \end{bmatrix}$$

Hence equation 3.3.30 will have the form:

$$\frac{1}{16}\left[\left(\frac{5}{\Delta_5\mu_5} + \frac{4}{\Delta_9\mu_9} + \frac{1}{\Delta_{10}\mu_{10}}\right)\bar{A}_7 + \frac{-4}{\Delta_5\mu_5}\bar{A}_4 + \left(\frac{-1}{\Delta_5\mu_5} - \frac{1}{\Delta_{10}\mu_{10}}\right)\bar{A}_8 + \frac{-4}{\Delta_9\mu_9}\bar{A}_{10}\right] = \frac{\Delta_5 J_5 + \Delta_9 J_9 + \Delta_{10} J_{10}}{3} \quad \ldots\ldots\ 3.3.31$$

Equation 3.3.31 can be written in its expanded form as;

$$\frac{1}{16}\left[0 \quad 0 \quad 0 \quad -\frac{4}{\Delta_5\mu_5} \quad 0 \quad 0 \quad \frac{5}{\Delta_5\mu_5} \quad \left(\frac{5}{\Delta_5\mu_5} + \frac{4}{\Delta_9\mu_9} + \frac{1}{\Delta_{10}\mu_{10}}\right)\right.$$

$$\left.\left(-\frac{1}{\Delta_5\mu_5} - \frac{1}{\Delta_{10}\mu_{10}}\right) \quad 0 \quad \frac{-4}{\Delta_9\mu_9} \quad 0 \quad 0 \quad 0 \quad 0 \quad 0\right][\bar{A}]$$

$$= \frac{I_5 + I_9 + I_{10}}{3} \quad \ldots\ldots\ 3.3.32$$

where $[\bar{A}] = \begin{bmatrix} \bar{A}_1 \\ \bar{A}_2 \\ \cdot \\ \cdot \\ \cdot \\ \bar{A}_{16} \end{bmatrix}$, $I_e = \Delta_e \cdot J_e$

For each nodal parameter in the system, an equation similar to equation 3.3.32 can be obtained. Assembling these equation into a single matrix equation gives:

$$[S][A] = [I] \quad \ldots \ldots \quad 3.3.33$$

which is the system matrix equation.

The boundary condition was inserted using, Dirichlet boundary condition, the method explained by Norrie [43] the method is summarised as follows if P is a node for which the nodal value is specified as A_p, so enter zero in the P^{th} row of the system matrix [S] except for the diagonal position, where it should be enterd 1, and enter A_p in the P^{th} row of the matrix [I].

CHAPTER 4

Computation and Application of Finite Element method

4.1 Computer program for the finite element method

The basic input data for the finite element program comprises

1) All the nodes and their x, y coordinates.

2) All the elements and their nodes identifiers.

3) The relationship between the node numbers and the node identifiers for all the elements.

4) The nodes numbers where the function is prescribed and its value.

The programming strategy is outlined in the flow chart (figure 4.1). The basic structure of the program is that of an assembly by nodes. The element K matrix is computed for all the elements and retained in storage for subsequent use since the assembly of the element matrix equations are by nodes. These elements that surround each node need to be ascertained. This information is compiled in the array, ICEV(I,J). The variable I specifies not only the matrix row but also which node is under consideration.

Column J = 1 lists the total number of elements surrounding node I, and columns J = 2, 3, 4,... record the identification numbers of these surrounding elements. Referring to figure 3.2 as an example, column 1 is initially set to zero for all nodes as shown in table 4.1, which contains data for only the first 6 nodes.

The first element to be processed is element 1, which can be seen from table 4.1, has the nodes numbered 4,1 and 5. In the array

the total number of surrounding elements listed for each of these nodes is incremented by one. The identification of element namely 1, is recorded for each node in the next available colum J = 2, as shown in table 4.2. Element 2, with nodes 2, 5 and 1, is the next element to be processed in the same way. The total number of surrounding elements listed for these nodes is incremented by one and the identificastion numbers of the element, namely 2, are recorded in the next available column,

as table 4.3 illustrates. Continuing with the above procedure we come to the array ICEV which is shown in table 4.4 afer all the elements have been processed in turn.

ICEV (I, J)						
Node	Total number of surrounding elements	Identification numbers of surrounding elements				
	J = 1	J = 2	J = 3	J = 4	J = 5	J = 6
1	0					
2	0					
3	0					
4	0					
5	0					
6	0					

Table 4.1 Array ICEV after initialization

Table 4.2

Array ICEV after processing of element 1

ICEV (I, J)

Node I	Total number of surrounding elements	Identification numbers of surrounding elements				
	J = 1	J = 2	J = 3	J = 4	J = 5	J = 6
1	1	1				
2	0	0				
3	0	0				
4	1	1				
5	1	1				
6	0	0				

Table 4.3

Array ICEV after processing of elements 1 and 2

ICEV (I, J)						
Node I	Total number of surrounding elements	Identification numbers of surrounding elements				
	J = 1	J = 2	J = 3	J = 4	J = 5	J = 6
1	2	1	2			
2	1	1				
3	0					
4	1	1				
5	2	1	2			
6	0					

Table 4.4

Array ICEV after processing of elements 1 - 16

ICEV (I, J)							
Node I	Total number of surrounding elements J = 1	Identification numbers of surrounding elements					
		J=2	J=3	J=4	J=5	J=6	J=7
1	2	1	2				
2	3	1	3	4			
3	1	4					
4	3	1	5	6			
5	6	1	2	3	6	7	8
6	3	3	4	8			
7	3	5	9	10			
8	6	5	6	7	10	11	12
9	3	7	8	12			
10	3	9	13	14			
11	6	9	10	11	14	15	16
12	3	11	12	16			
13	1	13					
14	3	13	14	15			
15	2	15	16				

4.2 The Iteration process for Finite Element Program

The saturation iteration procedure described by Demerdash [44] was used for solving the saturable magnetic field of shaded-pole motors.

Giving a guess for a set of reluctivity values over a continuum, solving the system equation for m.v.p (A), hence flux density (B) and field intensity (H) in each element. In this technique, one enters the B-H saturable characteristics, for the iron region, independently from B and H axes for each density and intensity of an element respectively. This yields two values of reluctivity, the assumed one ν_{as} and the calculated reluctivity ν_{cal}. In general ν_{as} and ν_{cal} will not be equal until the nonlinear saturation iteration is reached and the correct value of element reluctivity has been found. Before saturation iteration is completed a guess for the true reluctivity ν_{tr} is given as a linear combination of ν_{as} and ν_{cal} as follows:

$$\nu_{tr} = \nu_{as} + f_{\nu} \cdot (\nu_{ca-} - \nu_{as}) \quad \ldots \ldots y\ y$$

where f_{ν} is a deceleration factor which often takes a value as $0.001 < f_{\nu} < 0.1$.

The most recent values of reluctivity for all the element are used to obtain a new solution, from which new flux densities and field intensities are found. Then the process is repeated for a given excitation until convergence is achieved.

The criteria for reaching a satisfactory convergence is that the difference between the calculated m.v.p.s at two successive iteration must not be a predetermined precision value (ε) such as

$$\varepsilon = \sum_{i=1} \frac{A_{in} - A_{i\ n+1}}{A_{i\ n+1}} < 0.004 \quad \ldots \quad \ldots \quad X\ X$$

where

$i = 1, 2, \ldots,$ number of points.

A_{in} = m.v.p. value of node i at iteration n

$A_{i\ n+1}$ = m.v.p value of node i at iteration n + 1

The values of m.v.p's for all the nodes were set to zero at the very beginning (initial values).

The convergence of an iterative procedure, in which some or all of the results from one computation become the input for the next calculation, is when the difference between successive results continue to decrease, tending to zero in the limit.

4.3 Numerical Representation of Magnetization Curve

The magnetization curve, for steel sheets used for manufacturing shaded-pole motors, is numerically represented in a sub-program of the main finite-element program. Detailed tabulation of the magnetic flux densities corresponding to definite magnetic field intensities was available.

It is assumed that the nagnetization characteristics pass through the origin, so B = 0 when H = 0 and $\frac{dB}{dH}$ is always positive. The magnetization curve is subdivided into sections and an artifice has been incorporated for sensing the portion of the curve to be used to calculate the reluctivity for a given flux density.

The procedure of the numerical representation of the magnetizing curve is illustrated below Fig. 4.2

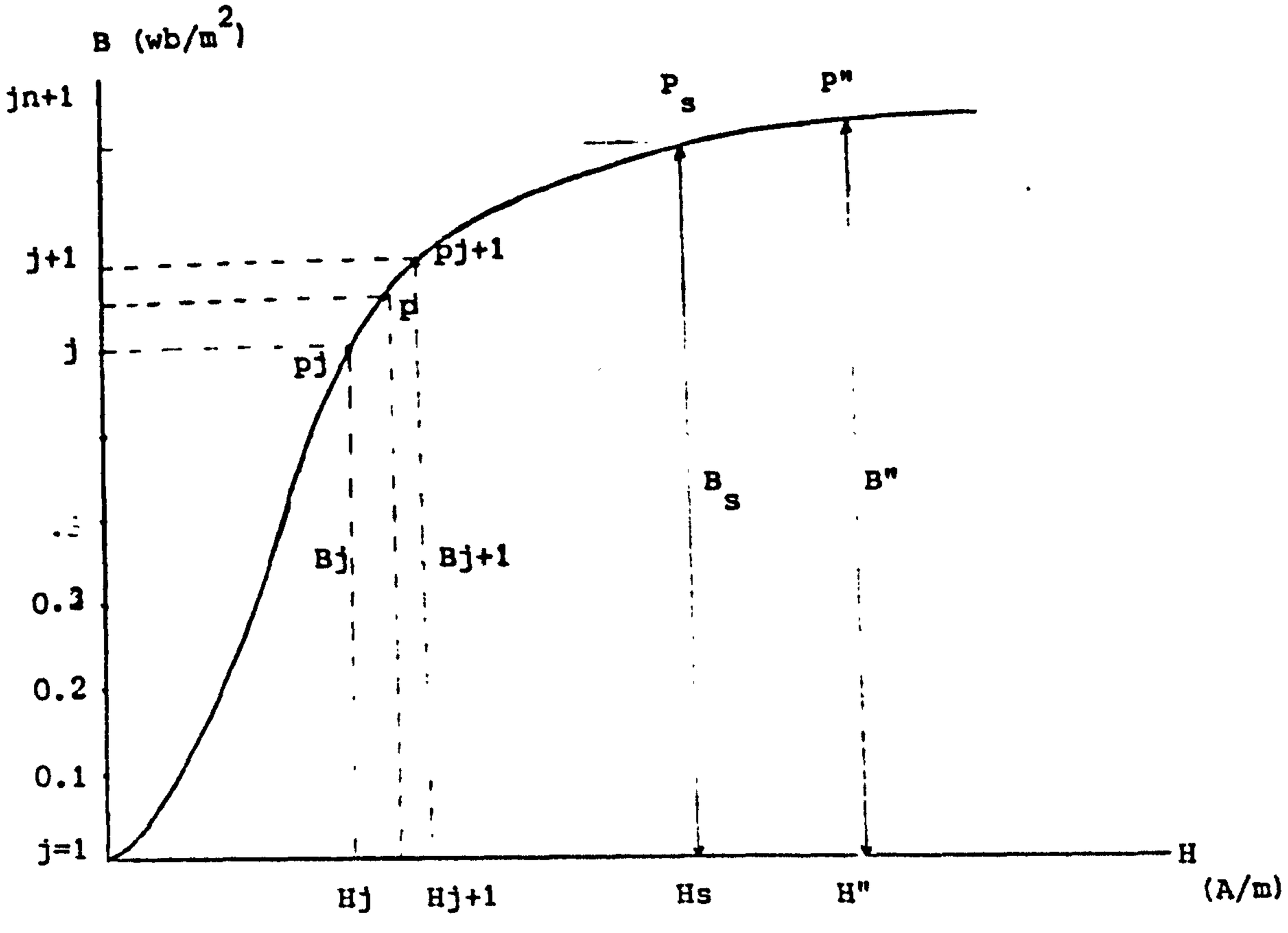

Figure 4.2.

It is assumed that beyond a saturated magnetic induction, (B_s), the slope of the B-H characteristics is given by the permeability of free space.

The distance or the range between B_s and the origin is sub-divided into equal sections, denoted as ΔB. The abscissae at J and J + 1 intersect the magnetizing curve at points P_J and P_{J+1}. Between these points the curve is replaced by the chord (P_J , P_{J+1}). At the origin J = 1 and at the saturation point J = n+1.

The next step is that all the values of H_J are read and the slope M_J, between two points of the curve, P_J and P_{J+1} is calculated using the method developed by Frederick and Edward [45]

$$M_J = \frac{H_{J+1} - H_J}{\Delta B} \quad \ldots\ \ldots\ 4.3.1$$

To find the reluctivity for a magnetic flux density $B < B_s$, at point p, the following steps are taken:

1) Find the section J in which B is situated

$$J = \frac{B}{\Delta B} + 1 \quad \ldots \ldots \quad 4.3.2$$

Only the integer parts of the results of equation 4.3.2 are used.

2) Using tabulated values of H_J and M_J, the value of the magentic intensity H is found as:

$$H = (B - B_J).\ M_J + H_J \quad \ldots \ldots \quad 4.3.3$$

3) The reluctivity at P is found to be

$$\nu = \frac{(B - B_J).M_J + H_J}{B} \quad \ldots \ldots \quad 4.3.4$$

In the case of a flux density greater than the saturated flux density value such that $B'' > B_5$, the reluctivity is found as:

$$\nu = \frac{(B'' - B_s).\nu_o + H_s}{B''} \quad \ldots \ldots \quad 4.3.5$$

Where $\nu_o = \frac{1}{\mu_o}$ is the reluctivity of free space. The flow chart of the computer sub-program is given in Fig. 4.3.2. B_s was chosen as 1.9 Wb/m^2 and n was chosen to be19 so ΔB was equal to 0.1 Wb/m^2.

4.4 Application of Finite Element Method

The finite element method described in the previous chapter, is applied to a shaded-pole induction motor (Figure 1.1) for investigating the flux distribution through the machine and to calculate the parameters of the machine. It is possible to carry out an investigation for half or part of the machine provided that the machine is symmetrical for the part being investigated. In the case of the shaded-pole motor there is a symmetry for half the machine. Coming back to finite element theory, to calculate the system matrix components, it requires a knowledge of all the elements and all the surrounding elements for each node. To calculate the system matrix components considering half the machine requires those elements surrounding each node of the symmetry line AB(Figure 4.3) to be ascertained. To overcome this problem, some elements were taken in the other half alongside the symmetry line. These element were chosen to be symmetrical with elements of the first half of the machine. The method was checked using a simple shape as shown in figure 4.4.

The region was divided into 92 elements, the symmetry line AB divides the problem into two symmetrical parts.

First of all the magnetic field was solved using th whole region. Second, the magnetic field was solved considering half the shape, because of the symmetry. Referring to figure 4.4 nodes 1, 2, 3,..., 8 are symmetrical with 1', 2', 3',..., 8' the system matrix will take the form:

$$S = \begin{bmatrix} a_{11} & a_{12} & a_{13} & a_{14} & \cdots & a_{1n} & b_{11'} & b_{12'} & \cdots & b_{18'} \\ a_{21} & a_{22} & a_{23} & \cdots & & a_{2n} & b_{21'} & b_{22'} & \cdots & b_{28'} \\ \vdots & \vdots & \vdots & \cdots & & \vdots & \vdots & \vdots & \cdots & \vdots \\ a_{n1} & a_{n2} & \cdot & \cdots & & a_{nn} & b_{n1'} & b_{n2'} & \cdots & b_{n8'} \\ b_{1'1} & b_{1'2} & b_{1'3} & \cdots & & b_{1'n} & b_{1'1'} & b_{1'2'} & \cdots & b_{1'8'} \\ \vdots & \vdots & \vdots & \cdots & & \vdots & \vdots & \vdots & \cdots & \vdots \\ b_{8'1} & b_{8'2} & b_{8'3} & \cdots & & b_{8'n} & b_{8'1'} & \cdot & \cdots & b_{8'8''} \end{bmatrix}$$

$$A = \begin{bmatrix} A_1 \\ A_2 \\ \vdots \\ A_n \\ A_{1'} \\ A_{2'} \\ \vdots \\ A_{8'} \end{bmatrix} \quad , \quad I = \begin{bmatrix} I_1 \\ I_2 \\ \vdots \\ I_n \\ I_{1'} \\ I_{2'} \\ \vdots \\ I_{8'} \end{bmatrix}$$

$$[S][A] = [I]$$

But $A_1' = A_1$, $A_2' = A_2$,...., $A_8' = A_8$

Substituting for A_1', A_2' ,...., A_8' and compressing the system matrix gives the system matrix for half the shape.

$$[S] = \begin{bmatrix} c_{11} & c_{12} & \cdots & c_{18} & a_{19} & a_{110} & \cdots & a_{1n} \\ c_{21} & c_{21} & \cdots & c_{28} & a_{29} & a_{210} & \cdots & a_{2n} \\ \vdots & \vdots & & \vdots & \vdots & \vdots & & \vdots \\ c_{n1} & c_{n1} & \cdots & c_{n8} & a_{n9} & a_{n10} & \cdots & a_{nn} \end{bmatrix}$$

$$[I] = \begin{bmatrix} I_1 \\ I_2 \\ \vdots \\ I_n \end{bmatrix} \quad , \quad [A] = \begin{bmatrix} A_1 \\ A_2 \\ A_3 \\ \vdots \\ A_n \end{bmatrix}$$

where I_n is third the sum of the currents of elements surrounding node n.

where $C_{kj} = a_{kj} + b_{kj'}$

$k = 1, 2, 3, \ldots, 8$

$j = 1, 2, 3, \ldots, 8$

$$[S][A] = [I] \quad \ldots \quad \ldots \quad 4.4.2$$

The compressed system matrix equation 4.4.2 was solved for A_1, A_2,...,A_n and then the values of A'_1, A'_2,...,A'_8 were substituted using equation 4.4.1. Reconstructing the system matrix and compressing it will be repeated for every iteration.

The flux density distribution was calculated and plotted on figure 4.5a for whole the shape, and figure 4.5b shows the flux distribution for half the shape.

From the comparison between figures 4.5a and 4.5b, it is clear that the flux distribuion is the same for the complete shape or half the shape.

The same method will be applied to investigate the magnetic field of half the shading-ring motor. In the study the following assumptions were made:

1. The magnetic vector potential has only a component along the axis of the machine.
2. The iron parts are isotropic and the B-H characteristics are single-valued.
3. The individual currents in the element forming the stator and rotor conductors are replaced by a uniform current density over the cross section of their coils.
4. The magnetic field outside the machine contour is negligible and therefore regions external to the stator are not considered.
5. The current density vector $\bar{J}$ has a component only in the axial direction.

Half the machine was considered in addition to extra elements alongside the symmetrical line were taken. The total number of

elements was 678 and 372 nodes before compressing the system matrix, the system then contained 634 elements and 344 nodes. The mesh generation was drawn by hand. Numbering the elements and the nodes it is possible to use a random procedure, but it is better to start numbering all the elements in each particular region as the elements in the air, the elements in the steel and the elements carrying current. The computer program devised by Norrie (43) was modified and used to calculate m.v.p.s, flux density and reluctivity for each element. Element numbers and their identifier nodes, node numbers and their x,y coordinates were supplied as an input data, from mesh drawing (figure 4.6).

From the flow chart figure 4.1 it is clear that the current density, for each element carrying current, must be known so the currents of the machine were found using the steady-state program developed by Lock (22). The currents were calculated at different values of speed. Three values of speed were chosen, s = 1, locked rotor, s = 0.05, no-load speed and s = 0.5, half speed.

For each value of speed the instantaneous currents were calculated at two instants of time t = 0 m.sec and t = 5 m.sec, where the currents have sinusoidal variation.

$i_m = \sqrt{2}\, I_m \, SIN(wt + \theta_1)$ For stator winding

$i_{sh} = \sqrt{2}\, I_{sh} \, SIN(wt + \theta_2)$ For shading ring

$i_{bar} = \sqrt{2}\, I_{bar} \, SIN(wt + \theta_3)$ For rotor bar

From the steady state program rms current values and their angles were obtained and the following table shows the instantaneous values of the currents.

Slip	time(m.sec)	i_m(amp)	i_{sh}(amp)	i_{bar}(amp)
1	0	3.25	-504	-100
	5	4.9	-214	52
0.05	0	1.3	-109	- 28
	5	3.05	-360	- 2
0.5	0	2.62	-407	- 78.7
	5	4.44	-221	33.6

i

The rotor bars have dfferent values of currents.

$$I_{bar_1} = I_{L_1} - I_{L_2} \quad , \quad I_{br_2} = I_{L_2} - I_{L_3} \, , \ldots$$

The bar currents are various, and differ from each other with respect to time. Loop current is calculated using the concept of forward and backward components as:

$$i_{L.m.} = \sum_n \left[\sqrt{2}\, \bar{I}_{f.n} \; \bar{e}^{j(m-1).n\alpha} \; e^{j(wt-n\theta)} \right.$$

$$\left. + \sqrt{2}\, \bar{I}_{b.n} \cdot e^{j(m-1).n\alpha} \; e^{j(wt+n\theta)} \right] \ldots \ldots \; 4.4.3$$

where

α = slot angle between adjacent bars.

n = order of harmonic current

m = loop number

$\theta = (1 - s).wt$, s = slip

First order only was considered, so equation 4.4.3 will be

$$i_{L.m} = \sqrt{2}\ \bar{I}_{f.1}\ \bar{e}^{j(m-1).\alpha}.\ e^{jswt} + \sqrt{2}\ \bar{I}_{b.1}\ e^{j(m-1)\alpha}.\ e^{j(2-s)wt}$$

... ... 4.4.4

Loops currents were calculated, using equation 4.4.4, at different instants of time and slip. The following table shows the variation of loops currents with time and slip.

Slip = 1		Slip = 0.05		Slip = 0.5	
t=o	t=5 m.sec	t=o	t=5 m.sec	t=o	t=5 m.sec
-643.4	-1.6	-189	-13.3	-508.6	-91
-543.3	-53.6	-160.7	-11.3	-430	-124.6
-270.7	-88.6	- 81.4	- 5.8	-214.6	-118.6
87.6	-95.4	23.7	1.5	68.8	- 74.9
418.2	-72	121.4	8.46	330.4	- 7.4
616.1	-25.7	180.5	12.6	487.1	62.5
618.6	28.7	182.3	12.8	489.2	112.6
424.7	74	126.3	9	336	127
96.1	95.9	30.2	2.2	76.1	101
-262.9	87.3	- 75.4	- 5.2	-207.9	43
-538.6	51	-157.2	-11	-425.9	- 28.5

Loops' currents. (amps)

The instantaneous current values are used as excitation currents in the finite element program.

The number of itrations required to reach convergence is depending on the value of ε (equation XX) where the computation results will be printed out when the value of ε becomes less or equal to the pre-determined value. The lower value gives better convergence and more accuracy. It is noted that the change in the results, for $\varepsilon < 0.005$, is very small so that value $\varepsilon_o = 0.004$ was taken as a predetermined value.

The following tables show the number of iterations and the corresponding value of ε.

slip = 1, t = o

N.ITR	ε
1	1.0
2	0.919
3	0.0502
4	0.0186
5	0.0093
6	0.0059
7	0.0044
8	0.0043
9	0.0034
10	0.0034

slip = 0.5, t = o

N. ITR	ε
1	1.0
2	0.636
3	0.0933
4	0.0309
5	0.0201
6	0.0164
7	0.0111
8	0.0086
9	0.0067
10	0.0055
11	0.0042

N.ITR	1	2	3	4	5	6	7
ε	1.0	0.203	0.0145	0.0076	0.0052	0.0032	0.0022

for slip = 0.05, t = 0.

The following results show the element number, flux density and reluctivity for slip = 0.05 and time = 0 as an example.

Element number	B(Wb/m^2)	$\nu = \frac{1}{\mu}$
1	1.35	1600
2	1.22	1140
3	1.47	2829
4	1.48	2872
5	1.3	1767
6	1.37	2425
7	0.8	1123
8	0.96	1125
9	0.35	1138
10	0.57	1130
11	0.04	1203
12	0.04	1203
13	0.57	1130
14	0.4	1135
15	0.83	1124
16	0.74	1124
17	1.27	1134
18	1.2	1131

The highest value of flux density was found to be 2.7 Wb/m^2, and the reluctivity was found to be 65556 for this particular case. The highest value of flux density reached 2.85 Wb/m^2 for locked rotor condition. Magnetic vector potentials were calculated for each node and printed out. The following table shows some points and their relative magentic potential values for slip = 0.5 and t = 0.

Element	Magnetic Potential (amp)	Element	Magnetic Potential (amp)	Element	Magnetic Potential (amp)
36	0.00192	37	-0.00022	38	-0.0022
39	-0.00404	40	-0.0066	41	-0.00783
42	-0.00577	43	-0.00662	44	-0.01178
45	-0.01359	46	-0.01344	47	-0.0134
48	-0.01335	49	-0.01112	50	-0.00862
51	-0.0045	52	-0.00079	53	0.00363
54	0.00866	55	0.01488	56	0.01786
57	0.01786	58	0.01789	59	0.01788
60	0.01521	61	0.00761	62	0.00675
63	0.01251	64	0.01782	65	0.01787
66	0.01789	67	0.01789	68	0.00973
69	0.0042	70	-0.00173	71	-0.00848
72	-0.01379	73	-0.01329	74	-0.01344

The highest value of magnetic potential was found to be 0.0195 Tesla/meter.

The magnetic vector potentials are used to obtain flux plots for any instant of time and speed.

Figures 4.7a and 4.7b illustrate the field patterns for slip = 1 and time = 0, slip = 1 and time = 5m.sec respectively. Figures 4.8a and 4.8b show the field patterns for slip = 0.5, t = 0 and t = 5 m.sec respectively. Figures 4.9a, 4.9b illustrate the field patterns for slip = 0.05 and times t = 0, t = 5m.sec.

The finite element method was also applied to the reversing-speed motor (Figure 4.10). The flux plot was obtained using only the stator current as an exciting current and figure 4.11 shows the field pattern for this motor.

A computer program was developed to obtain the flux lines distribution for each element. Figure 4.12 gives the flow chart of this program.

CHAPTER 5

FINITE ELEMENT AND PARAMETERS CALCULATION

5.1 Theory

The main purpose of using the finite element method is to introduce an alternative approach to parameter calculations. The aim of this method is to achieve better accuracy than the normal way which is mentioned in Chapter 2.

The procedure of the method is outlined as follows: All the instantaneous currents are calculated, for a given speed and time, and used as excitation currents in the finite element program. Flux density and reluctivity is calculated for each element after a good convergence is achieved.

At this stage the reluctivity is fixed for all the elements. The fixed reluctivity is used as input data. The self inductance of any coil is calculated using the concept of stored energy.

$$W_s = \int_v \cdot \int_o^B H.db \cdot dv \quad \ldots \quad \ldots \quad 5.1.1$$

$$= \int_v \frac{B^2}{2\mu_r} \cdot dV = \frac{B^2}{2\mu_r} \cdot A.L$$

$$W_s = 0.5\ li^2 \quad \ldots \quad \ldots \quad 5.1.2$$

so

$$l = \frac{B^2}{\mu_r . i^2} \cdot A.L \quad \ldots \quad \ldots \quad 5.1.3$$

where L is the stack length of the machine

A is the area of any element under consideration

B is the flux density in an element

μ_r is the fixed permability of any element

i is the conductor current of the coil being considered.

The value of flux density is calculated, for the existing current and fixed permability, for each element in the region. Using equation 5.1.3 over all the elements of the machine to get the partial inductances, then taking the summation, of these inductances, gives the self inductance of the winding being considered.

Mutual inductance between two coils is calculated using the flux linkage concept. Flux produced by one coil and links another coil, where the value of flux density and its angle is calculated for each element and printed out.

Mutual inductance can be expressed as

$$M_{1.2} = \frac{N_2 \phi_{1.2}}{I_1} \quad \ldots \ldots \quad 5.1.4$$

$$\phi_{1.2} = \phi_1 + \phi_2 + \ldots + \phi_n \quad \ldots \ldots \quad 5.1.5$$

$$= B_1 \cdot L_1 \cdot L + \bar{B}_2 \cdot L_2 L + \ldots + \bar{B}_n \cdot L_n \cdot L$$

$$\phi_{1.2} = L \cdot \Sigma_n \bar{B}_n \cdot L_n = L \cdot \Sigma_n \cdot B_n \cdot L_n \cdot \cos \theta_n$$

where N = number of turn, I_1 = conductor current of first coil

L = stack length, L_n = length of element n

B_n = flux density of element n

$\bar{B}_n = B_n \cdot \cos(\theta_n)$ or $\bar{B}_n = B_n \cdot \sin(\theta_n)$.

The expression having cos θ_n or sin θ_n depends on the position of the coil with respect to X.Y coordinates. If the centre of the coil is in the X direction so $\bar{B}_n = B_n \cos(\theta_n)$ and if the centre is in Y direction then $\bar{B}_n = B_n \cdot \sin(\theta_n)$. Figure 5.1.1 shows part of the machine and illustrates the elements to be used to calculate a mutual inductance and the cross length of each element (L_1 , L_2 ,.., L_n).

5.2 RESULTS

Equation 5.1.2 is used to calculate the self inductances of the main winding, shading ring and rotor loops.

The following table shows the self inductance of the main winding at slips equal 1, 0.5 and 0.05

Slip	Time (m.sec)	I_m (amp)	1 (H)	
	0	3.25	0.1584	
1	5	4.9	0.1834	
	0	2.62	0.1792	
0.5	5	4.44	0.1863	μ = constant
	0	1.3	0.2411	
0.05	5	3.05	0.2352	

Self inductance of mainwinding

Self inductance of the ring and mutual inductance between two rings for constant permeability and different speeds are illustrated in the following table.

Slip	Time (m.sec)	I_{sh} (amp)	l (H)	M (H)
1	0	-503.8	0.1083×10^{-5}	0.433×10^{-7}
	5	-214.5	0.85×10^{-6}	0.355×10^{-7}
0.5	0	-407	0.1116×10^{-5}	0.475×10^{-7}
	5	-221	0.9097×10^{-6}	0.468×10^{-7}
0.05	0	-109	0.1174×10^{-5}	0.431×10^{-7}
	5	-360	0.118×10^{-5}	0.473×10^{-7}

Self inductance of one ring and mutual inductance between two rings

From the results shown in the table it is clear that the ring inductance and mutual inductance between two rings do not have significant variation with speed or time so they will be considered constant.

Variations of rotor loop self inductance with position is calculated, the self inductances are found for all the loops at one speed and instant of time. The following table shows the values of rotor loops self inductances.

Loop No.	Slip = 1		Slip = 0.5		Slip = 0.05	
	time = o	time = 5 (m.sec)	time = o	time = 5 (m.sec)	time = o	time = 5 (m.sec)
	$\ell(10^{-6}H)$	$\ell(10^{-6}H)$	$\ell(10^{-6}H)$	$\ell(10^{-6}H)$	$\ell(10^{-6}H)$	$\ell(10^{-6}H)$
1	0.944	1.8	1.16	2.22	2.46	7.6
2	1.07	2.15	1.23	3.35	1.82	8.86
3	1.08	2.36	1.19	3.45	1.73	6.51
4	0.838	1.66	0.956	1.64	1.87	3.4
5	0.688	0.922	0.768	0.904	1.85	1.3
6	0.734	0.858	0.834	0.853	1.91	1.51
7	0.868	1.17	0.997	1.68	1.73	5.47
8	0.96	2.4	1.04	3.12	1.62	6.83
9	0.976	1.11	1.17	2.36	2.07	3.46
10	0.78	1.1	0.955	1.06	2.03	1.56
11	0.98	1.42	1.19	1.34	2.66	3.84

Self inductances of rotor loops at different time and speed

Variations of rotor loop self inductance are plotted on figures (5.2.1.a) for slip = 1, (5.2.1.b) for slip = 0.5 and (5.2.1.c) for slip = 0.05.

Field plottings of rotor loops are plotted on figures, $5.2.2.a_1$, $5.2.2.a_2$,..., $5.2.2.a_{11}$ for (slip = 1, time = 0), $5.2.3.a_1$, $5.2.3.a_2$,..., $5.3.2.a_{11}$ for (slip = 1, t = 5 m.sec). Field plottings of rotor loops are illustrated on figures $5.2.4.b_1$,

5.2.4.b_2 ,..., 5.2.4.b_{11} for (slip = 0.05, t = 0). Figures 5.2.5.a, 5.2.5.b and 5.2.5.c show flux distribution, produced by rotor bars, for (slip = 1, t = 0), (slip = 1, t = 5 m.sec), and (slip = 0.05, t = 0) respectively.

Flux of the main winding is obtained at different speed of the motor at time = 0. Field maps of the main windings are plotted on figures (5.2.6.a for S = 1, t = 0), (5.2.6.b for S = 0.5, t = 0) and (5.2.6.c for S = 0.05, t = 0).

Shading ring flux is calculated considering one ring carrying current, for (slip = 1, 0.5, 0.05) and also is calculated for two rings carrying currents. Flux produced by one ring is plotted on figures (5.2.7), (5.2.8) and (5.2.9) for (slip = 1, 0.5, 0.05) respectively and time = 0.

Mutual inductance between main winding and shading ring is calculated, at t = 0 and t = 5 m.sec, for locked rotor condition, half speed and no load speed. Also mutual inductance between main winding and rotor loops is calculated for the same above conditions. The following tables show the results which are obtained

slip	time (m.sec)	M (H)
1	0	1.018×10^{-4}
	5	0.876×10^{-4}
0.5	0	0.969×10^{-4}
	5	0.895×10^{-4}
0.05	0	1.105×10^{-4}
	5	1.06×10^{-4}

Mutual inductance between main winding and shading ring

Loop No.	Slip = 1		Slip = 0.5		Slip = 0.05	
	time = 0	time = 5 (m.sec)	time = 0	time = 5 (m.sec)	time = 0	time = 5 (m.sec)
	$Mx10^{-4}$ (H)	$Mx10^{-4}$ (H)	$Mx10^{-4}$ (H)	$Mx10^{-4}$ (H)	$Mx10^{-4}$ (H)	$Mx10^{-4}$ (H)
1	0.397	0.519	0.47	0.46	0.65	0.57
2	0.553	0.427	0.6	0.38	0.52	0.46
3	0.4	0.359	0.45	0.32	0.45	0.33
4	0.548	0.69	0.65	0.62	1.1	0.97
5	0.532	0.78	0.64	0.78	1.15	1.08
6	0.471	0.67	0.56	0.66	0.99	0.94
7	0.495	0.58	0.6	0.53	0.73	0.61
8	0.206	0.144	0.23	0.185	0.21	0.26
9	0.63	0.612	0.74	0.62	0.95	0.72
10	0.47	0.712	0.57	0.71	1.09	1.02
11	0.55	0.88	0.7	0.87	1.24	1.26

Mutual inductance between main winding and rotor loops

Mutual inductance between shading ring and rotor loops is calculated considering one ring carries current, the results are listed in the following table.

Loop No.	Slip = 1		Slip = 0.5		Slip = 0.05	
	time = 0	time = 5	time = 0	time = 5	time = 0	time = 5
	(m.sec) $M(10^{-7}H)$	(m.sec) $M(10^{-7}H)$	(m.sec) $M(10^{-7}H)$	(m.sec) $M(10^{-7}H)$	(m.sec) $M(10^{-7}H)$	(m.sec) $M(10^{-7}H)$
1	0.336	0.25	0.46	0.35	0.34	0.22
2	0.39	0.14	0.21	0.65	0.37	0.299
3	3.1	2.5	3.4	2.7	3.1	2.6
4	1.1	1.07	1.55	1.8	1.09	0.898
5	0.614	0.59	0.76	0.77	0.516	0.508
6	0.52	0.47	0.63	0.64	0.44	0.43
7	0.48	0.38	0.44	0.5	0.44	0.368
8	0.48	0.37	0.37	0.41	0.48	0.466
9	0.5	0.37	0.61	0.56	0.53	0.401
10	0.4	0.42	0.7	0.697	0.34	0.394
11	0.5	0.55	0.82	0.868	0.49	0.49

Mutual inductance between shading ring and rotor loops

The results, listed in the last two tables, were checked by finding the mutual inductances between rotor loops and main winding, also between rotor loops and ring, where the current exists in one rotor loop at a time.

Figure 5.2.10 shows mutual inductance waveform between main winding and rotor loop. Variations of mutual inductance between one ring and a rotor loop, considering each loop represents a position, are plotted on figure 5.2.11.

Mutual inductances between rotor loops are calculated for each individual loop at two times and three values of speed. The calculated results are tabulated to be used for plotting the waveform of mutual inductance between any two loops. The following tables show the results at time = 5 m.sec and different speeds.

	Mutual inductance between loop I and loop J $M_{I,J}$ (H x 10^{-7})							
I/J	1	2	3	4	5	6	7	8
1		6.75	0.946	0.41	0.41	0.342	0.274	0.34
2	6.2		5.48	0.466	0.335	0.27	0.233	0.293
3	0.779	5.22		7.4	0.534	0.429	0.363	0.414
4	0.394	0.465	7.57		0.69	0.532	0.437	0.479
5	0.393	0.362	0.615	0.756		1.51	0.551	0.572
6	0.323	0.29	0.481	0.571	1.49		0.899	0.54
7	0.272	0.239	0.389	0.448	0.522	0.864		4.56
8	0.323	0.286	0.39	0.436	0.475	0.485	4.09	
9	0.41	0.357	0.427	0.434	0.468	0.402	0.504	10.1
10	0.508	0.381	0.467	0.477	0.514	0.44	0.378	0.645
11	2.35	0.834	0.68	0.631	0.671	0.568	0.488	0.689

I/J	9	10	11
1	0.37	0.451	2.46
2	0.381	0.404	0.782
3	0.44	0.447	0.606
4	0.454	0.453	0.578
5	0.538	0.536	0.686
6	0.448	0.446	0.565
7	0.539	0.364	0.462
8	9.45	0.518	0.588
9		1.74	0.983
10	2.09		2.06
11	1.07	1.94	

Mutual inductances between rotor loops for s = 1, t = 5 m.sec

Mutual inductance between loop I and loop J

$M_{I,J}$ (H x 10^{-7})

I/J	1	2	3	4	5	6	7	8
1		8.82	2.21	0.367	0.342	0.289	0.245	0.328
2	8.15		11.5	0.687	0.331	0.269	0.299	0.322
3	1.94	11		7.02	0.62	0.494	0.423	0.553
4	0.343	0.691	7.35		0.655	0.481	0.4	0.5
5	0.346	0.352	0.713	0.734		1.43	0.536	0.638
6	0.287	0.286	0.547	0.499	1.38		0.971	0.661
7	0.223	0.223	0.428	0.38	0.48	0.892		0.875
8	0.29	0.282	0.498	0.427	0.502	0.535	7.85	
9	0.435	0.385	0.496	0.392	0.463	0.407	0.753	11.8
10	0.477	0.394	0.552	0.417	0.491	0.428	0.36	0.65
11	1.98	0.909	0.759	0.527	0.622	0.533	0.451	0.703

I/J	9	10	11
1	0.369	0.417	2.21
2	0.385	0.4	0.872
3	0.448	0.49	0.683
4	0.406	0.401	0.496
5	0.52	0.511	0.634
6	0.439	0.426	0.525
7	0.737	0.329	0.408
8	10.3	0.504	0.564
9		1.62	0.939
10	1.92		1.93
11	1.02	1.78	

Mutual inductances between rotor loops for s = 1, t = 5 m.sec

Mutual inductance between loop I and loop J $M_{I,J}$ (H x 10^{-7})								
I/J	1	2	3	4	5	6	7	8
1		3.2	3.75	0.769	0.473	0.405	0.317	0.357
2	29.5		23	2.3	0.464	0.376	0.323	0.292
3	3.44	23		16	0.561	0.447	0.396	0.326
4	0.679	2.56	15.6		1.28	0.676	0.555	0.428
5	0.463	0.492	0.618	1.18		2.71	0.761	0.561
6	0.389	0.389	0.473	0.75	2.6		3.17	0.89
7	0.268	0.302	0.386	0.579	0.708	2.95		33
8	0.319	0.256	0.295	0.416	0.46	0.761	30.3	
9	0.486	0.418	0.421	0.541	0.606	0.552	2.75	15.6
10	0.774	0.505	0.508	0.716	0.769	0.665	0.498	0.818
11	14	3.184	0.996	0.958	0.964	0.842	0.627	0.82

I/J	9	10	11
1	0.467	0.676	14.2
2	0.378	0.49	3.09
3	0.391	0.483	0.912
4	0.485	0.69	0.858
5	0.645	0.783	0.984
6	0.564	0.654	0.827
7	2.649	0.469	0.585
8	14.9	0.647	0.689
9		2.68	1.14
10	2.87		2.89
11	1.19	2.7	

Mutual inductances between rotor loops for s = 1, t = 5 m.sec

Using the results listed in the tables, waveforms are plotted, to show the variation of mutual inductance, between rotor loops, when they change their position. Mutual inductance between loop 1 and 2 is plotted against rotor position as shown by figure 5.2.12. Figures 5.2.13, 5.2.14, 5.2.15, 5.2.16, 5.2.17, 5.2.18, 5.2.19, 5.2.20 and 5.2.21 illustrate the variation of mutual inductance between loops 1 and 3, 1 and 4, 1 and 5, 1 and 6, 1 and 7, 1 and 8, 1 and 9, 1 and 10 and 1 and 11 respectively.

CHAPTER 6

TRANSIENT ANALYSIS OF SHADED-POLE MOTOR

Performance differential equations of the machine were derived from the electro-physical construction of the machine. Half the machine was considered because of the symmetry, so three stator equations and eleven rotor equations were derived.

Electrical machine can be treated, in general, as a configuration of coils interacting with each other through self and mutual inductance. The performance of electrical machines can be described by a set of voltage equations:

$$v_m = i_m . R_m + P(l_m l_m) + P\phi_m \quad \ldots \ldots \quad 6.1$$

where m = 1, 2, 3 ...., c

c = total number of coils

The flux linkage ϕ_m of coil m will be a function of every current in the multi-coil system as well as their relative positions.

$$\phi_m = f\ (i_1, i_2, i_3, \ldots, i_c, \theta_1, \theta_2, \ldots, \theta_c)$$

$$P\phi_m = \sum_{n=1}^{c} \frac{\partial \phi_m}{\partial i_n} p i_n + \sum_{n=1}^{c} \frac{\partial \phi_m}{\partial \theta_n} p \theta_n \quad \ldots \ldots \quad 6.2$$

In equation (6.2), the first summation involving rate of change of currents is referred to as the emf of pulsation or transformation since it is caused by the pulsation of flux. the latter summation is the emf of rotation because it depends on relative motion between the coils.

In addition to the electrical equations (6.1) and (6.2), the mechanical equation was introduced to investigate the speed behaviour of the machine.

$$T_e = J\ddot{\theta} + T_L \quad \ldots \ldots \quad 6.3$$

where T_e is the electromagnetic torque developed

J = moment of inertia

$\ddot{\theta}$ = acceleration of the rotor

and T_L = load torque including friction and windage

6.1 Derivation of Differential Performance Equations

Figure (6.1) shows the physical representation of half the shaded-pole motor. The main winding voltage equation was derived as follows

$$v_1 = R_1 i_1 + p(\ell_1\ i_1) + p(M_{1.2}\ \ i_2) + p(M_{1.3}\ i_3) + p(M_{1.4}\ \ i_4) + p(M_{1.5}\ \ i_5) + \ldots\ldots + p(M_{1.15}\ \ i_{15})$$

$$v_2 = R_2 i_2 + p(\ell_2\ i_2) + p(M_{2.1}\ \ i_1) + p(M_{2.3}\ i_3) + p(M_{2.4}\ \ i_4) + p(M_{2.5}\ \ i_5) + \ldots\ldots + p(M_{2.15}\ \ i_{15})$$

But $i_1 = i_2 = i_s$, $v_1 + v_2 = v_s$

$$v_s = R_s i_s + p(L_s\ i_s) + p(M_{s.q1}\ i_{q1}) + p(M_{s.q2}\ i_{q2}) + p(M_{s.r1}\ \ i_{r1}) + \ldots\ldots + p(M_{s.r11}\ \ i_{r11})$$

$$v_s = R_s i_s + L_s.pi_s + M_{s.q1}.pi_{q1} + M_{s.q2}pi_{q2} + \sum_{n=1}^{11} P(M_{s.rn}\ i_{rn}) \qquad \ldots\ \ldots\ 6.1.1$$

where $M_{s.q}$ = constant, L_s = constant

$L_s = l_1 + l_2 + 2M_{1.2}$, $M_{1.3} + M_{2.3} = M_{s.q1}$

$M_{1.4} + M_{2.4} = M_{s.q2}$, $M_{1.5} + M_{2.5} = M_{s.r1}$

$M_{1.6} + M_{2.6} = M_{s.r2}$ and so on

Because the shading ring has a closed circuit its voltage is zero. The voltage equation for ring one is

$$v_3 = 0 = R_3 i_3 + \ell_3 pi_3 + M_{q1.s}.pi_s + M_{q1.q2}pi_{q2} + p(M_{q1.r1}\ i_{r1}) + p(M_{q1.r2}.i_{r2}) + \ldots + p(M_{q1.r11}.i_{r11})$$

$$v_{q1} = R_{q1} i_{q1} + \ell_{q1} pi_{q1}, + M_{q1.s} pi_s + M_{q1.q2} \cdot pi_{q2} + \sum_{n=1}^{11} p(M_{q1.rn} \cdot i_{rn}) \quad \ldots\ \ldots\ 6.1.2$$

and the voltage equation for ring two is

$$v_{q2} = R_{q2} i_{q2} + \ell_{q2} \cdot pi_{q2} + M_{q2.s} \cdot pi_s + M_{q2.q1} \cdot pi_{q1} + \sum_{n=1}^{11} p(M_{q2.rn} i_{rn}) \quad \ldots\ \ldots\ 6.1.3.$$

6.2 Representation of cage rotor

The cage rotor is represented, in the present investigation, by a number of cascaded loops, each formed by two adjacent bars and the two interconnecting portions of the rings. The number of loops is equal to the number of rotor bars. Each loop is considered as a single turn coil having flux linkage with itself, with other rotor loops and with the stator windings. An equivalent circuit of the cage rotor by this representation is shown in figure (6.2).

The voltage equation for n^{th} loop is

$$0 = R_{rn} i_{rn} - R_b (i_{r.n+1} + i_{r.n-1}) + \sum_{m=1}^{11} p(M_{rn.m} i_{rm}) + p(M_{rn.s} i_s) + p(M_{rn.q1} i_{q1}) + p(M_{rn.q2} i_{q2}) \quad \ldots\ \ldots\ 6.2.1$$

6.3 Representation of Self and Mutual Inductance

Both self and mutual inductances were calculated, for each winding in the machine, using finite-element methods. The results were obtained at two times and different speeds.

The Self-inductance of the main winding and shading ring were found to be constants. The mutual inductance between the main winding and shading ring was also taken to be constant. The mutual inductance between two rings was constant and the self inductance of

rotor loop with the speed of the machine and the position of the loop. Under locked rotor condition where the slip = 1 the variation of the rotor loop self inductance is not significant. The rotor loop self inductance variations appear clearly when the speed of the motor was increased. This is noticed from the comparison between figures (5.1.2.a) and (5.1.2.b) and between figures (5.1.2.a) and (5.1.2.c). The purpose of representing a rotor loop self inductance in this chapter is to be used in the transient equations where the speed of the motor is initially zero thus the self inductance of a rotor loop was considered constant.

6.3.1 Mutual inductance between main winding and a rotor loop

Field plotting of main winding and rotor loops show different flux linkage between the main winding and each rotor loop. The flux linkage is both speed and position dependant as shown in figures (5.2.2.), (5.2.3) and (5.2.4).

Mutual inductance between main winding and a rotor loop was calculated by finite element methods. The variation of mutual inductance between main winding and a rotor loop is illustrated by figure (5.2.10). From the waveform it is clear that the mutual inductance varies sinusoidally.

so

$$M_{s.r} = \hat{M}_{s.r} \cos(\theta + \alpha)$$

where θ is the angular displacement between a reference point on the stator and a reference point on the rotor

and α is the initial angle between the main winding and a rotor loop. Such an expression may be written for each loop.

Considering the space displacement between each loop, the mutual inductance between main winding and loop n will be

$$M_{s.rn} = \hat{M}_{s.rn} \cos (\theta + \alpha + (n-1)\ \alpha_1)$$

where α_1 is the slot angle

6.3.2 Mutual inductance between shading-ring and a rotor loop

Field maps of the shading-ring show different flux distirbution for different speed as shown in figures (5.2.7, 5.2.8, 5.2.9).

Flux linkage with a rotor loop depends on the position of the loop with respect to the shading ring. Mutual inductance between shading ring and a rotor loop was calculated for each loop at two times and three values of slip. Mutual inductance waveform against the rotor position is shown by figure (5.2.11). It is obvious, from the waveform, that the mutual inductance is a maximum when the loop is co-axial with the ring, and it is very small in all other positions.

The mutual inductance expression was derived considering two cases:

1. The rotor loop is co-axial with the ring. This position occupies two slots only.

$$M_{q.r} = \hat{M}_{q.r} \cos (2(\theta + \alpha + \delta))$$

where δ is the angle between main winding and the ring so the mutual inductance between shading-ring one and a rotor loop was expressed as

$$M_{q.rn} = \hat{M}_{q.rn} \cos(2(\theta + \alpha + \delta + (n-1)\alpha_1)) \quad \ldots \ldots \quad 6.3.2.1$$

where n indicates to loop number was considered.

Equation (6.3.2.1) is applicable to this region if the angle $-\alpha_1 < \theta_1 < \alpha_1$ where $\theta_1 = \theta + \alpha + \delta + (n-1)\alpha_1$.

2. The rotor loop is outside the co-axial region. In this region the mutual inductance is small for all the loops in this region and it may be considered constant. An expression is given for loop n in this region as:

$$M_{q.rn} = \hat{M}_{q.rn} \cos(\theta + \alpha + \delta + (n-1)\alpha_1) \quad \ldots \ldots \quad 6.3.2.2$$

Shading-ring two is displaced 180 electrical degrees from shading-ring one. Equation (6.3.2.1) will take, for shading-ring two, the form

$$M_{q.rn} = -\hat{M}_{q.rn} \cos(2(\theta + \alpha + \delta + (n-1)\alpha_1)) \quad \ldots \ldots \quad 6.3.2.3$$

and equation (6.3.2.2) will be

$$M_{q.rn} = -\hat{M}_{q.rn} \cos(\theta + \alpha + \delta + (n-1)\alpha_1) \quad \ldots \ldots \quad 6.3.2.4$$

Equations (6.3.2.3) and (6.3.2.4) express the mutual inductance between a rotor loop and shading-ring two in the co-axial and the non co-axial regions respectively.

6.3.3. Mutual Inductance between Rotor Loops

Each rotor loop was treated as a single turn coil. Flux

distribution for each coil was calculated at two times and three values of speed. Field maps are shown by figures (5.2.2), (5.2.3) and (5.2.4).

Flux linkages between one rotor loop and the rest of the loops depends on the position of the loop under consideration as well as the speed of the machine. Therefore the mutual inductance between rotor loops was calculated by finite element methods for each individual loop. The results were obtained considering different speed of the machine. Variation of mutual inductance, between a rotor loop and other loops, are shown by figures (5.2.1.2), (5.2.13), ... (5.2.21).

Mutual inductance between rotor loops has a high value when the machine is running at no load speed and it decreases with speed deceleration of the machine. The mutual inductance is significant between the adjacent loops as appears from the comparison between figure (5.2.12) and figures (5.2.13, 5.2.14, 5.2.15). An expression was obtained from the waveform of mutual inductance between the loops:

$$M_{r.n} = \pm \hat{M}_{r.n} + (1 + 0.5 \cos(k.\alpha_1 + \theta))$$

where $K\alpha_1 = (n-r)\alpha_1$

The sign (+) or (-) depends on the value of the angle $k.\alpha_1$.

6.4 Torque Evaluation

The induced voltage of a single coil carrying current i and setting up flux linkage with itself is

$$e = \frac{d\phi}{dt} \quad \ldots \quad \ldots \quad 6.4.1$$

Neglecting the power loss in the resistance of coil, the electrical energy input will be stored in the field as magnetic energy w_s. The energy stored in a time period t_1 t_o t_2 is

$$\int_{t_1}^{t_2} e.i.\ dt = \int_{t_1}^{t_2} \frac{d\phi}{dt}\, i\ dt$$

i.e. $$w_s(t_1, t_2) = \int_{t_1}^{t_2} i\ d\ \phi \quad \ldots \quad \ldots \quad 6.4.2$$

The flux linkage and current are related by the magnetising curve as shown in figure 6.3

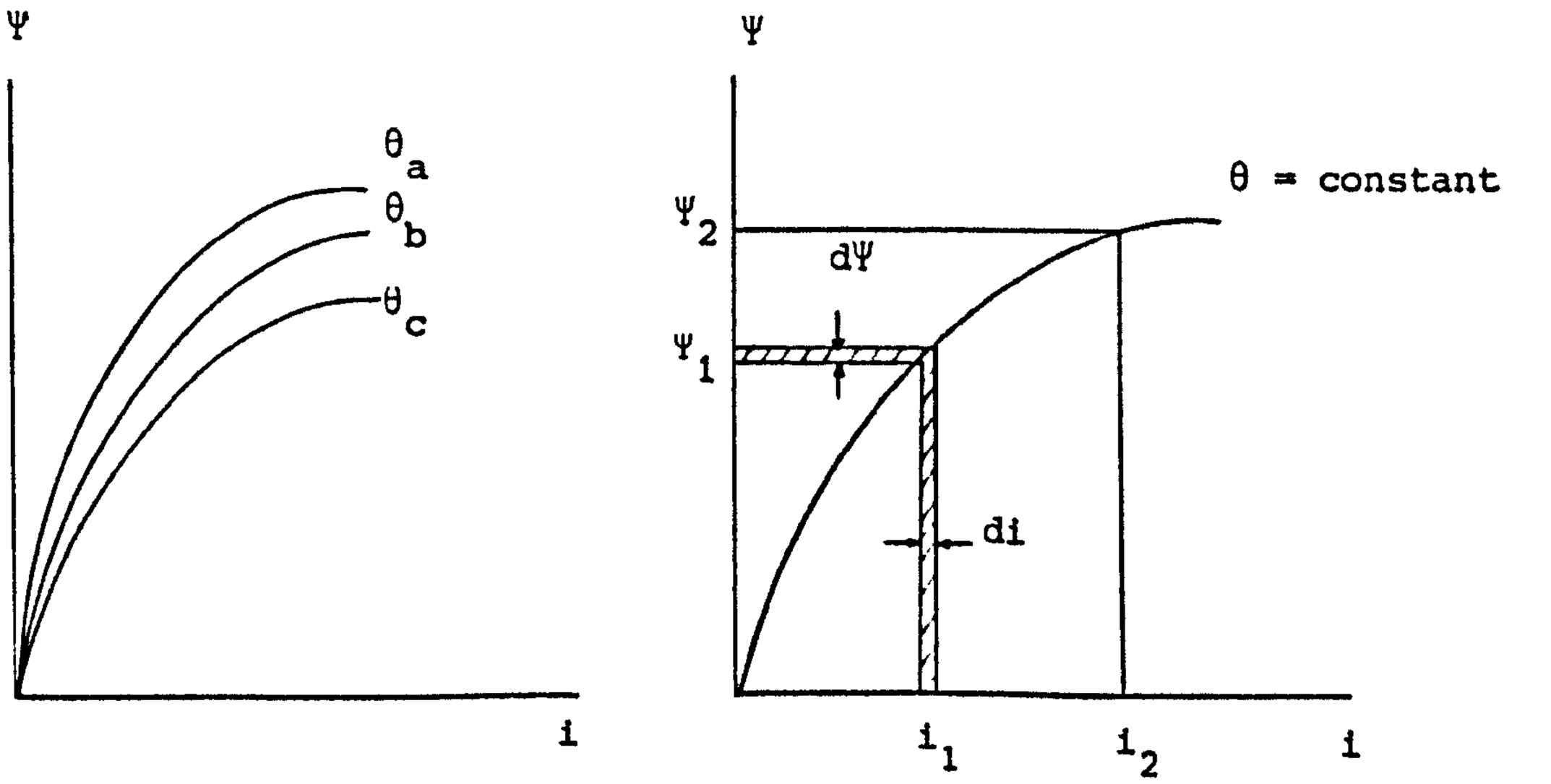

Figure 6.3

Replacing the limits in equation 6.4.2

$$\int_{\phi_1}^{\phi_2} i \, d\phi = w_s(\phi_1, \phi_2) \quad \ldots \ldots \quad 6.4.3$$

The co-energy w'_s is defined with reference to figure 6.1 as

$$w'_s(i_1, i_2) = \int_{i_1}^{i_2} \phi \, di \quad \ldots \ldots \quad 6.4.4.$$

The co-energy is related to the stored energy by

$$w_s = \sum_{n=1}^{K} \int i d\phi = \sum_{n=1}^{K} i\phi - \sum_{n=1}^{K} \int \phi di$$

therefore

$$w_s = \sum_{n=1}^{K} i\phi - w'_s \quad \ldots \ldots \quad 6.4.5$$

The power balance equation for any electro-mechanical system, assuming the absence of electric fields is:

$$p_e = p_m + \frac{d}{dt} w_s \quad \ldots \ldots \quad 6.4.6$$

where p_e = electrical power input

p_m = mechanical power output

w_s = energy stored in the magnetic field.

Consider a multi-coil system

$$i_1 \frac{d\phi_1}{dt} + i_2 \frac{d\phi_2}{dt} + \ldots = T_1 \frac{d\theta_1}{dt} + T_2 \frac{d\theta_2}{dt} + \ldots + \frac{d}{dt} w_s$$

For K coil system

$$\sum_{n=1}^{K} i_n \frac{d\psi_n}{dt} = \sum_{n=1}^{K} T_n \frac{d\theta_n}{dt} + \frac{d}{dt} w_s \quad \ldots \quad \ldots \quad 6.4.7$$

$$w_s = \sum_{n=1}^{k} \int i_n d\psi_n \quad \ldots \quad \ldots \quad 6.4.8$$

where T = Torque,

θ = angular position

and ψ = flux linkage

Neglecting the effects of hysteresis the energy stored in the magnetic field depends only on the final values of the variables and not on the way in which they reached those values. One method of evaluating the total stored energy is to set all the flux linkages to zero then increase each one in turn to its final values. Once a flux linkage reaches its final value it is kept at that value and a flux in the next coil is then allowed to increase to its final value until all coils are considered.

w_s should be expressed as a function of flux linkages and positions of coils, $w_s = \sum_{n=1}^{K} w_s (\theta_n , \psi_n)$

$$\frac{d}{dt} w_s = \sum_{m=1}^{K} \frac{\partial}{\partial \psi_m} w_s \frac{d\psi_m}{dt} + \sum_{m=1}^{K} \frac{\partial}{\partial \theta_m} w_s \frac{d\theta_m}{dt}$$

$$\frac{\partial}{\partial \psi_m} w_s = \frac{\partial}{\partial \psi_m} \sum_{n=1}^{K} \int i_n d\psi_n = i_m$$

therefore

$$\frac{d}{dt} w_s = \sum_{m=1}^{K} i_m \frac{d\psi_m}{dt} + \sum_{m=1}^{K} \frac{\partial}{\partial \theta_m} w_s \frac{d\theta_m}{dt}$$

Substituting in equations 6.4.7 gives

$$\sum_{n=1}^{K} T_n \frac{d\theta_n}{dt} = - \sum_{m=1}^{K} \frac{\partial}{\partial\theta_m} w_s \frac{d\theta_m}{dt}$$

therefore

$$T_n = - \frac{\partial}{\partial\theta_n} w_s (\psi, \theta) \quad \ldots \quad \ldots \quad 6.4.10$$

w_s must be a function of ψ and θ

From equations (6.4.7) and (6.4.5)

$$\sum_{n=1}^{K} i_n \frac{d\psi_n}{dt} = \sum_{n=1}^{K} T_n \frac{d\theta_n}{dt} + \frac{d}{dt} \sum_{n=1}^{K} i_n\psi_n - \frac{d}{dt} w'_s$$

$$\ldots \quad \ldots \quad 6.4.11$$

$$\frac{d}{dt} \sum_{n=1}^{K} i_n\psi_n = \sum_{n=1}^{K} i_n \frac{d\psi_n}{dt} + \sum_{n=1}^{K} \psi_n \frac{di_n}{dt}$$

$$\frac{d}{dt} w'_s = \sum_{m=1}^{K} \frac{\partial}{\partial i_m} w'_s \frac{di_m}{dt} + \sum_{m=1}^{K} \frac{\partial}{\partial\theta_m} w'_s \frac{d\theta_m}{dt}$$

$$\frac{\partial}{\partial i_m} w'_s = \psi_m$$

Substituting in equation 6.4.11 and simplifying.

$$\sum_{n=1}^{K} T_n \frac{d\theta_n}{dt} = \sum_{m=1}^{K} \frac{\partial}{\partial\theta_m} w'_s \frac{d\theta_m}{dt} \quad .. \quad .. \quad 6.4.12$$

$$\sum_{n=1}^{K} T_n = \sum_{n=1}^{K} \frac{\partial}{\partial\theta_n} w'_s \quad \ldots \quad \ldots \quad 6.4.13$$

or for coil n the torque will be

$$T_n = \frac{\partial}{\partial \theta_n} w'_s \quad \ldots \ldots \quad 6.4.14$$

The co-energy must be a function of currents and positions $w'_s = w'_s(i, \theta)$.

The co-energy method is easier to employ in practical machines than the stored energy method, since it is simpler mathematically to keep the currents constant rather than flux linkages during the virtual displacement. In the linear system $w'_s = w_s$. Consider a coil system such as in a rotating machine, with m rotor coils and n stator coils the torque exerted on the rotor is

$$T_{rotor} = \sum_{K=1}^{K} \frac{\partial}{\partial \theta_k} w'_s$$

$$\text{Let } \theta_k = \theta + \alpha_k$$

where θ is the angular displacement between stator and rotor reference points.

α_k is the constant displacement between coil K and reference point of the rotor

Therefore

$$\frac{\partial}{\partial \theta} w'_s = \sum_{K=1}^{m} \frac{\partial}{\partial \theta_K} w'_s \frac{\partial \theta_k}{\partial \theta}$$

$$\frac{\partial \theta_K}{\partial \theta} = 1$$

Therefore

$$T = \frac{\partial}{\partial \theta} w'_s \quad \ldots \ldots \quad 6.4.15$$

The co-energy w'_s, for c coils systems, in matrix form will be

$$w'_s = 0.5[i_1, i_2, \ldots, i_c]\begin{bmatrix} L_{11} & M_{12} & \cdots & M_{1c} \\ M_{21} & L_{22} & \cdots & M_{2c} \\ \vdots & \vdots & \vdots & \vdots \\ M_{c1} & \cdot & \cdots & L_{cc} \end{bmatrix}\begin{bmatrix} i_1 \\ i_2 \\ \vdots \\ i_c \end{bmatrix} \quad 6.4.16$$

From equations (6.4.15) and (6.4.16) the matrix torque equation is

$$T = 0.5[i_1, i_2, \ldots, i_c]\frac{d}{d\theta}\begin{bmatrix} L_{11} & M_{12} & M_{13} & \cdots & M_{1c} \\ M_{21} & L_{22} & M_{23} & \cdots & M_{2c} \\ \vdots & \vdots & \vdots & \vdots & \vdots \\ M_{c1} & M_{c2} & \cdot & \cdots & L_{cc} \end{bmatrix}\begin{bmatrix} i_1 \\ i_2 \\ \vdots \\ i_c \end{bmatrix} \quad \ldots\ \ldots\ 6.4.17$$

6.5 Solution of Performance Equations

To solve equations (6.1.1), (6.1.2), (6.1.3) and (6.2.1) for the unknown currents, these equations were rewritten in differential shape as follows:

For main winding

$$v_s - R_s i_s - \sum_{n=1}^{11} i_{rn}\, pM_{s.rn} = L_s.pi_s + M_{s.q1}pi_{q1} + M_{s.q2}pi_{q2} + \sum_{n=1}^{11} M_{s.rn}pi_{rn} \quad \ldots\ \ldots\ 6.5.1$$

For ring one

$$-R_{q1}i_{q1} - \sum_{n=1}^{11} i_{rn}\, pM_{q1.rn} = M_{s.q1}\cdot pi_s + l_{q1}pi_{q1} + M_{q1.q2}pi_{q2} + \sum_{n=1}^{11} M_{q1.rn}pi_{rn} \quad \ldots\ \ldots\ 6.5.2$$

For ring two

$$- R_{q2} i_{q2} - \sum_{n=1}^{11} i_{rn}\, pM_{q2.rn} = M_{s.q2} \cdot pi_s + M_{q1.q2} \cdot pi_{q1} + l_{q2} pi_{q2}$$

$$+ \sum_{n=1}^{11} M_{q2.rn} pi_{rn} \quad \ldots\ \ldots\ 6.5.3$$

For rotor loop one

$$-R_{r1} i_{r1} + R_b(i_{r2} + i_{r11}) - \sum_{m=1}^{11} i_{rm} pM_{r1.m} - i_s \cdot pM_{r1.s}$$

$$-i_{q1} \cdot pM_{r1.q1} - i_{q2} \cdot pM_{r1.q2} = M_{r1.s} \cdot pi_s + M_{r1.q1} \cdot pi_{q1}$$

$$+M_{r1.q2} \cdot pi_{q2} + \sum_{m=1}^{11} m_{r1.m} \cdot pi_{rm} \quad \ldots\ \ldots\ 6.5.4$$

Rotor loop two

$$-R_{r2}\, i_{r2} + R_b(i_{r1} + i_{r3}) - \sum_{m=1}^{11} i_{rm} \cdot pM_{r2.m} - i_s pM_{r2.s}$$

$$-i_{q1} \cdot pM_{r2.q1} - i_{q2} \cdot\ pM_{r2.q2} = M_{r2.s} pi_s + M_{r2.q1} \cdot pi_{q1}$$

$$+M_{r2.q2} pi_{q2} + \sum_{m=1}^{11} M_{r2.m} \cdot pi_{rm} \quad \ldots\ \ldots\ 6.5.5.$$

and so on for all the rotor loops.

These differential equations are simplified and written in matrix form as

$$\begin{bmatrix} K_1 \\ K_2 \\ K_3 \\ K_4 \\ K_5 \\ K_6 \\ \cdot \\ \cdot \\ \cdot \\ \cdot \\ \cdot \\ K_{14} \end{bmatrix} = \begin{bmatrix} L_s & M_{sq1} & M_{sq2} & M_{sr1} & M_{sr2} & \cdots\cdots\cdots & M_{sr11} \\ M_{sq1} & l_{q1} & M_{q1q2} & M_{q1r1} & M_{q1r2} & \cdots\cdots\cdots & M_{q1r11} \\ M_{sq2} & M_{q1q2} & l_{q2} & M_{q2r1} & M_{q2r2} & \cdots\cdots\cdots & M_{q2r11} \\ M_{sr1} & M_{q1r1} & M_{q2r1} & L_{r1} & M_{r1r2} & \cdots\cdots\cdots & M_{r1r11} \\ M_{sr2} & M_{q1r2} & M_{q2r2} & M_{r1r2} & L_{r2} & \cdots\cdots\cdots & M_{r2r11} \\ \cdot & \cdot & \cdot & \cdot & \cdot & \cdots\cdots\cdots & \cdot \\ \cdot & \cdot & \cdot & \cdot & \cdot & \cdots\cdots\cdots & \cdot \\ \cdot & \cdot & \cdot & \cdot & \cdot & \cdots\cdots\cdots & \cdot \\ \cdot & \cdot & \cdot & \cdot & \cdot & \cdots\cdots\cdots & \cdot \\ \cdot & \cdot & \cdot & \cdot & \cdot & \cdots\cdots\cdots & \cdot \\ M_{sr11} & M_{q1r11} & M_{q2r11} & M_{r11r1} & M_{r11r2} & \cdots\cdots\cdots & L_{r11} \end{bmatrix} \begin{bmatrix} pi_s \\ pi_{q1} \\ pi_{q2} \\ pi_{r1} \\ pi_{r2} \\ \cdot \\ \cdot \\ \cdot \\ \cdot \\ \cdot \\ pi_{r11} \end{bmatrix}$$

$$\ldots\ \ldots\ 6.5.6$$

where $K_1 = v_s - R_s i_s - \sum_{n=1}^{11} i_{rn} \cdot \dot{\theta} \cdot \sin(\theta+\alpha+(n-1)\alpha_1) \cdot M_{srn}$

$$K_2 = -R_{q1} i_{q1} - \sum_{n=1}^{11} i_{rn} \dot{\theta} \cdot \sin(\theta+\alpha+\delta+(n-1)\alpha_1) \cdot M_{q1rn}$$

$$K_3 = -R_{q2} i_{q2} + \sum_{n=1}^{11} i_{rn} \dot{\theta} \cdot \sin(\theta+\alpha+\delta+(n-1)\alpha_1) \cdot M_{q2rn}$$

$$K_4 = -R_{r1} i_{r1} + R_b(i_{r2} + i_{r11}) - \sum_{m=1}^{11} i_{rm} p M_{rn}$$

$$-M_{r1s} i_s \dot{\theta} \sin(\theta+\alpha) - M_{r1q1} \dot{\theta} \sin(\theta+\alpha+\delta)$$

$$+M_{r1q2} \cdot i_{q2} \dot{\theta} \sin(\theta+\alpha+\delta)$$

$$K_5 = -R_{r2} i_{r2} + R_b(i_{r1} + i_{r3}) - \sum_{m=1}^{11} i_{rm} p M_{rn}$$

$$- M_{r2s} i_s \dot{\theta} \sin(\theta+\alpha+\alpha_1)$$

$$-M_{r2q1} i_{q1} \dot{\theta} \cdot \sin(\theta+\alpha+\delta+\alpha_1) + M_{r2q2} i_{q2} \dot{\theta} \sin(\theta+\alpha+\delta+\alpha_1)$$

$$K_6 = -R_{r3} + R_b(i_{r2} + i_{r4}) - \sum_{m=1}^{11} i_{rm} \cdot pM_{rn} - M_{r3.s} i_s \dot{\theta} \cdot \sin(\theta+\alpha+2\alpha_1)$$

$$-M_{r3.q1} i_{q1} \cdot \dot{\theta} \cdot \sin(\theta+\alpha+\delta+2\alpha) + M_{r2.q2} \cdot i_{q2} \dot{\theta} \sin(\theta+\alpha+\delta+2\alpha_1)$$

K_7, K_8, K_9, K_{10}, K_{11}, K_{12}, K_{13} and K_{14} are obtained in the same way as K_4, K_5 and K_6.

Equations (6.3) and (6.5.6) were solved numerically for currents and speed. Runge-Kutta 4^{th} order method was employed to obtain the numberical solution. The method may be summarised as follows:

if

$$\frac{dy}{dx} = f(x, y)$$

then

$$y(n+1) = y(n) + \frac{H_1 + 2H_2 + 2H_3 + H_4}{6}$$

where

$$H_1 = h.f(x_n, y_n)$$

$$H_2 = h.f(x_n + 0.5h, y_n + 0.5H_1)$$

$$H_3 = h.f(x_n + 0.5h, y_n + 0.5H_2)$$

$$H_4 = h.f.(x_n + h, y_n + H_3)$$

h is step length in x.

pi_s, pi_{q1}, pi_{q2}, pi_{r1}, pi_{r2} ,...., pi_{r11} were obtained at every step by solving matrix equation (6.5.6) using Gauss Elimination method.

Experimental results of transient torque-time were obtained for the test motor, using the procedure which is mentioned in section (2.3.3). Figure (6.4) illustrates the transient torque and speed characteristics. Transient current-time patterns of main winding are shown by figure (6.5). Figure (6.6) shows transient current of shading ring.

CHAPTER 7

STEADY STATE SOLUTION

The steady-state performance of small induction machines is more significant than the transient characteristics in respect to machine design. The basic differential equations are derived in order to build a steady state solution which takes into consideration unsymmetrical windings, non-uniform air-gap and distrj bution of the windings. Self and mutual inductances of all the windings are calculated, by finite element methods, and represented in the performance equations. Variation of harmonic rotor currents are also considered. Voltage equations are formed in terms of harmonic currents and harmonic inductance coefficients. Any number of space harmonics can be taken into consideration by including the appropriate number of inductance coefficient terms. Because the performance of a shaded-pole motor is greatly affected by the presence of space harmonics, Lock (22) examined briefly their origin as shown in Appendix A.

7.1 Steady State Performance Equations

The stator harmonic currents are very small in comparison with the fundamental so the harmonic currents will be ignored in the stator windings. Voltage equations derived in Chapter 6 are the basic equations of the steady state performance. For the main winding the voltage equation is.

$$v_s = i_s R_s + P(l_s i_s) + P\Psi_s \quad \ldots \quad \ldots \quad 7.1.1.$$

The flux linkage Ψ_s is the contribution of all harmonic currents of

all windings.

Similarly the voltage equations of the shading rings are

$$0 = i_{q1}R_{q1} + P(l_{q1}i_{q1}) + P\Psi_{q1} \quad \ldots \ldots \quad 7.1.2.$$

$$0 = i_{q2}R_{q2} + P(l_{q2}i_{q2}) + P\Psi_{q2} \quad \ldots \ldots \quad 7.1.3$$

Because the mutual inductances between stator windings are constants, equations 7.1.1., 7.1.2 and 7.1.3 will take the following forms,

$$V_s = R_s i_s + L_s\, pi_s + M_{sq1}pi_{q1} + M_{sq2}pi_{q2} + \sum_{n=1}^{11} p(M_{srn}i_{rn})$$

$$\ldots \ldots \quad 7.1.4$$

$$0 = R_{q1}i_{q1} + L_{q1}pi_{q1} + M_{sq1}pi_s + M_{q1q2}pi_{q2} + \sum_{n=1}^{11} P(M_{q1rn}i_{rn})$$

$$\ldots \ldots \quad 7.1.5$$

$$0 = R_{q2}i_{q2} + L_{q2}pi_{q2} + M_{sq2}pi_s + M_{q1q2}pi_{q1} + \sum_{n=1}^{11} P(M_{q2rn}i_{rn})$$

$$\ldots \ldots \quad 7.1.6.$$

The cage rotor is represented by cascade loops as discussed in section 6.2. This yields voltage equations for the n^{th} rotor loop as follows:

$$0 = R_{rn}i_{rn} - R_b(i_{rn+1}+i_{rn-1}) + p(l_{rn}i_{rn}) + P\Psi_{rn}$$

$$= R_{rn}i_{rn} - R_b(i_{rn+1}+i_{rn-1}) + P(M_{srn}i_s)$$

$$+ P(M_{q1rn}i_{q1}) + P(M_{q2rn}i_{q2}) + \sum_{n=1}^{11} P(M_{rnm}i_{rm})$$

$$\ldots \ldots 7.1.7$$

Referring to the series of space harmonic fields produced by the stator windings, each rotor loop current consists of a series of harmonic currents.

Considering only the real part of the exponential series, the current for n^{th} loop is

$$i_n = \sum_k \left[\sqrt{2}\, \bar{I}_{fk} e^{-j(n-1)k\alpha}\, e^{j(\omega t - k\theta)} \right.$$

$$\left. + \sqrt{2}\, \bar{I}_{bk} e^{j(n-1)k\alpha}\, e^{j(\omega t + k\theta)} \right] \quad \ldots\ \ldots\ 7.1.8$$

where α is the slot angle between adjacent bars

and k = order of harmonic current.

The loop currents have the same magnitude but are displaced by a phase angle which is a multiple of the slot angle α. Thus for the k^{th} order harmonic current.

$$i_{(n-1)k} + i_{(n+1)k} = 2i_{nk} \cos(k\alpha) \quad \ldots\ \ldots\ 7.19$$

Subsituting in equation 7.1.7. gives

$$0 = (R_{rn} - 2R_b \cos(k\alpha))\, i_{rn} + P(M_{srn} i_s)$$

$$+P(M_{q1rn} i_{q1}) + P(M_{q2rn} i_{q2}) + \sum_{n=1}^{11} P(M_{rnm}\, i_{rm}) \quad \ldots\ \ldots\ 7.1.10$$

assuming N is the highest order of rotor harmonic currents considered.

Since there are two components for each order of harmonic, a forward and a backward component, there are 2(N+1) rotor equations. Neglecting saturation effects, the stator harmonic currents can be ignored. There are therefore three voltage equations of the stator to be solved. The number of rotor equation can be reduced by the fact that the flux linkage between the rotor and stator windings produces only odd order of rotor harmonic currents. Thus the voltage equations are (N+1) for the rotor and three equations for the stator.

7.2 Representation of Inductances

For steady-state analysis, it is necessary to represent the inductances as functions of rotor position θ. The position of the rotor is a simple function of time when the speed is constant, i.e.

$$\theta = (1 - s)\,\omega t \quad \ldots \quad \ldots \quad 7.2.1.$$

Self inductances of the stator windings and the mutual inductances between stator windings are assumed to be constant. The mutual inductance between the main winding and a rotor loop is shown by figure (5.2.10). From the curve given by (5.2.10) it is obvious that there are significant harmonic contents. Lock (22) calculated the percentage of each harmonic and he found that the harmonic above the 7^{th} order is very small, less that 1%.

the mutual inductance between a rotor loop and the shading rings

is illustrated by figure (5.2.11). From the waveform it is obvious that the mutual inductance between the shading rings and a rotor loop is very small over a wide region of the rotor position and it has a significant value in the co-axial position.

The mutual inductance between a rotor loop and the main winding is expressed as

$$M_{sr} = \sum_{k=1}^{H_1} \bar{M}_{srk} e^{jk\theta} \quad \ldots \ldots \quad 7.2.2.$$

Similarly the mutual inductance between the shading ring and a rotor loop is

$$M_{qr} = \sum_{k=1}^{H_1} \bar{M}_{qrk} e^{jk\theta} \quad \ldots \ldots \quad 7.2.3$$

where k = 1, 3, 5, 7

H_1 = highest harmonic inductance coefficient

$\bar{M}_{srk} = M_{srk}^{d} e^{j\alpha_{ks}}$

$\bar{M}_{qrk} = M_{qrk}^{e} e^{j\alpha_{kq}}$

and α_{ks} and α_{kq} are the angles of phase shift.

Since the net flux entering the rotor produced by a stator coil must be zero the average terms in these inductance series are zero. In

the case of rotor loops the average terms are the predominant terms for the self and mutual inductances which are approximated by

$$M_{rr} = \sum_{k=o}^{H_1-1} \bar{M}_{rk} e^{jk\theta} \quad \ldots \ldots \quad 7.2.4.$$

7.3 Evaluation of Flux Linkages

In order to solve the set of voltage equations, discussed in section 7.1, the flux linkage must be evaluated. The inductance coefficients will be employed for this purpose.

7.3.1 Flux linkage on a rotor loop

Considering the axis of the main winding as reference, the m^{th} rotor loop posituion is

$$p_m = \theta + (m-1)\alpha \quad \ldots \ldots \quad 7.3.1.$$

where α is the fundamental slot angle

$\theta = (1-s)\omega t$ is the position of the first rotor loop

and s = slip of the rotor

The flux linkages on a rotor loop are due to flux produced by the main windings, shading rings and all rotor loops.

$$\Psi_r = \Psi_{rs} + \Psi_{rq} + \Psi_{rr} \quad \ldots \ldots \quad 7.3.2$$

The flux linkage on rotor loop n by the main winding

$$\Psi_{rs} = \sqrt{s}\,\bar{I}_s e^{j\omega t} \sum_{k=1}^{H_1} \bar{M}_{rsk} e^{j(k\theta+k(n-1)\alpha)}$$

$$= \frac{\sqrt{2}}{2}\bar{I}_s \sum_{k=1}^{H_1} [\bar{M}_{rsk} e^{j(\omega t+k\theta)}\, e^{jk(n-1)\alpha}$$

$$+ \bar{M}^*_{srk} e^{j(\omega t-k\theta)} e^{-jk(n-1)\alpha}] \quad \ldots\ \ldots\ 7.3.3$$

This expression shows that each harmonic mutual inductance induces two harmonic currents in the rotor. Their frequencies are dependent on the speed of the rotor, the frequency of the stator current and the order of the harmonic inductance coefficient.

$$f_r = [1 \pm k(1-s)]f_o \quad \ldots\ \ldots\ 7.3.4$$

The flux linkage on rotor loop n by the shading ring is

$$\Psi_{rq} = \sqrt{2}\,\bar{I}_q e^{j\omega t} \sum_{k=1}^{H_1} \bar{M}_{rqk} e^{j(k\theta+k(n-1)\alpha)}$$

$$= \frac{\sqrt{2}}{2}\bar{I}_q \sum_{k=1}^{H_1} [\bar{M}_{rqk} e^{j(\omega t+k\theta)}\, e^{jk(n-1)\alpha}$$

$$+ \bar{M}^*_{rqk} e^{j(\omega t-k\theta)}\, e^{-jk(n-1)\alpha}] \quad \ldots\ \ldots\ 7.3.5.$$

Since the magnitude of all rotor loop currents are the same, for the same harmonic order, with a phase shift due to space displacement, it is only necessary to find the harmonic currents in a reference loop which is taken as loop 1. The flux linkages on rotor loop 1 by the n^{th} harmonic current of m^{th} rotor loop is

$$\Psi_{1mn} = \left[\sqrt{2}\bar{I}_{fn} e^{-j(m-1)n\alpha_e} j(\omega t - n\theta) + \sqrt{2}\bar{I}_{bn} e^{j(m-1)n\alpha_e} j(\omega t - n\theta)\right] \sum_{k=o}^{H_1-1} \bar{M}_{mk} e^{j(k\theta + k(m-1)\alpha)}$$

$$= \frac{\sqrt{2}}{2} \bar{I}_{fn} \sum_{k=o}^{H_1-1} \left[\bar{M}_{mk} e^{j(m-1)(k-n)\alpha_e} j[\omega t-(n-k)\theta]\right.$$

$$+ \bar{M}^{*}_{mk} e^{-j(m-1(n+k)\alpha} {}_e j[\omega t-(n+k)\theta]\left.\right]$$

$$+ \frac{\sqrt{2}}{2} \bar{I}_{bn} \sum_{k=o}^{H_1-1} \left[\bar{M}_{mk} e^{j(m-1)(k+n)\alpha} {}_e j[\omega t+(n+k)\theta]\right.$$

$$+ \bar{M}^{*}_{mk} e^{j(m-1)(n-k)\alpha} {}_e j[\omega t+(n-k)\theta]\left.\right] \quad \ldots\ \ldots\ 7.3.6$$

The total flux linkages on rotor loop 1 by the n^{th} harmonic due to the complete rotor is the sum of sub-flux linkages

$$\Psi_{1n} = \sum_{m=1}^{NL} \Psi_{1mn} \quad \ldots\ \ldots\ 7.3.7.$$

7.3.2. Flux linkage on a stator winding

The flux linkages on a stator winding are due to the flux of both stator and rotor windings

$$\Psi_s = \Psi_{ss} + \Psi_{sr} \quad \ldots \ldots \quad 7.3.8$$

Consider the flux linkagte on the main winding by n^{th} rotor harmonic current

$$\Psi_{srn} = \sum_{m=1}^{NL} i_m \sum_{k=1}^{H_1} \bar{M}_{rsk} e^{j[k\theta + k(m-1)\alpha]}$$

$$= \sum_{m=1}^{NL} \sum_{k=1}^{H_1} \Big[\frac{\sqrt{2}}{2} \bar{I}_{fn} \Big[\bar{M}_{rsk} e^{-j(m-1)(n-k)\alpha} e^{j[\omega t-(n-k)\theta]} + \bar{M}^{*} e^{-j(m-1)(n+k)\alpha} e^{j[\omega t-(n+k)\theta]} \Big] + \frac{\sqrt{2}}{2} \bar{I}_{bn} \Big[\bar{M}_{rsk} e^{j(m-1)(k+n)\alpha} e^{j[\omega t+(n+k)\theta]} + \bar{M}^{*}_{rsk} e^{j(m-1)(n-k)\alpha} e^{j[\omega t+(n-k)\theta]} \Big] \Big] \quad \ldots \ldots \quad 7.3.9$$

Similar equations apply for the shading rings.

The flux linkages on a stator winding due to a flux of a stator winding is not a function of rotor position and it is expressed, for the main winding, as

$$\Psi_{ss} = L_s \bar{I}_s e^{j\omega t} + M_{sq1} \bar{I}_{q1} e^{j\omega t} + M_{sq2} \bar{I}_{q2} e^{j\omega t} \quad \ldots \ldots \quad 7.3.10$$

Differentiation of the flux linkages with respect to time are required in the voltage equations which are discussed in section

(7.1). These are obtained by direct differentiation of the flux linkages expressions which are simple functions of time. After the substitution, in the voltage equations, and simplification the steady state equations are written in matrix form as shown in appendix B.

7.4 Torque Evaluation

In order to calculate the steady state torque it is essential to find the torque contribution of all harmonic currents. The torque expression derived in section (6.4) was employed for this purpose. For a c-coil system equation (6.4.17) will take the form.

$$T = \frac{1}{2} i_1^2 \frac{dl_1}{d\theta} + i_1 i_2 \frac{dM_{12}}{d\theta} + i_1 i_3 \frac{dM_{13}}{d\theta} + \ldots + i_1 i_c \frac{dM_{1c}}{d\theta}$$

$$+ \frac{1}{2} i_2^2 \frac{dl_2}{d\theta} + i_2 i_3 \frac{dM_{23}}{d\theta} + i_2 i_4 \frac{dM_{24}}{d\theta} + \ldots + i_2 i_c \frac{dM_{2c}}{d\theta}$$

$$+ \frac{1}{2} i_3^2 \frac{dl_3}{d\theta} + i_3 i_4 \frac{dM_{34}}{d\theta} + i_3 i_5 \frac{dM_{35}}{d\theta} + \ldots + i_3 i_c \frac{dM_{3c}}{d\theta}$$

$$+ \frac{1}{2} i_4^2 \frac{dl_4}{d\theta} + i_4 i_5 \frac{dM_{45}}{d\theta} + i_4 i_5 \frac{dM_{45}}{d\theta} + \ldots + i_4 i_c \frac{dM_{4c}}{d\theta}$$

$$+ \ldots\ldots\ldots\ldots\ldots\ldots\ldots\ldots\ldots\ldots\ldots\ldots\ldots\ldots\ldots\ldots$$

$$+ \ldots\ldots\ldots\ldots\ldots\ldots\ldots\ldots\ldots\ldots\ldots\ldots\ldots\ldots\ldots\ldots$$

$$+ \ldots\ldots\ldots\ldots\ldots\ldots\ldots\ldots\ldots\ldots\ldots\ldots\ldots\ldots\ldots\ldots$$

$$+ \frac{1}{2} i_{c-1}^2 \frac{dL_{c-1}}{d\theta} + i_{c-1} i_c \frac{dM_{c-1c}}{d\theta}$$

$$+ \frac{1}{2} i_1^2 \frac{dL_c}{d\theta} \quad \ldots \quad \ldots \quad (7.4.1)$$

Since the self inductances of the stator windings and the mutual inductance between stator windings are considered to be constant, there are no torque contribution from these self and mutual inductances. The torque is due to the mutual inductance between stator and rotor windings as well as the self inductance of rotor loops and mutual inductance between the loops.

7.4.1. Torque due to interaction between stator and rotor currents

The average torque produced from the interaction between main winding and rotor currents is evaluated by considering each harmonic current of the rotor loops

$$T_{sr} = i_s \sum_{m=1}^{NL} i_{rmn} \sum_{h=1}^{H_1} \frac{d}{d\theta} M_{srh}$$

$$= \sqrt{2}\, \bar{I}_s\, e^{j\omega t} P_o \sum_{m=1}^{NL} \left[\left(\sqrt{s}\, \bar{I}_{fmn} e^{-j(m-1)n\alpha}\, e^{j(\omega t - n\theta)} \right. \right.$$

$$\left. \left. + \left(\sqrt{2}\, \bar{I}_{bmn} e^{-j(m-1)n\alpha}\, e^{j(\omega t + n\theta)} \right) \right] \cdot \right.$$

$$\sum_{h=1}^{H_1} jh\, \bar{M}_{srh} e^{jh[\theta + (m-1)\alpha]} \quad \ldots\ \ldots\ 7.4.2$$

Equation (7.4.2.) simplifies to give the average torque produced by the interaction between main winding and rotor currents.

$$T_{sr} = \sum_{n=1}^{H_1} \frac{jnP_o NL\, \bar{I}_s}{2} \left[\bar{I}^*_{fn}\ \bar{M}^*_{srn} + \bar{I}^*_{bn}\, \bar{M}_{srn} \right] \quad \ldots\ \ldots\ 7.4.3$$

A similar torque expression is obtained from the interaction between shading rings and rotor harmonic currents

$$T_{qr} = \sum_{n=1}^{H_1} \frac{jnP_o NL\ \bar{I}_q}{2} [\bar{I}^*_{fn}\ \bar{M}^*_{qrn} + \bar{I}^*_{bn}\ \bar{M}_{qrn}] \ldots \ldots 7.4.4$$

7.4.2. Torque due to rotor currents interaction -

Since the self inductance of the rotor loops and the mutual inductance between the loops are variable with the rotor position, the torque is produced by the interaction between the loops. Consider the contribution of the n^{th} forward harmonic current of loop 1 and the k^{th} forward harmonic current of the rest of the loops

$$T_{ff} = \sqrt{2}\ \bar{I}_{fn}\ e^{j(\omega t - n\theta)} \sum_{m=1}^{NL} \sqrt{2}\ \bar{I}_{fk} e^{j(\omega t - k\theta)} e^{-j(m-1)k\alpha} \frac{dM_{mh}}{d\theta}$$

$$= P_o \sqrt{2}\ \bar{I}_{fn} e^{j(\omega t - n\theta)} \sum_{m=1}^{NL} \sqrt{2}\ \bar{I}_{fk}\ e^{j(\omega t - k\theta)} e^{-j(m-1)k\alpha} jh\bar{M}_{mh} e^{jh\theta}$$

After the multiplication and simplification the torque expression is

$$T_{ff} = \frac{jhP_o \bar{I}_{fn}}{2} \sum_{m=1}^{NL} \bar{I}_{fk} e^{-j(m-1)k\alpha} \left[\bar{M}_{mh} e^{j[2\omega t - (k-h+n)\theta]}\right.$$

$$\left. + \bar{M}^*_{mh} e^{j[2\omega t - (k+h+n)\theta]}\right]$$

$$+ \bar{I}_{fk} e^{j(m-1)k\alpha} \left[\bar{M}^*_{mh} e^{j(k-h-n)\theta} + \bar{M}_{mh} e^{j(k+h-nm)\theta}\right] \ldots \ldots 7.4.5$$

The first two terms produce average torque only at certain sub-synchronous speeds and therefore are neglected. The third term produces average torque under the condition

$$k - h - n = 0 \quad \text{or } h = k - n$$

For $h > 0$ or $h = 0$, $k > n$ or $k = n$ and the torque expression for this case is

$$T_{fnfk} = \frac{jhP_o \bar{I}_{fn}}{2} \sum_{m=1}^{NL} \bar{I}^{*}_{fk} \bar{M}^{*}_{mh} e^{j(m-1)k\alpha} \quad \ldots\ldots\ 7.4.6.$$

where $\bar{M}_{mh}$ is the h^{th} harmonic mutual inductance between loop 1 and loop m

The fourth term produces average torque if the following condition is satisfied:

$$k + h - n = 0 \quad \text{or } h = n - k$$

Therefore $n > k$ or $n = k$ and the torque is

$$T_{fnfk} = \frac{jhP_o \bar{I}_{fn}}{2} \sum_{m=1}^{NL} \bar{I}^{*}_{fk} \bar{M}_{mh} e^{j(m-1)k\alpha} \quad \ldots\ldots\ 7.4.7$$

The torque expression in respect to self inductances is

$$T_{fnfn} = \frac{jhP_o \bar{I}_{fn}^{2} \; NL}{2} \bar{M}_{mo}$$

Similar expressions are derived for the interaction between I_{fn}/I_{bk}, I_{bk}/I_{fn} and I_{bn}/I_{bk}. In the case of forward/backward currents the torque expression is

$$T_{fnbk} = \frac{jhP_o \bar{I}_{fn}}{2} \sum_{m=1}^{NL} \bar{I}_{fk}^{*} \; \bar{M}_{mh} \; e^{-j(m-1)k\alpha} \quad \text{for } h = n + k$$

The contribution of backward/forward currents is

$$T_{bnfk} = \frac{jhP_o \bar{I}_{bn}}{2} \sum_{m=1}^{NL} \bar{I}_{fk}^{*} \; \bar{M}_{mh}^{*} \; e^{j(m-1)k\alpha} \quad \text{for } h = k + n$$

Torque contribution of backward/backward currents is

$$T_{bnbk} = \frac{jhP_o I_{bn}}{2} \sum_{m=1}^{NL} \bar{I}_{bk}^{*} \; \bar{M}_{mh}^{*} \; e^{-j(m-1)k\alpha} \quad \text{for } h = n - k$$

$$T_{bnbn} = \frac{jhP_o \bar{I}_{bn}}{2} \sum_{m=1}^{NL} \bar{I}_{bn}^{*} \; \bar{M}_{mh} \; e^{-j(m-1)k\alpha} \quad \text{for } h = k - n$$

After finding the contribution of torque due to stator and rotor currents interaction and as well as the contribution from rotor

currents interaction, the electric torque is calculated by taking the summation of all the torque contributions. In order to find the currents, and hence the torque, the set of voltage equation (1.B) is solved after separation into real and imaginary parts. The method will be illustrated, considering three voltage equations, as follows:

If the complex system matrix has the following form

$$\begin{bmatrix} v_1 \\ v_2 \\ v_3 \end{bmatrix} = \begin{bmatrix} R_1+jx_1 & jx_{12} & jx_{13} \\ jx_{21} & R_2+jx_2 & jx_{23} \\ jx_{31} & jx_{32} & R_3+jx_3 \end{bmatrix} \begin{bmatrix} i_1 \\ i_2 \\ i_3 \end{bmatrix} \quad \ldots\ \ldots\ 7.4.8$$

Equation 7.4.8, after the separation, will take the form

$$\begin{bmatrix} v_{r1} \\ v_{r2} \\ v_{r3} \\ v_{m1} \\ v_{m2} \\ v_{m3} \end{bmatrix} = \begin{bmatrix} R_1 & 0 & 0 & -X_1 & -X_{12} & -X_{13} \\ 0 & R_2 & 0 & -X_{21} & -X_2 & -X_{23} \\ 0 & 0 & R_3 & -X_{31} & -X_{32} & -X_3 \\ X_1 & X_{12} & X_{13} & R_1 & 0 & 0 \\ X_{21} & X_2 & X_{23} & 0 & R_2 & 0 \\ X_{31} & X_{32} & X_3 & 0 & 0 & R_3 \end{bmatrix} \begin{bmatrix} I_{r1} \\ I_{r2} \\ I_{r3} \\ I_{m1} \\ I_{m2} \\ I_{m3} \end{bmatrix} . \quad \ldots\ \ldots\ 7.4.9$$

The complex voltage equation of the shaded pole motor has a similar form as equation (7.4.8), therefore an equation similar to equation (7.4.9) is used to find the currents of the stator, shading ring and rotor harmonic currents. For each value of speed, currents and torque are calculated. Torque/speed and current/speed characteristics are shown by figure (7.1) and figure (7.2) respectively for both measured and calculated results.

CHAPTER 8

GENERAL CONCLUSIONS AND SUGGESTIONS FOR FURTHER WORK

In the present investigation, the finite element method is employed to solve magnetic field problems of electrical machines. A general approach is derived to solve the two-dimensional electromagnetic field of the whole or part of the machine.

The finite element method described in Chapter 3 is based on minimising an energy function satisfying natural boundary conditions. This method of discretizing the two-dimensional field problem, coupled with the convergence of Newton-Raphson algorithm, yields a unique and stable solution.

The attraction of this method consists of its use as a practical design tool for machine field analysis, especially where different magnetic characteristics and different current densities exist. Comprehensive information about the effect of saturation in different parts of the machine is obtained from the flux plots.

Flux distribution of the machine is plotted for all the currents existing in the coils as well as the flux distribution due to each coil of the machine.

In order to calculate the self inductance of machine's coils the concept of stored energy is employed for this purpose. Mutual inductance between every pair of coils of the machine is calculated by finite element methods. The method of calculating self and mutual inductance is generalised to every electromagnetic multi-coil system.

Referring to the results obtained, in Chapter 6, by finite element method, self inductance of stator windings and mutual

inductance between stator windings are assumed to be constant because the changes of their values are relatively small. Self inductance of rotor loops is both speed and position dependent. From the results obtained by finite element, it is obvious that the self inductance of a rotor loop increases with the increase of speed. It reaches ($0.88x10^{-5}$H) when the motor is running near the synchronous speed and ($0.108x10^{-5}$H) for the locked rotor case. The mutual inductance between rotor loops is variable and for this reason the mutual inductances between a reference loop and the rest of the loops are calculated at different speeds as shown by figures (5.2.12), (5.2.13) ,..., and (5.2.21). The mutual inductance between a rotor loop and the reference loop is both speed and position dependent and is a maximum at no-load speed and decreases with speed deceleration of the machine, and is particularly significant between the adjacent loops. Field plotting of main winding shows different flux linkage with each loop. This depends on the speed of the machine as well as the position of the loop. Mutual inductance between main winding and a rotor loop is shown by figure (5.2.10). From the waveform it is obvious that there are harmonic contents. Mutual inductance between shading ring and a rotor loop is calculated at different values of speed. The mutual inductance is a maximum when the loop is co-axial with the shading ring, and it is a minimum in all other positions. Figure (5.2.11) illustrates the variation of mutual inductance with rotor loop position.

The speed of the machine has little effect on the mutual

inductance between stator main windings and a rotor loop.

From the results obtained by finite element methods, the self and mutual inductances of each winding of the machine are represented as a function of position. The cage rotor is represented by cascaded loops and each loop is considered to be a single turn coil. A general approach is established for analysing the shaded pole motor. The basic performance equations are derived from the electrophysical construction of the machine. A step-by-step numerical method is used for solving the basic performance equations to study the transient behaviour of the machine. The computed and experimental results, as shown by figures (6.4), (6.5) and figure (6.6), are not exactly the same. Peak values of experimental torque-time are greater than the computed values by 30% and the shape of the computed and the experimental pattern are not exactly identical. Computed transient current-time of the main winding has the same shape as the experimental one. The peak values of the measured transient current is higher than the predicted peak values.

The author believes that the difference between the experimental and the computed results is due to the approximation which was made for representing the parameters as a function of rotor position and the fact that the effect of the speed was neglected. In addition to this there are harmonic contents in the parameters waveforms which were ignored. In order to improve the computed results a substantial modification of parameter representation should be made. In the case of the steady state performance the torque-speed and current-speed characteristics of both computed and measured results are shown by figure (7.1) and

and figure (7.2). The predicted current is lower than the experimental current by 15%, also the computed torque-speed is lower than the measured torque-speed. The difference between the predicted and measured results of steady state is also due to the parameters representation in the steady state equations.

For the future work on machine analysis and design the finite element method is sufficiently accurate for analysing the two-dimensional field of any electromagnetic circuit. In order to improve the method and to get more accurate parameters the author proposes the following:

1. Extending the finite element method for solving the three-dimensional field of electrical machines.

2. Using an iterative solution between the finite element and the performance equations, where a computer program, coupling the finite element and the performance programs, is necessary to be established. This method of study will enble the researcher to calculate the parameters instantaneously by the finite element method used in the performance equations.

3. Consider the system to be non-linear when calculating the stored energy and the torque. This means that the parameters are both current and position dependent $M = M(i,\theta)$.

4. Application of the present finite element method to calculate the parameters of the three-phase induction motor and transformers.

ACKNOWLEDGEMENTS

The author wishes to express his thanks to Professor D.J. Tedford and Professor M.J. Grimble for providing the facilities in this department for undertaking the present investigation.

Thanks are due to Prfessor W.S. Wood and Dr. R.D. Slater for their invaluable guidance, advice and criticism through the investigation and the writing. Thanks are also due to Dr. R.S. Simpson and Dr. F.P. Flynn for their stimulating discussions and encouragement.

Appreciation is expressed to Mr. J. Dickson and the other department technicians for their services towards the experimental work.

Finally, thanks to Ann Hall for typing the manuscript.

REFERENCES

1. Trickey, P.H. : 'An analysis of the shaded pole motor', AIEE Trans., 1936, 55, pp. 1007-1014.

2. Trickey, P.H. : 'Performance calculations on shaded pole motors', AIEE Trans., 1947, 66, pp. 1431-1438.

3. Kron, G. : 'Equivalent circuits of the shaded pole motor with space harmonics', AIEE Trans., 1950, 69, pp. 735-741.

4. Chang, S.S.L. : 'Equivalent circuits and their application in designing shaded pole motors', AIEE Trans., 1951, 70, pp. 690-699.

5. Sherer, F.W. and Hertzog, G.E. : 'The calculation of shaded pole motor performance using a digital computer', AIEE Trans., 1959, 78, pp. 1607-1610.

6. Surh, F.W. : 'A theory for shaded-pole induction motors', AIEE Trans., 1958, 77, Pt. 3, pp. 509-515.

7. Desai, B.G. and Mathew, M.A. : 'Transient analysis of shaded pole motor', IEEE Trans., 1971, PAS-90, pp. 484-494.

8. Butler, O.I. and Wallace, A.K. : 'Generalised theory of induction motors with asymmetrical primary windings and its application to the analysis and performance prediction of shaded-pole motors', Proc. IEE, 1968, 115, (5), pp. 685-694.

9. Butler, O.I. and Wallace, A.K. : 'Equivalent circuit for non-quadrature, tapped-quadrature and shaded-pole single-phase induction motor', Proc. IEE, 1968, 115 (12), pp. 1767-1771.

10. Butler, O.I. and Wallace, A.K. : 'Effects of parameter changes on the performance of shaded-pole motors', Proc. IEE, 1969, 116 (5), pp. 732-736.

11. Perret, R. and Poloujadoff, M. : 'Characteristics analysis of saturated shaded-pole motors', IEEE Trans., 1976, PAS-95, pp. 1347-1353.

12. Ooka, H. : 'Analysis of the reluctance-augmented shaded pole motor', J. Inst. Elect. Eng., Japan, 1971, 91, pp. 145-153.

13. Ooka, H. : 'Effect of wide air gap part in shaded pole motors', Hitachi Hyoron, 1972, 54, pp. 203-206.

14. Ooka, H. : 'Analysis of shaded-pole motor with double shading coils', Electr, Eng. Japan, 1972, 92, pp. 54-62.

15. Ooka, H. : 'Distribution of flux, current and torque of a reluctance-augmented shaded pole motor operating under locked rotor conditions', Electr. Eng. Japan 1973, 93, pp. 46-53.

16. Eastham, J.F. and Williamson, S. : 'Generalised theory of induction motors with asymmetrical airgaps and primary windings', Proc. IEE, 1973, 120, (7), pp. 767-775.

17. Eastham, J.F. and Williamson, S. : 'Design and analysis of close-ratio two-speed shaded-pole induction motors', Proc. IEE, 1973, 120, (10), pp. 1243-1249.

18. Williamson, S. and Breese, P. : 'Effect of airgap-profile variations on the performance of reluctance-augmented shaded-pole motors', Proc. IEE, 1977, 124, (10), pp. 860-864.

19. Williamson, S. and Breese, P. : 'Evaluation of the reluctance-augmentation principle in shaded-pole motors', Proc. IEE, 1978, 125, (9), pp. 831-835.

20. Cullen, A.L., and Barton, T.H. : 'A simplified electromagnetic theory of the induction motor, using the concept of wave impedance', Proc. IEE, 1958, 105C, (8), pp. 331-336.

21. Chin, N.F. : 'Machine representation', M.Sc. Thesis, University of Strathclyde, 1975.

22. Kai Sang Lock, B.Sc. : "Machine Representation', Ph.D. Thesis, University of Strathclyde.

23. Silvester, P. and Chari, M.V.K. : 'Finite Element solution of saturable magnetic field problems', IEEE Trans. Vol, PAS-89, Sep-Oct, 1970.

24. Chari, M.V.K., Sharma, A.K. and Kudlacik, H.W. : 'No-load magnetic field analysis in the end region of a turbine generator by finite element method', IEEE Power Engineering Society Winter meeting, New York, Jan. 1976.

25. Brandl, P., Reichet, K., and Vogt, W. : 'Simulation of turbo-generators on steady-state load', Boveri Rev., 1975, 9, pp. 444-449.

26. Williamson, S. and Ralph, J.W. : 'Finite element anlysis for nonlinear magnetic field problem with complex current sources' IEE Proc., Vol. 129, Pt. A, No. 6, August, 1982.

27. Williamson, S. anmd Ralph, J.W., : 'Finite element analysis of an induction motor fed from a constant-voltage source', IEE Proc., Vol. 130, Pt. B, No. 1, January, 1983.

28. Wood, W.S. : 'Transient in electrical machines', Ph.D. Thesis, University of Strathclyde, 1965.

29. Slater, R.D. : 'Transient in electrical machines", Ph.D. Thesis, University of Strathclyde, 1966.

30. Simpson, R.R.S. : 'Transient torque in a salient pole machine', Ph.D. Thesis, University of Strathclyde, 1966.

31. Flynn, F.P. : 'Transient in induction motors with particular reference to transient torques in large machines', Ph.D. Thesis, University of Strathclyde, 1970.

32. Simpson, R.R.S., and Slater, R.D. : 'Heavy duty switching angle selector', Proc. IEE, 1967, 114, (1), P. 115.

33. Wood, W.S., and McNaul, J. : 'A simple method of recording angular acceleration', Engineer, 1962, 213, p. 569.

34. Wood, W.S., and Shanmugasundaram, A. : 'Performance of a type E-5-A/1, 2" induction generator as an angular accelerometer', Muirhead Tech., 1963, 17, (4), pp. 30-32.

35. Trickey, P.H. : 'Induction motor resistance ring width, Electrical Eng., 1936, 55, pp. 144-150.

36. Alger, P.L. : 'The nature of polyphase induction machine' (John Wiley and Sons Inc., New York, 1951).

37. Say, M.G. : 'The performance and design of alternating current machines', Pitman Ltd. 1958.,

38. Fulton, N.N. : 'Design optimisation of small induction motors', Ph.D. Thesis, University of Strathclyde, 1973.

39. Vickers, H. : 'The induction motor', (Pitman and Sons Ltd., 1953).

40. Christofides, N. : 'Origin of load losses in induction motors with cast aluminum rotors', Proc. IEE, 1965, 112, (12), pp. 2317-2331.

41. Subba Rao, V., and Butler, O.I. : 'Stray losses of polyphase cage-induction motors with particular reference to the condition of imperfect rotor-bar iron insultation', Proc. IEE. 1969, 116, (5), pp. 737-751.

42. Silvester and Chari : 'Finite element solution of saturable magnetic field problem', IEEE Trans. Vol, PAS-89, Sep-Oct 1970.

43. Norrie, D.H. and Devries, G. : 'An introduction to finite element analysis".

44. Demerdash, N.A. and Nehl, T.W. : 'An evaluation of the method of finite element and finite differences in the solution of nonlinear electromagnetic fields in electrical machines", IEEE, Trans. Vol. PAS-98, No. 1, Jan-Feb 1979.

45. Frederick, C. Trutt, Edward, A : 'Representation of the magnetisation characteristic of D.C machine for computer use', IEEE Trans. PAS Vol. 87, No. 3, March, 1968.

APPENDIX A

Origin of Space Harmonics and Harmonics Currents

The air gap flux ϕ is related to the mmf F and permeance λ by the simple relation

$$\phi = F \cdot \lambda \text{ ... ... } (1.A)$$

Thus space harmonic flux may arise due to mmf harmonics or permeance harmonics or a combination of both depending on the distribution of the windings and the shape of the air gap. For a uniform air gap machine, the permeance is a constant so the mmf harmonics are the only source of harmonic flux. In the case of reluctance-augmented shaded pole motors, they are the result of both the mmf harmonics from a concentrated stator windings and the permeance wave due to the non-uniform air gap. Lock (22) in Section 4.4 showed that by applying Fourier series analysis to the mmf waveform, a uniform air gap machine was considered and then

$$F = \sum_{h=1}^{\infty} \frac{2N1}{\pi h} \sin(h\beta/2) \cos h\gamma \text{ ... ... } (2.A)$$

With a sinusoidal current

$$i = I_k \cos(kwt)$$

Each harmonic mmf wave can be resolved into a forward and a backward rotating component.

$$F_{hk} = \frac{I_k N K_{sh}}{\pi h} (\cos(h\gamma - kwt) + \cos(h\gamma + kwt)) \quad \ldots \quad \ldots \quad (3.A)$$

where F_{hk} is the h^{th} mmf harmonic produced by

k^{th} harmonic current

and $k_{sh} = \sin(h\beta/2)$ is the coil span factor of h^{th} harmonic field. Each component in equation (3.A) is a rotating wave having a sinusoidal distribution in space with h times the basic number of poles. It rotates relative to the stator with velocity $\mp$ kw/h electrical radians per second, or k/h times the basic synchronous speed. With respect to the rotor which rotates at a speed of w_r, the wave of harmonic field moves at a speed of $(kw \mp hw_r)/h$. This movement of the field over the rotor induces in the rotor winding two harmonic currents which in turn induce harmonic currents in the stator. This is a chain reaction with the magnitude of the harmonic currents decreasing rapidly at the later stages of the interaction. Lock (22) illustrated by figure (5.1) the interaction of a stator and a rotor coil through h^{th} harmonic field.

The frequencies of the harmonic currents in the rotor windings are dependent on the speed of the rotor, the frequency of the stator current as well as the order of the harmonic field. Thus, with a stator frequency f_o and a rotor slip s, the frequencies of the rotor harmonic currents produced by the h^{th} harmonic field is

$$f_r = [1 \pm h(1-s)]f_o \quad \ldots \quad \ldots \quad (4.A)$$

APPENDIX B

Steady State Matrix Performance Equations

Up to the 5^{th} order of rotor harmonic currents are considered and the fundamental of the stator currents. Voltage equations are written in partitioned matrix form as follows

$$\begin{bmatrix} V_d \\ \hline V_r \end{bmatrix} = \begin{bmatrix} Z_{dd} & \vdots & Z_{dr} \\ \hline Z_{rd} & \vdots & Z_{rr} \end{bmatrix} \begin{bmatrix} I_d \\ \hline I_r \end{bmatrix} \quad \ldots\ldots \text{1.B}$$

All the voltages are zero except the main winding voltage which equal to the supply voltage and where the current matrices are

$$[I_d] = \begin{bmatrix} I_s \\ I_{q1} \\ I_{q2} \end{bmatrix} \quad \text{and} \quad [I_r] = \begin{bmatrix} I_{rf1} \\ I_{rb1} \\ I_{rf3} \\ I_{rb3} \\ I_{rf5} \\ I_{rb5} \end{bmatrix}$$

The impedance matrix Z_{dd} is

$$[Z_{dd}] = \begin{bmatrix} Z_s & j\omega M_{sq1} & j\omega M_{sq2} \\ j\omega M_{q1s} & Z_{q1} & j\omega M_{q1q2} \\ j\omega M_{q2s} & j\omega M_{q2q1} & Z_{q2} \end{bmatrix}$$

where $Z_s = R_s + j\omega L_s$

$Z_q = R_q + j\omega L_q$

$$[Z_{dr}] = j\omega \frac{NL}{2} \begin{bmatrix} M_{dr1} & M^{*}_{dr1} & M_{dr3} & M^{*}_{dr3} & M_{dr5} & M^{*}_{dr5} \\ M_{q1r1} & M^{*}_{q1r1} & M_{q1r3} & M^{*}_{q1r3} & M_{q1r5} & M^{*}_{q1r5} \\ M_{q2r1} & M^{*}_{q2r1} & M_{q2r3} & M^{*}_{q2r3} & M_{q2r5} & M^{*}_{q2r5} \end{bmatrix}$$

$$[Z_{dr}] = j\omega \frac{NL}{2} \begin{bmatrix} S_{f1}M^{*}_{dr1} & S_{f1}M^{*}_{q1r1} & S_{f1}M^{*}_{q2r1} \\ S_{b1}M_{dr1} & S_{b1}M_{q1r1} & S_{b1}M_{q2r1} \\ S_{f3}M^{*}_{dr3} & S_{f3}M^{*}_{q1r3} & S_{f3}M^{*}_{q2r3} \\ S_{b3}M_{dr3} & S_{b3}M_{q1r3} & S_{b3}M_{q2r3} \\ S_{f5}M^{*}_{dr5} & S_{f5}M^{*}_{q1r5} & S_{f5}M^{*}_{q2r5} \\ S_{b5}M_{dr5} & S_{b5}M_{q1r5} & S_{b5}M_{q2r5} \end{bmatrix}$$

$$[Z_{rr}] = \begin{bmatrix} Z_{f1} & Z_{f1b1} & Z_{f1f3} & Z_{f1b3} & Z_{f1f5} & Z_{f1b5} \\ Z_{b1f1} & Z_{b1} & Z_{b1f3} & Z_{b1b3} & Z_{b1f5} & Z_{b1b5} \\ Z_{f3f1} & Z_{f3b1} & Z_{f3} & Z_{f3b3} & Z_{f3f5} & Z_{f3b5} \\ Z_{b3f1} & Z_{b3b1} & Z_{b3f3} & Z_{b3} & Z_{b3f5} & Z_{b3b5} \\ Z_{f5f1} & Z_{f5b1} & Z_{f5f3} & Z_{f5b3} & Z_{f5} & Z_{f5b5} \\ Z_{b5f1} & Z_{b5b1} & Z_{b5f3} & Z_{b5b3} & Z_{b5f5} & Z_{b5} \end{bmatrix}$$

where $Z_{fh} = R_{rn} - 2R_b\cos(h\alpha) + j\omega S_{fh} \sum_{m=1}^{NL} M_{mo}\, e^{-j(m-1)h\alpha}$

$$Z_{bh} = R_{rn} - 2R_b\cos(h\alpha) + j\omega S_{bh} \sum_{m=1}^{NL} M_{mo}\, e^{-j(m-1)h\alpha}$$

$$Z_{fhfn} = j\omega\, S_{fh} \sum_{m=1}^{NL} \bar{M}_{mk}\, e^{-j(m-1)h\alpha} \qquad \text{for } h = n - k$$

$$= j\omega\, S_{fh} \sum_{m=1}^{NL} \bar{M}^{*}_{mk}\, e^{-j(m-1)h\alpha} \qquad \text{for } h = n + k$$

$$Z_{fhbn} = j\omega\, S_{fh} \sum_{m=1}^{NL} \bar{M}^{*}_{mk}\, e^{-j(m-1)h\alpha} \qquad \text{for } h = k - n$$

$$Z_{bhfn} = j\omega S_{bh} \sum_{m=1}^{NL} \bar{M}_{mk}\, e^{j(m-1)h\alpha} \qquad \text{for } h = k - n$$

and

$$Z_{bhbn} = j\omega S_{bh} \sum_{m=1}^{NL} \bar{M}_{mk} e^{j(,m-1)h\alpha} \qquad \text{for } h = n + k$$

$$= j\omega\, S_{bh} \sum_{m=1}^{NL} \bar{M}^{*}_{mk} e^{j(m-1)h\alpha} \qquad \text{for } h = n - k$$

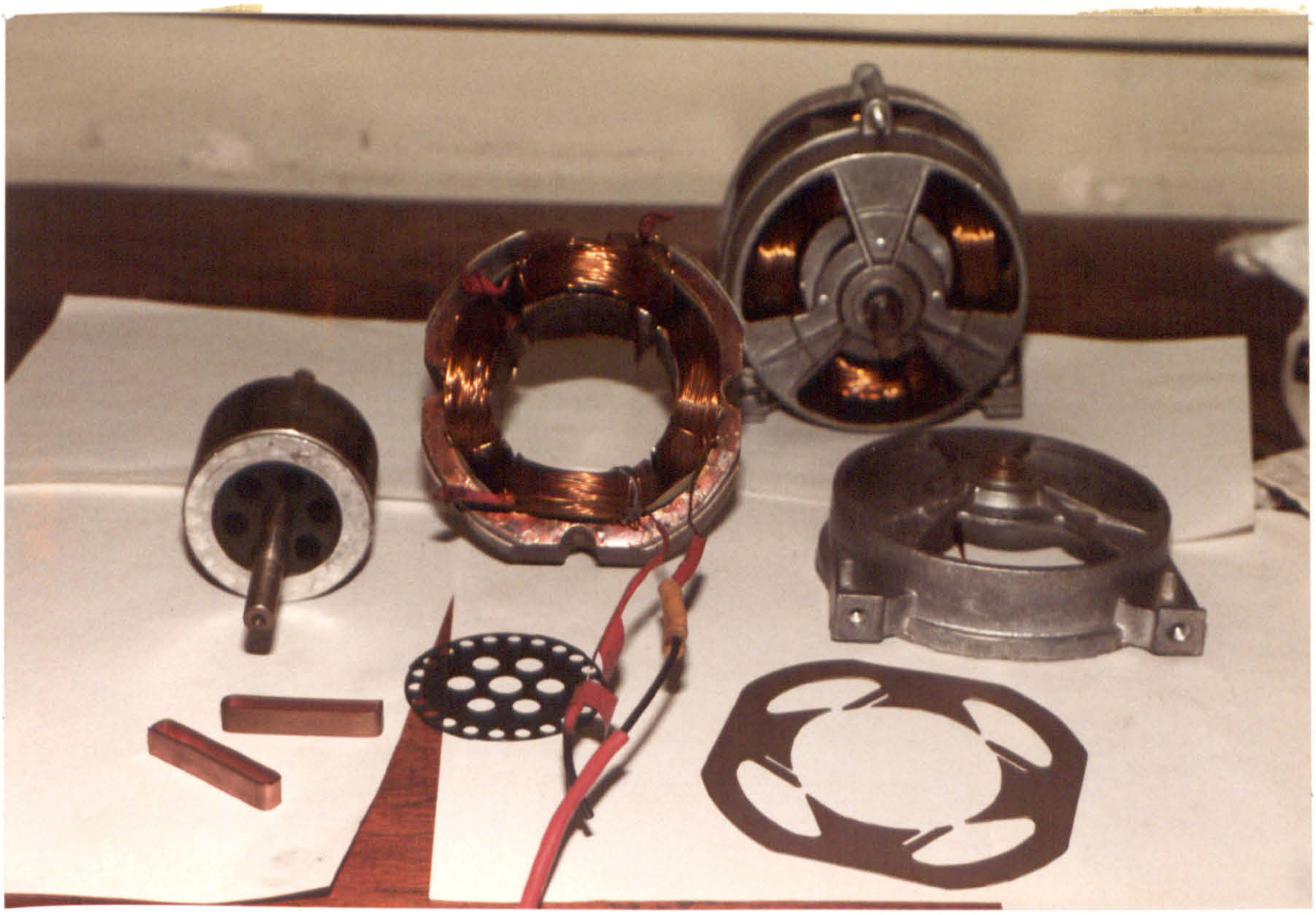

Figure 1.1 Practical shaded-pole motor

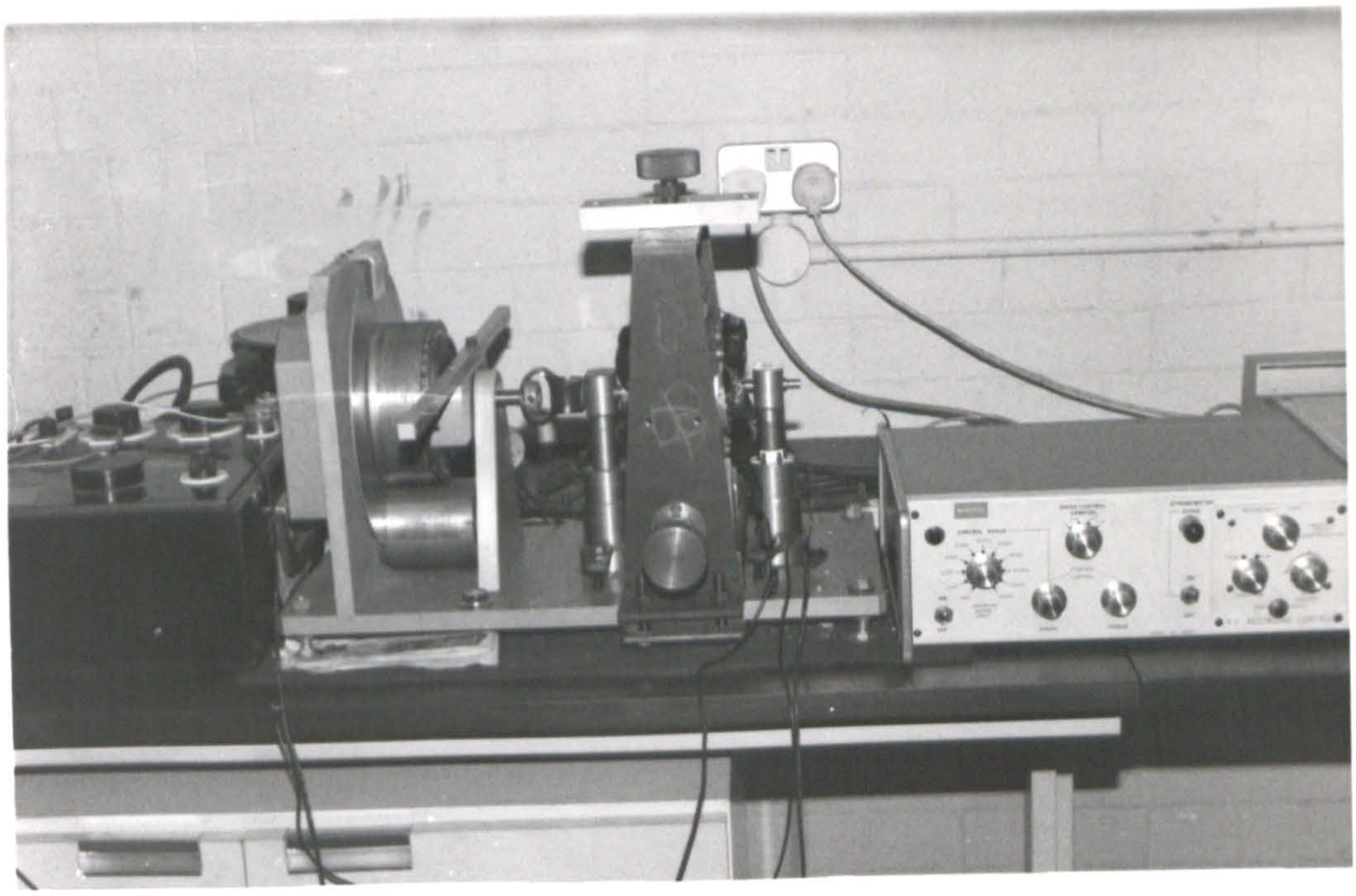

Figure 2.1 Test rig, control unit and magtrol dynamometer

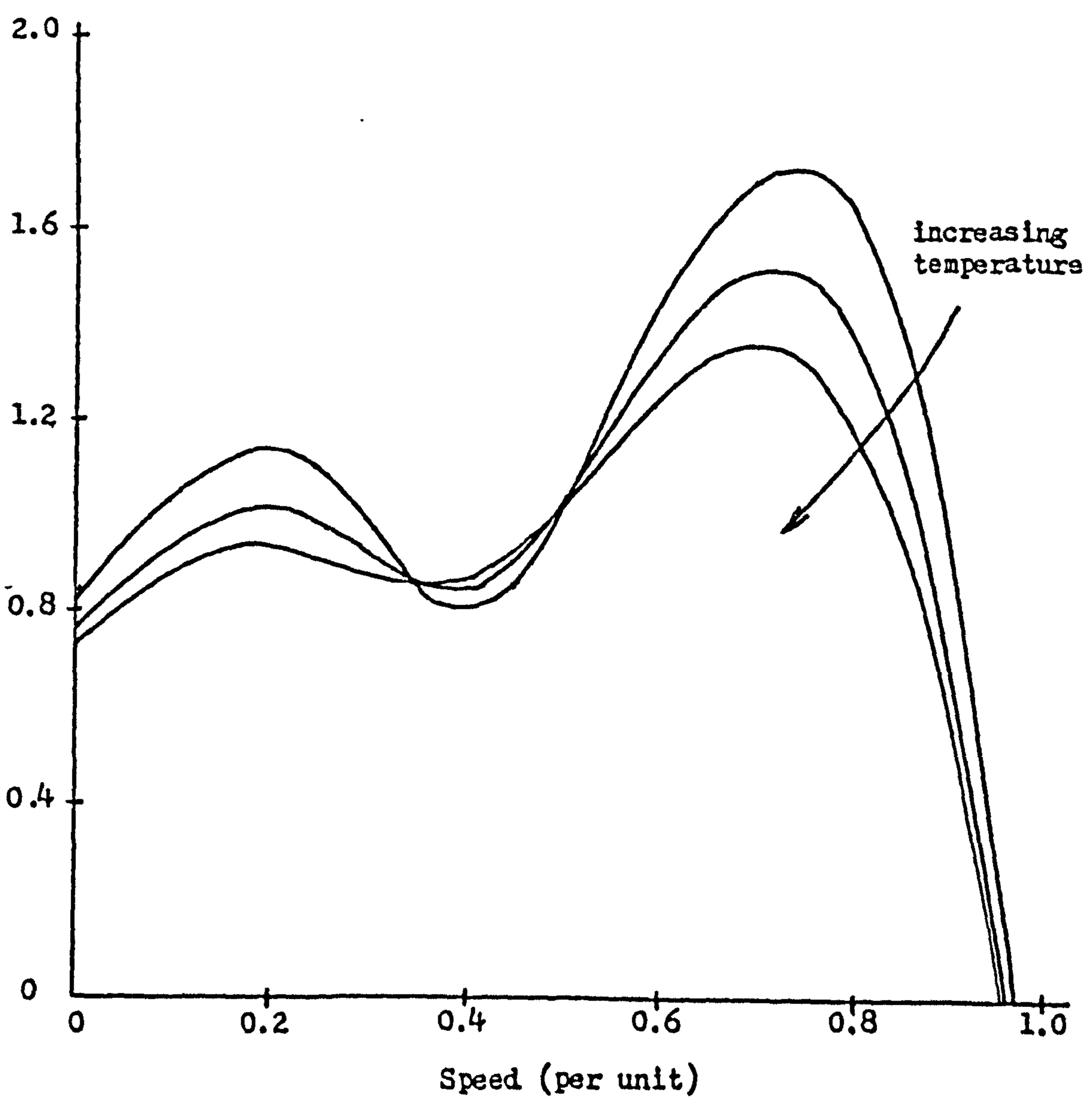

Figure 2.2 Variation of torque/speed with winding temperature

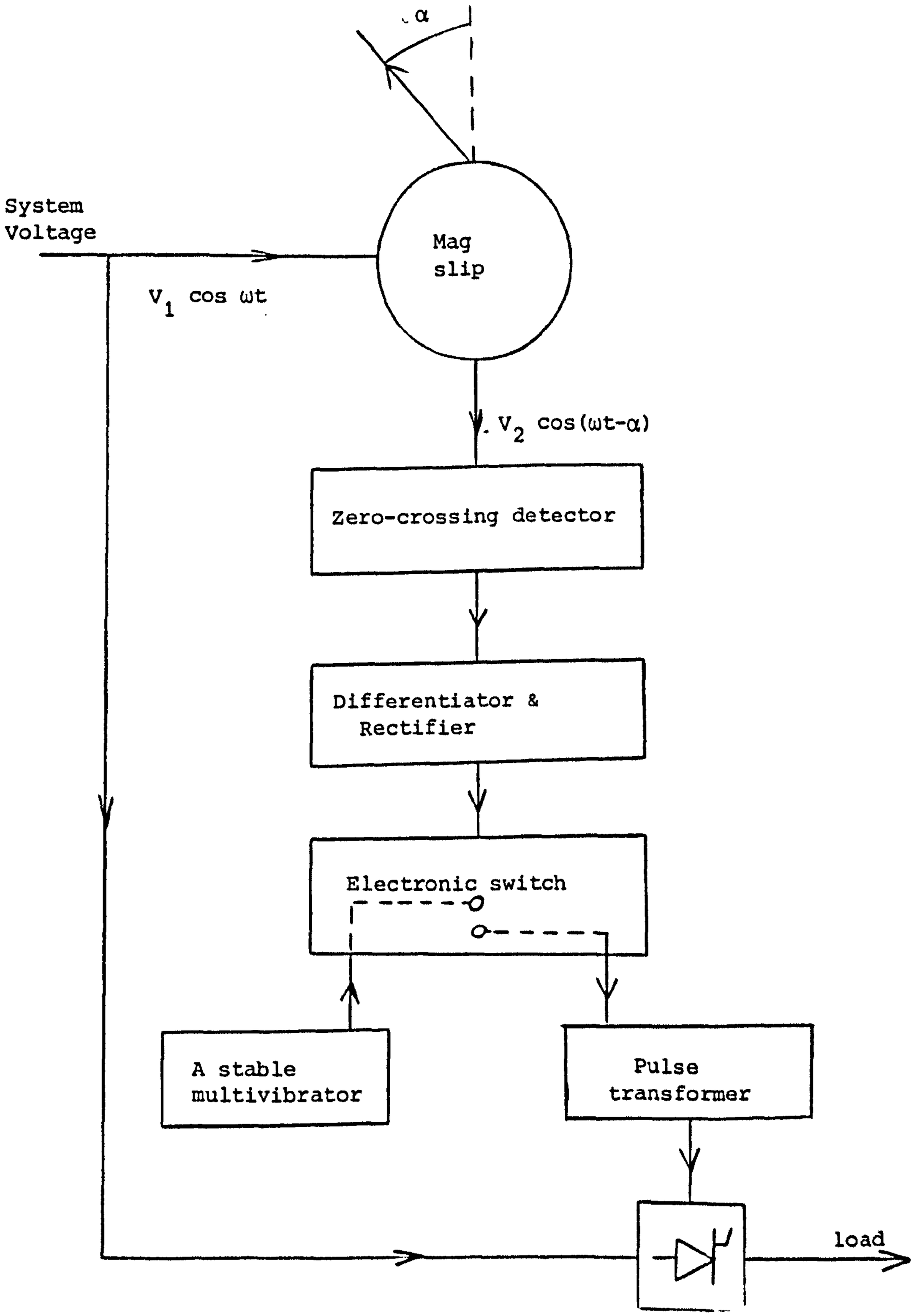

Figure 2.3 Block diagram of a switching angle selector

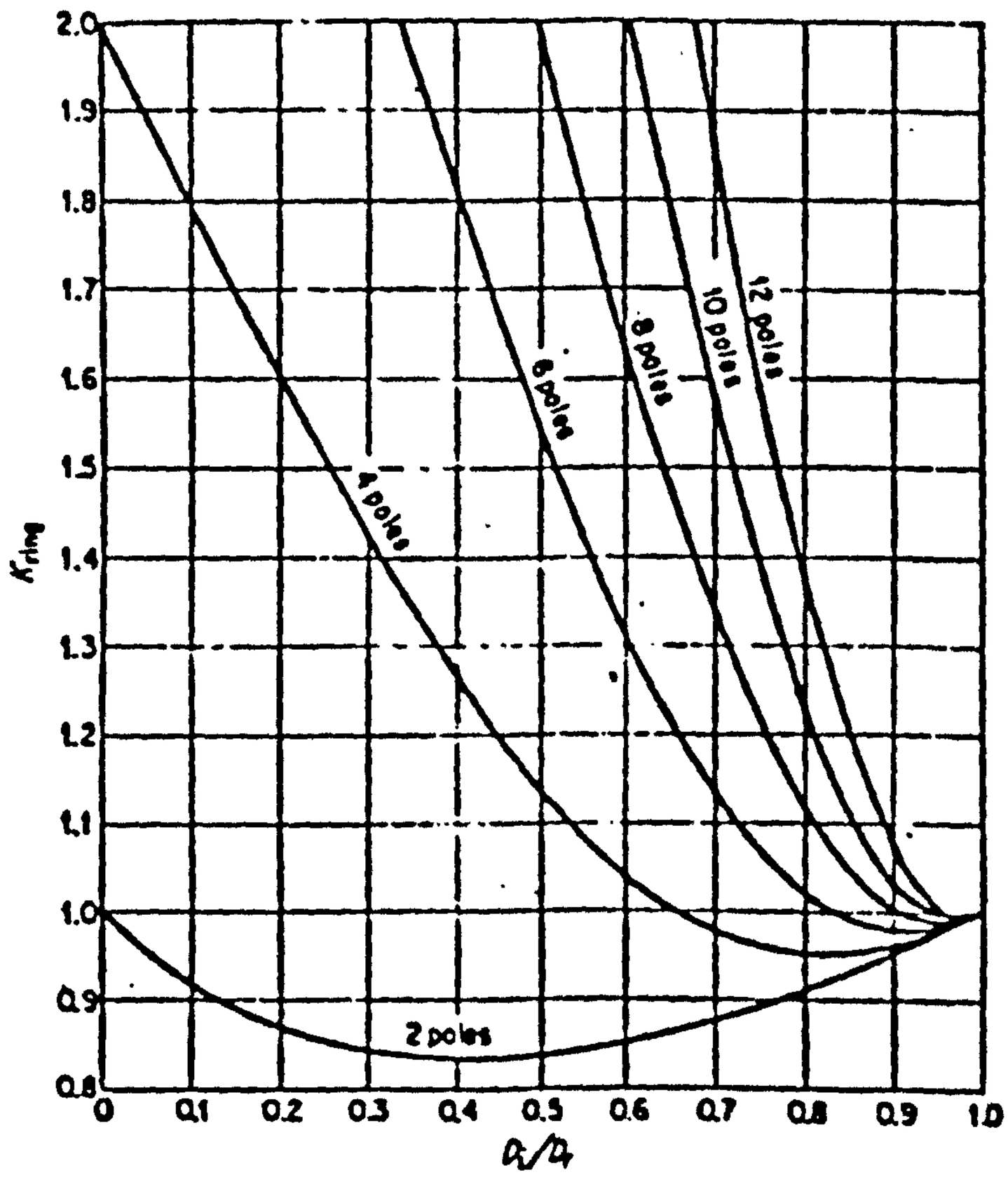

Figure 2.4 Effect of width of ring on ring resistance (from Trickey's)

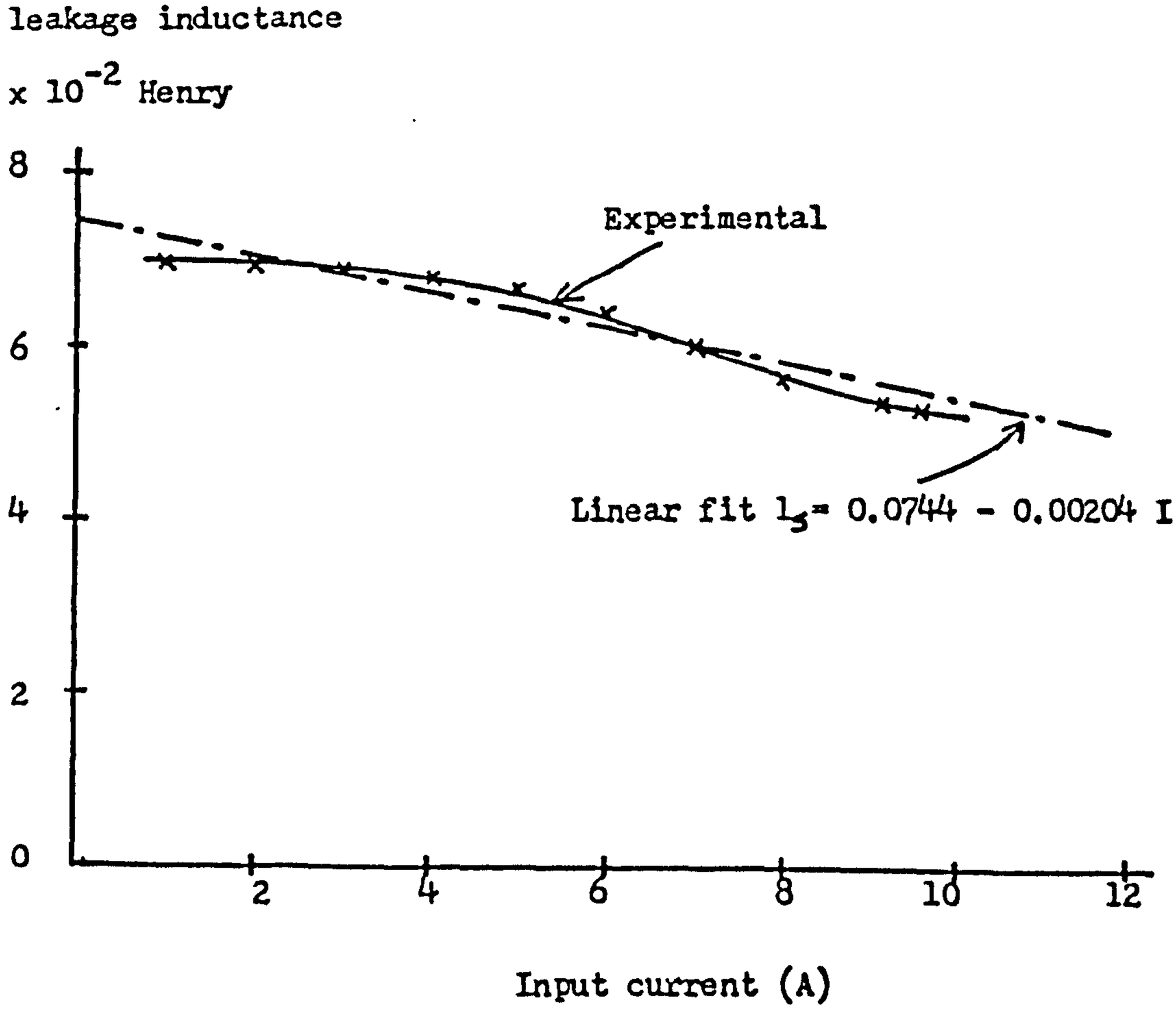

Figure 2.5 Main winding leakage inductance measured by 'Rotor-out' method

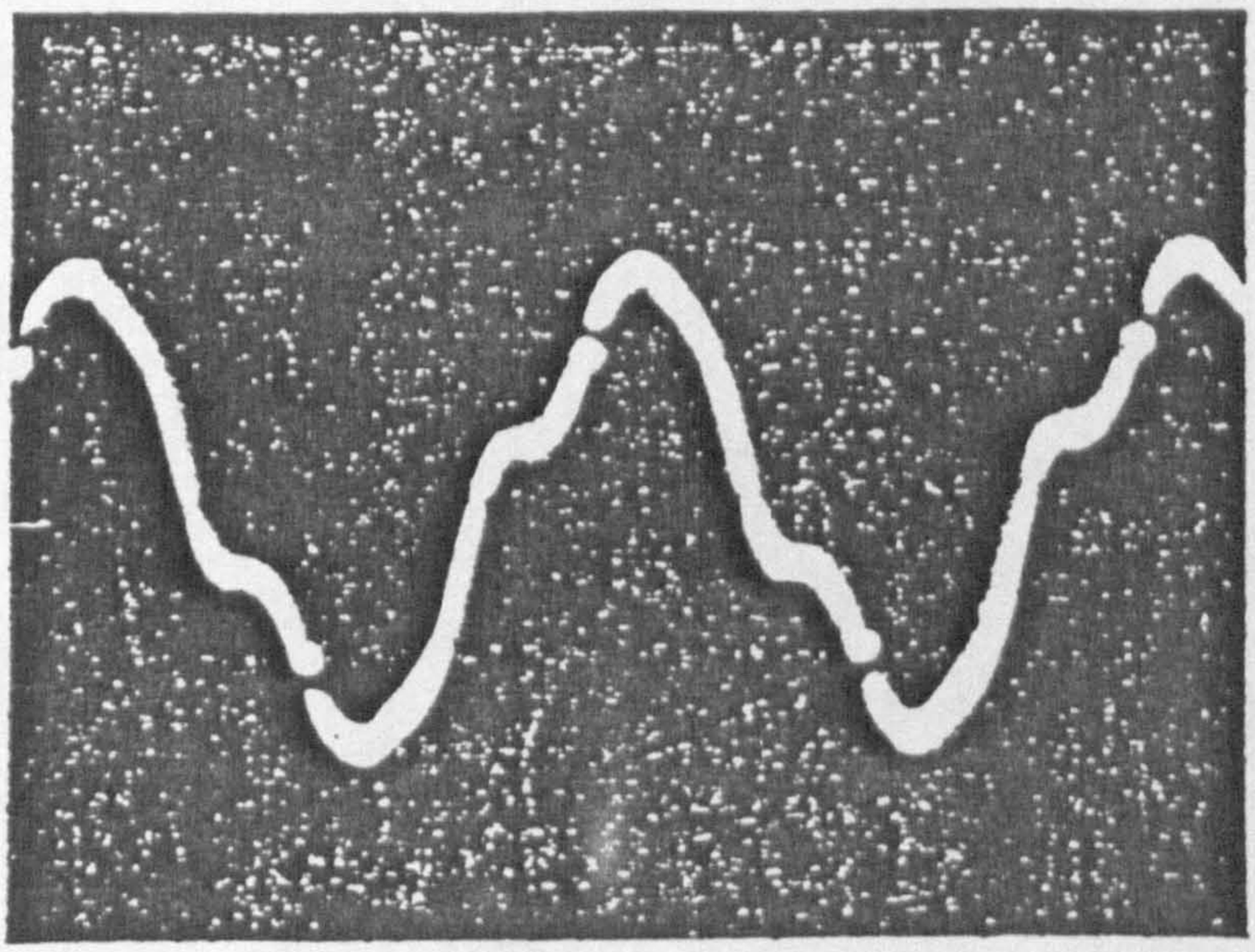

Figure 2.6 Oscillogram showing variation of mutual inductance between main winding and a rotor loop as a function of rotor position

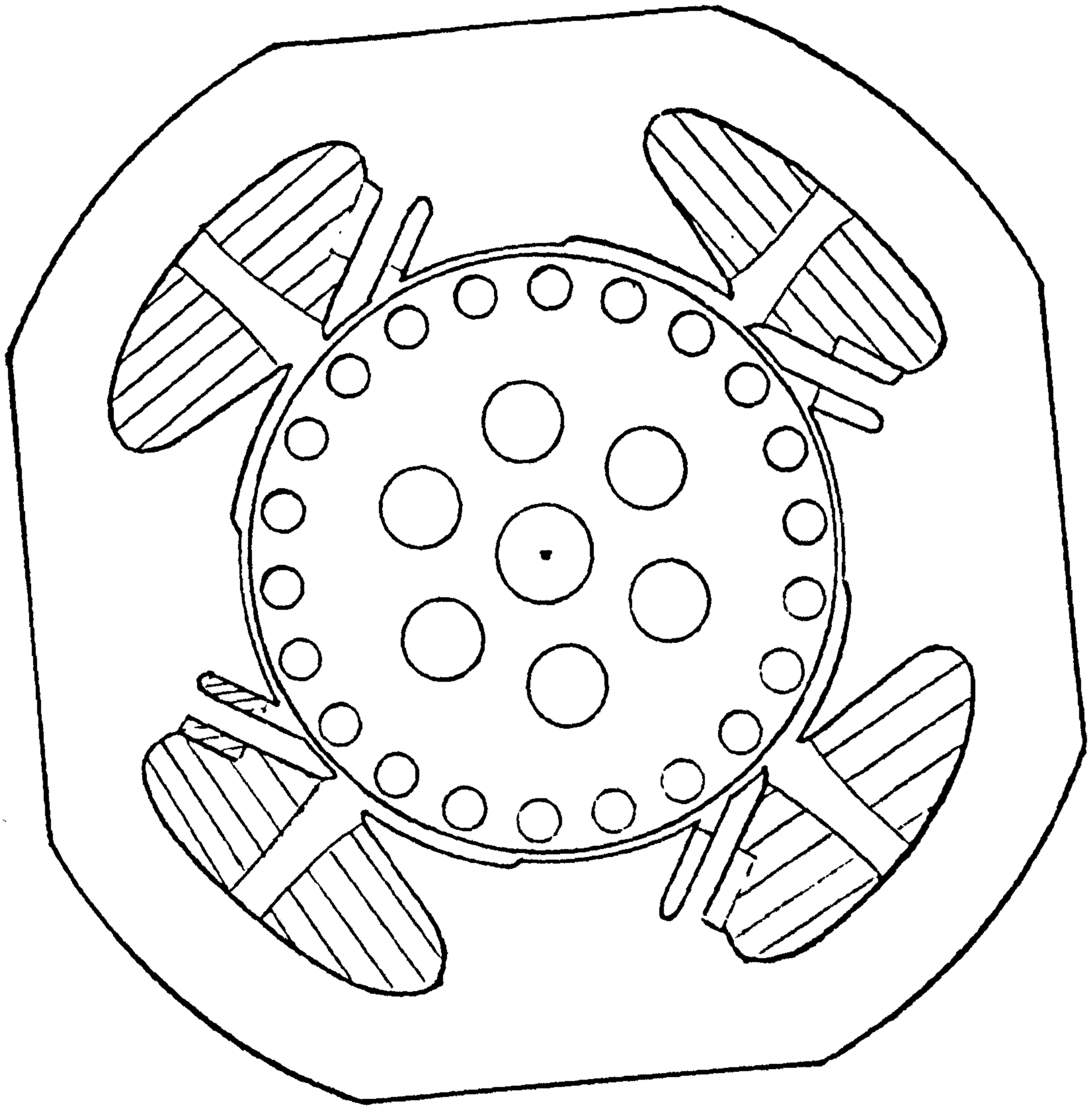

Figure 3.1 Shaded-pole motor

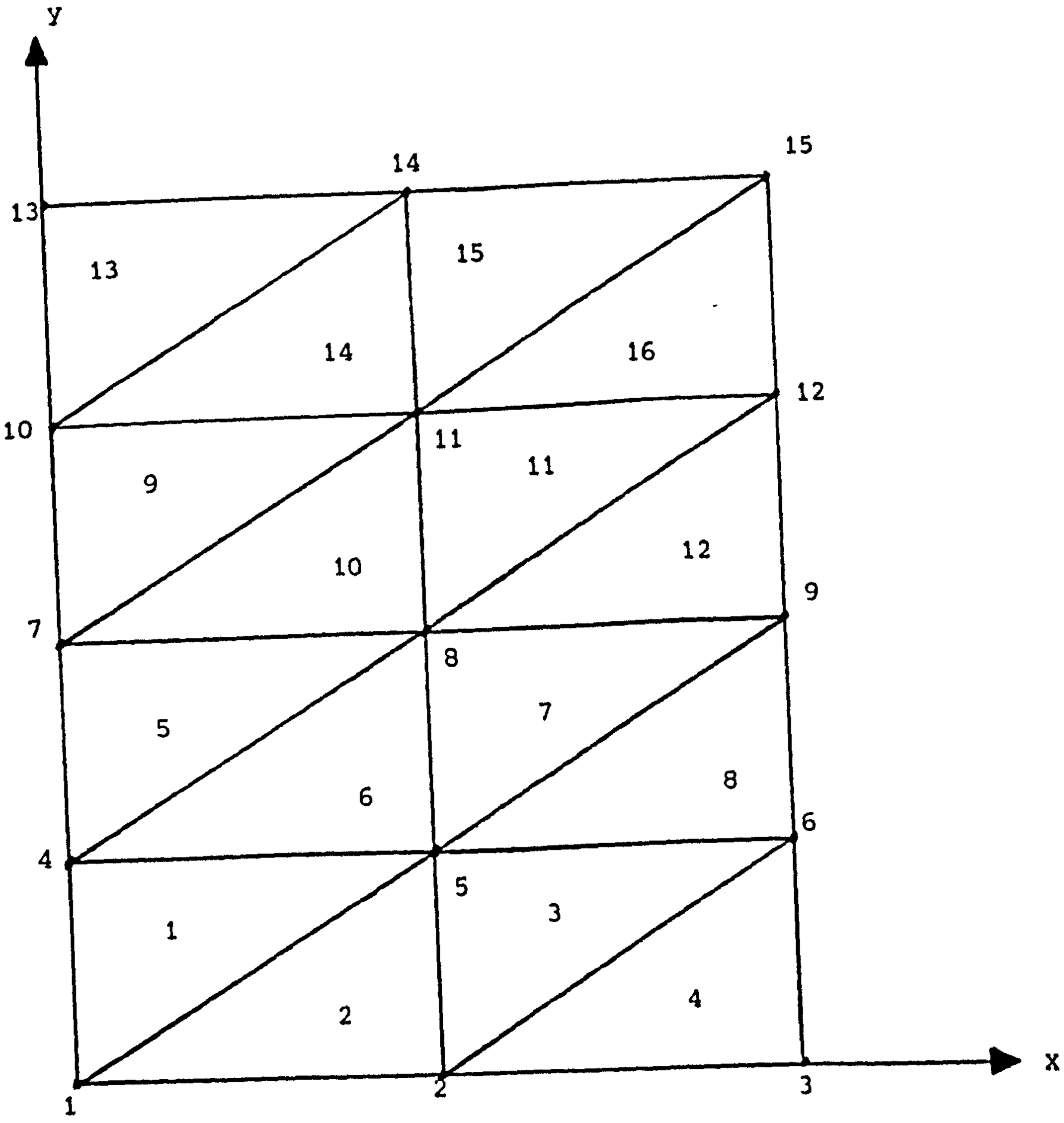

Figure 3.2 Region subdivided into 16 finite elements

Figure 4.1 Flow chart of computer program for finite element method

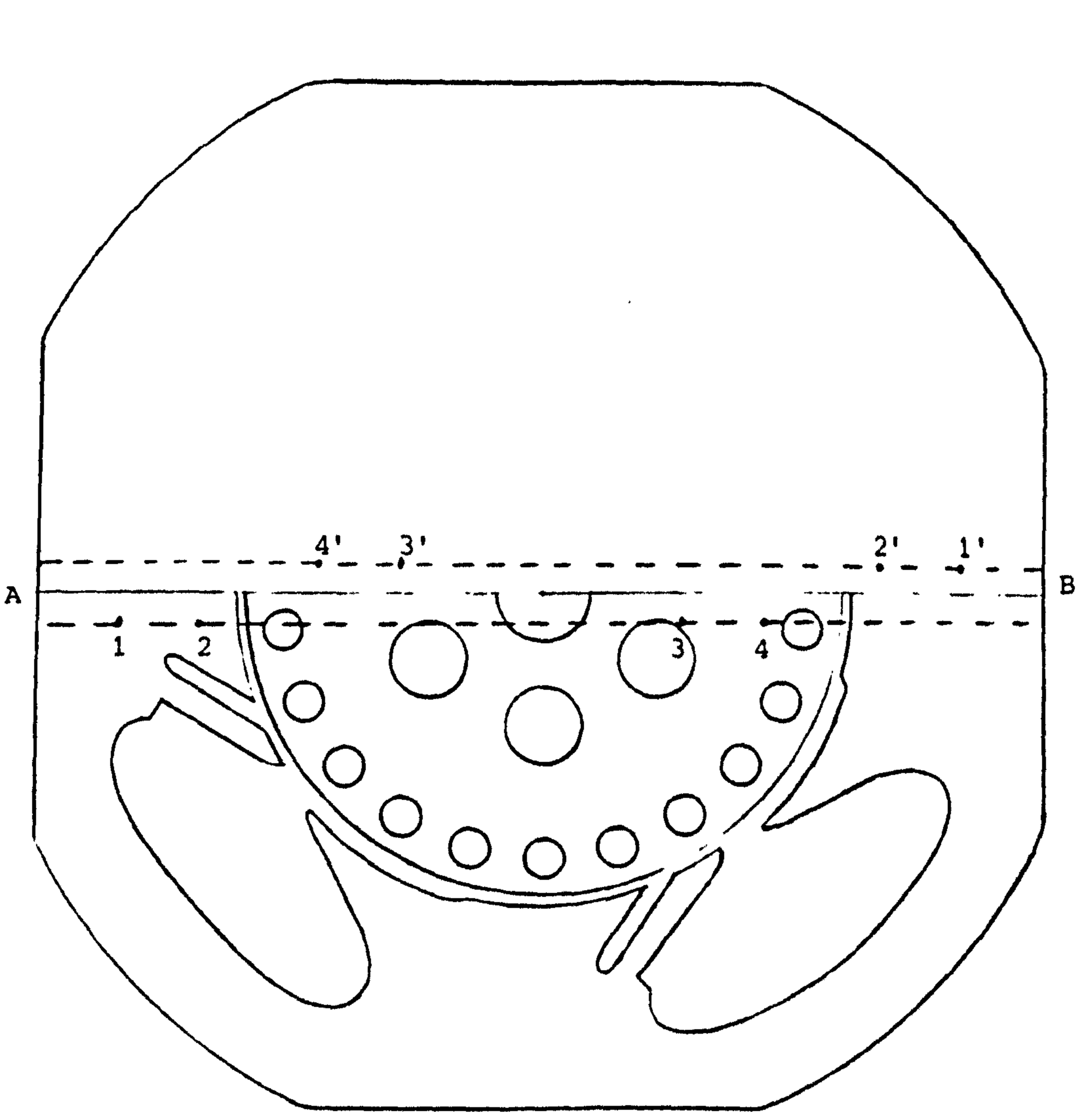

Fig. 4.3.

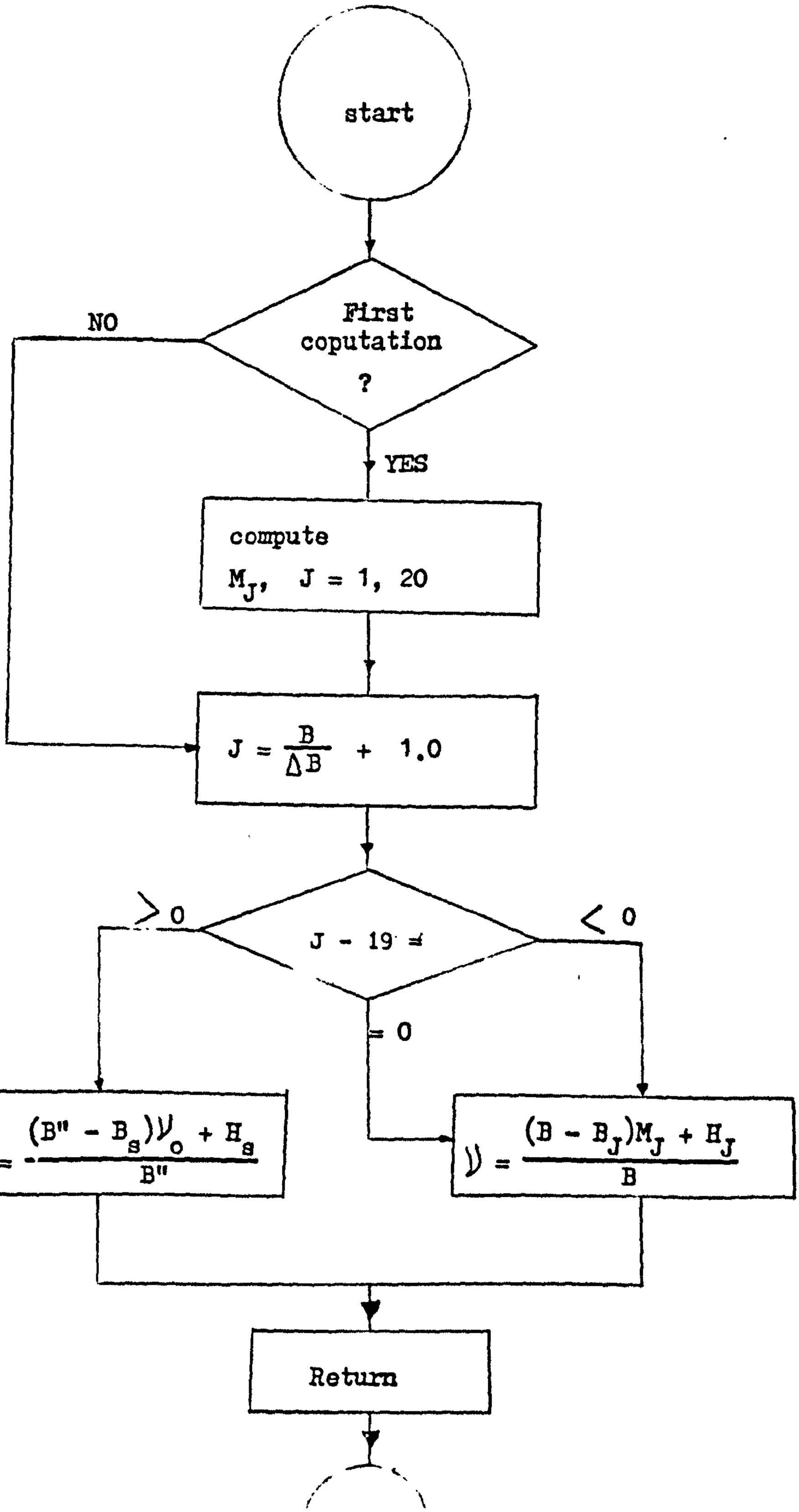
start
First coputation ?
NO
YES
compute
M_J, J = 1, 20
$J = \frac{B}{\Delta B} + 1.0$
J - 19 ≤
> 0
< 0
= 0
$\nu = \frac{(B'' - B_s)\nu_o + H_s}{B''}$
$\nu = \frac{(B - B_J)M_J + H_J}{B}$
Return
stop

Figure 4.3.2

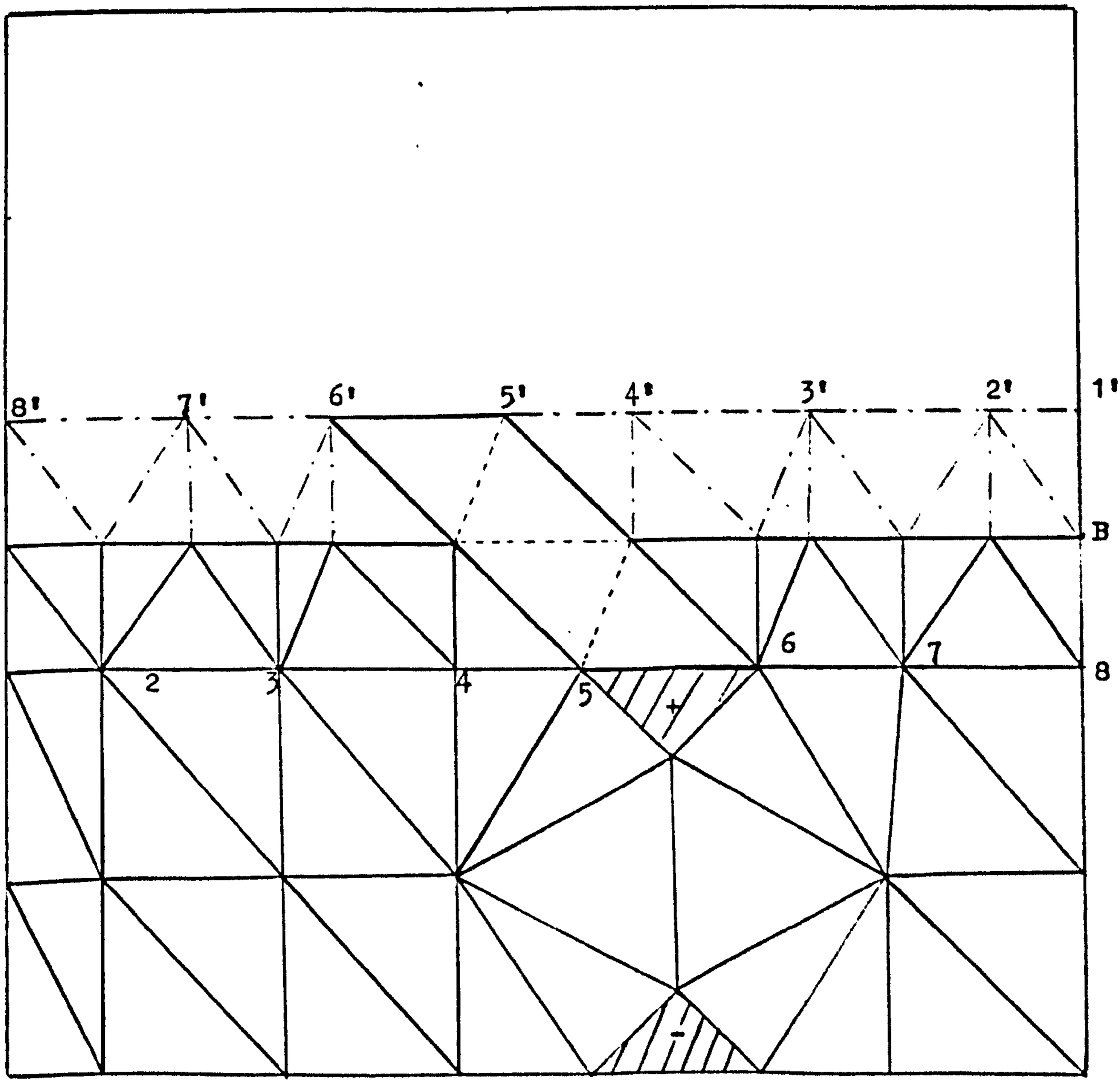

Fig. 4.4

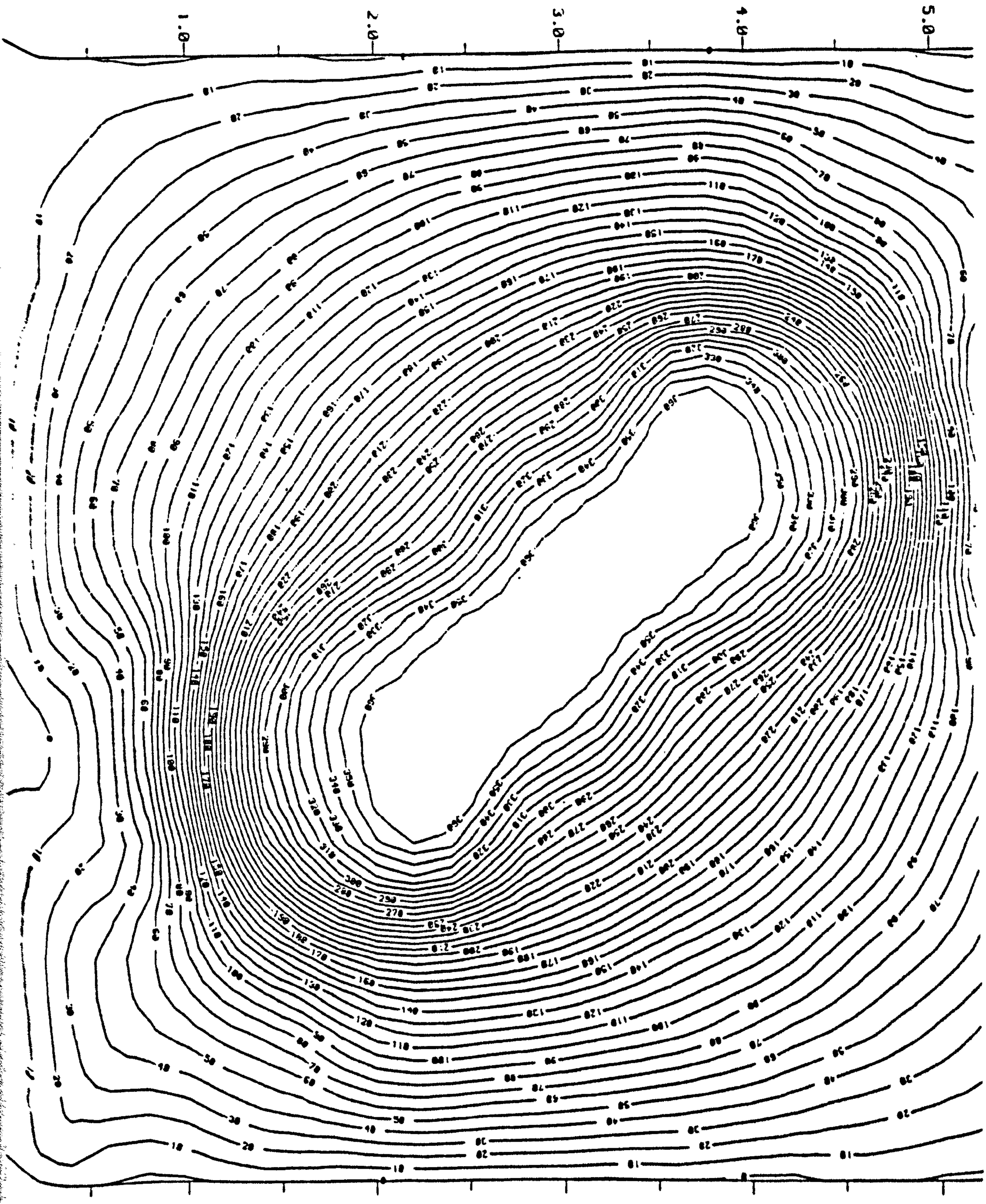

Fig. 4.5a

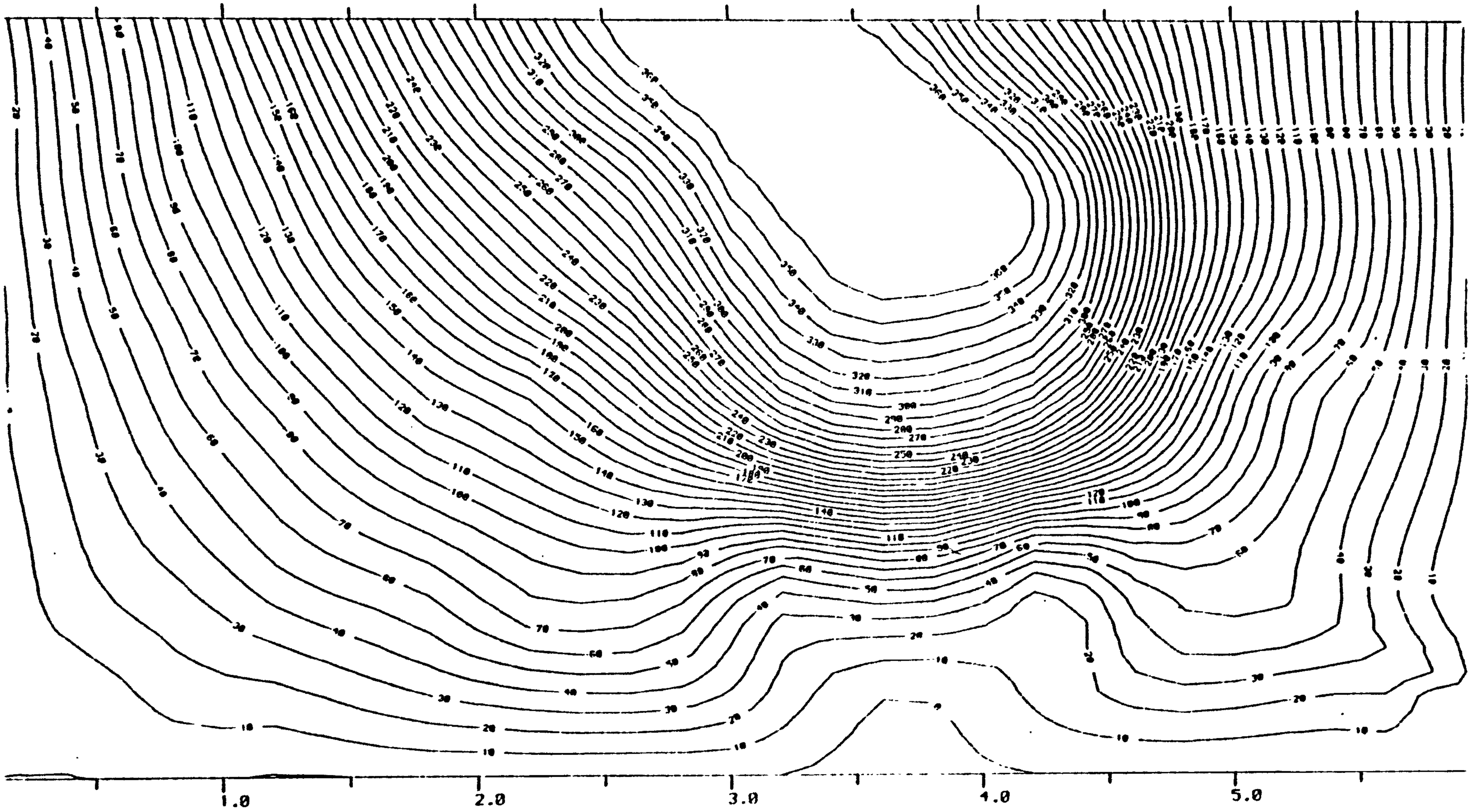

Fig. 4.5b

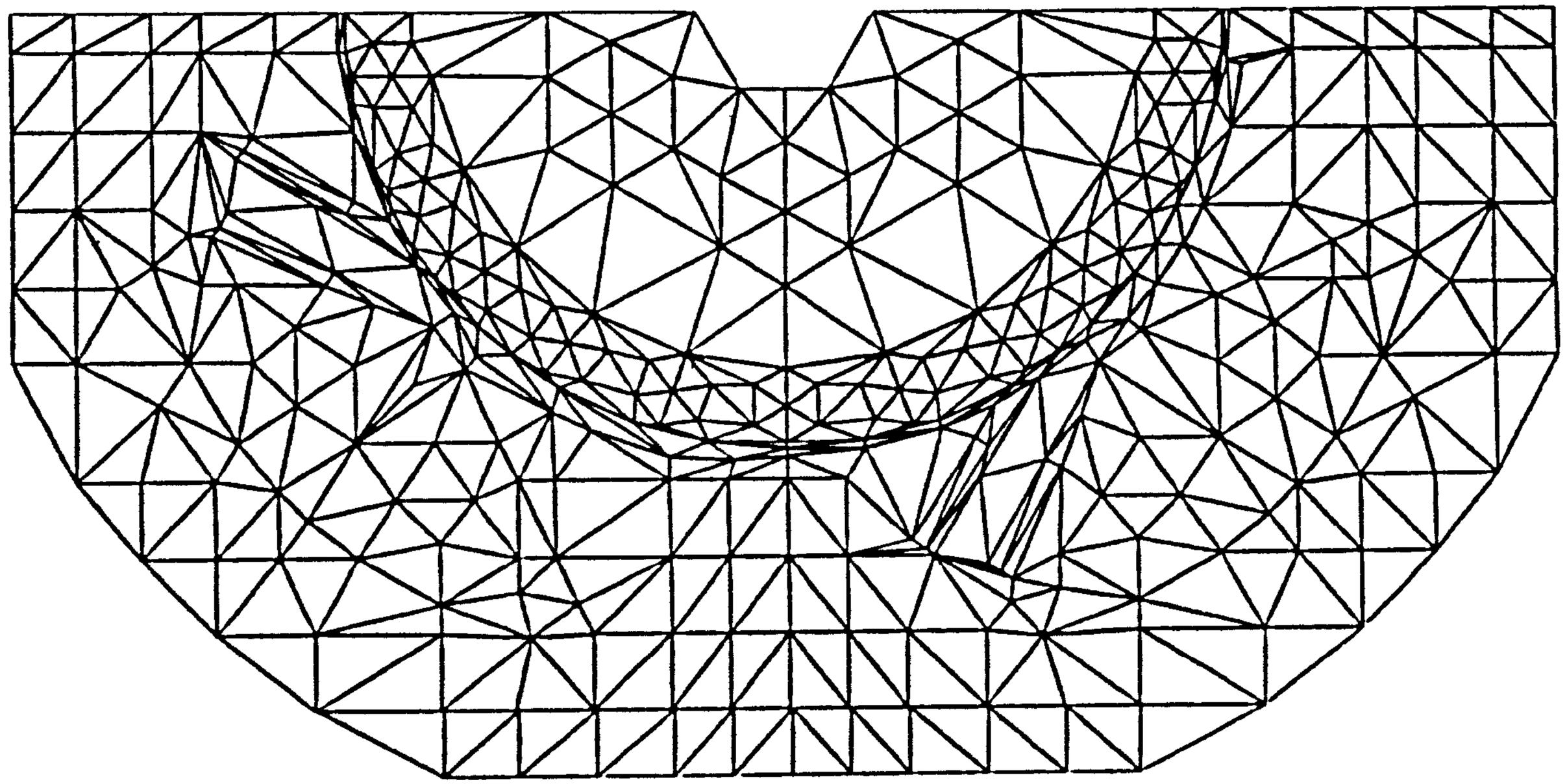

Fig. 4.6 Mesh drawing of shaded-pole motor

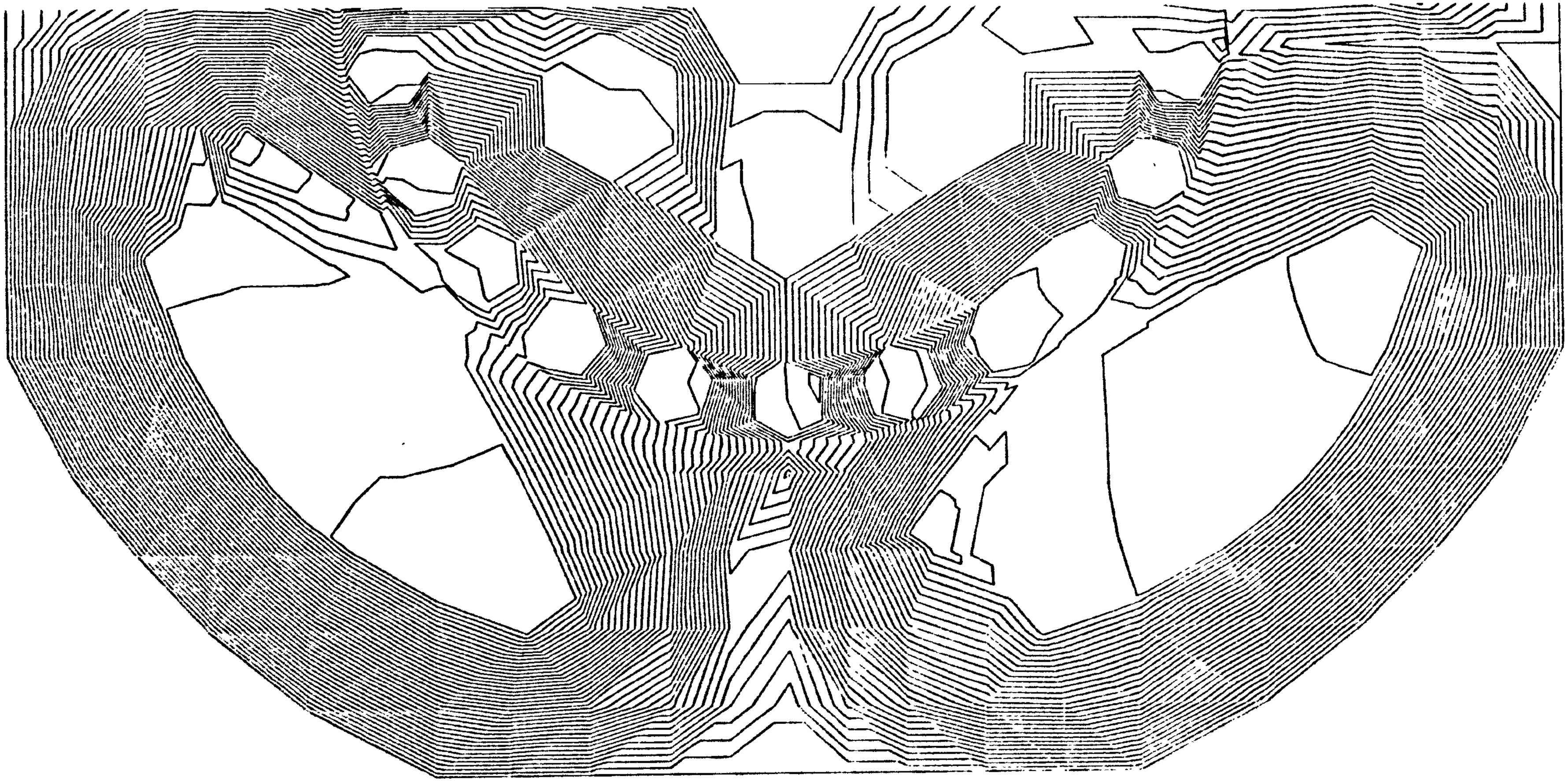

Fig. 4.7a Flux plotting for s = 1, t = 0

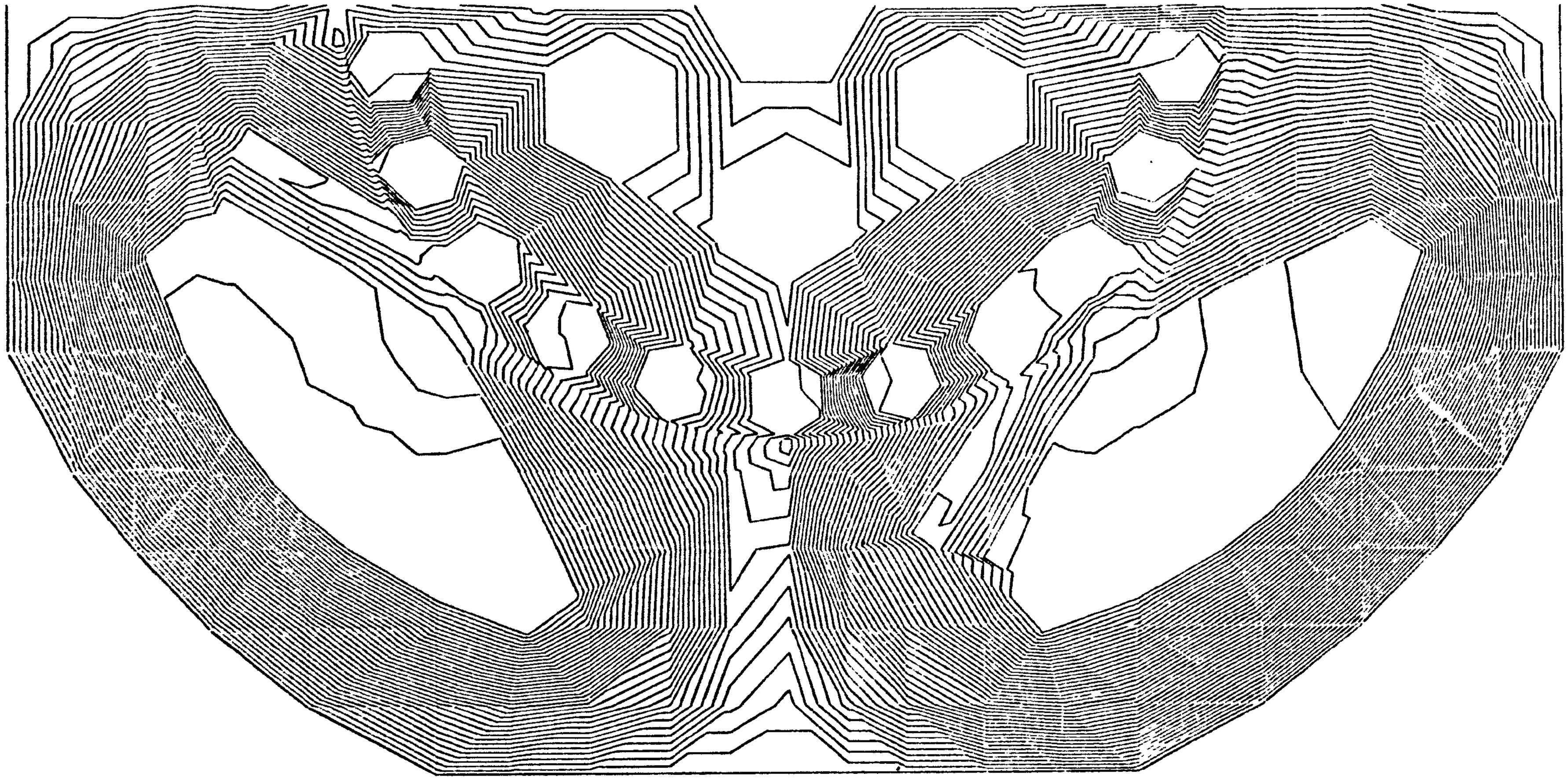

Fig. 4.7b Flux plotting for s = 1, t = 5 m.sec

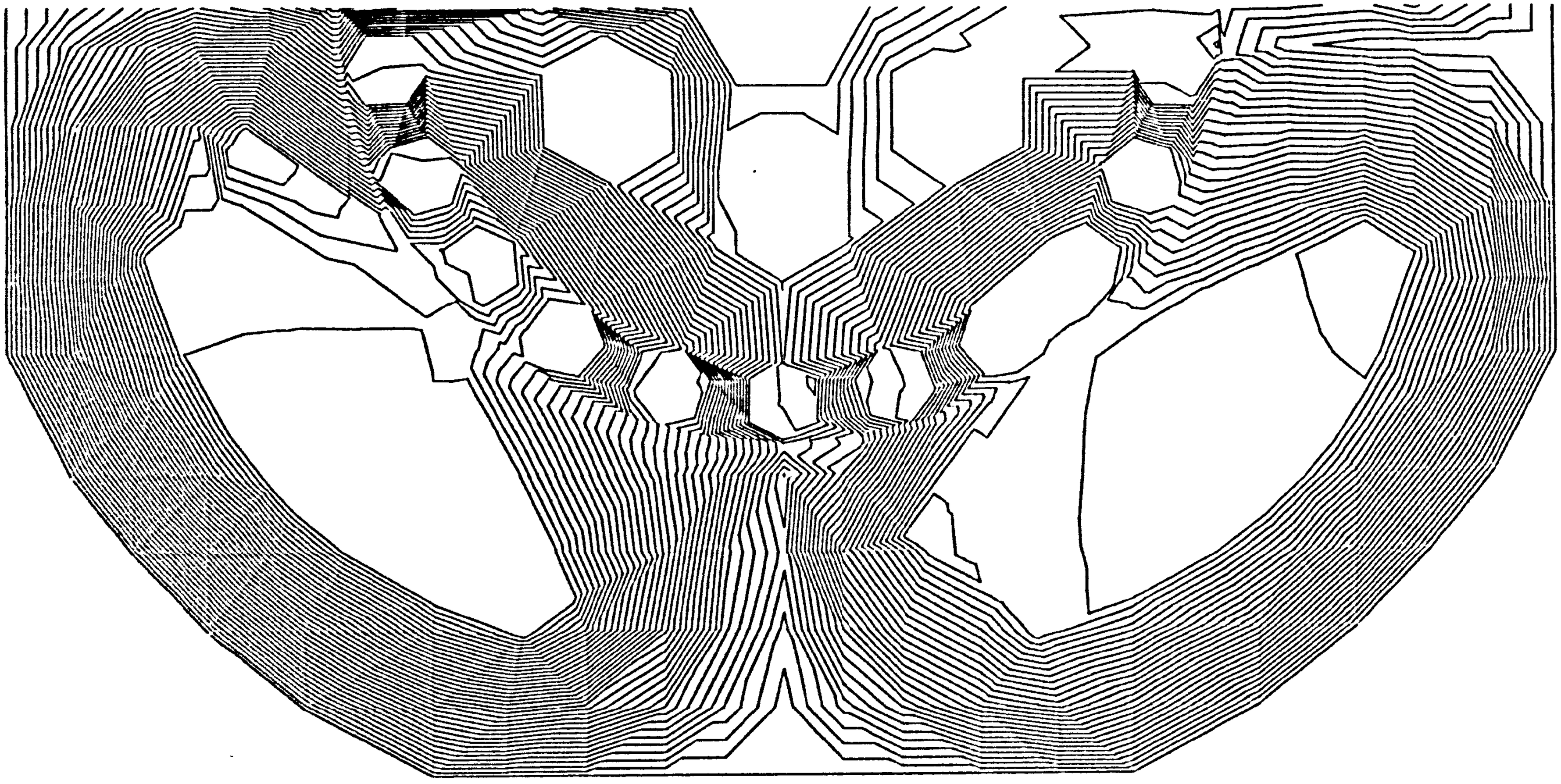

Fig. 4.8.a Flux plotting of the motor for s = 0.5, t = 0

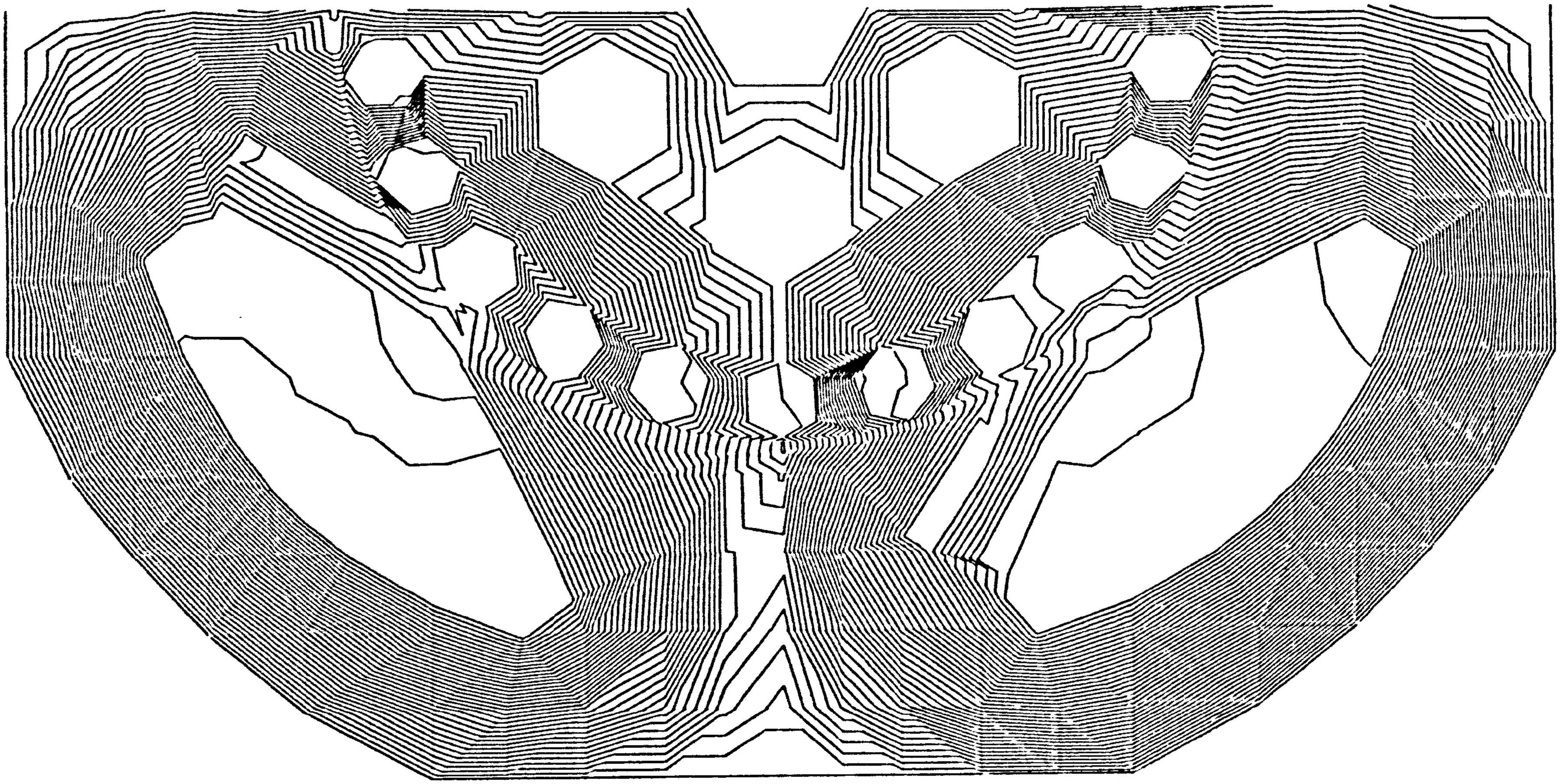

Fig. 4.8.b Flux plotting of the motor for s = 0.5, t = 5 m.sec

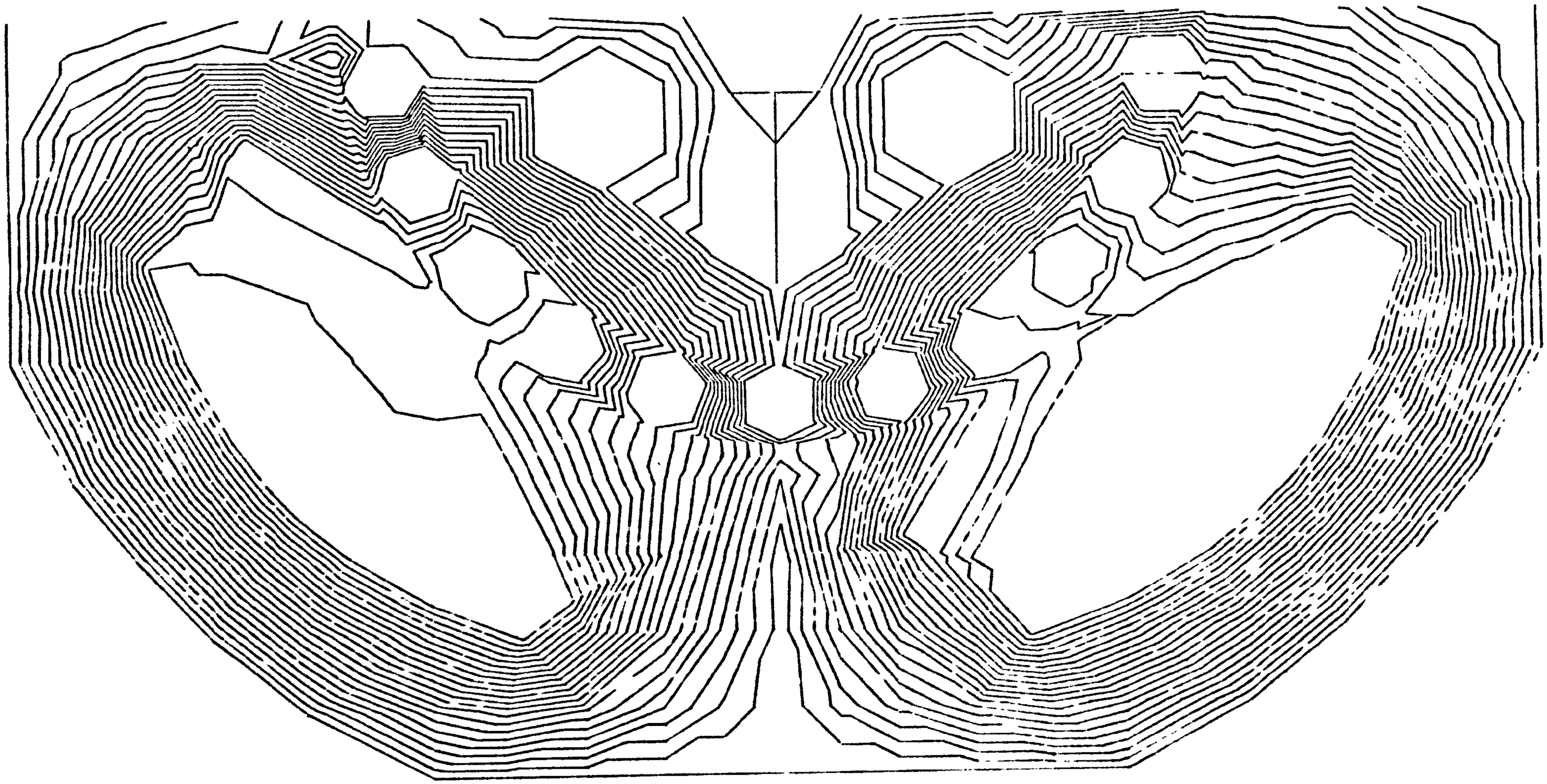

Fig. 4.9a Flux plotting of the motor for s = 0.05, t = 0

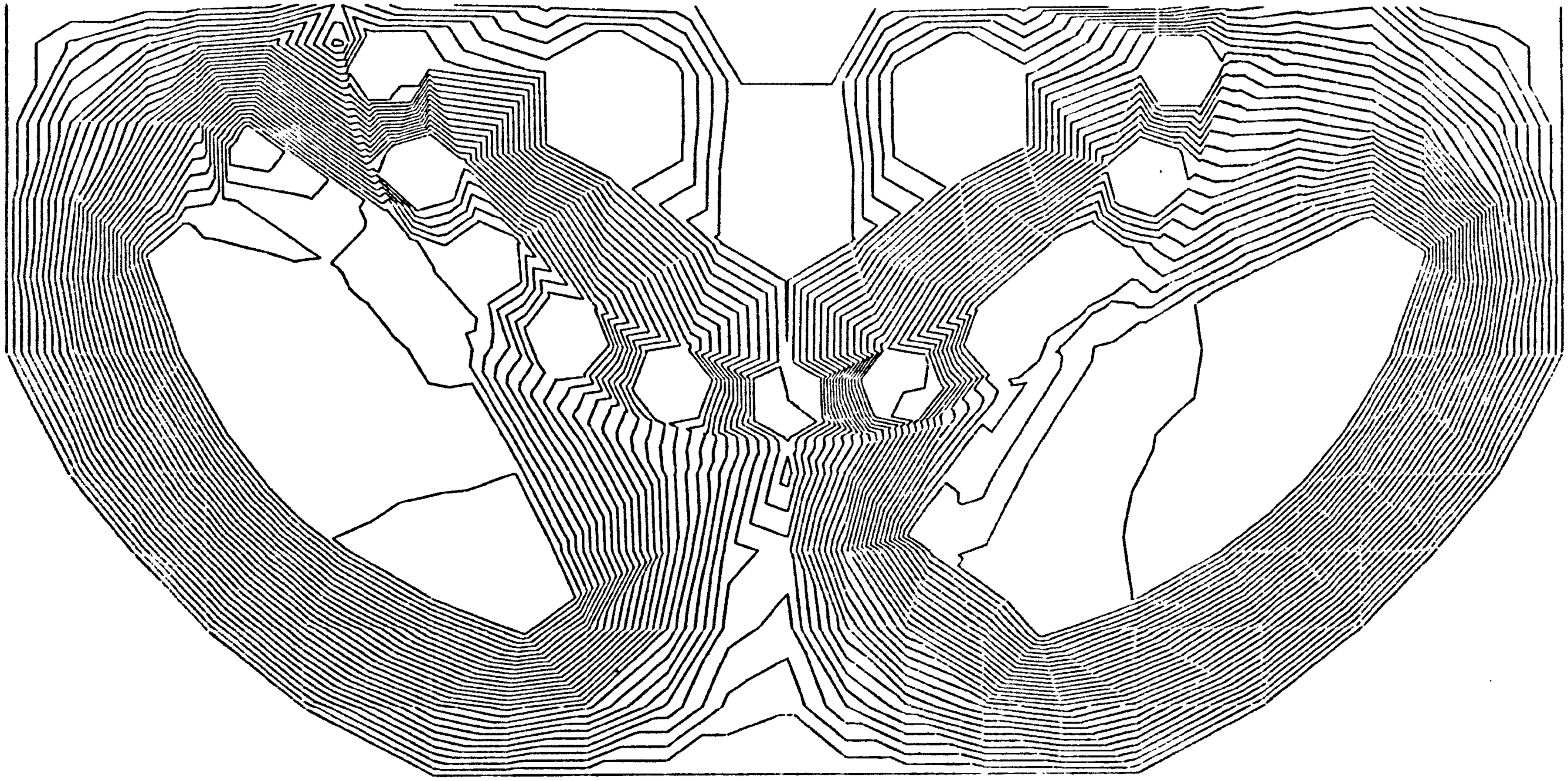

Fig. 4.9b Flux plotting for s = 0.05, t = 5 m.sec

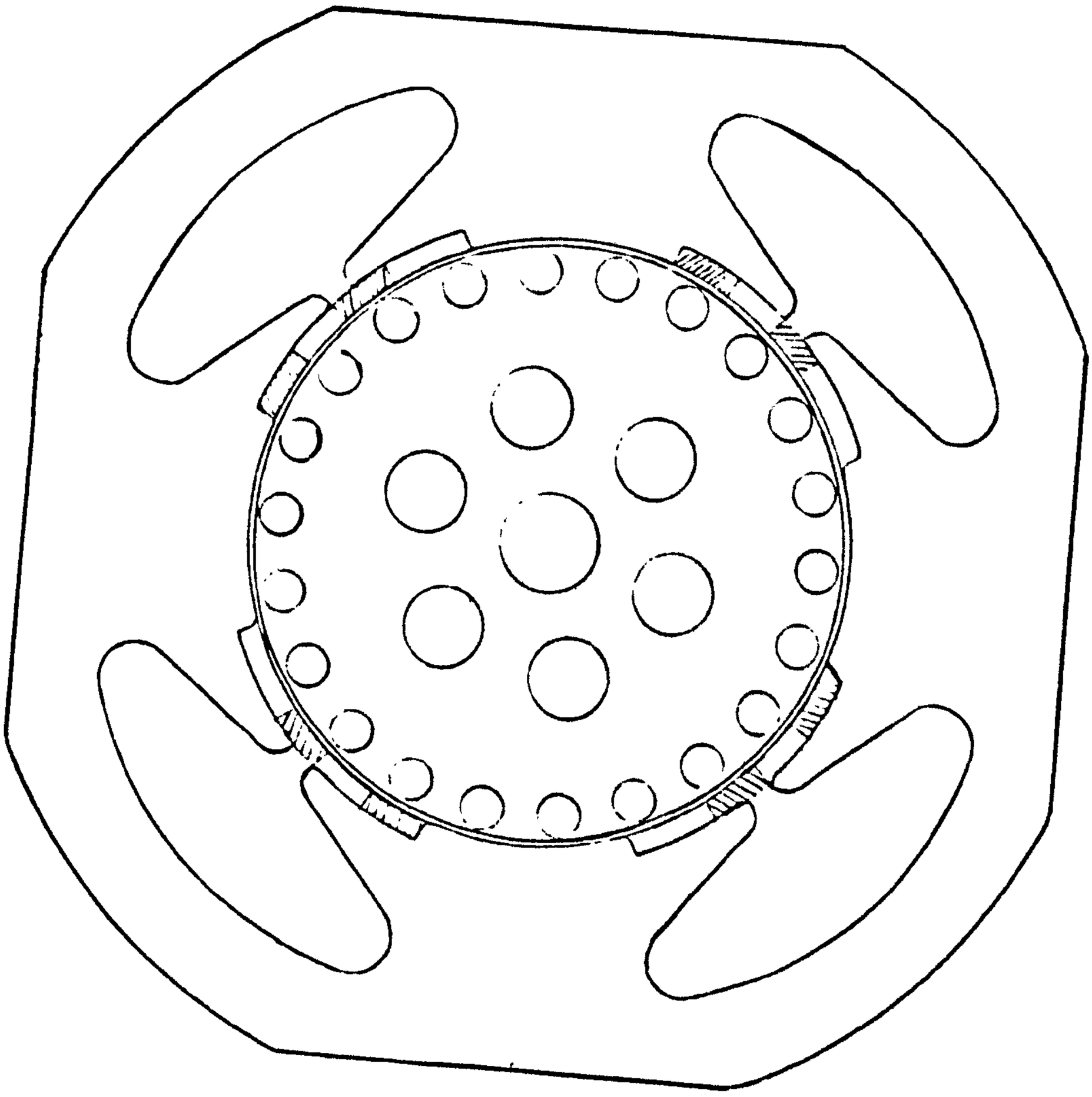

Figure 4.10 Reversing speed motor

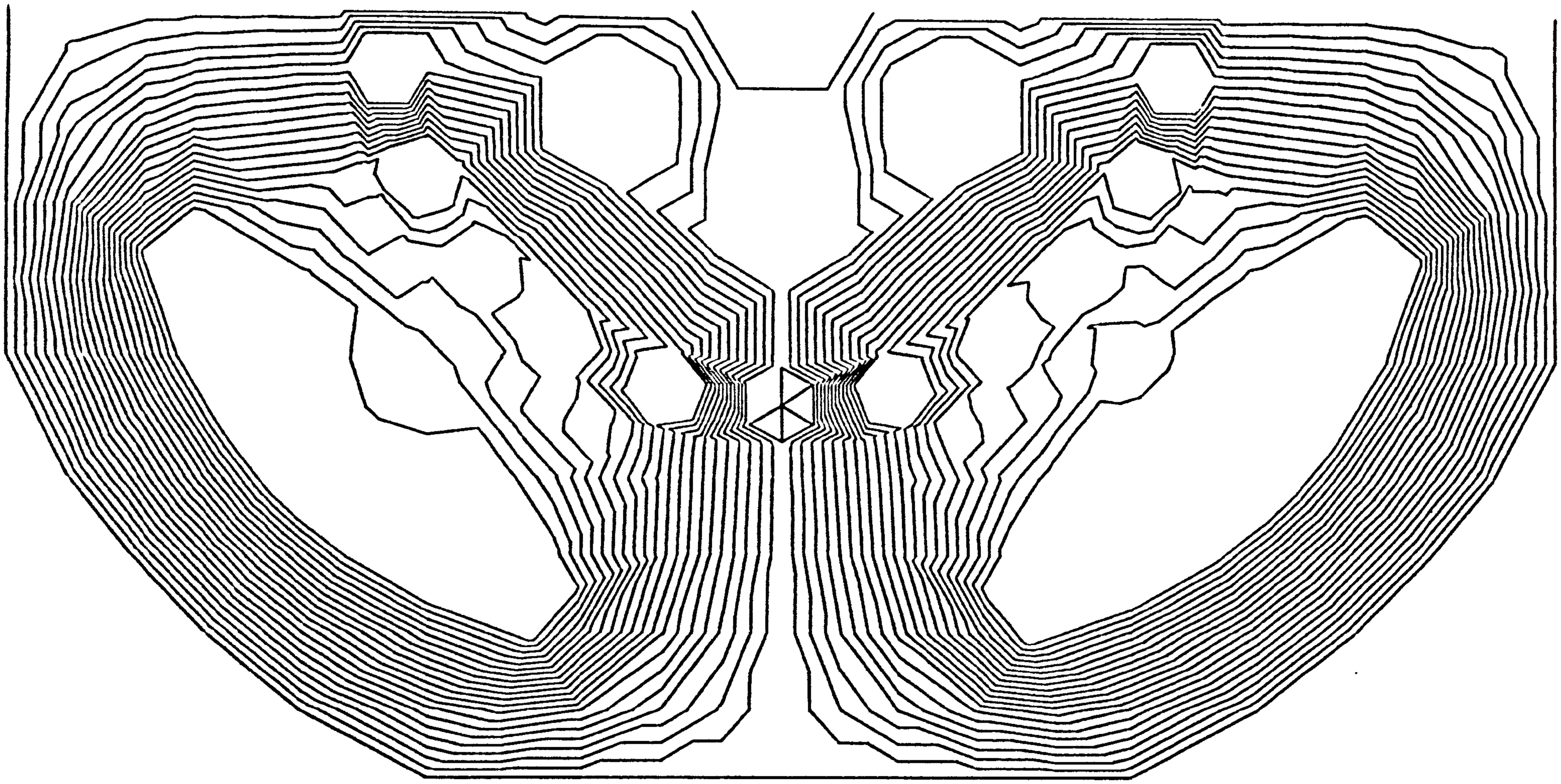

Fig. 4.11

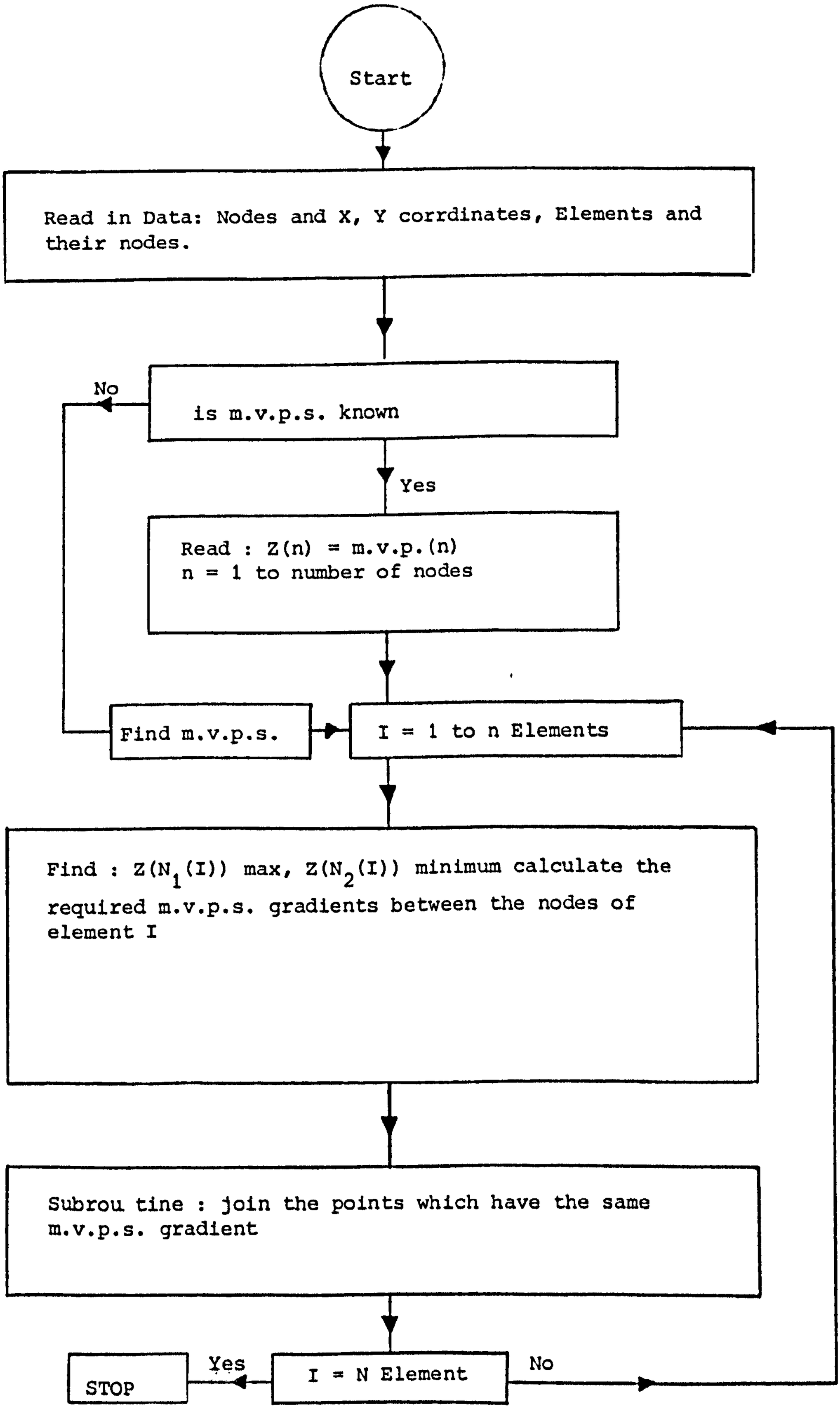

Figure 4.12 Flow chart of plotting program

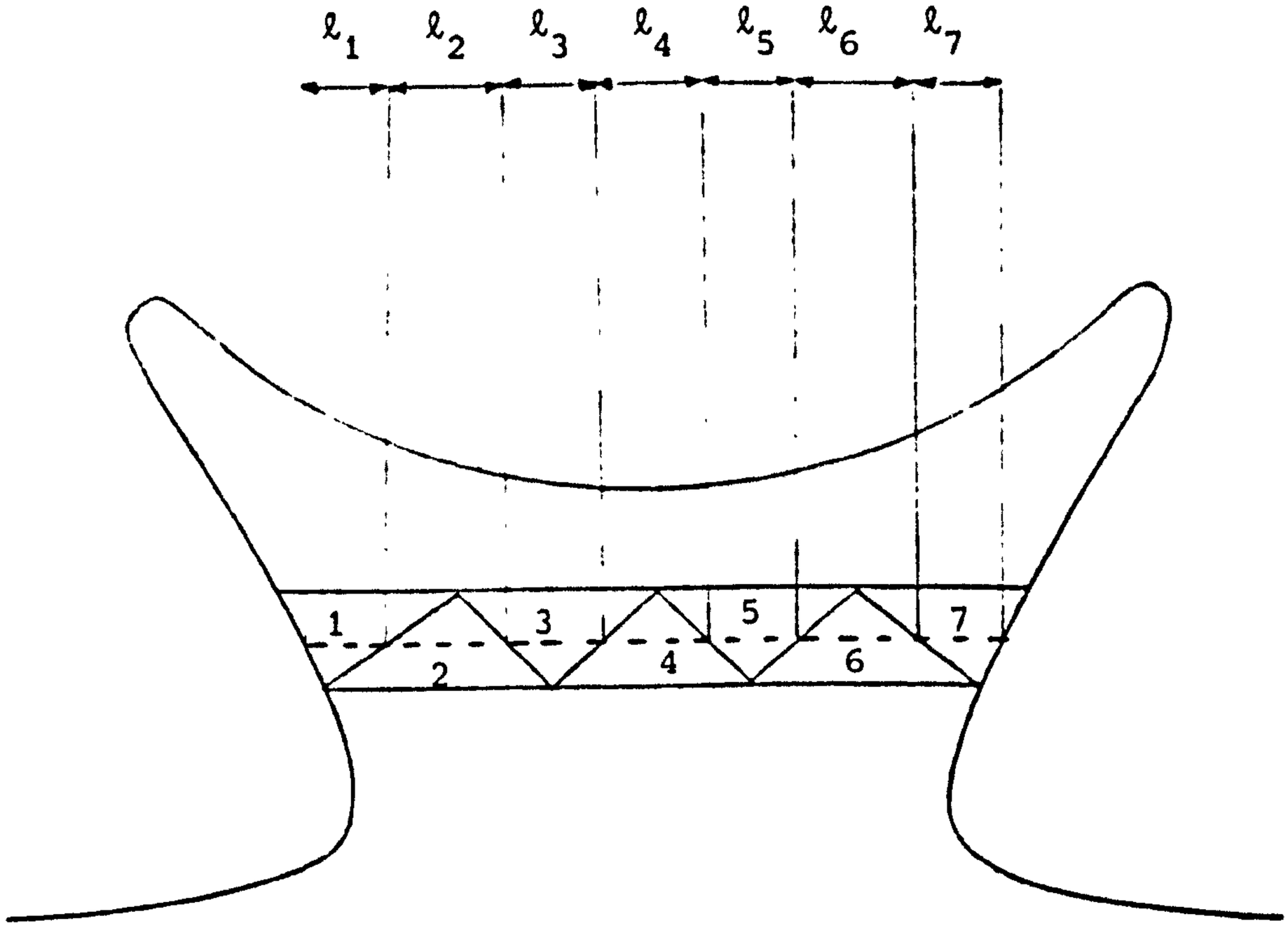

Fig. 5.1.1. Pole of the machine

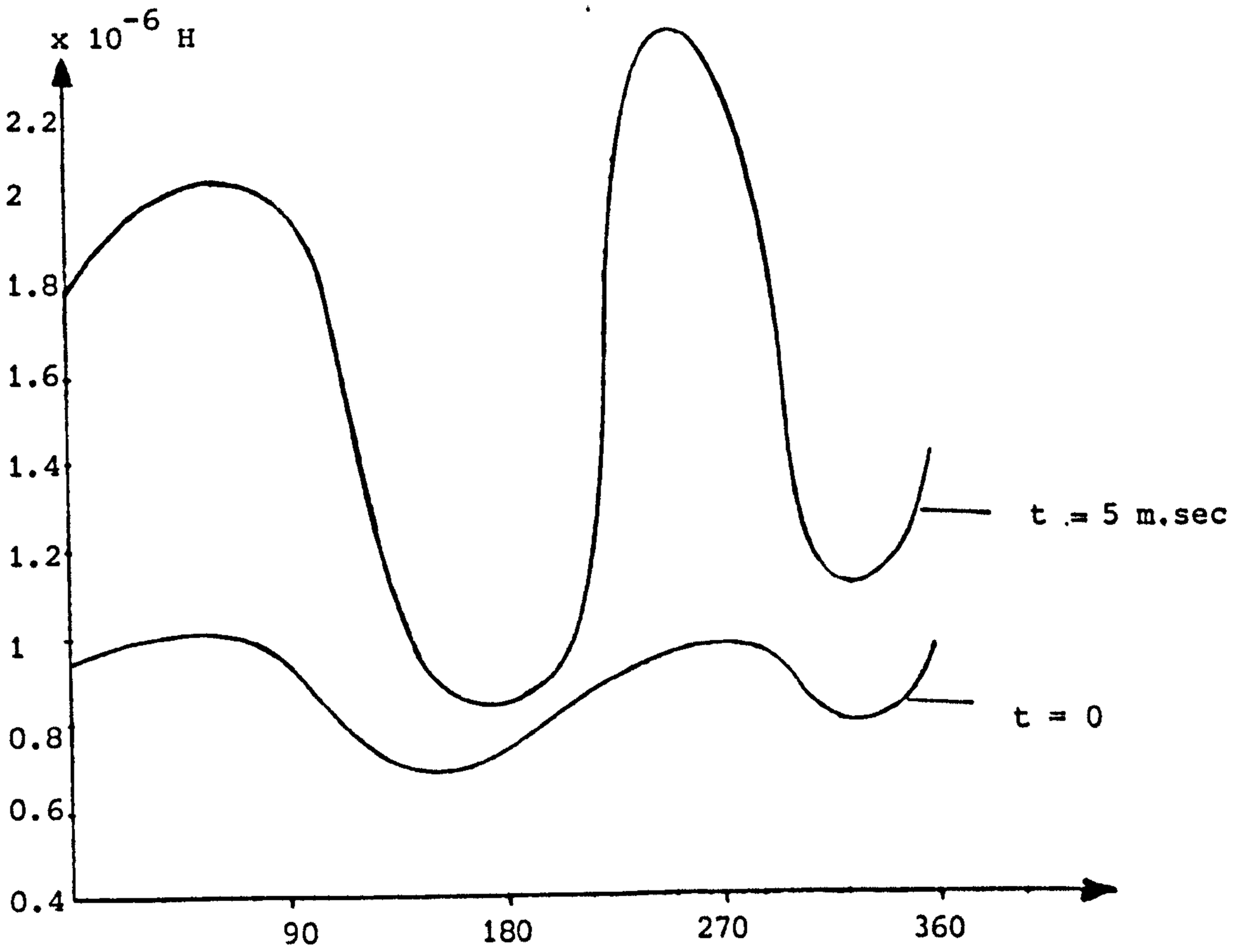

Fig: 5.2.1a Variation of rotor loop self inductance, slip = 1

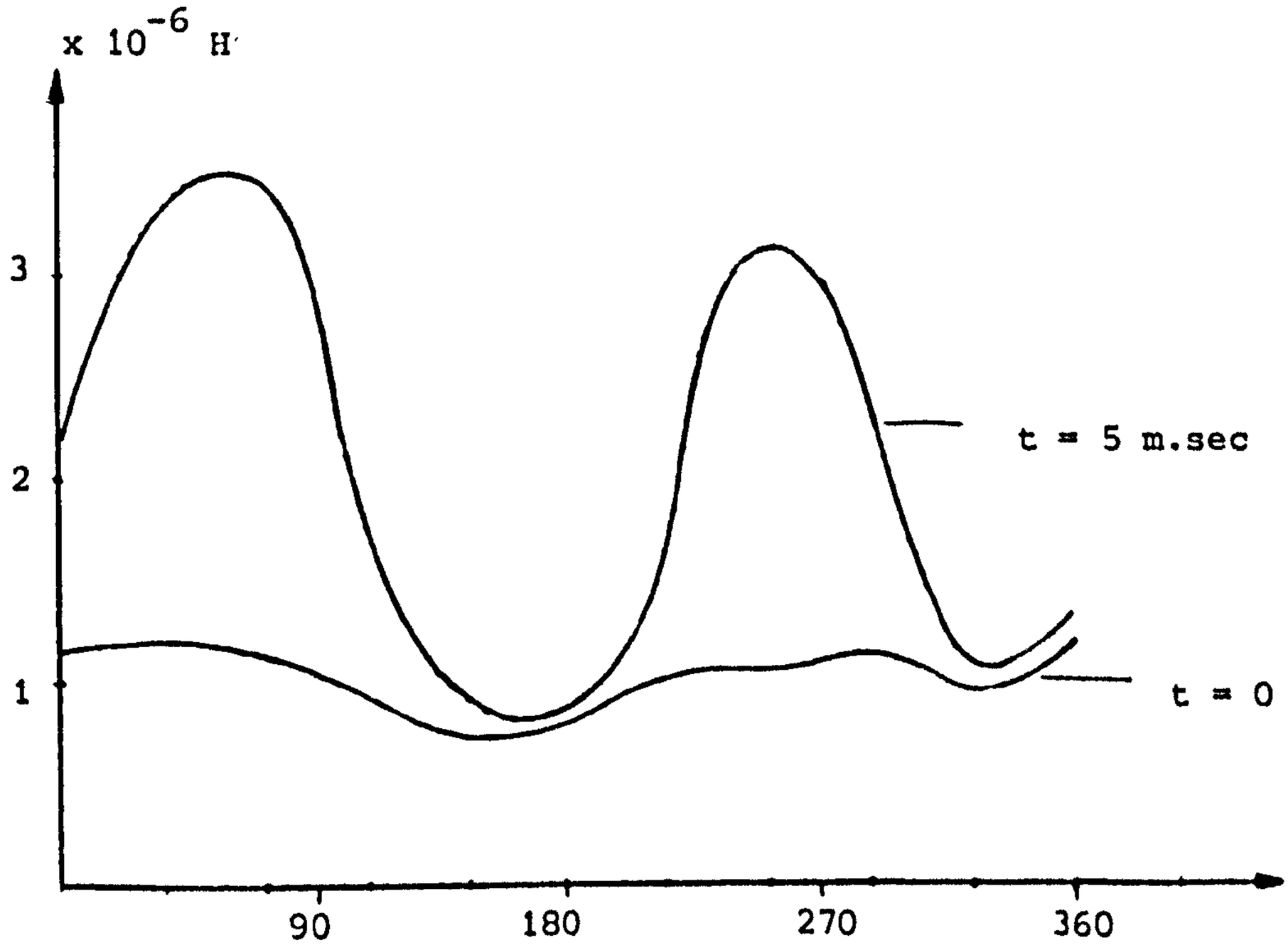

Fig. 5.2.1b Variation of rotor loop self inductance, slip = 0.5

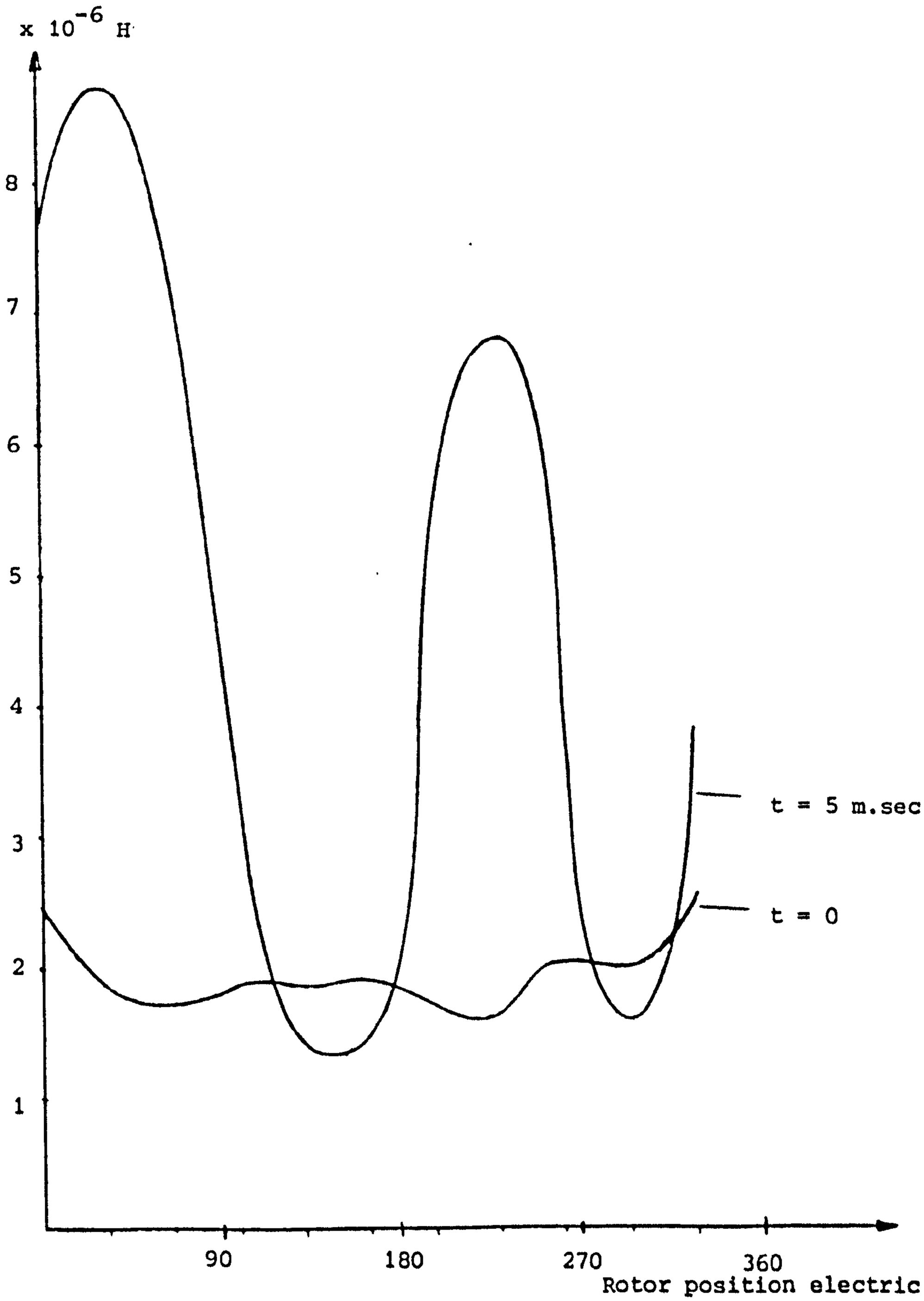

Figure 5.2.1c Variation of rotor loop self inductance for, slip = 0.05

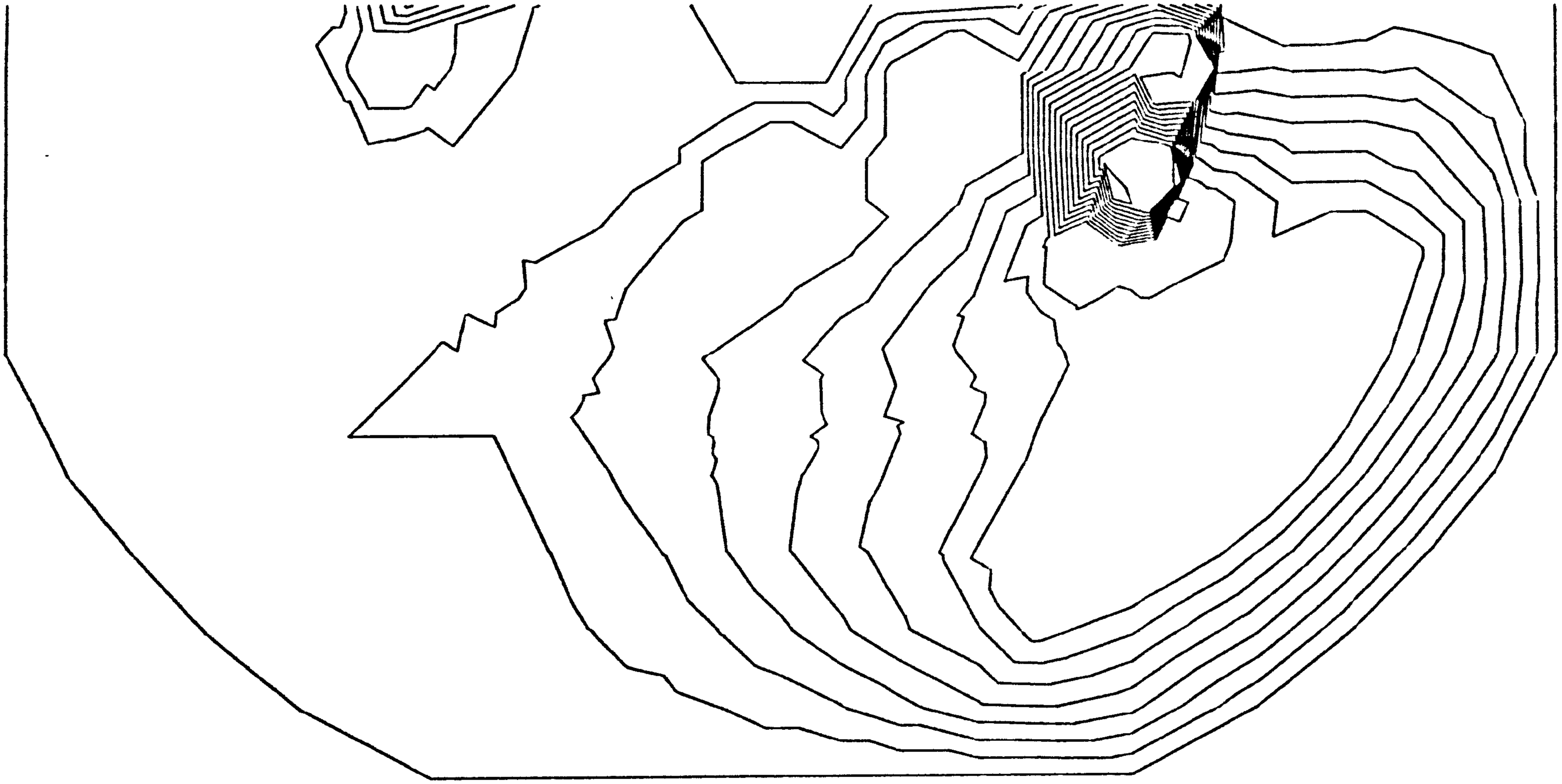

Fig. 5.2.2.a_1 Flux of loop 1 for s = 1, t = 0

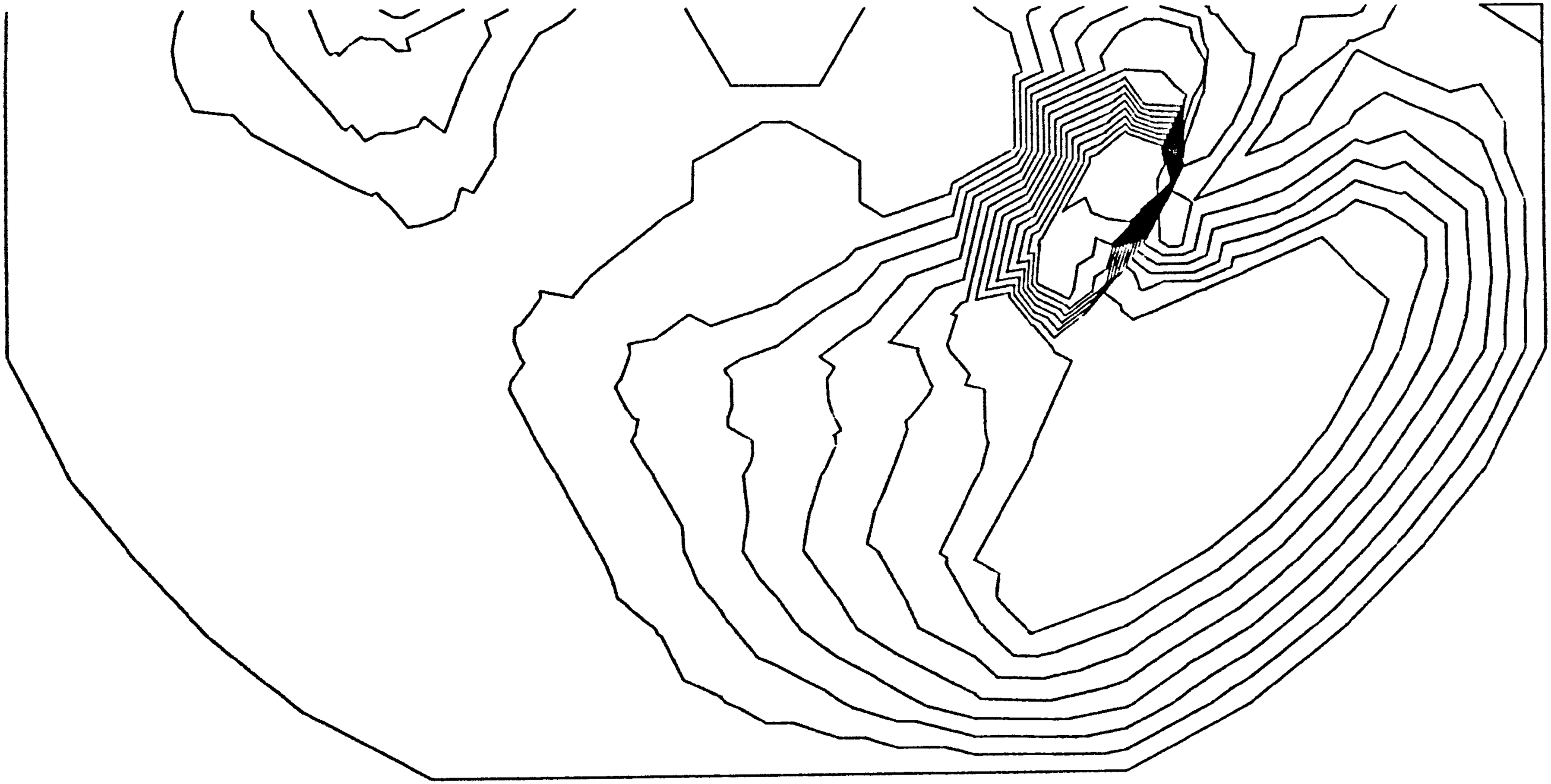

Fig. 5.2.2.a2 Flux of loop 2 for s = 1, t = 0

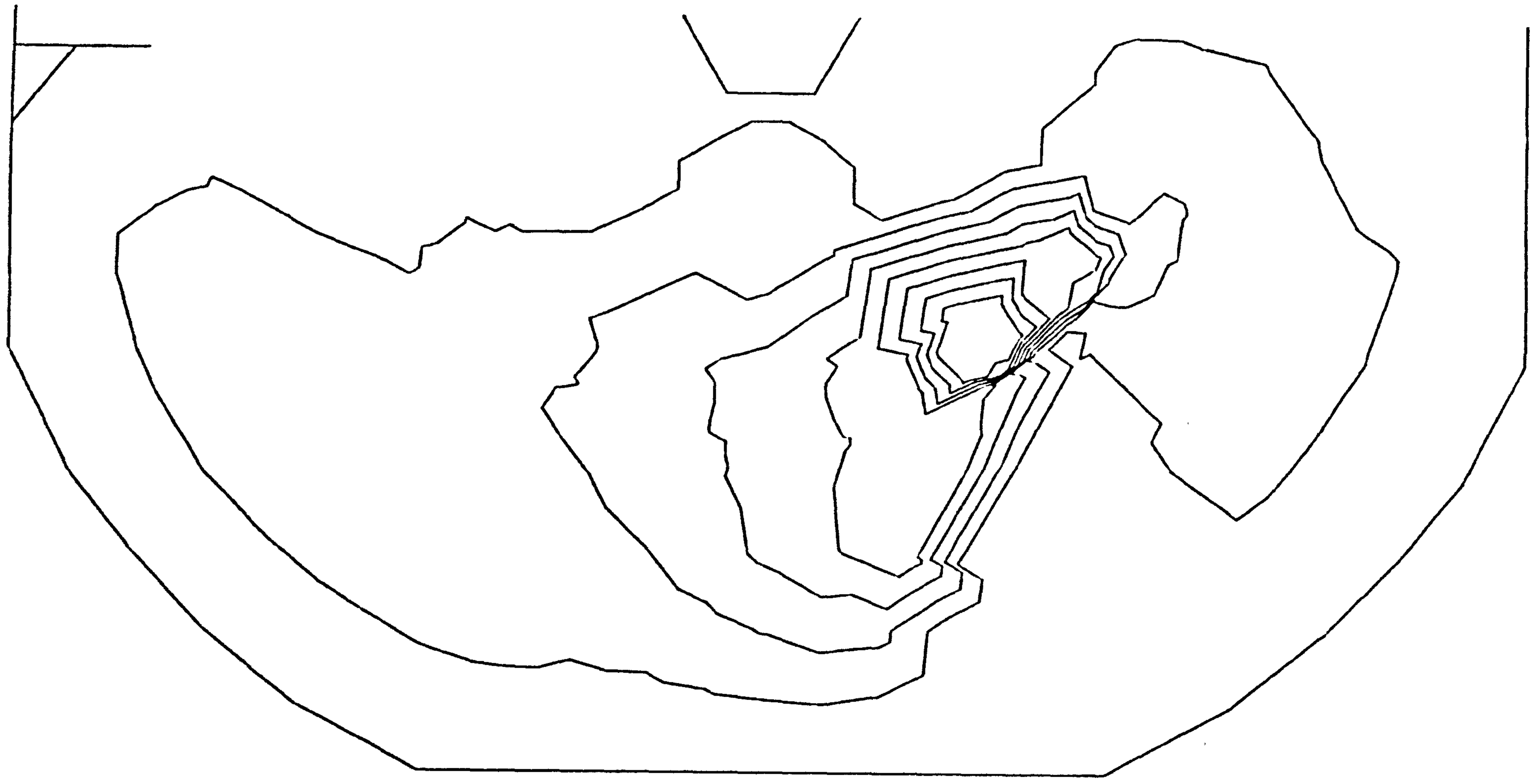

Fig. 5.2.2.a_3 Flux of loop 3 for s = 1, t = 0

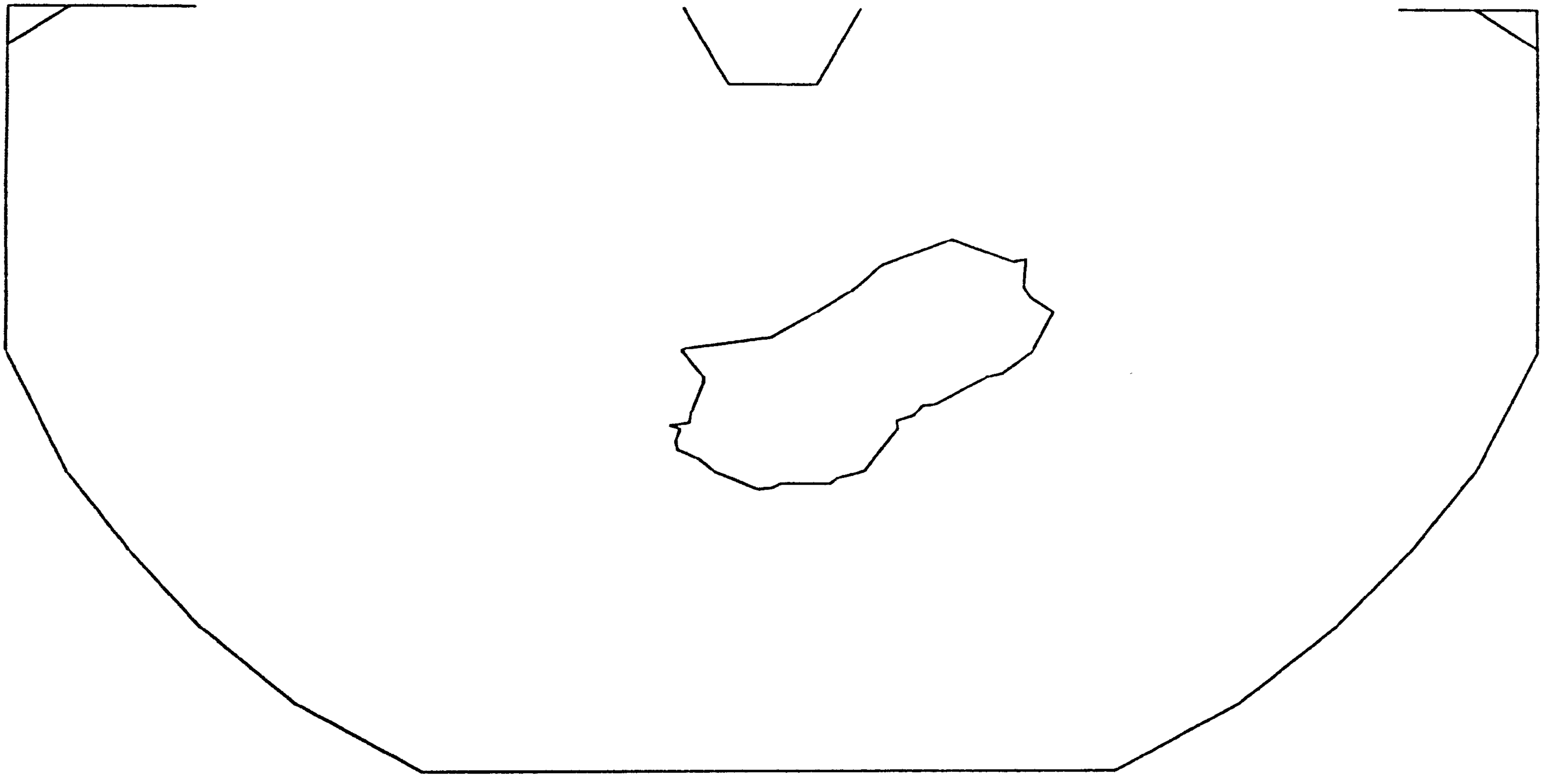

Fig. 5.2.2.a_4 Flux of loop 4 for s = 1, t = 0

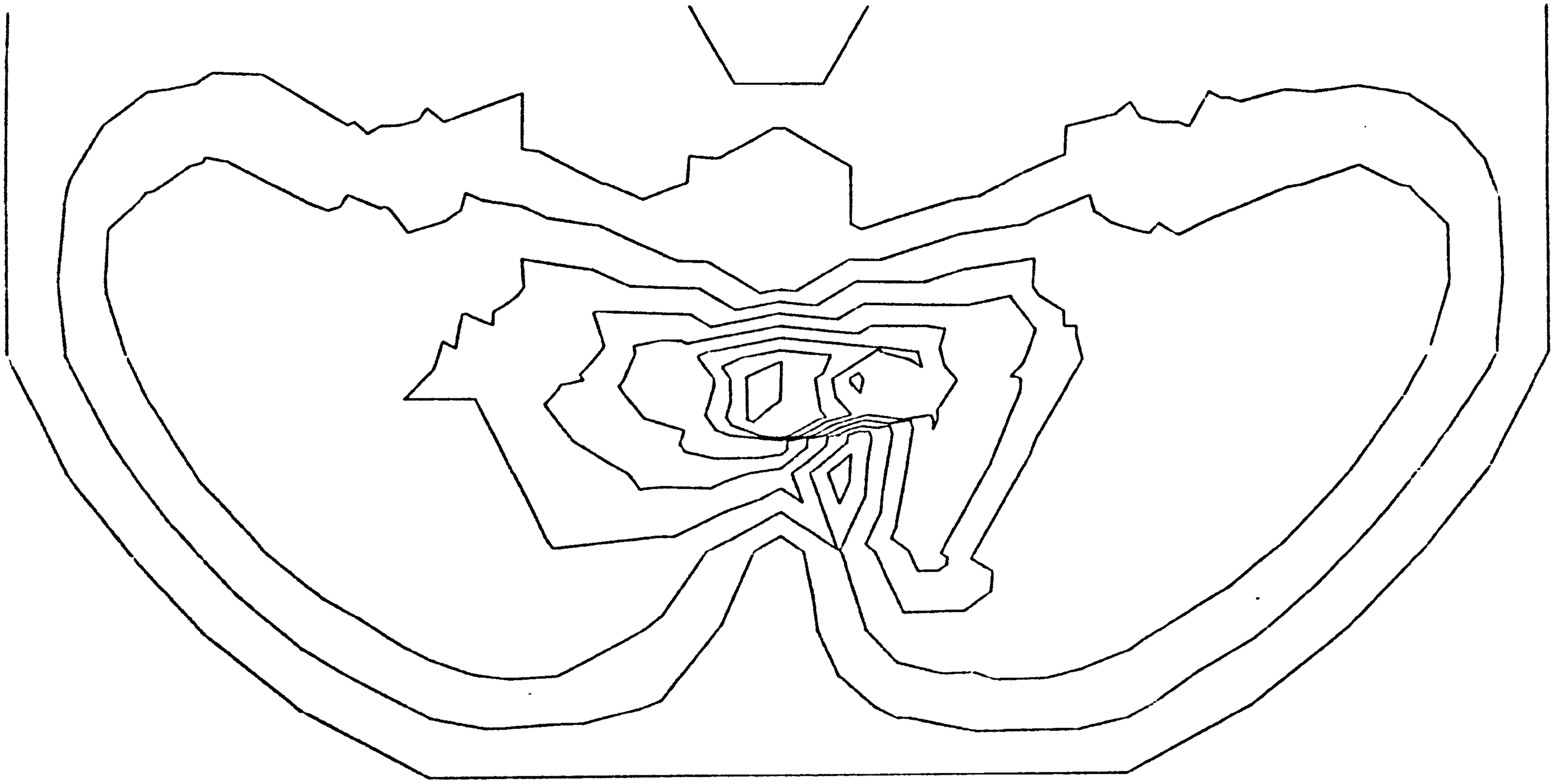

Fig. 5.2.2.a_5 Flux of loop 5 for s = 1, t = 0

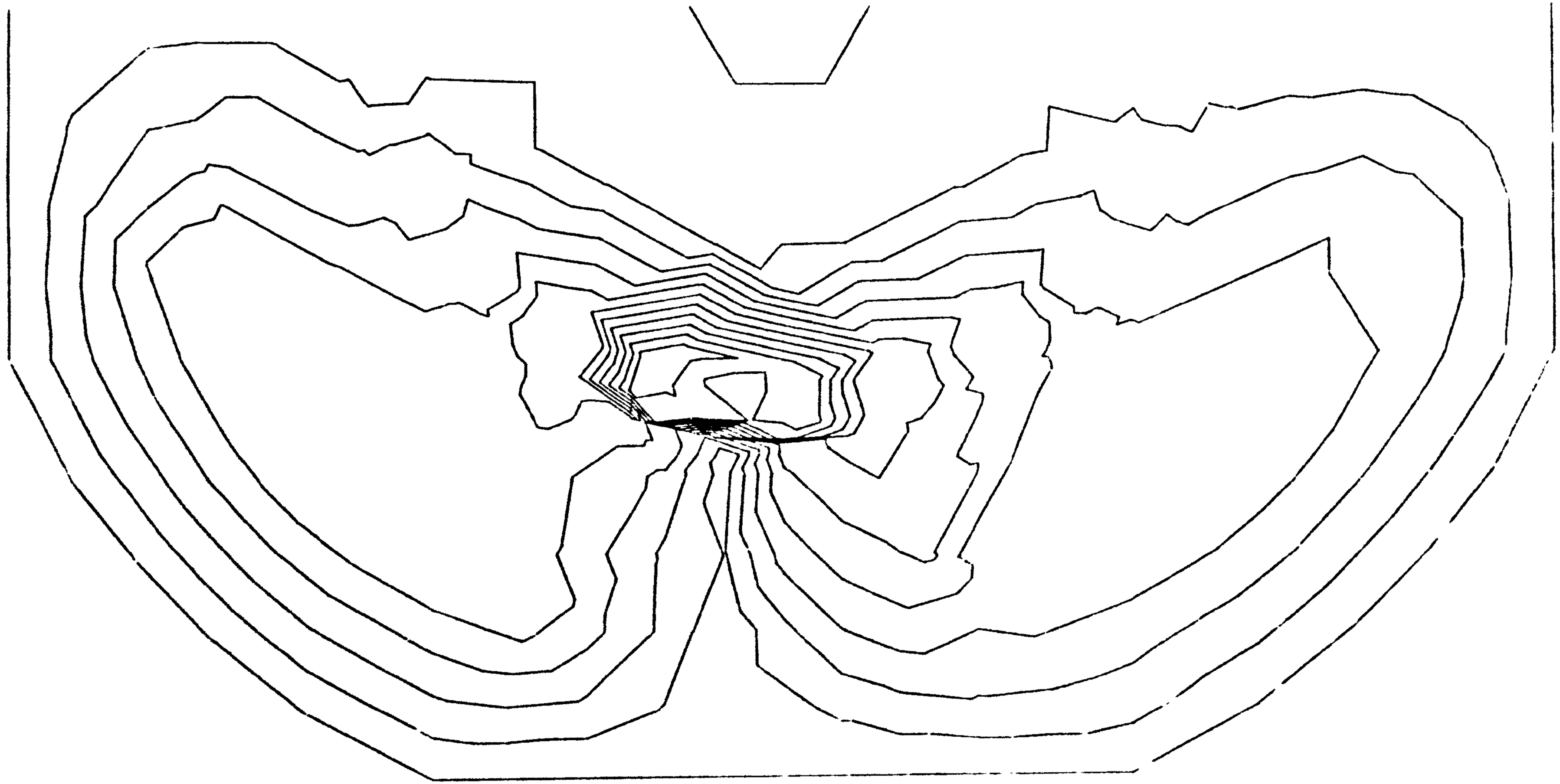

Fig. 5.2.2.a_6 Flux of loop 6 for s = 1, t = 0

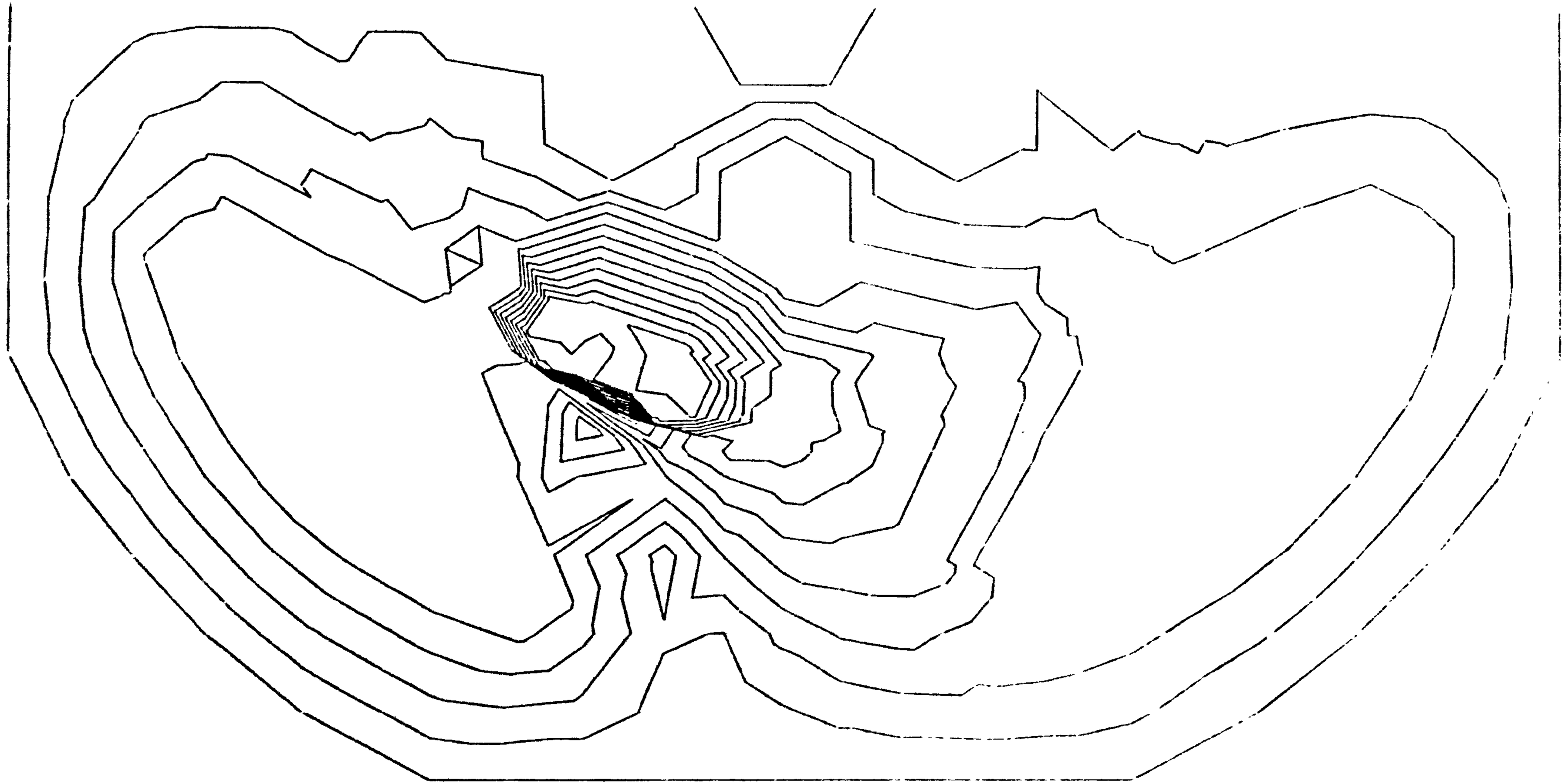

Fig. 5.2.2.a$_7$ Flux of loop 7 for s = 1, t = 0

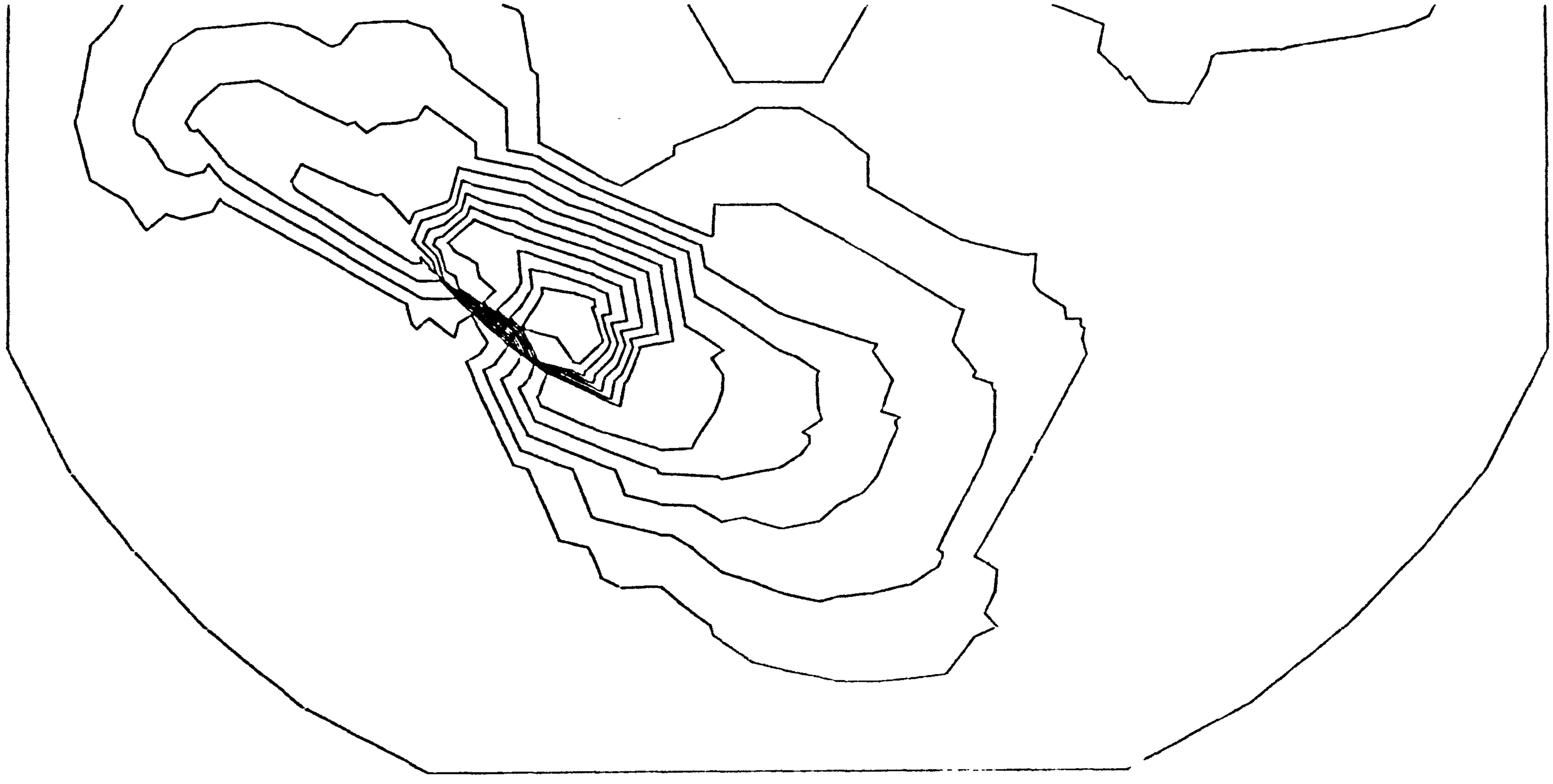

Fig. 5.2.2.a_8 Flux of loop 8 for s = 1, t = 0

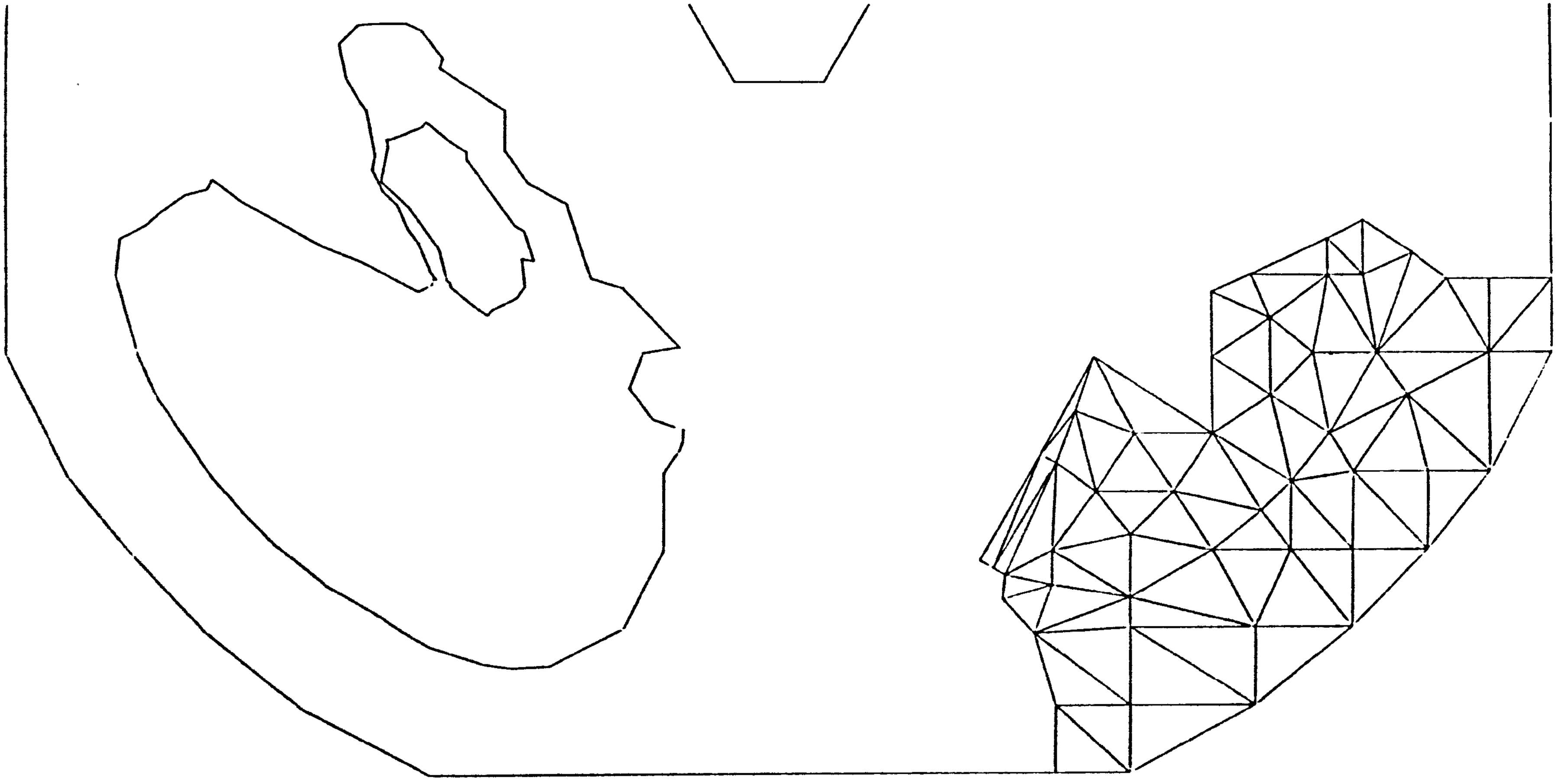

Fig. 5.2.2.ag Flux of loop g for s = 1, t = 0

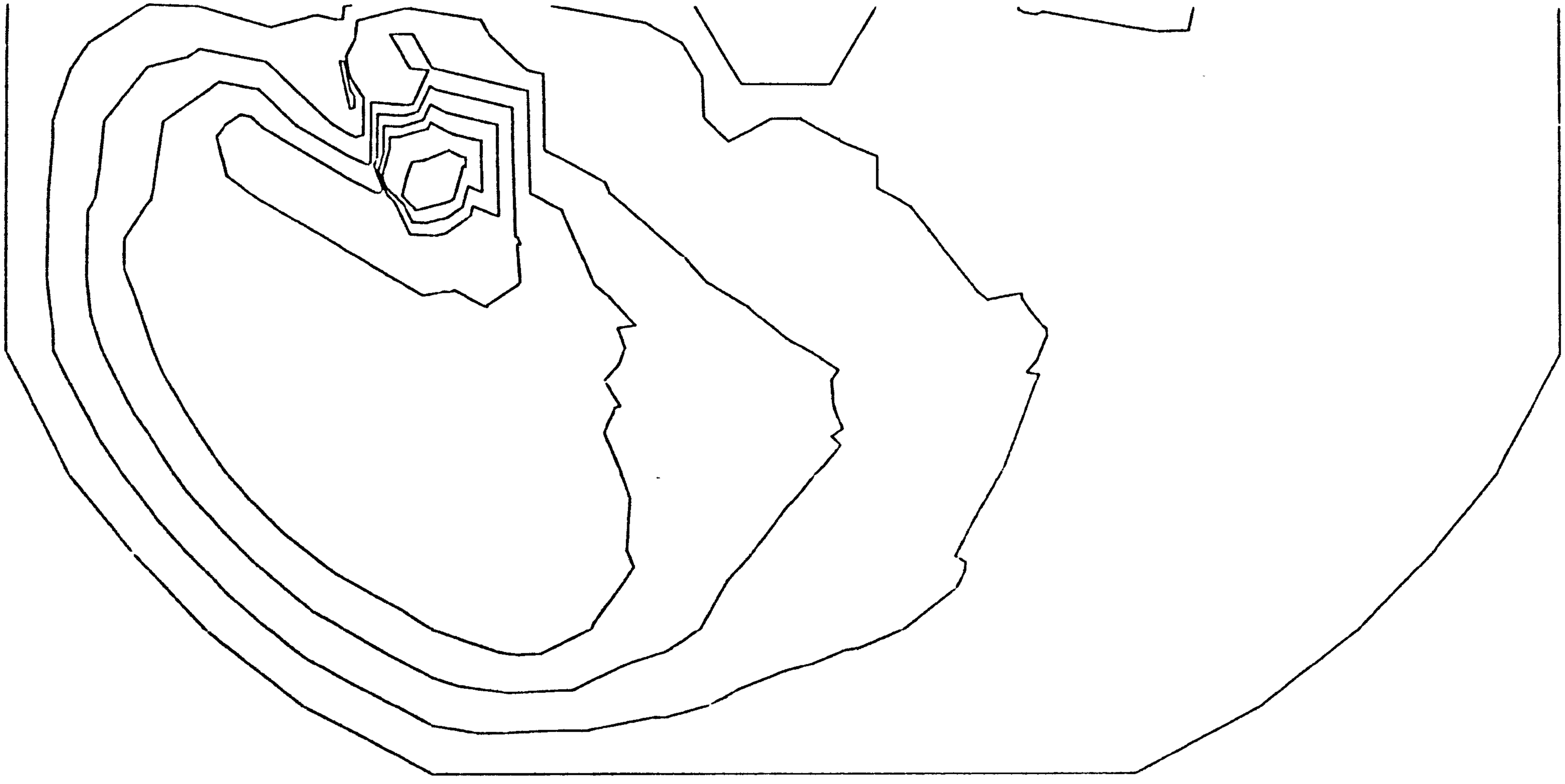

Fig. 5.2.2.a_{10} Flux of loop 10 for s = 1, t = 0

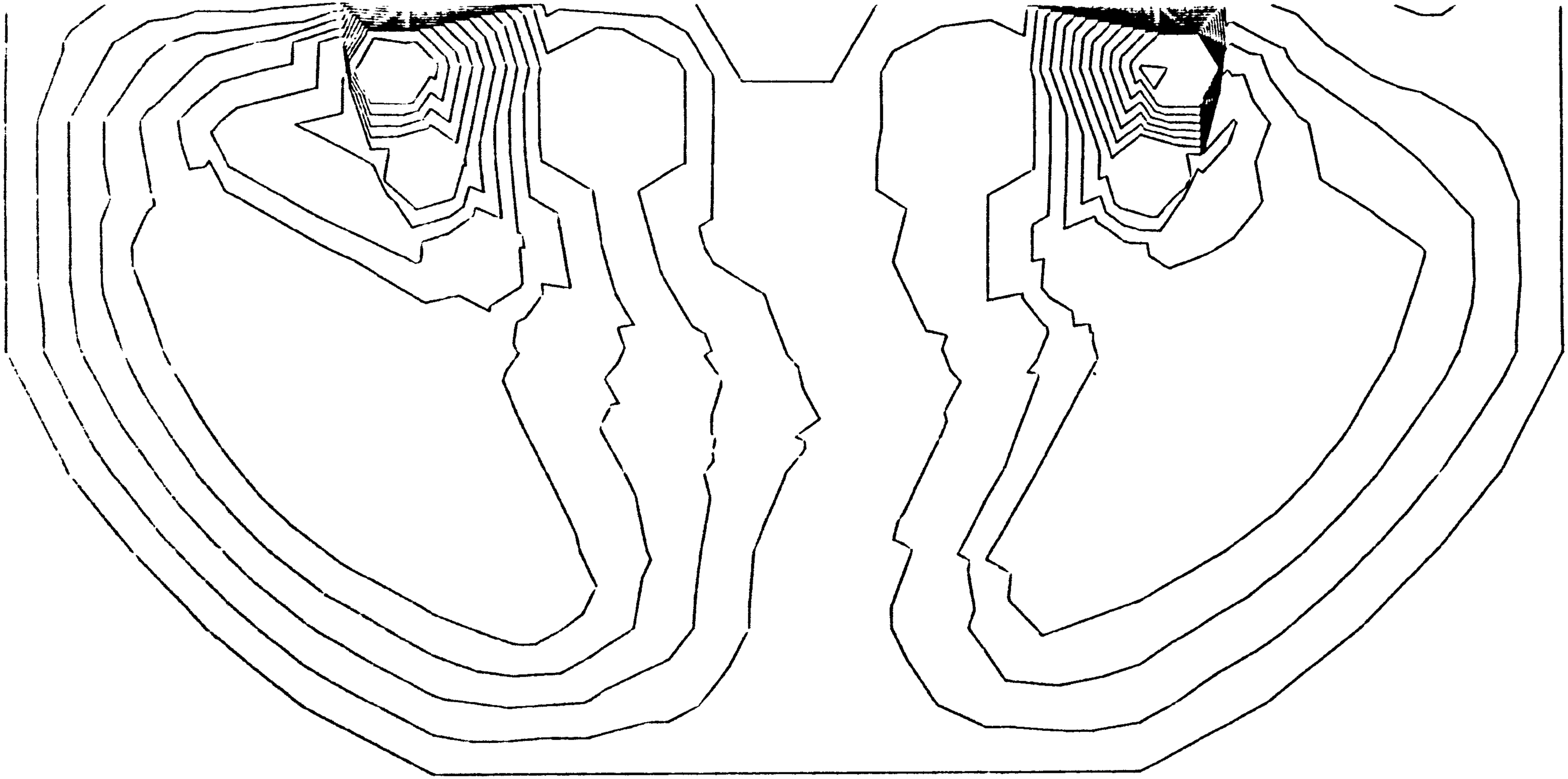

Fig. 5.2.2.a_{11} Flux of loop 11 for s = 1, t = 0

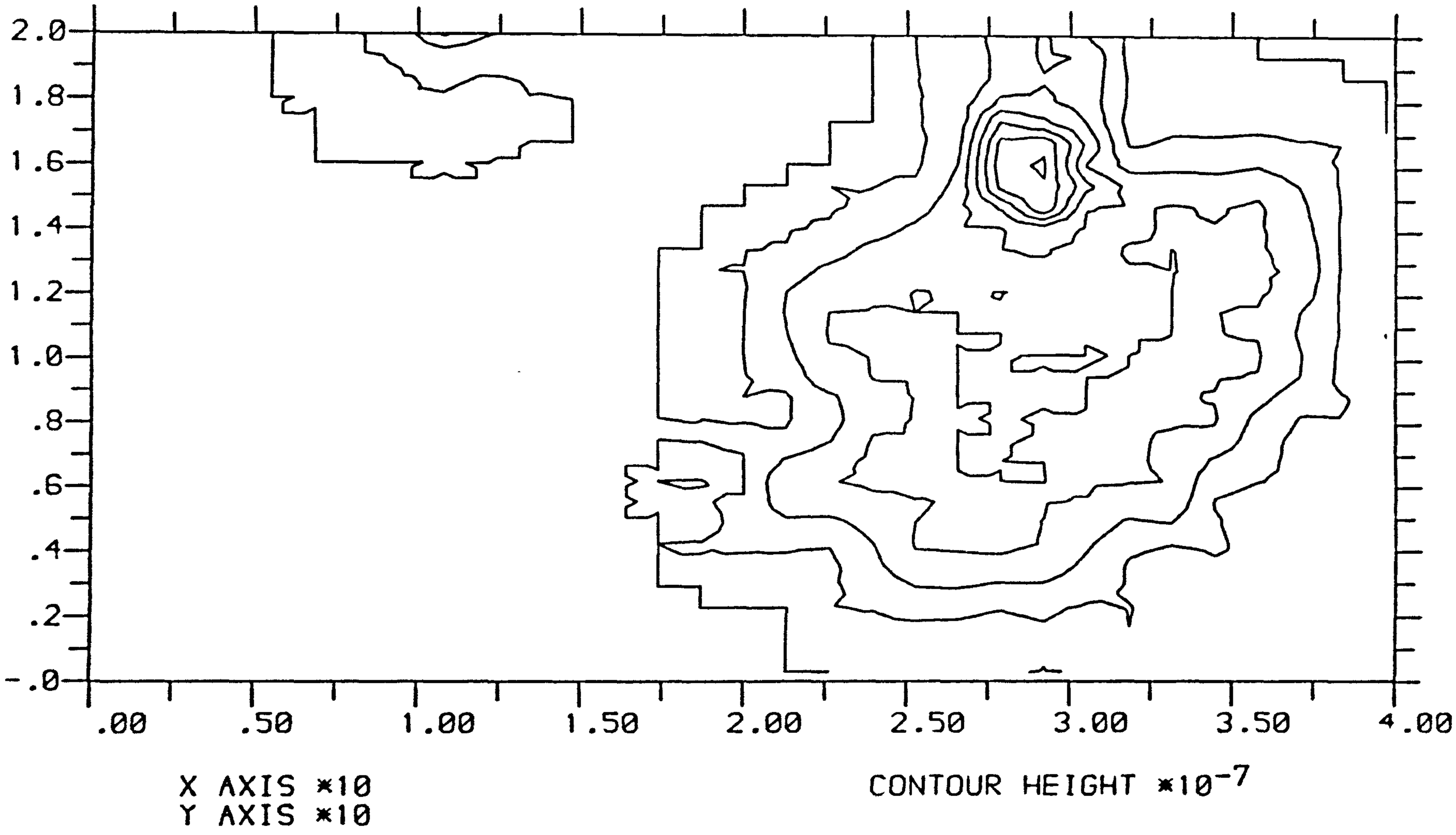

Fig. 5.2.3.a_1 Flux of loop 1 for s = 1, t = 5 m.sec

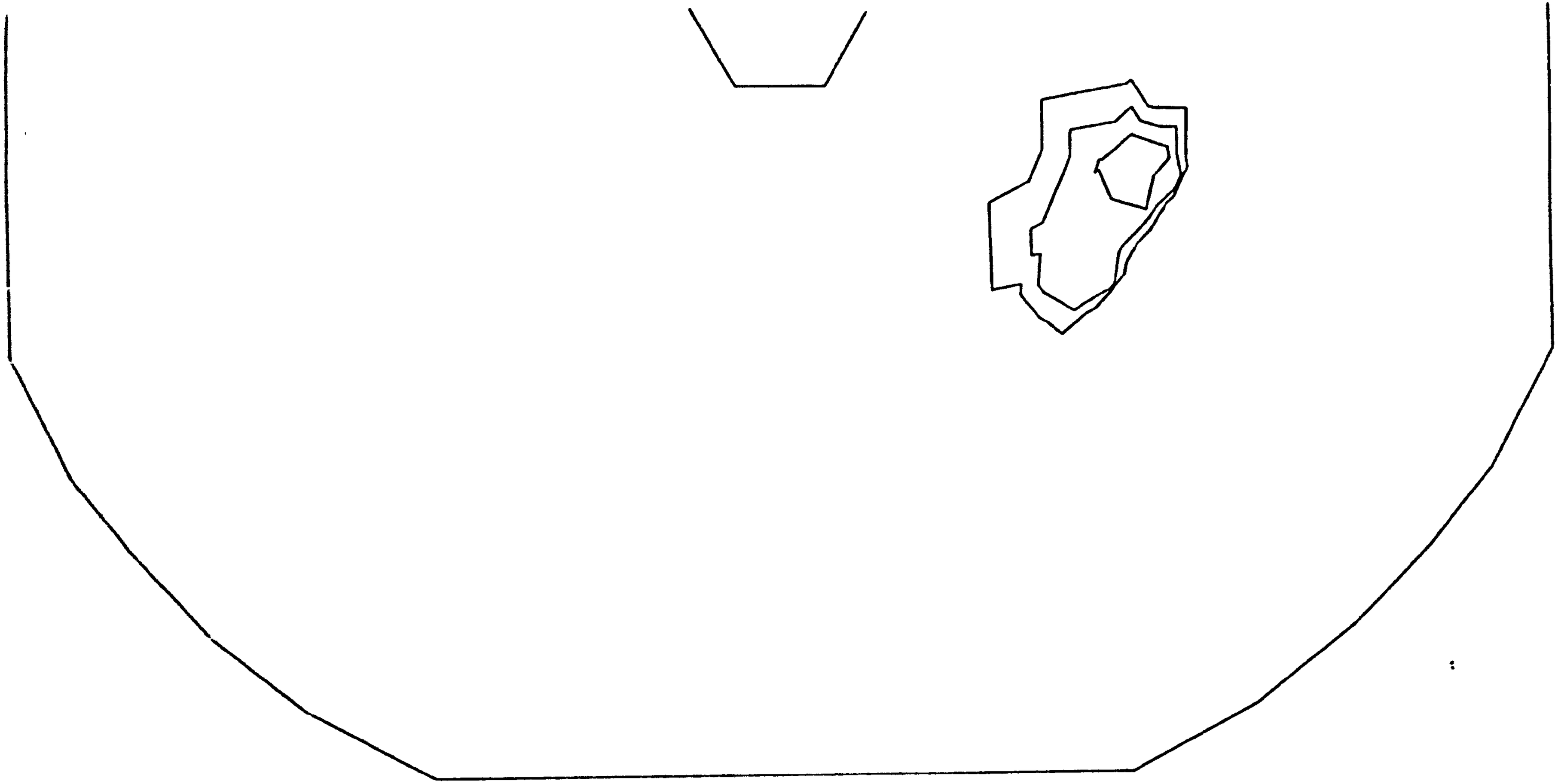

Fig. 5.2.3.a_2 Flux of loop 2 for s = 1, t = 5 m.sec

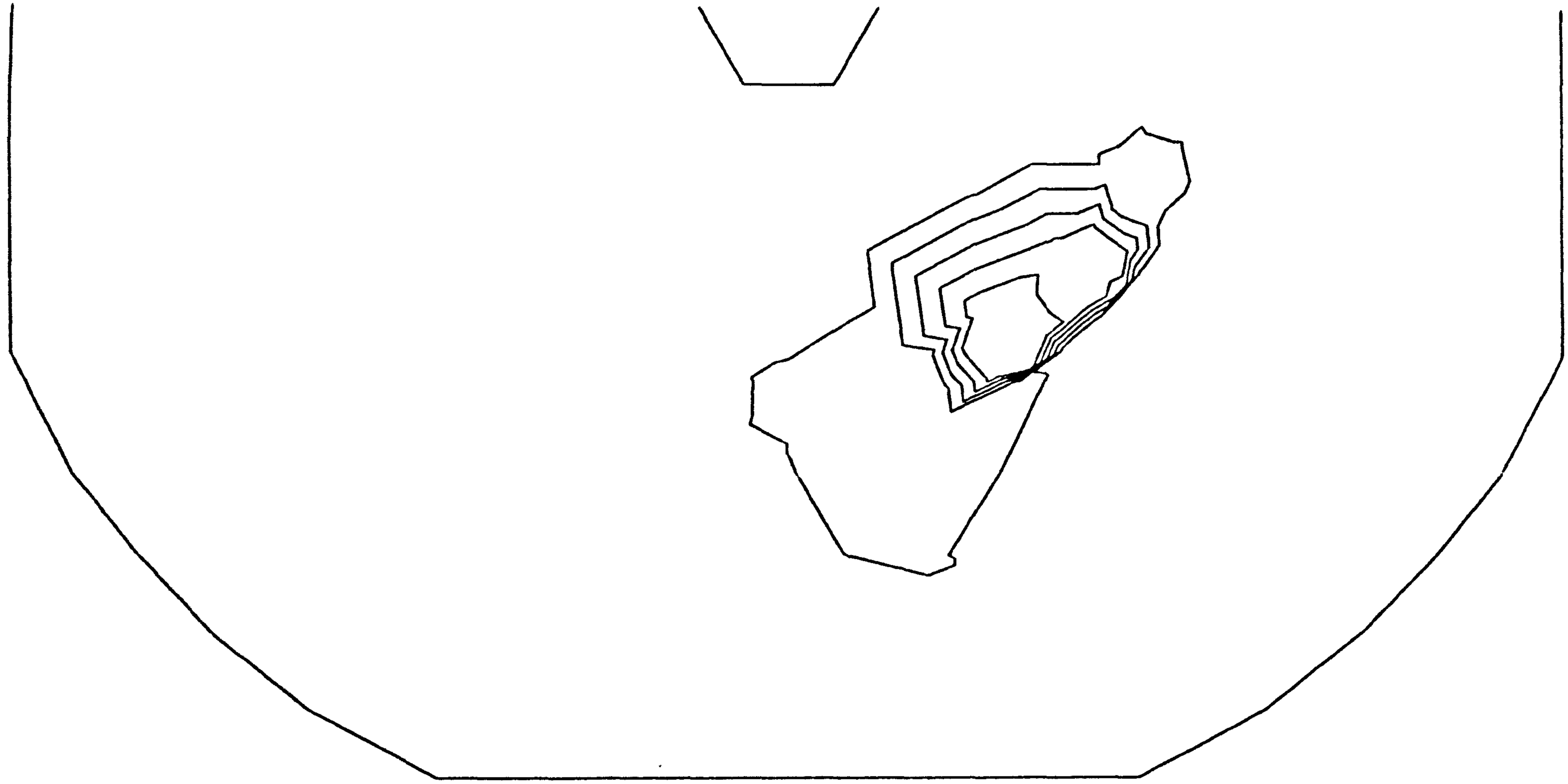

Fig. 5.2.3.a_3 Flux of loop 3 for s = 1, t = 5 m.sec

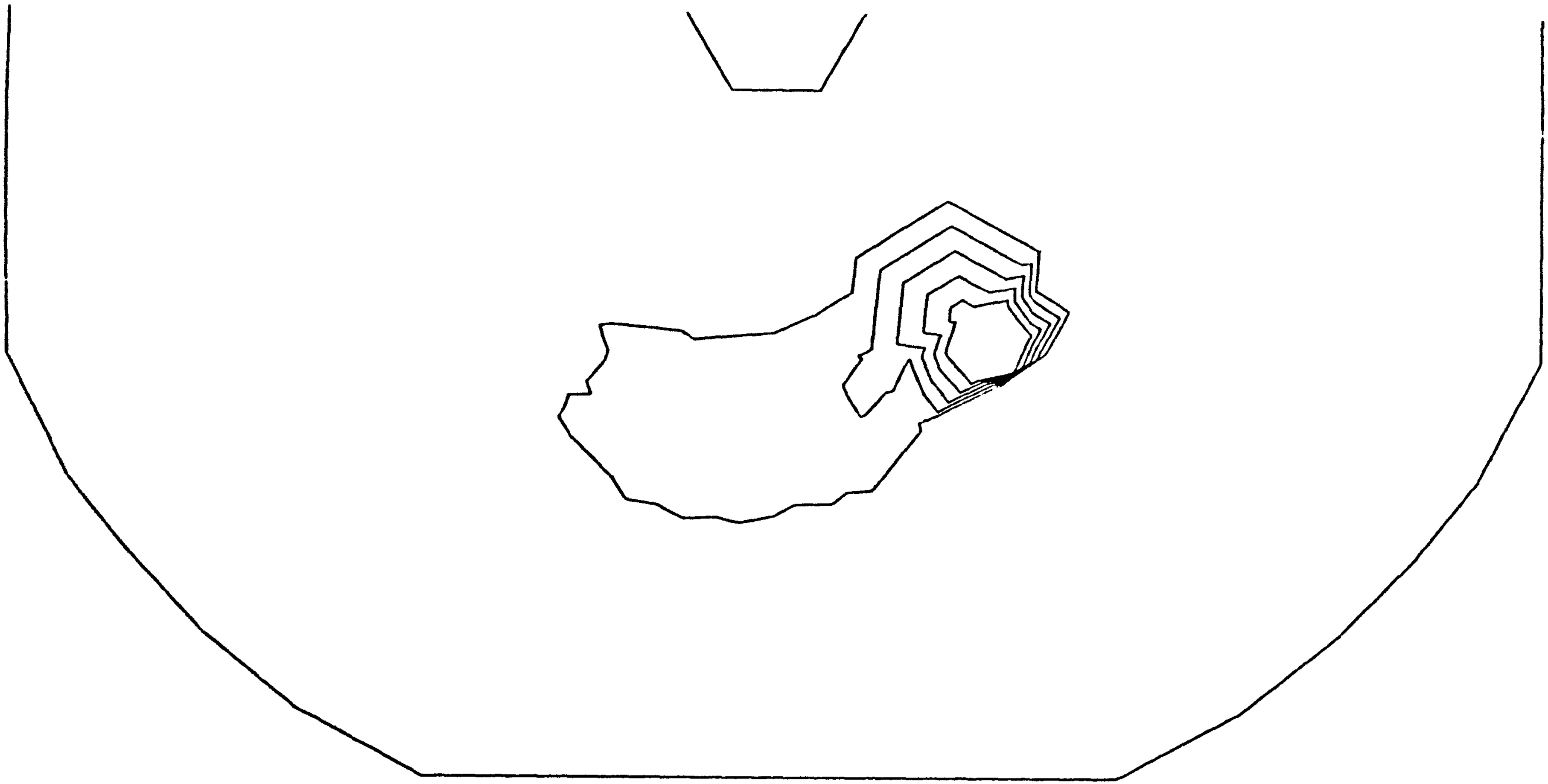

Fig. 5.2.3a$_4$ Flux of loop 4 s = 1, t = 5 m.sec

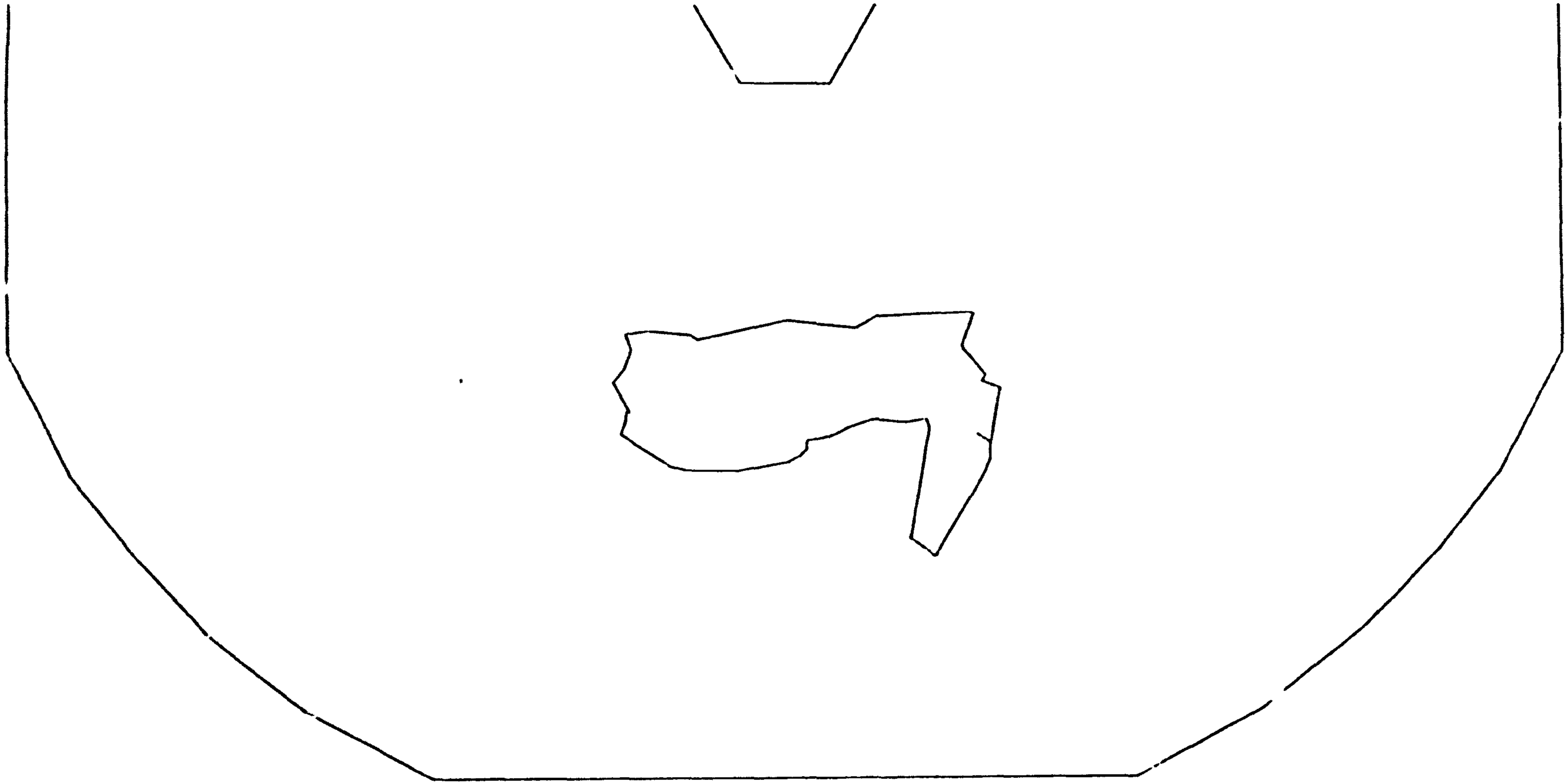

Fig. 5.2.3.a_5 Flux of loop 5 s = 1, t = 5 m.sec

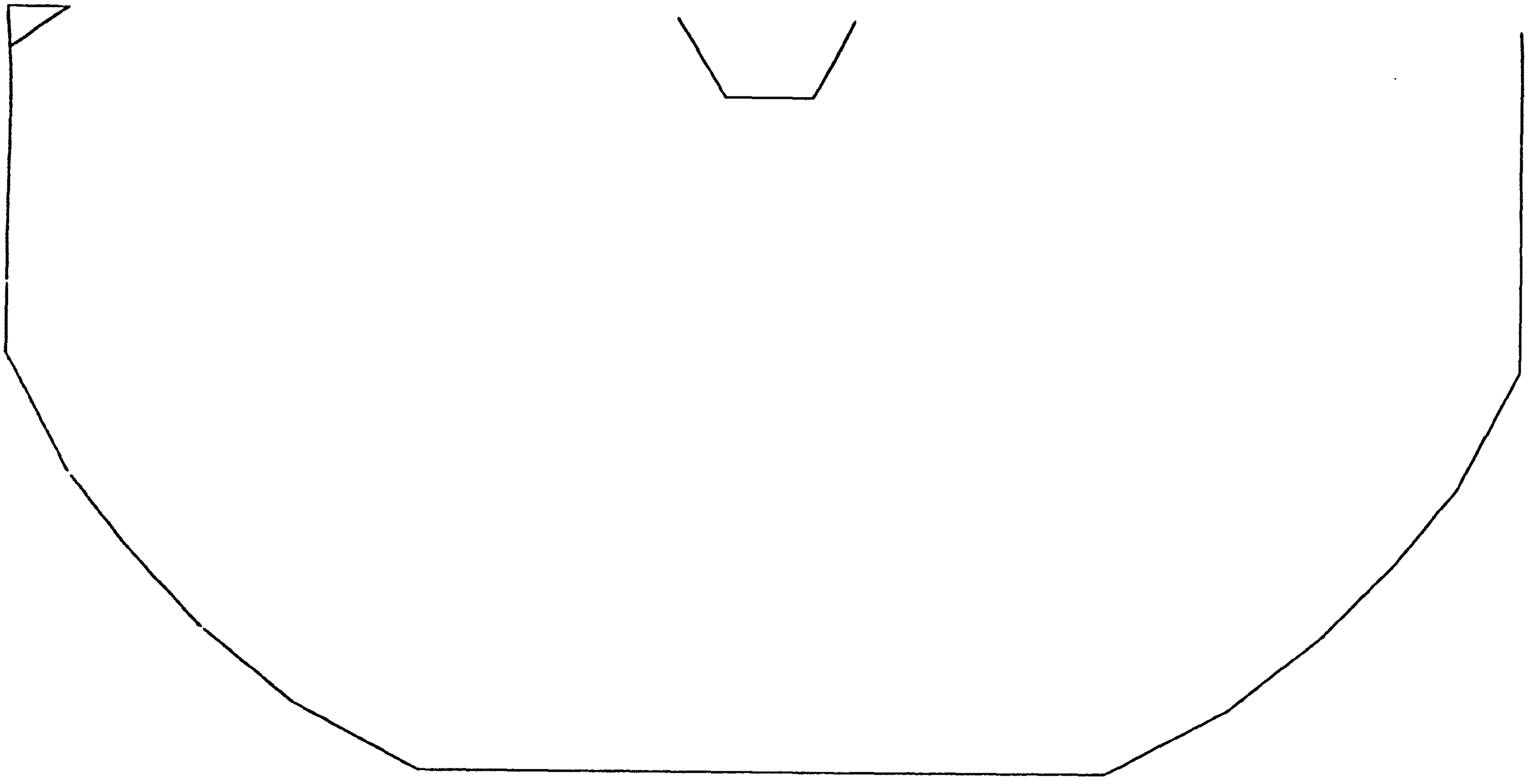

Fig. 5.2.3.a_6 Flux of loop 6 for s = 1, t = 5 m.sec

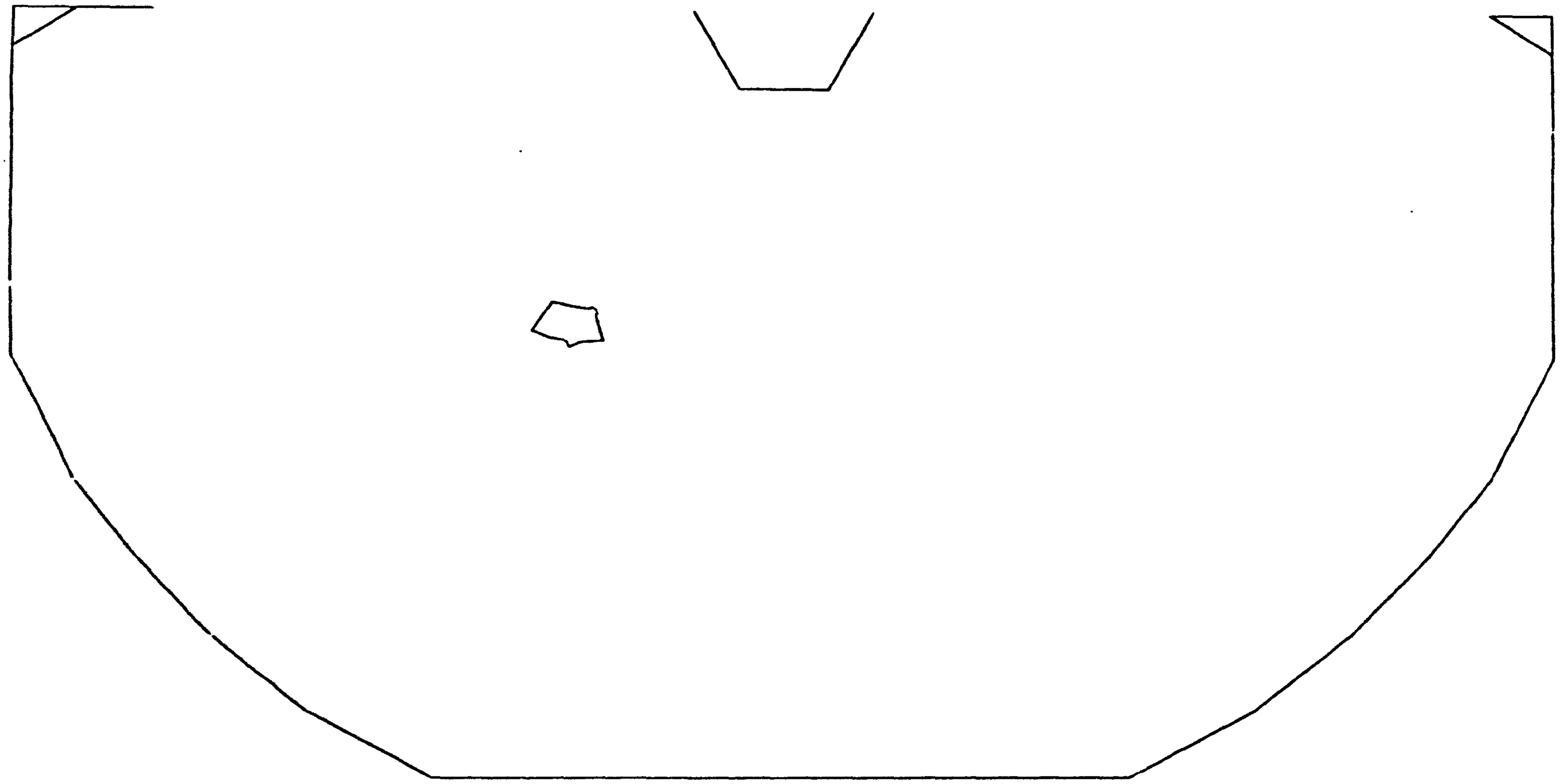

Fig. 5.2.3.a_7 Flux of loop 7 for s = 1, t = 5 m.sec

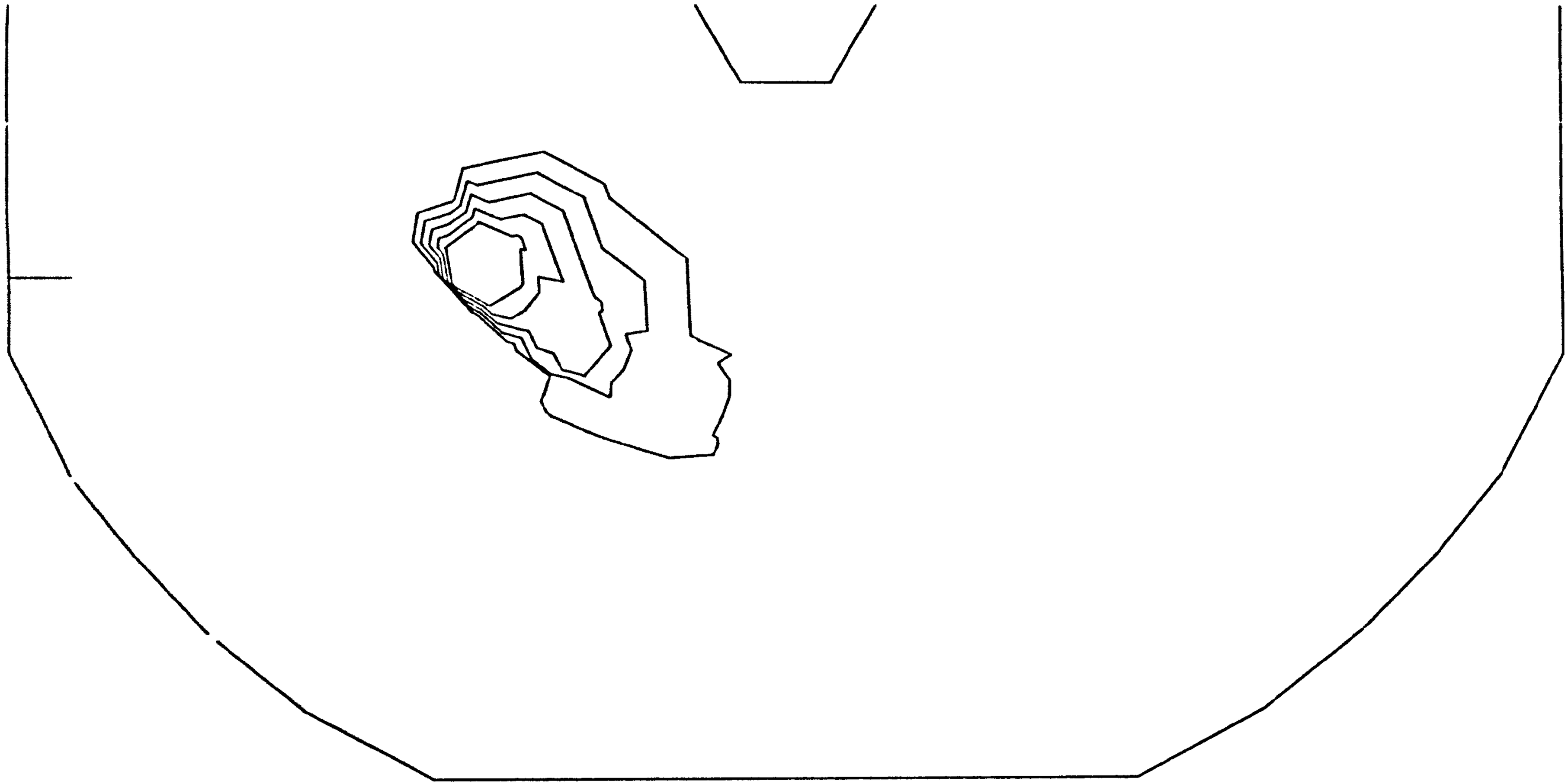

Fig. 5.2.3.a_8 Flux of loop 8 for s = 1, t = 5 m.sec

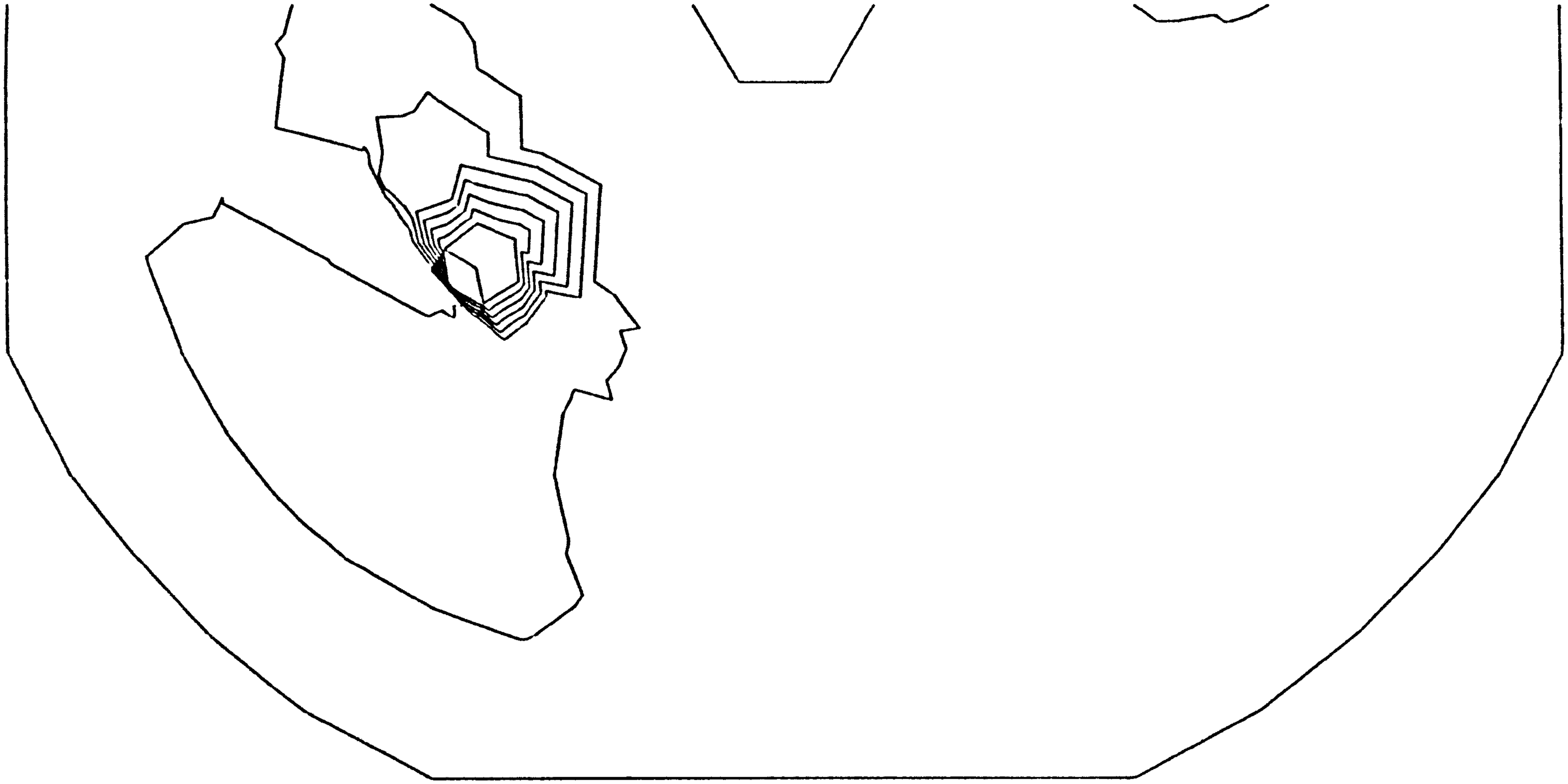

Fig. 5.2.3.a_9 Flux of loop 9 for s = 1, t = 5 m.sec

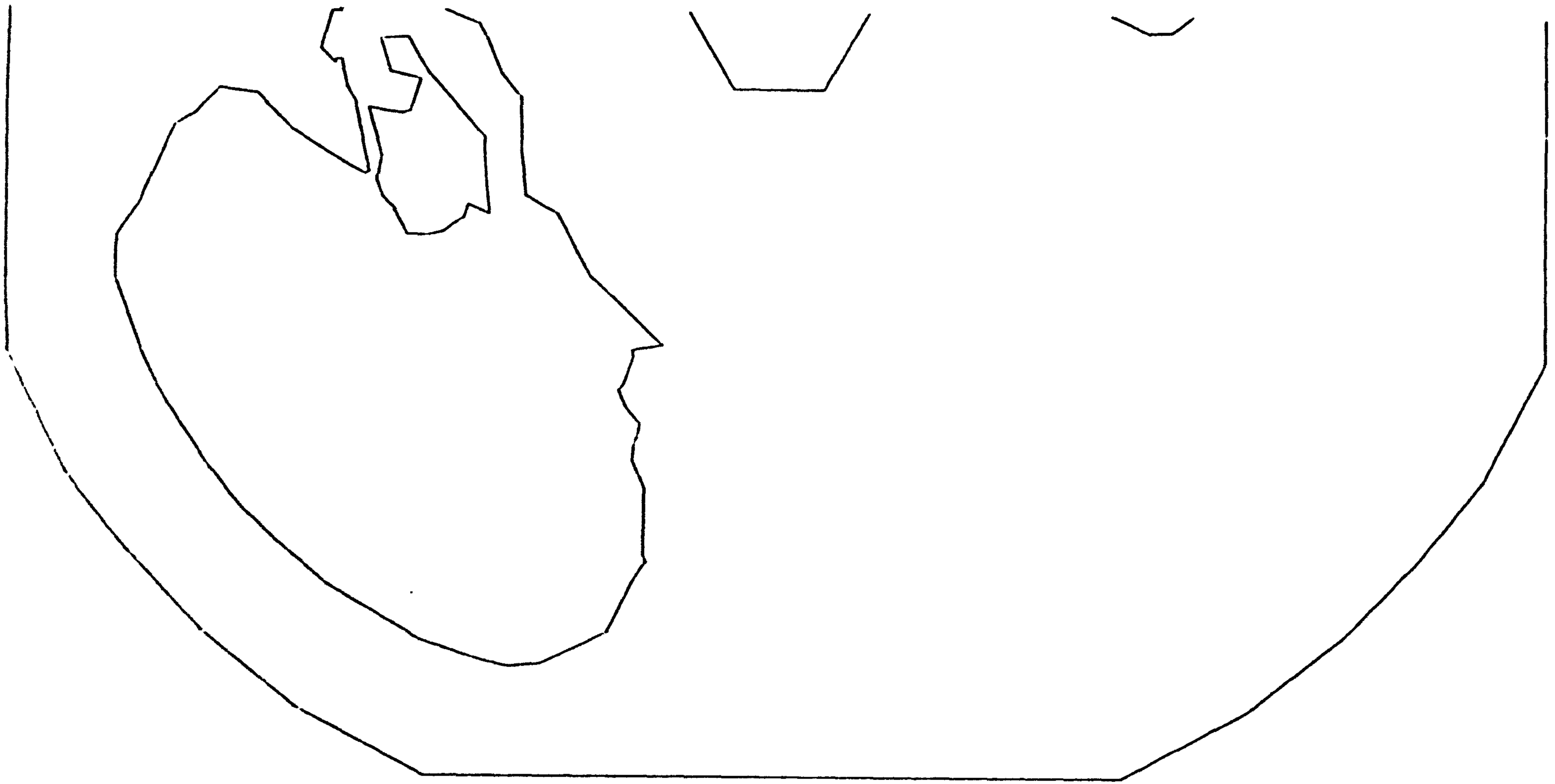

Fig. 5.2.3.a_{10} Flux of loop 10 for s = 1, t = 5 m.sec

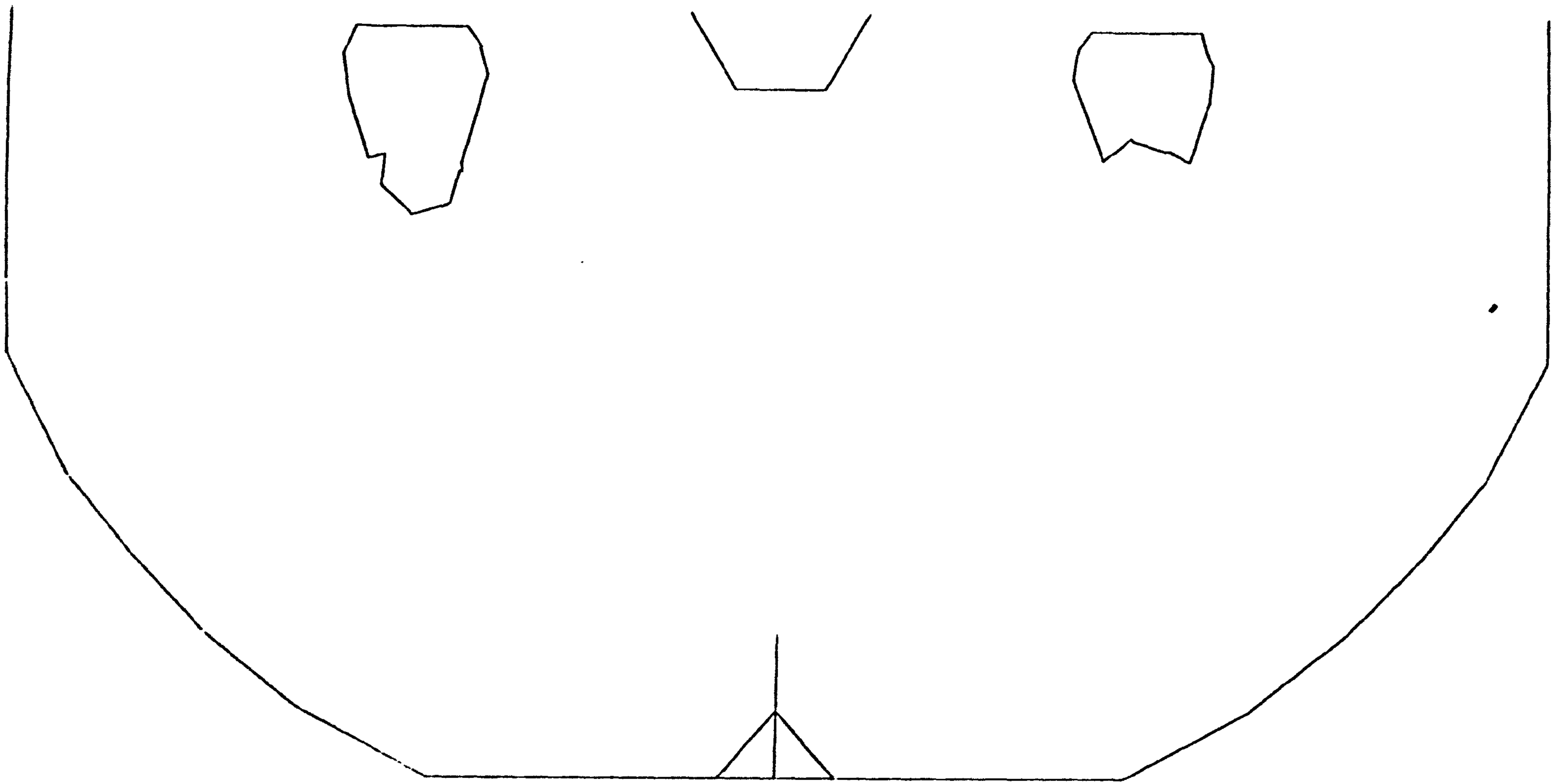

Fig. 5.2.3.a_{11} Flux of loop 11 for s = 1, t = 5 m.sec

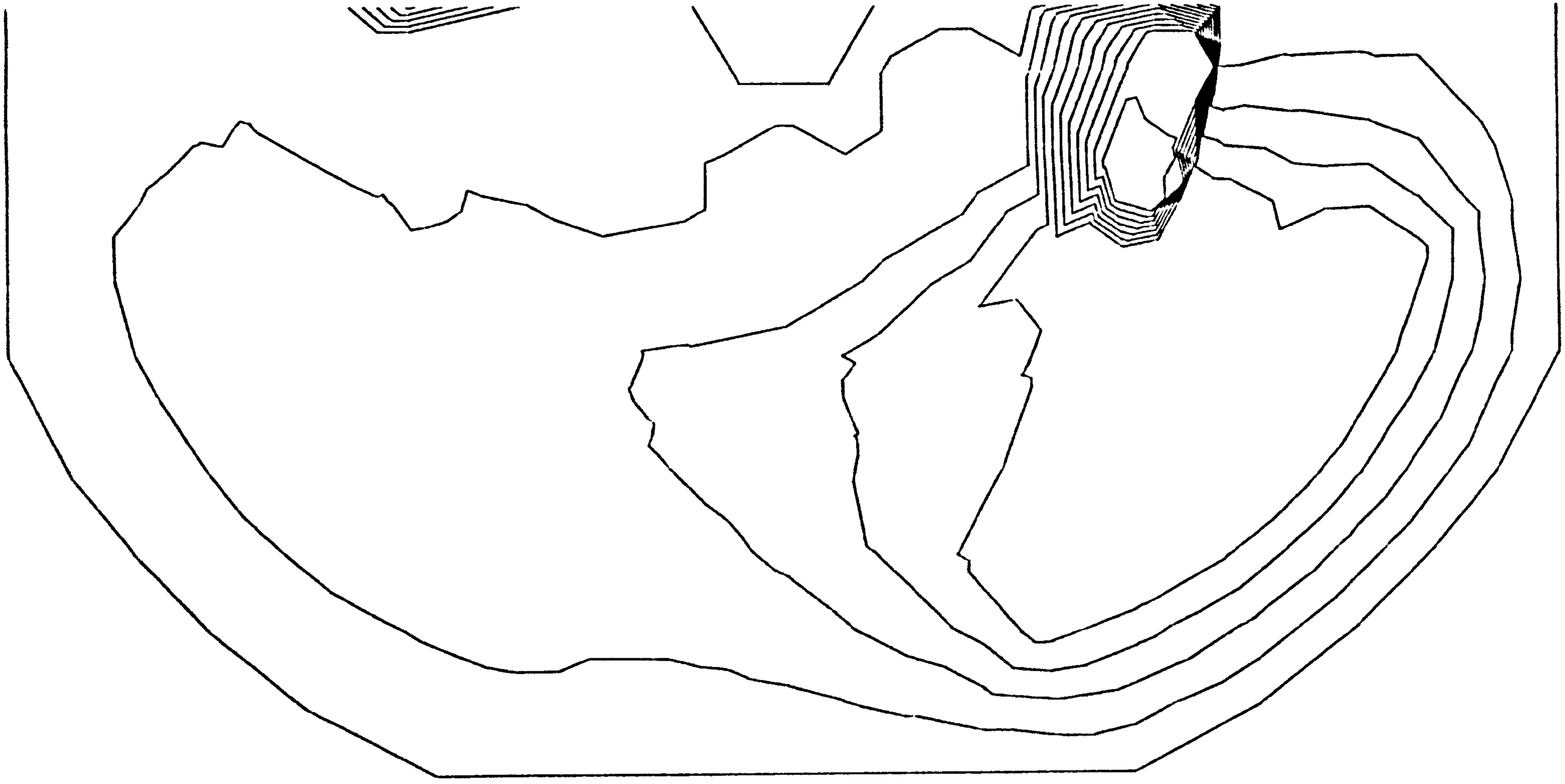

Fig. 5.2.4.b_1 Flux of loop 1 for s = 0.05, t = 0

Fig. 5.2.4.b_2 Flux of loop 2 for s = 0.05, t = 0

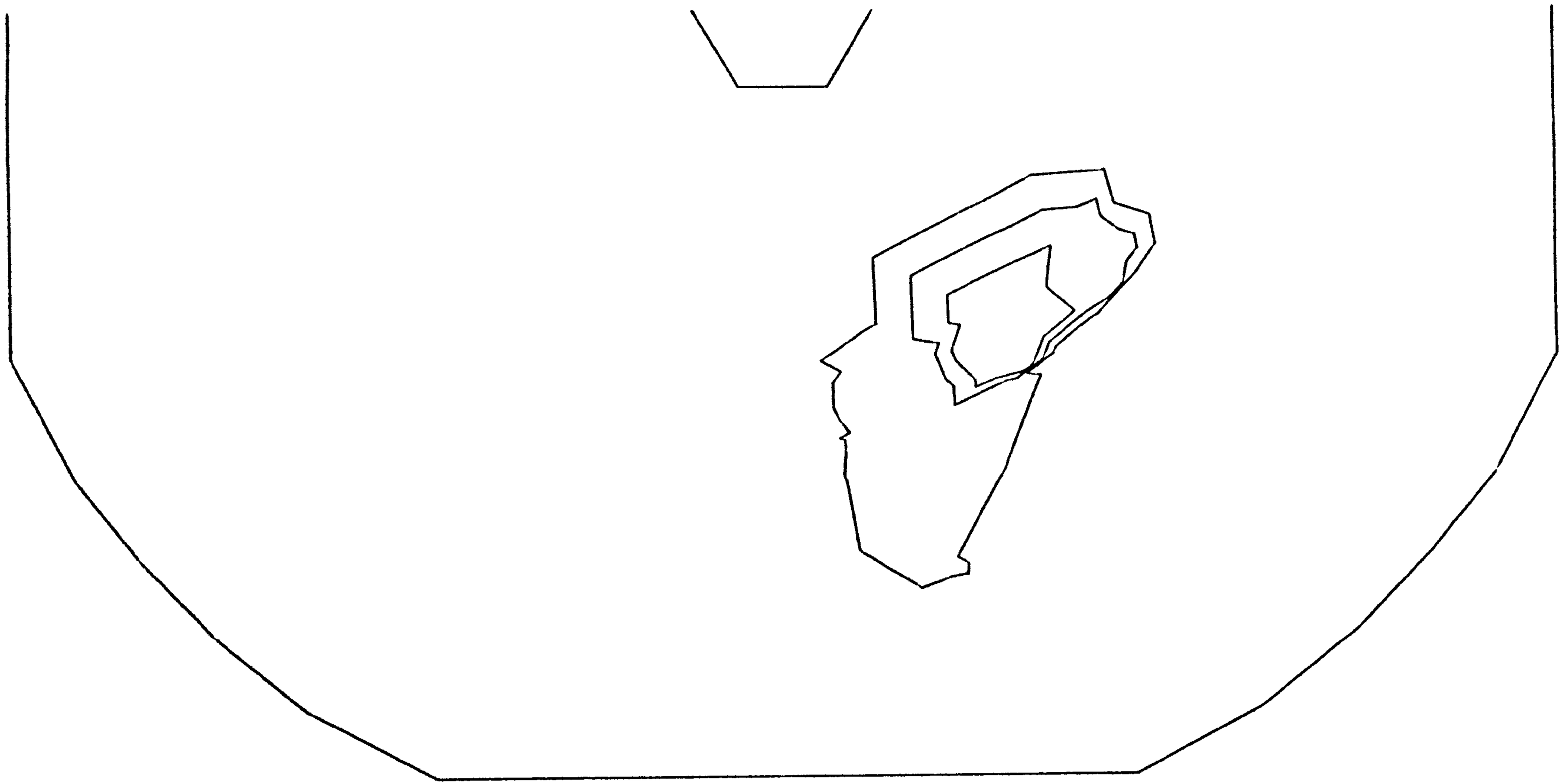

Fig. 5.2.4.b_3 Flux of loop 3 for s = 0.05, t = 0

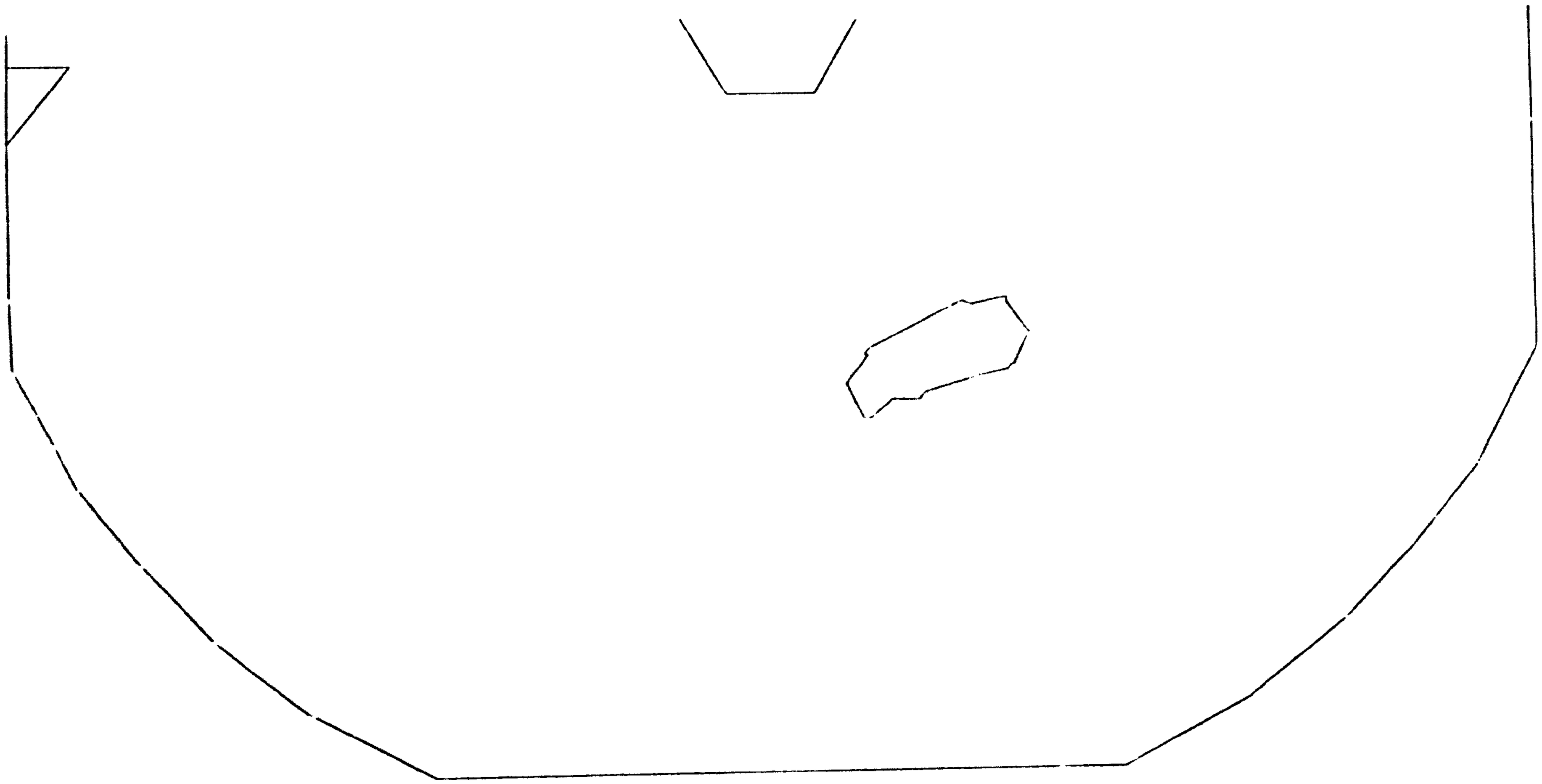

Fig. 5.2.4.b_4 Flux of loop 4 for s = 0.05, t = 0

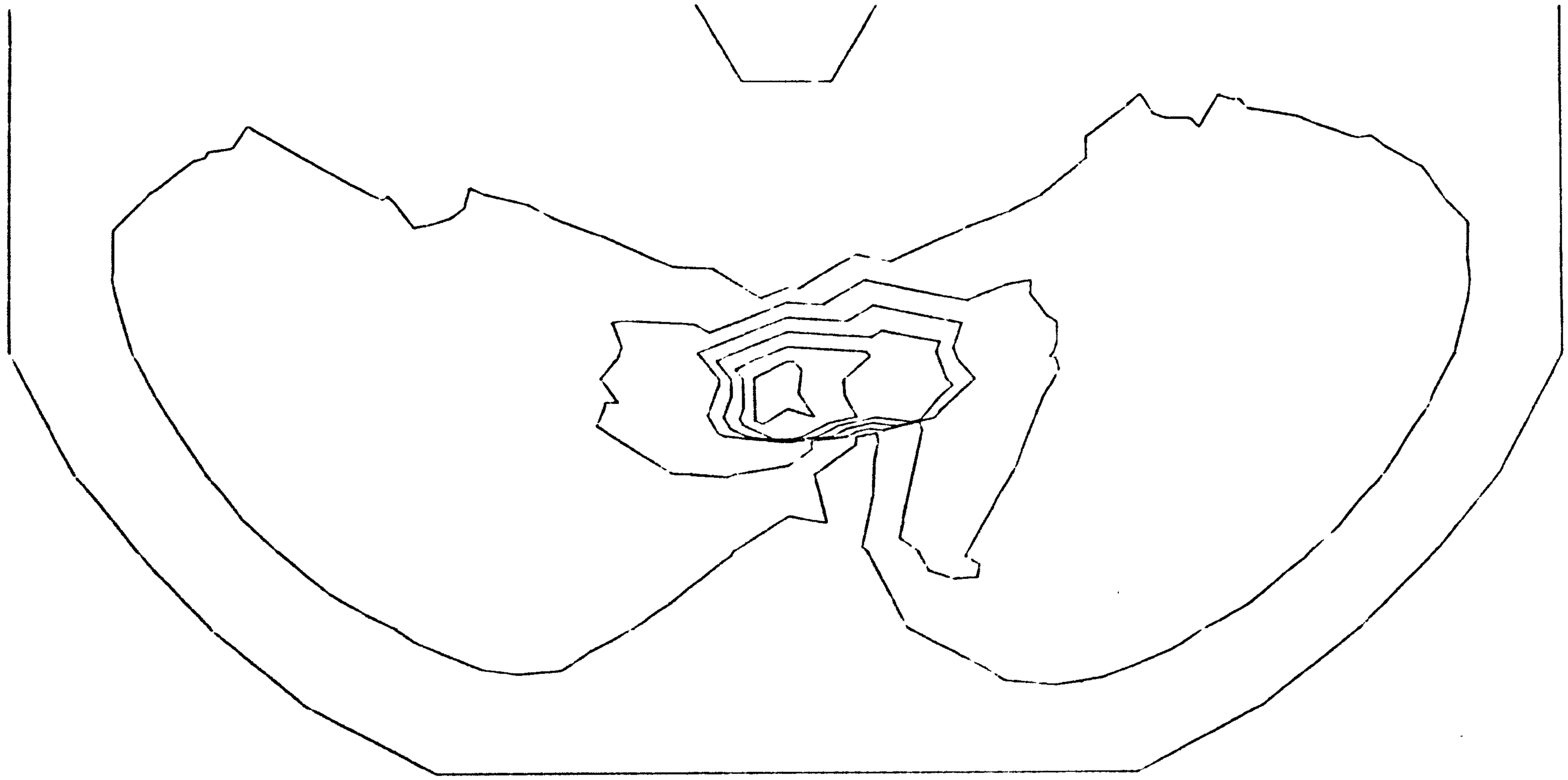

Fig. 5.2.4.b_5 Flux of loop 5 for s = 0.05, t = 0

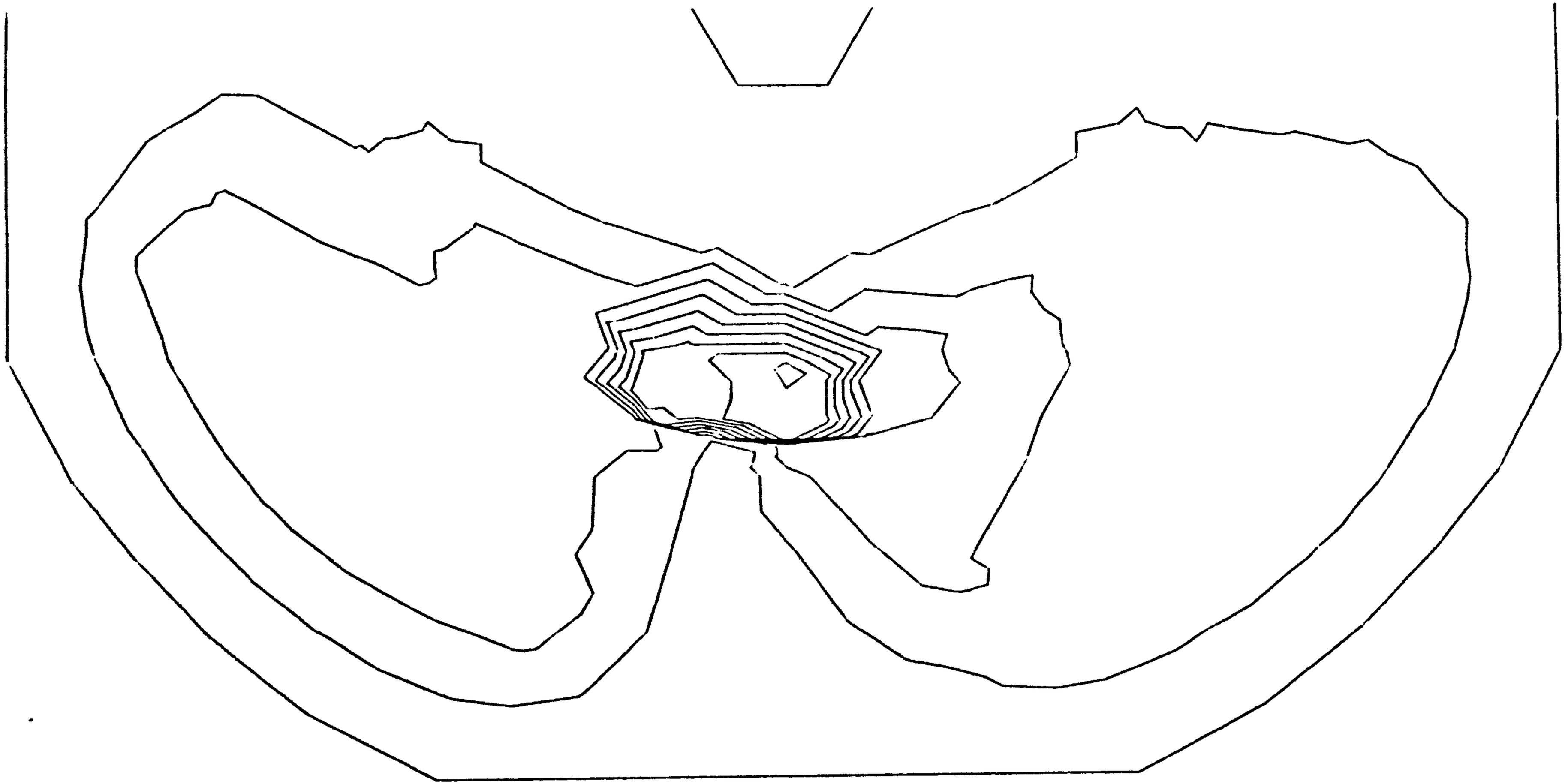

Fig. 5.2.4.b_6 Flux of loop 6 for s = 0.05, t = 0

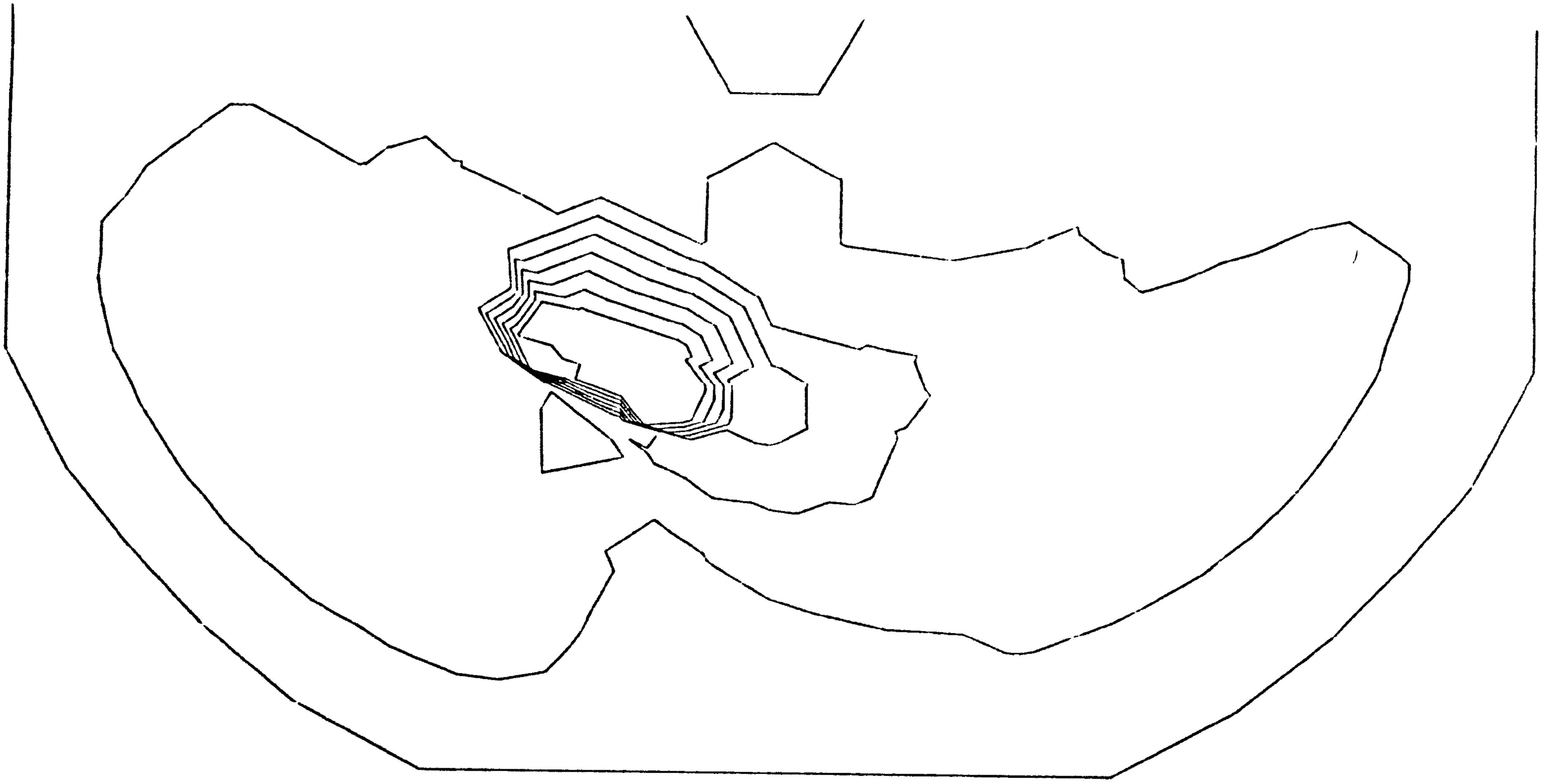

Fig. 5.2.4.b$_7$ Flux of loop 7 for s = 0.05, t = 0

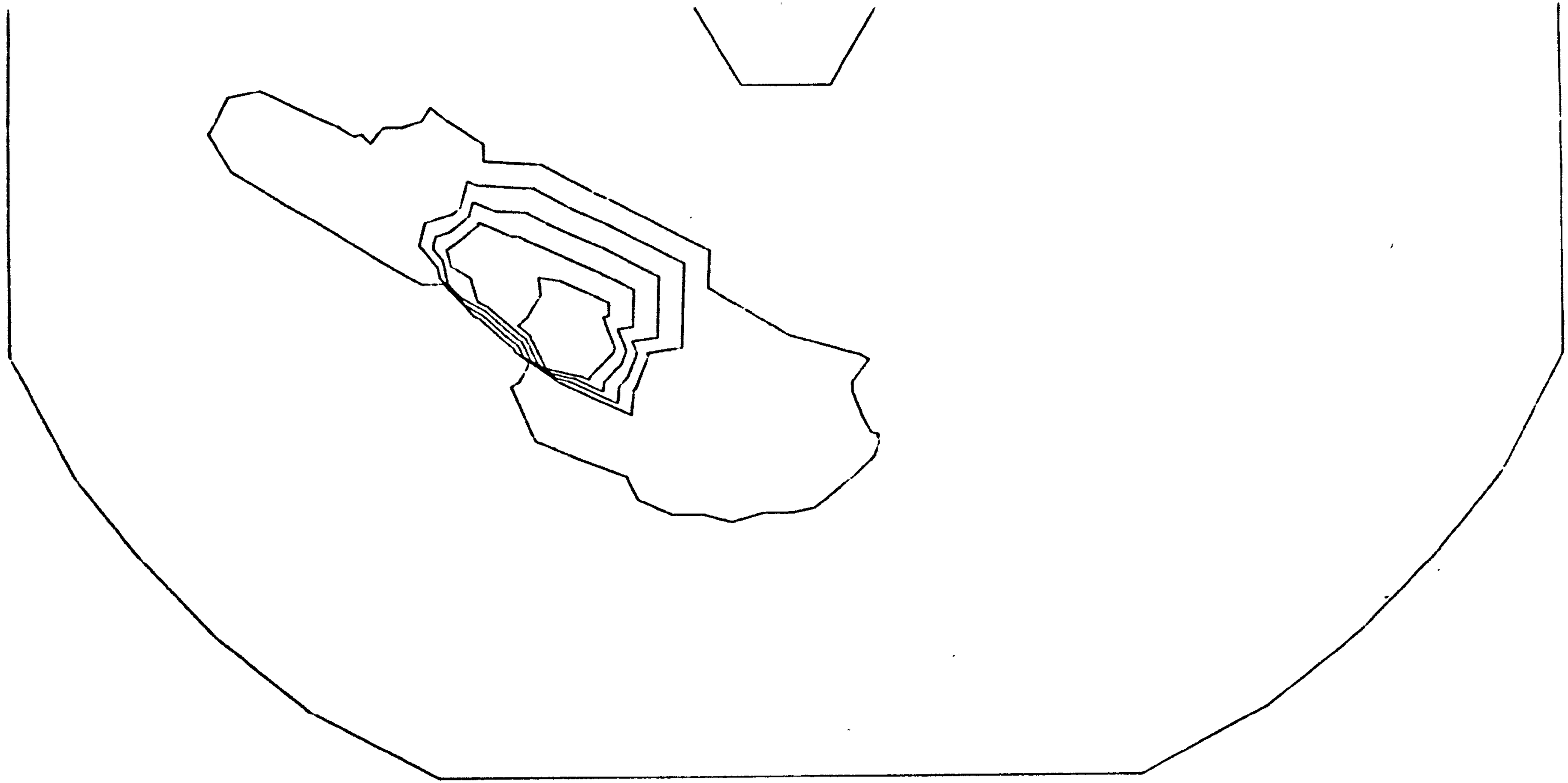

Fig. 5.2.4.b_8 Flux of loop 8 for s = 0.05, t = 0

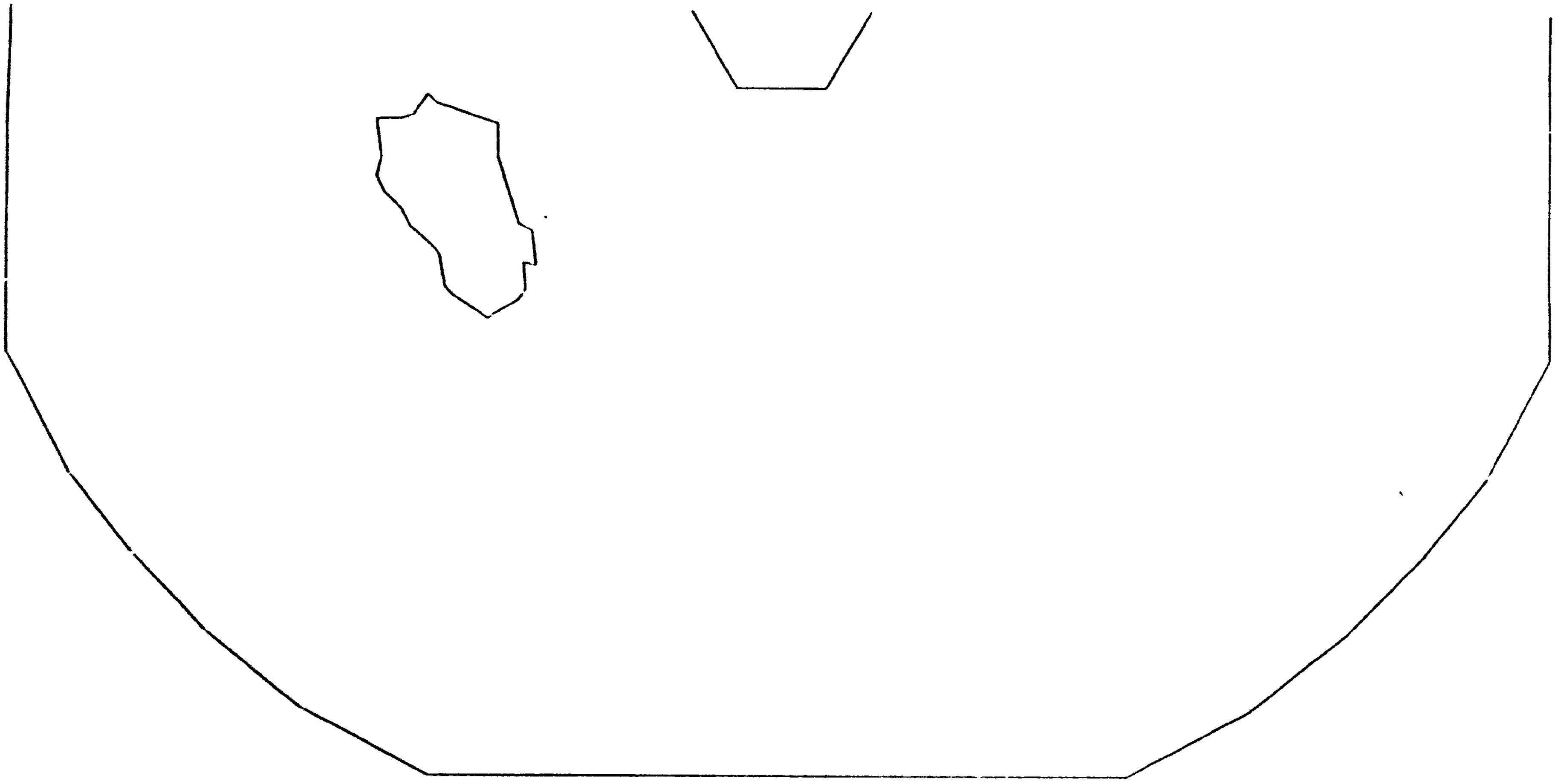

Fig. 5.2.4.b_9 Flux of loop 9 for s = 0.05, t = 0

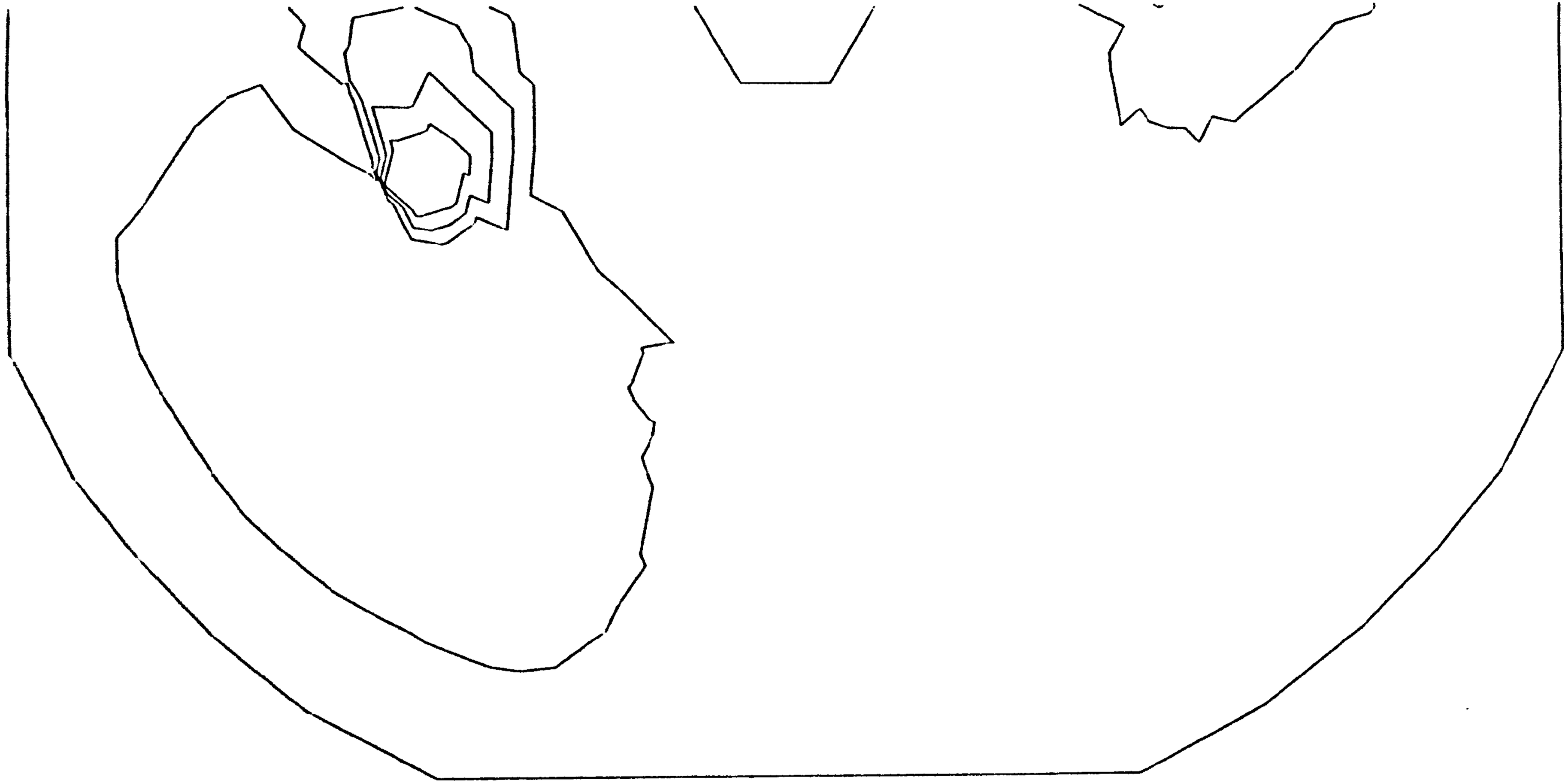

Fig. 5.2.4.b_{10} Flux of loop 10 for s = 0.05, t = 0

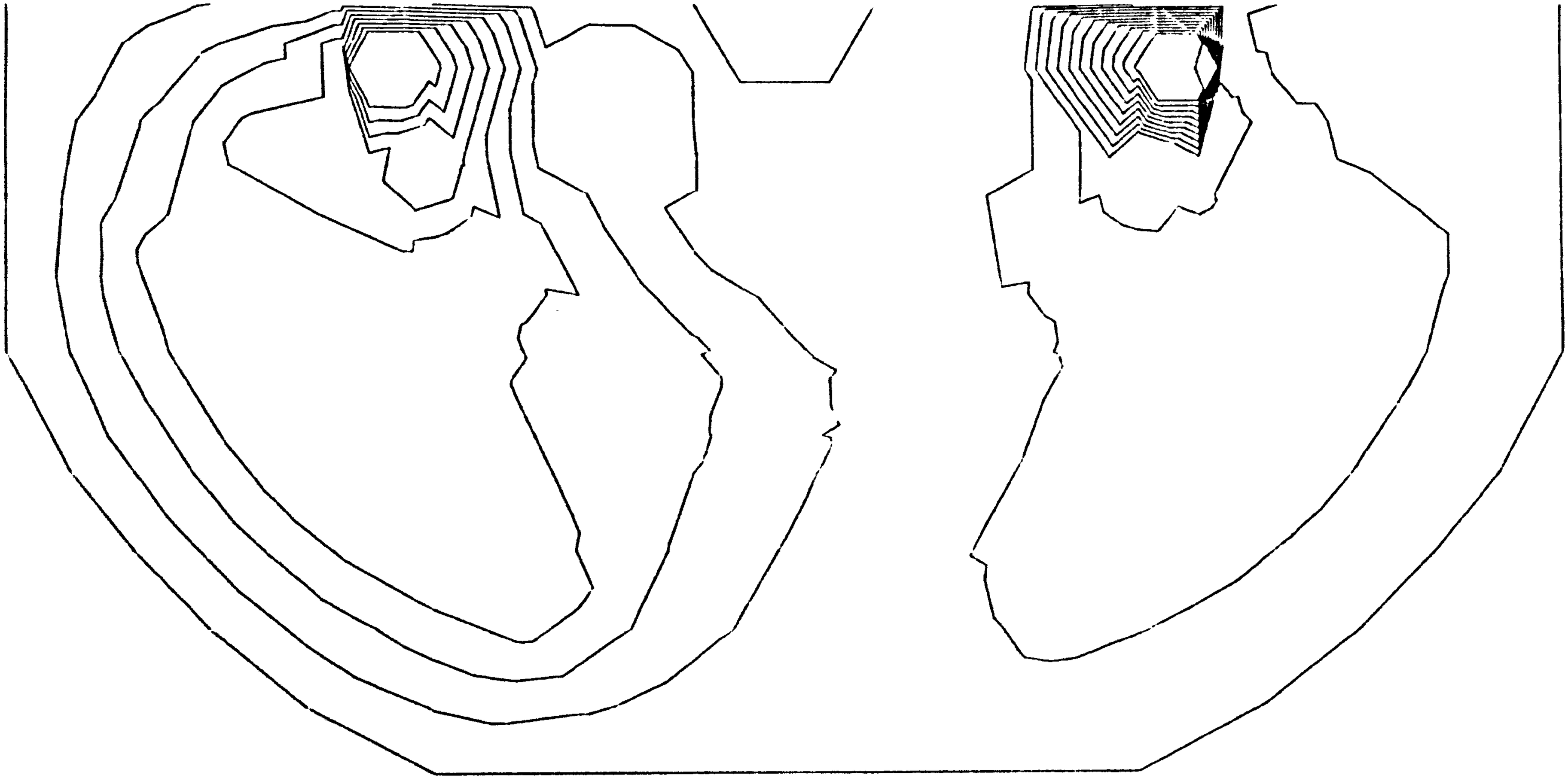

Fig. 5.2.4.b_{11} Flux of loop 11 for s = 0.05, t = 0

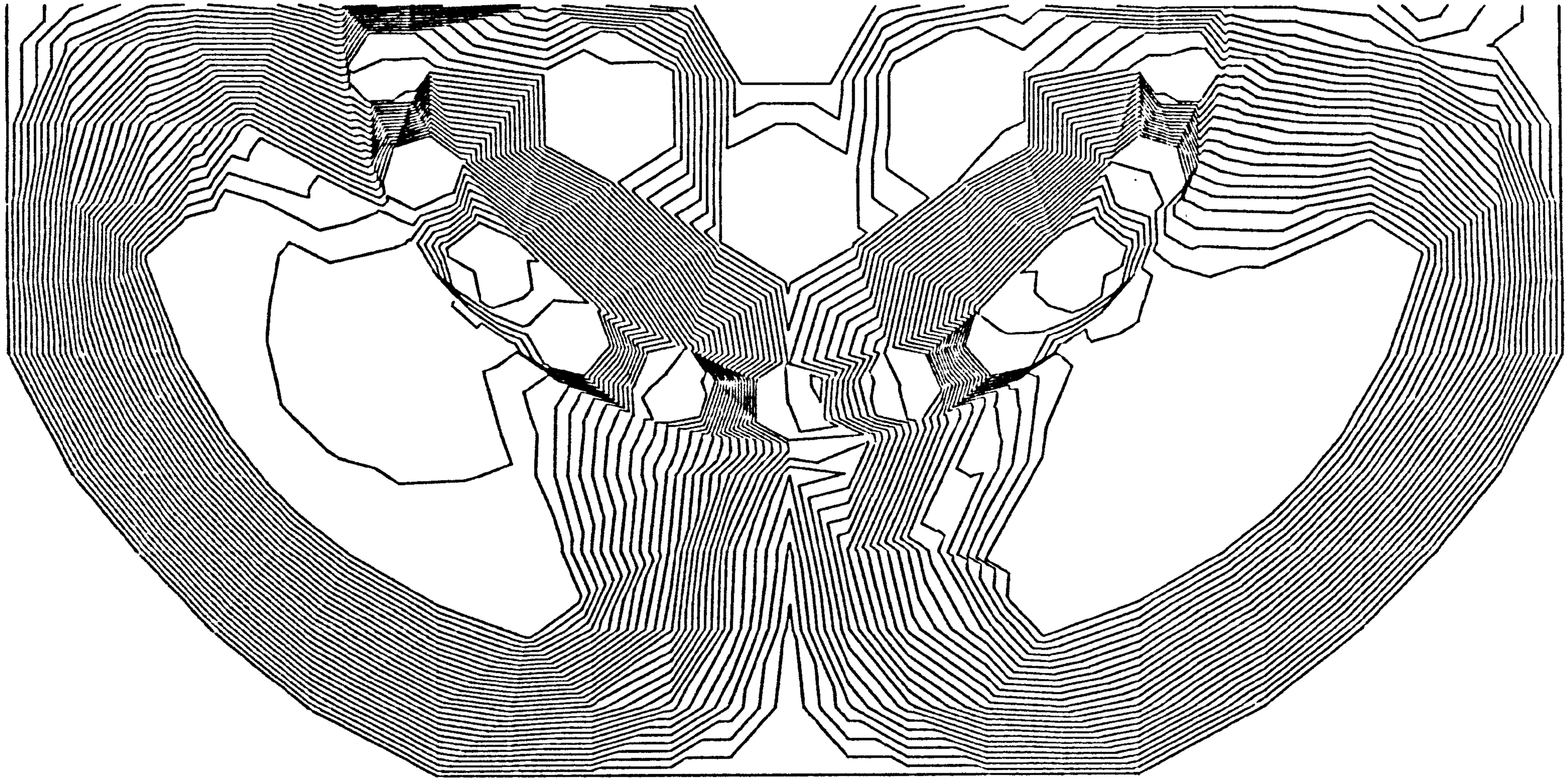

Fig. 5.2.5a Flux of rotor bars (s = 1, t = 0)

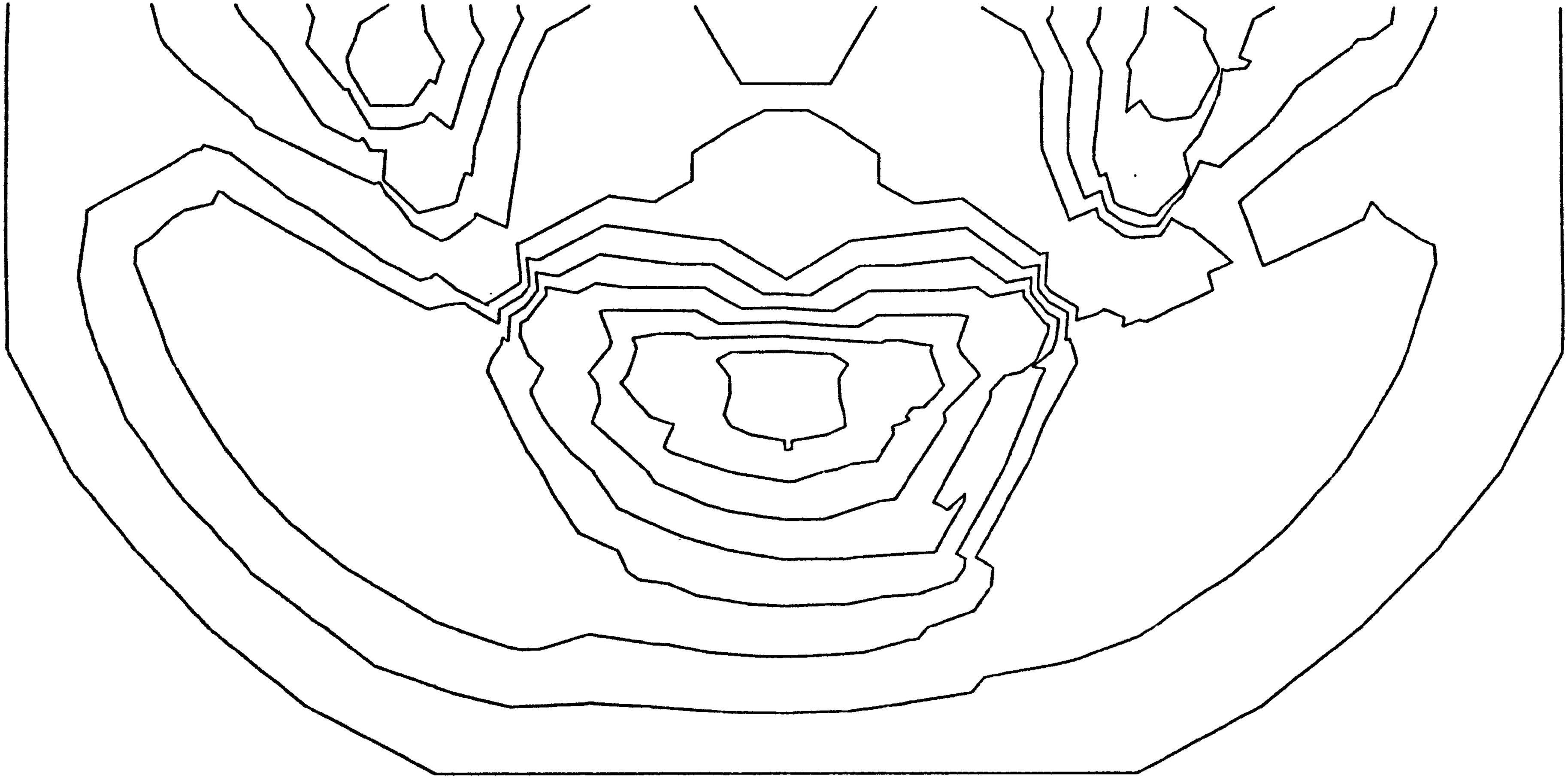

Fig. 5.2.5b Flux of rotor bars s = 1, t = 5 m.sec

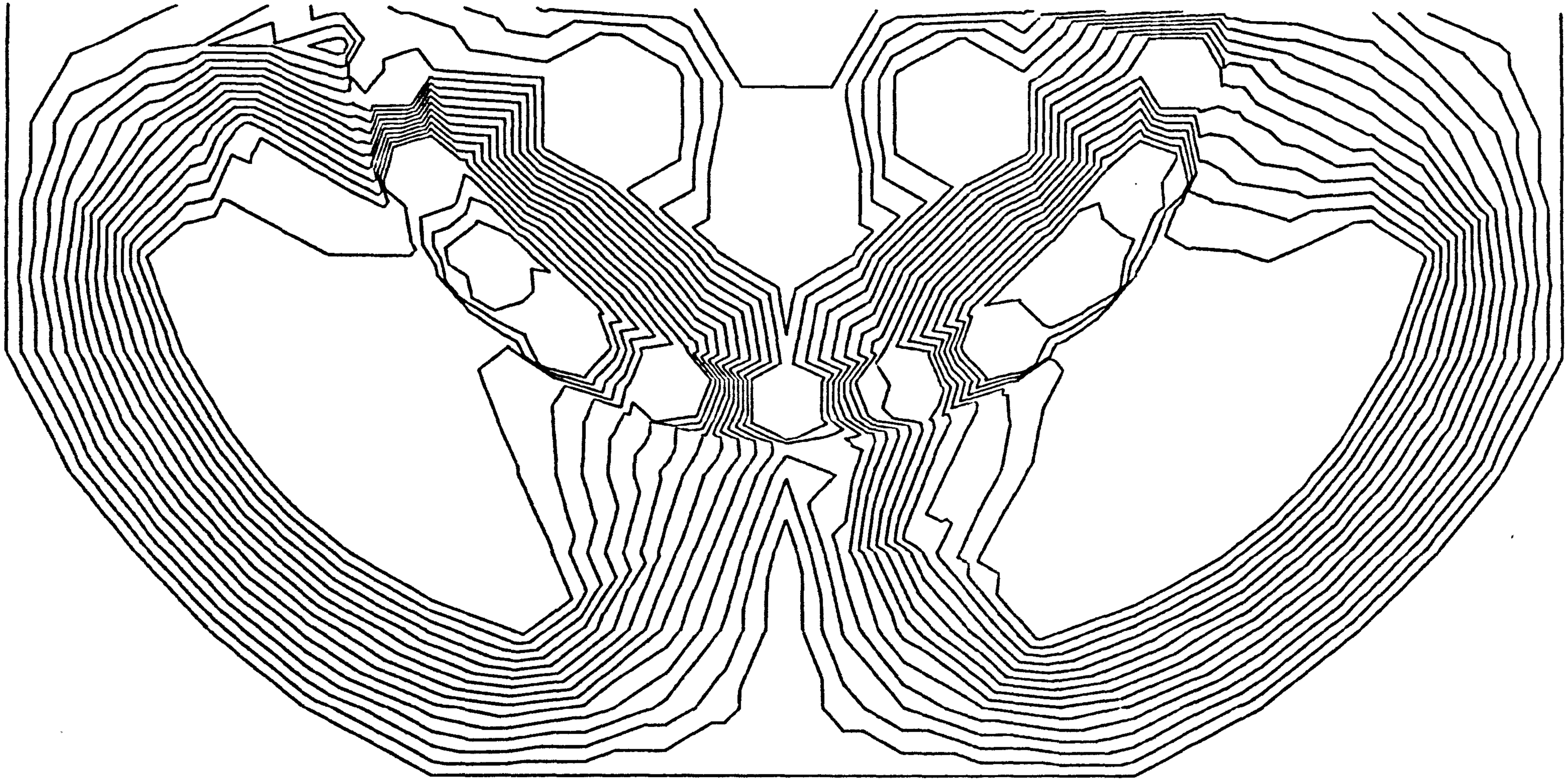

Fig. 5.2.5c Flux of rotor bars for s = 0.05, t = 0

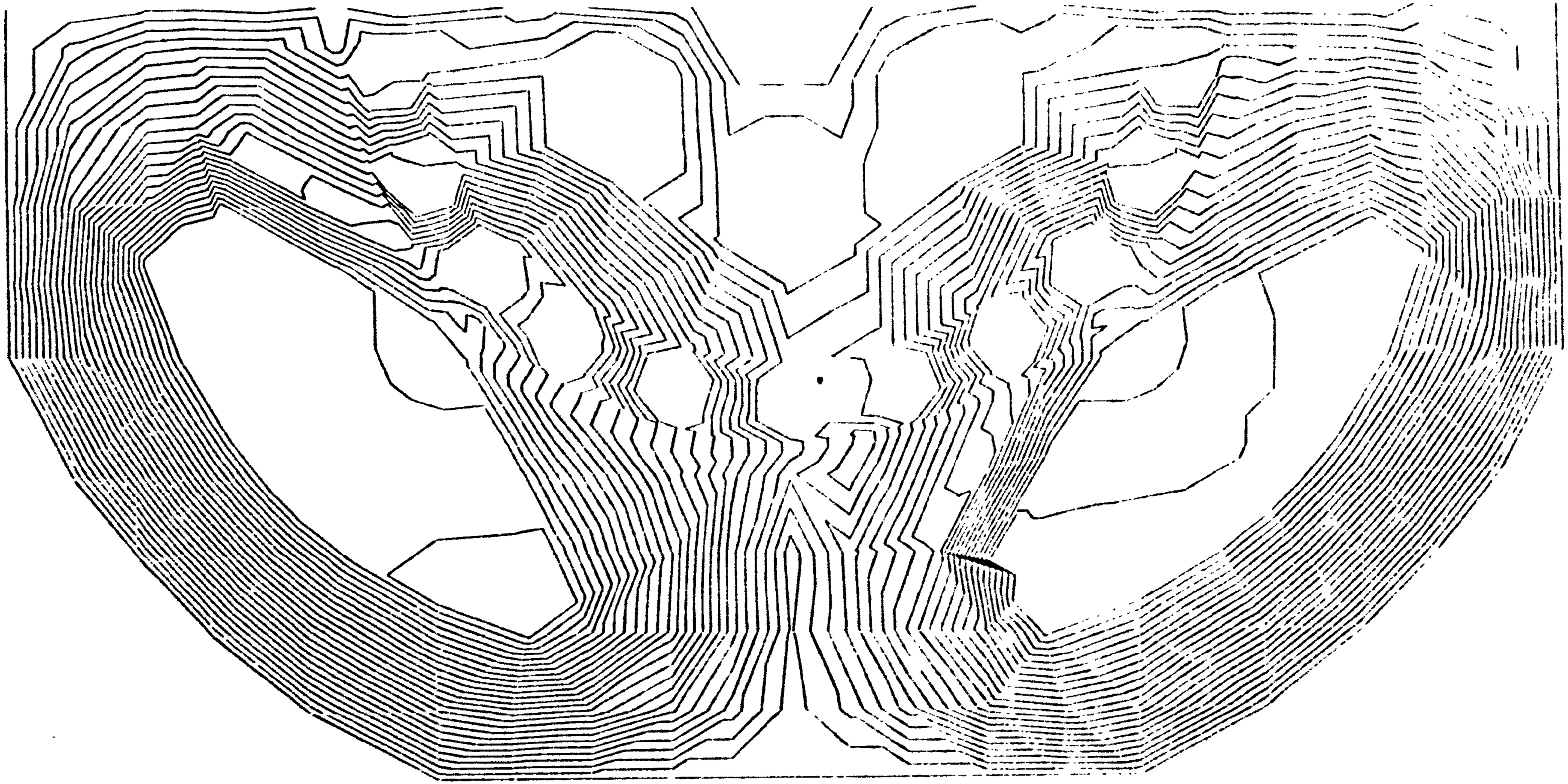

Fig. 5.2.6a Flux of main winding (s = 1, t = 0) ψ = constant

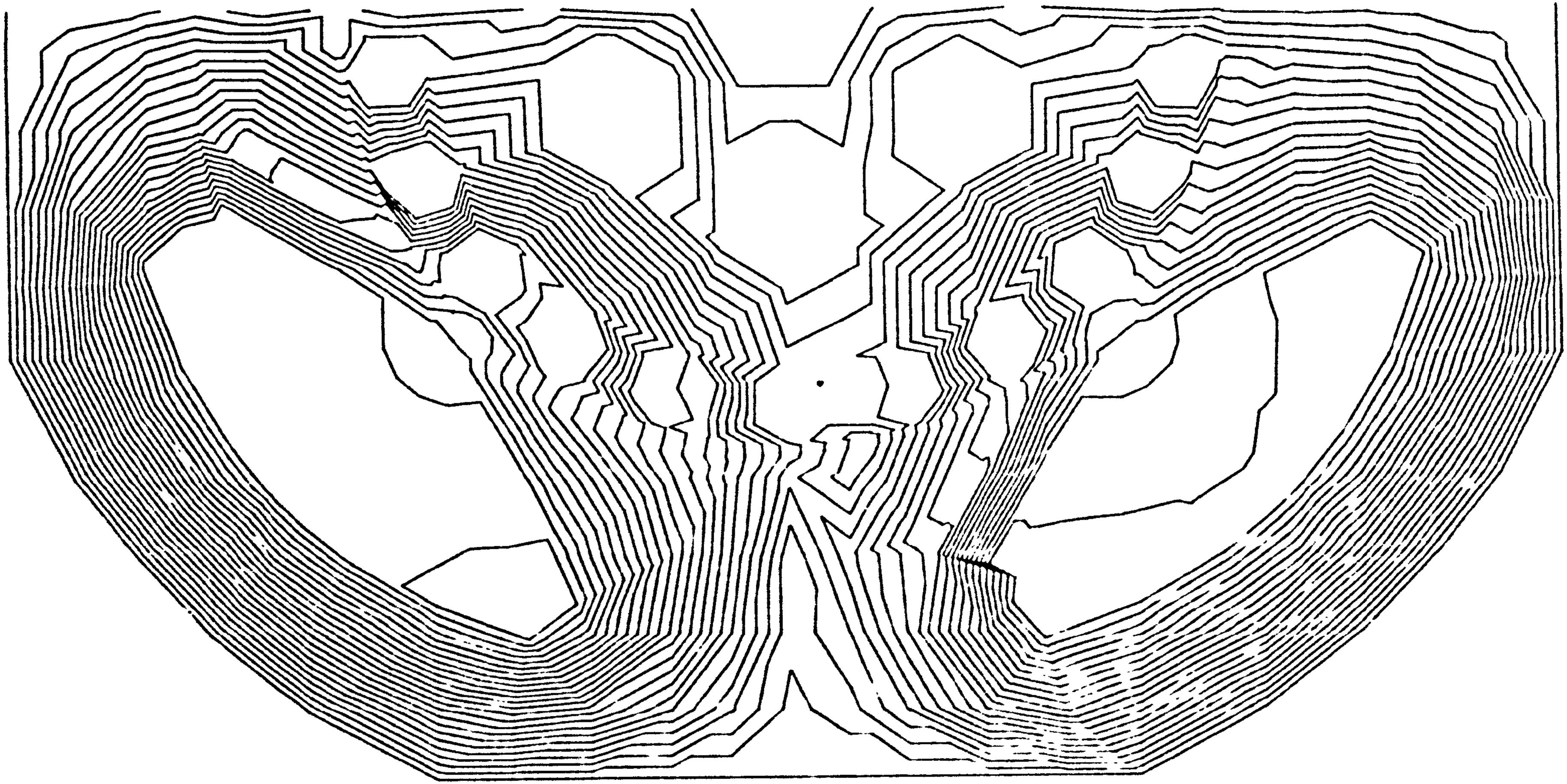

Fig. 5.2.6.b Flux of main winding (s = 0.5, t = 0) ν = constant

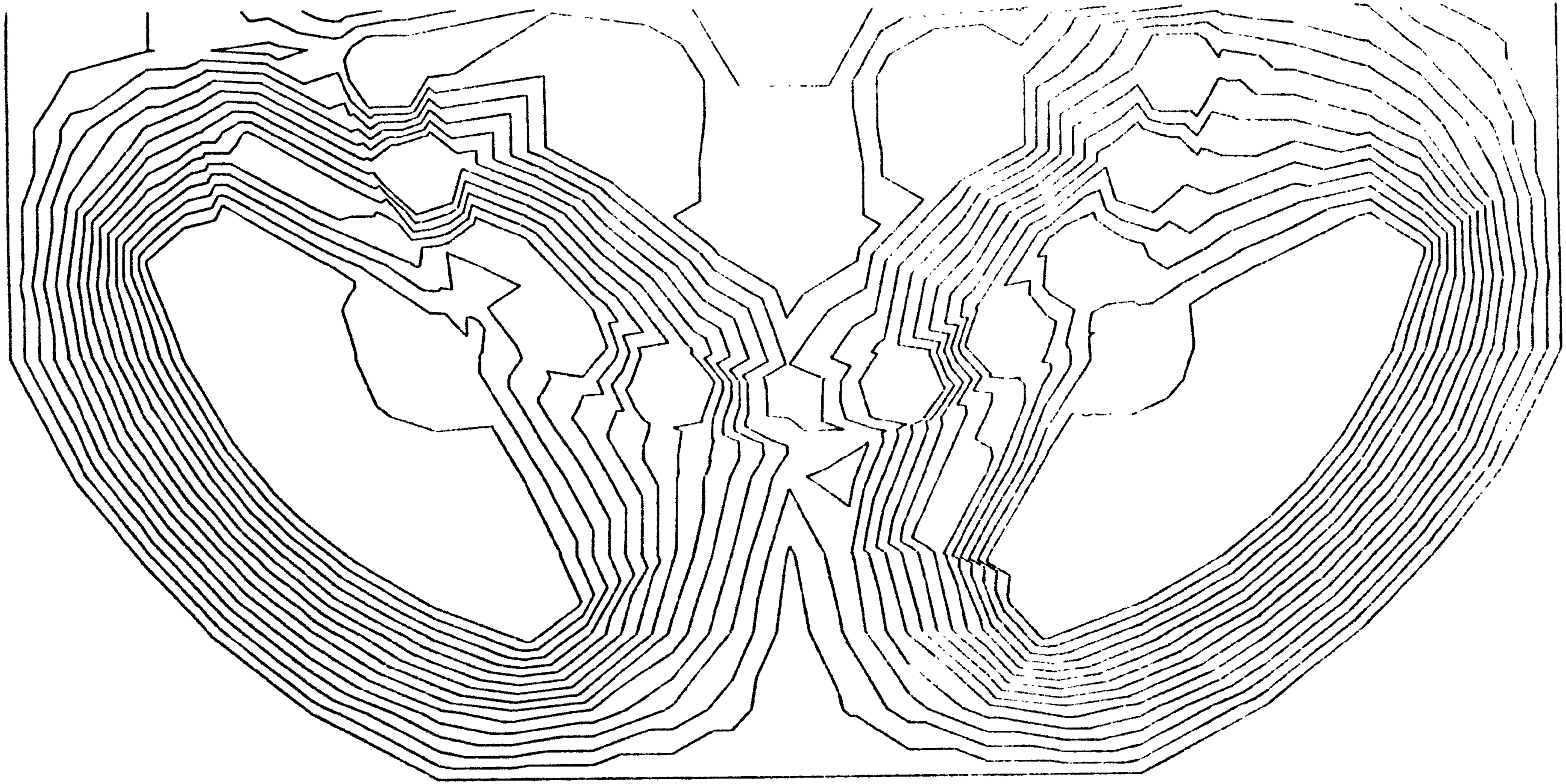

Fig. 5.2.6c Flux of mainwinding (s = 0.05, t = 0) ν = constant

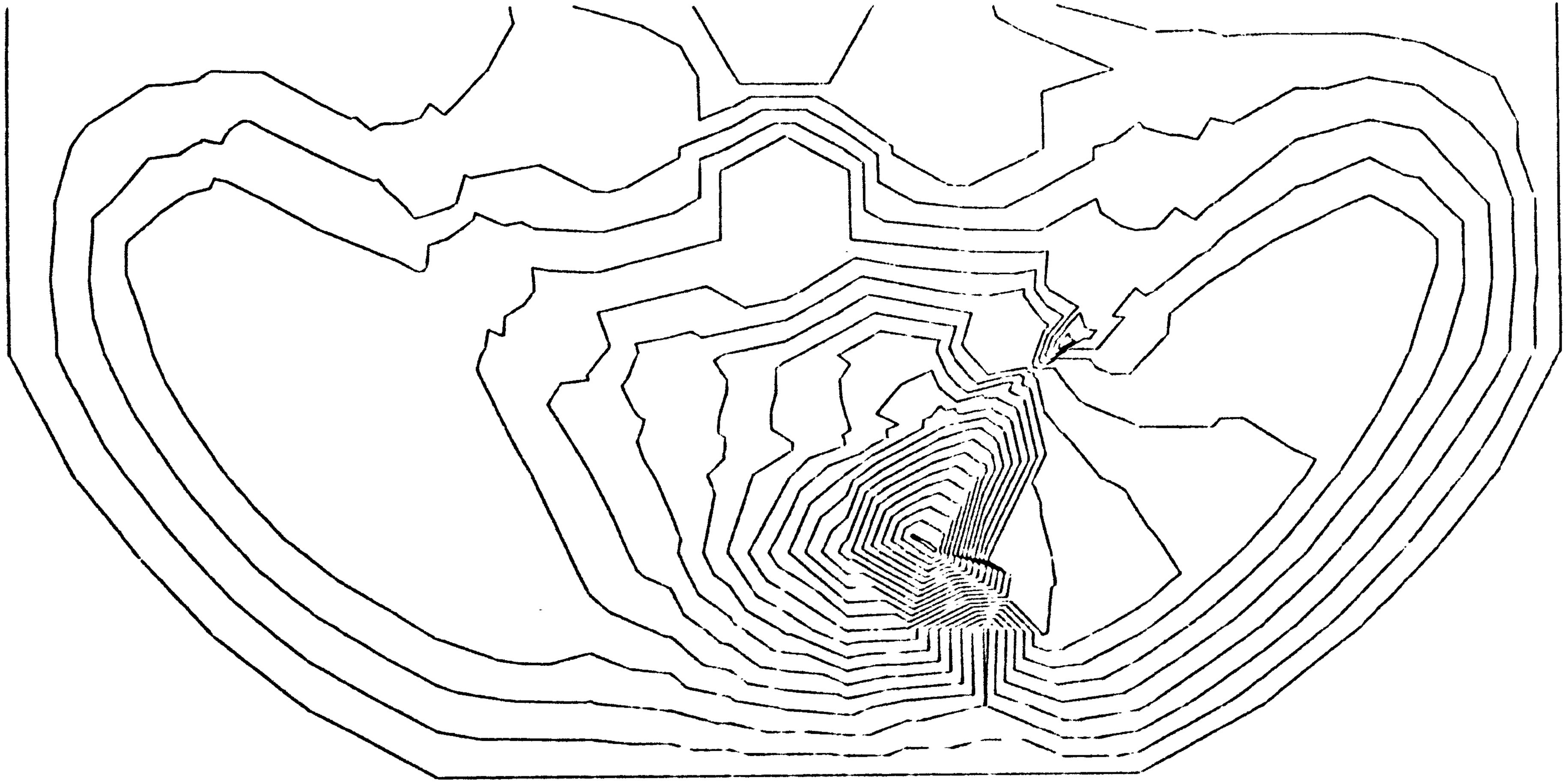

Fig. 5.2.7 Flux of one shading ring (s = 1, t = 0), ν = constant

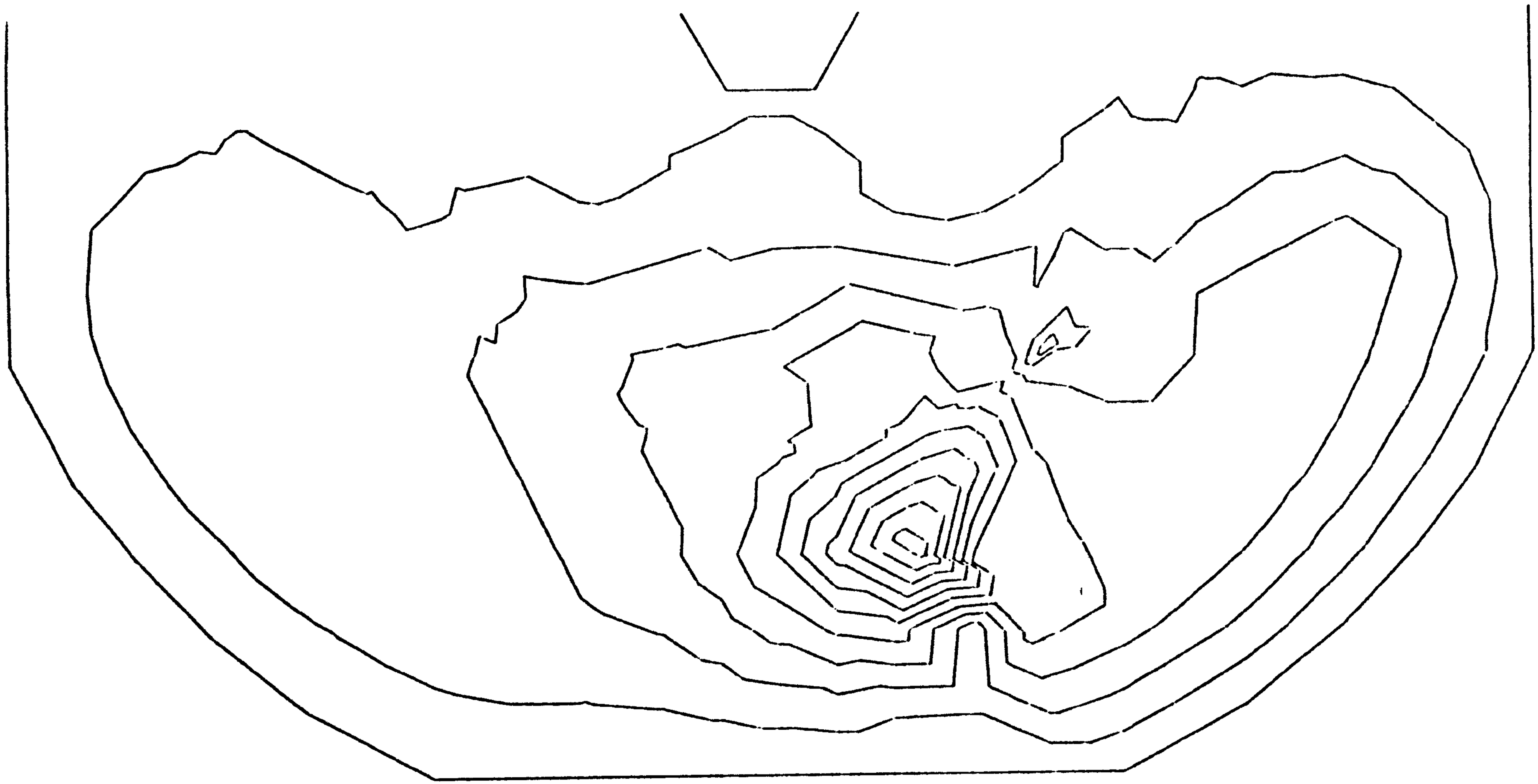

Figure 5.2.8 Flux of one ring (s=0.5, t = 0)

Fig. 5.2.9 Flux of one shading ring (s = 0.05, t = 0), ν = constant

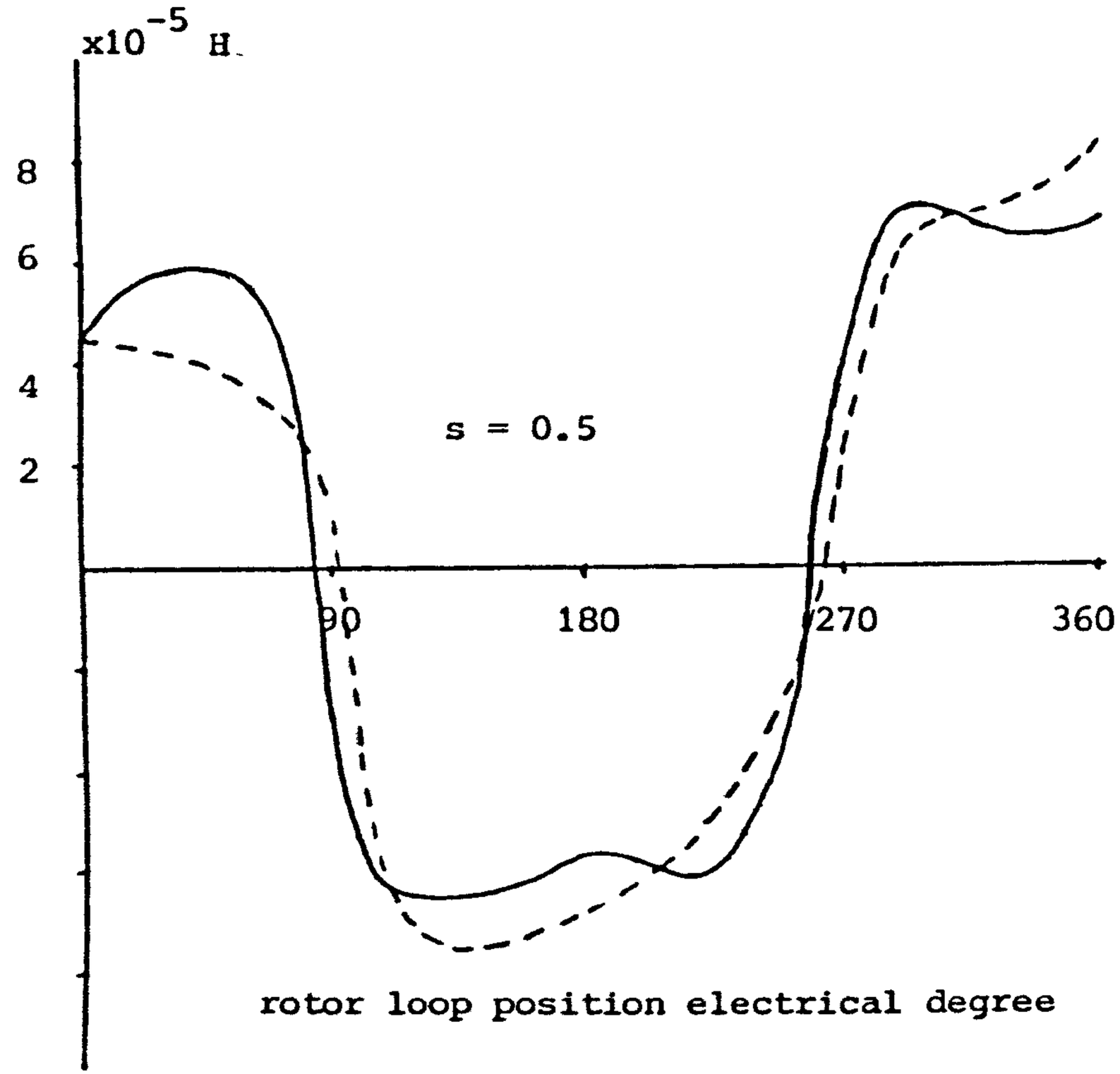

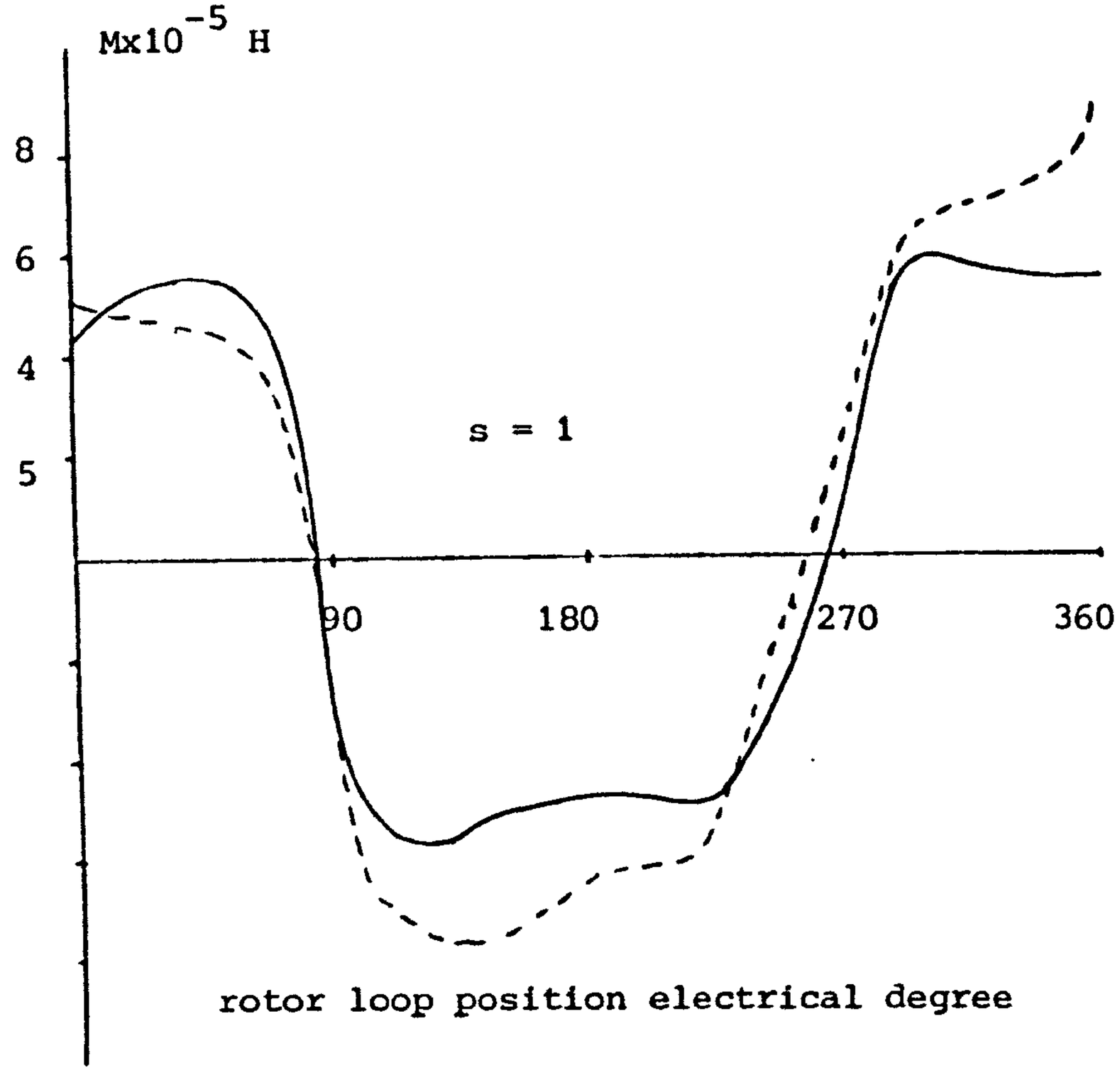

Figure 5.2.10 Mutual inductance between main winding and a rotor loop

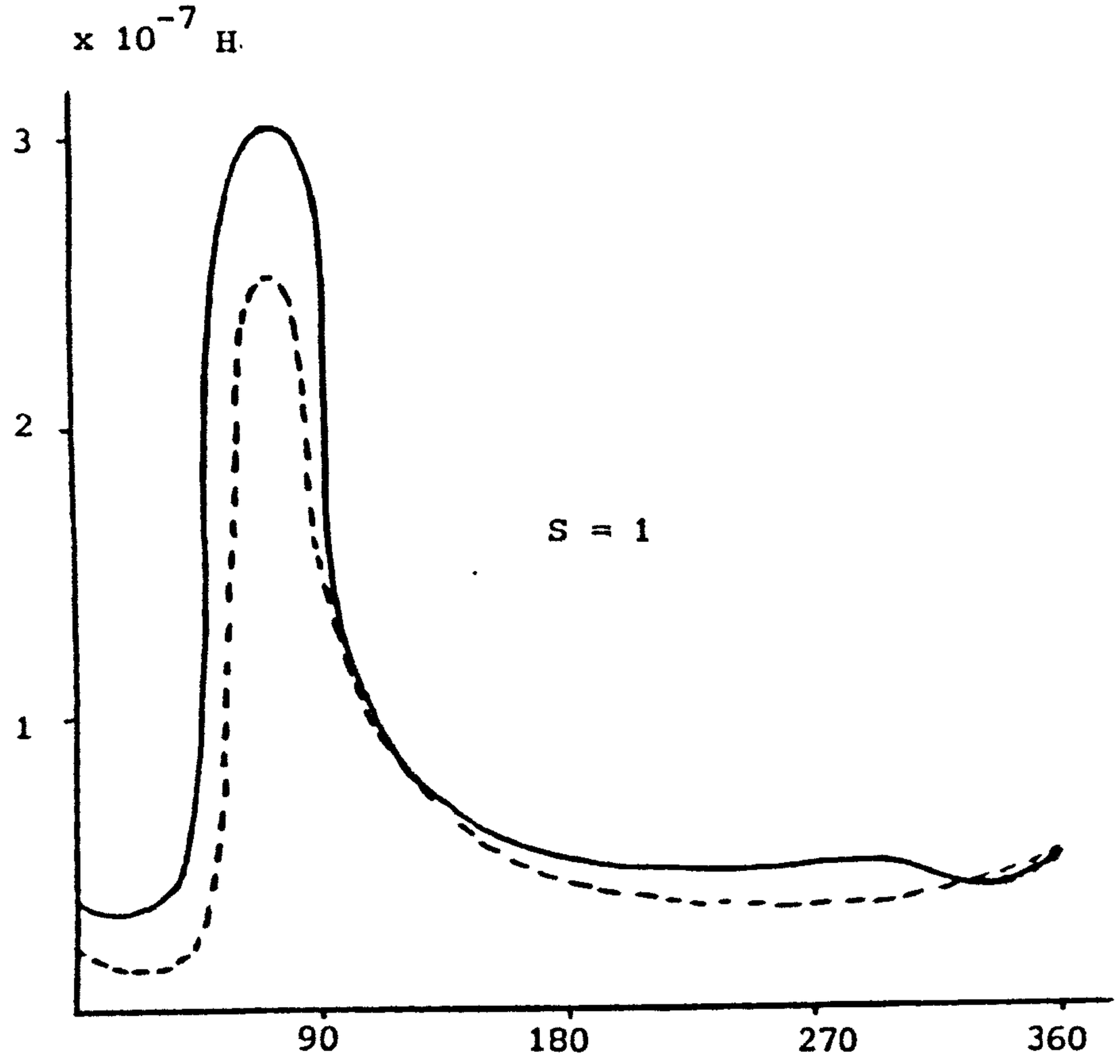

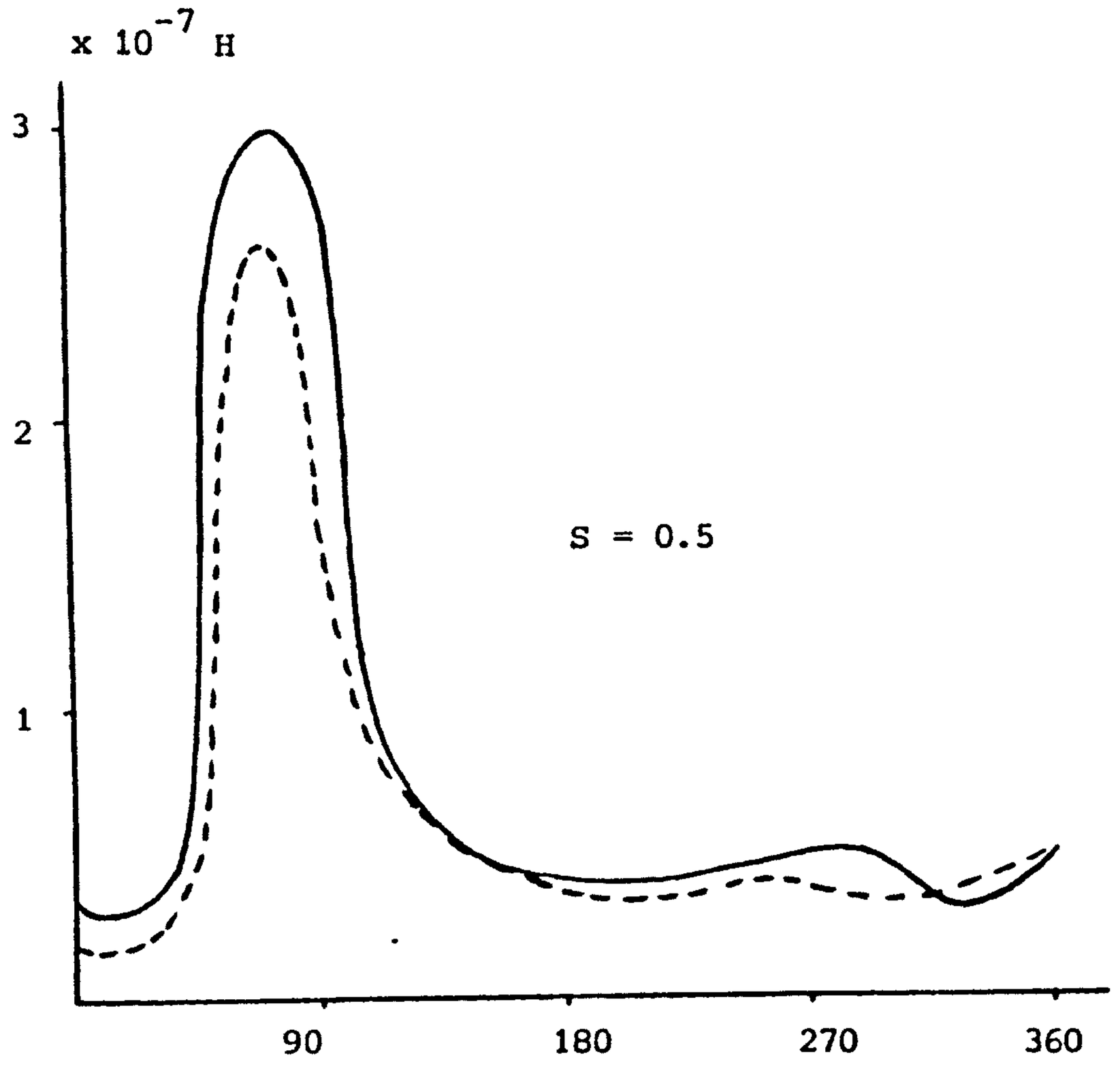

Figure 5.2.11 Mutual inductance between shading ring and a rotor loop

---- t = 5 m.sec

—— t = 0

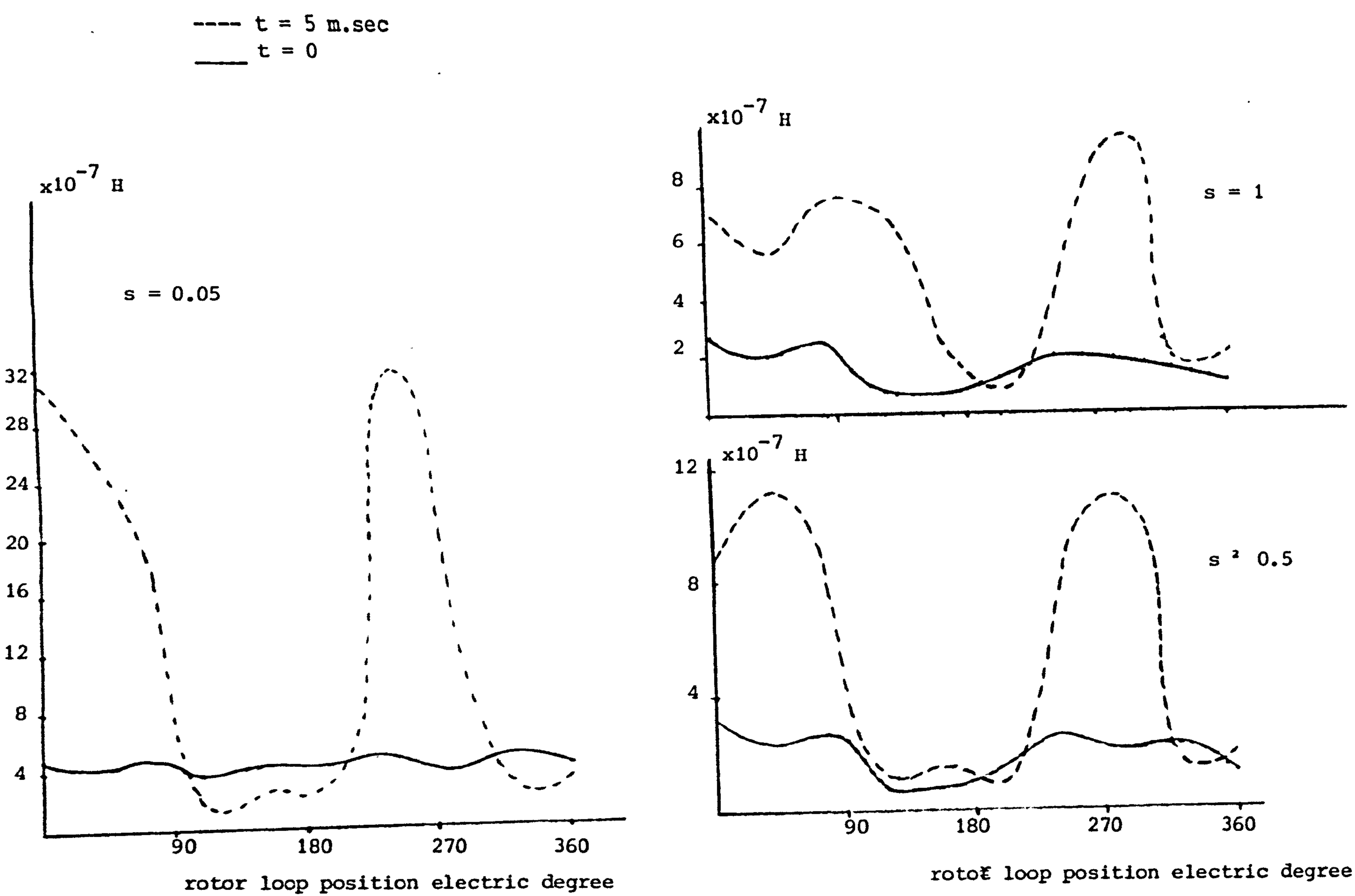

Figure 5.2.12 Mutual inductance between loop 1 & 2

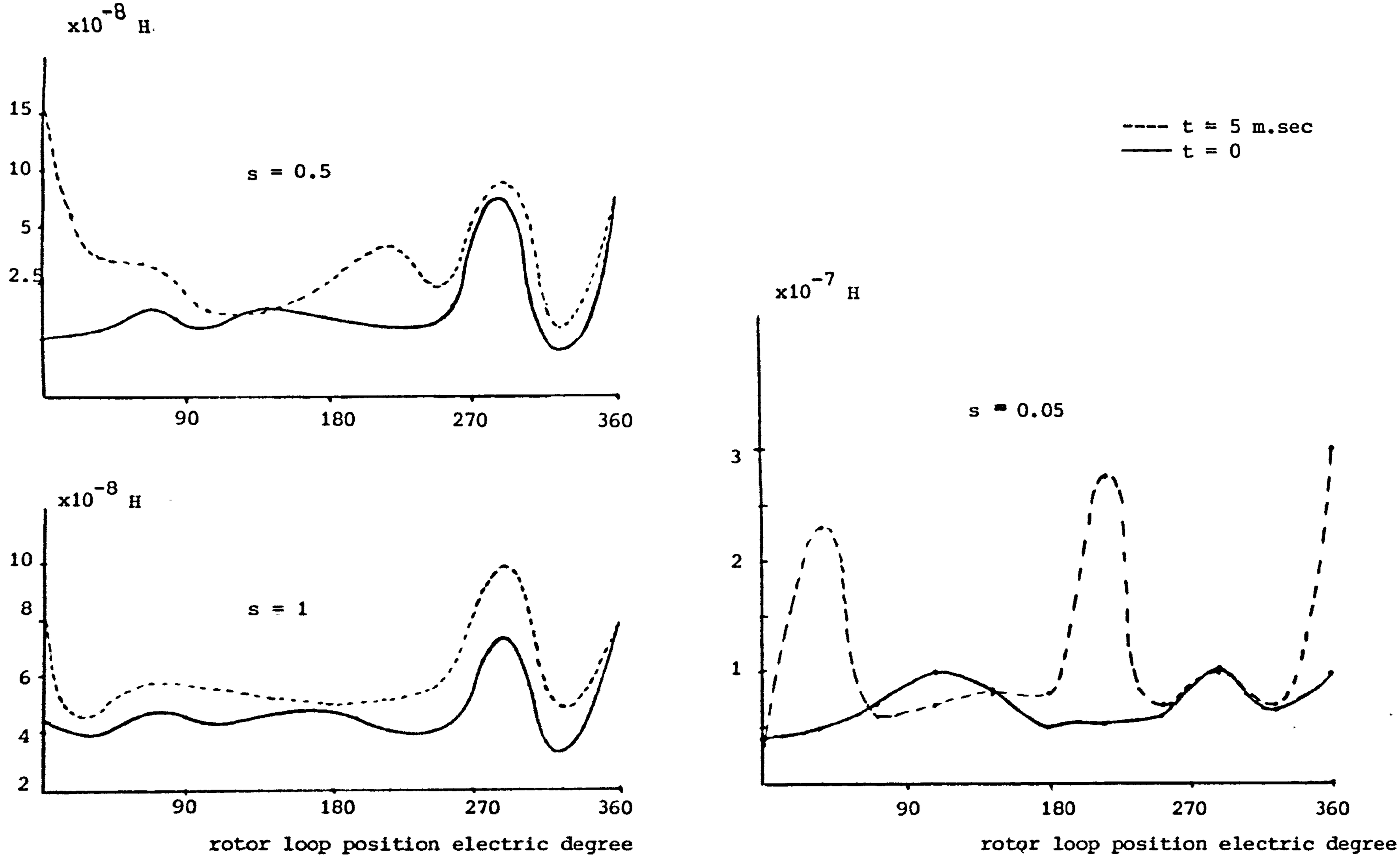

Figure 5.2.13 Mutual inductance between loop 1 & 3

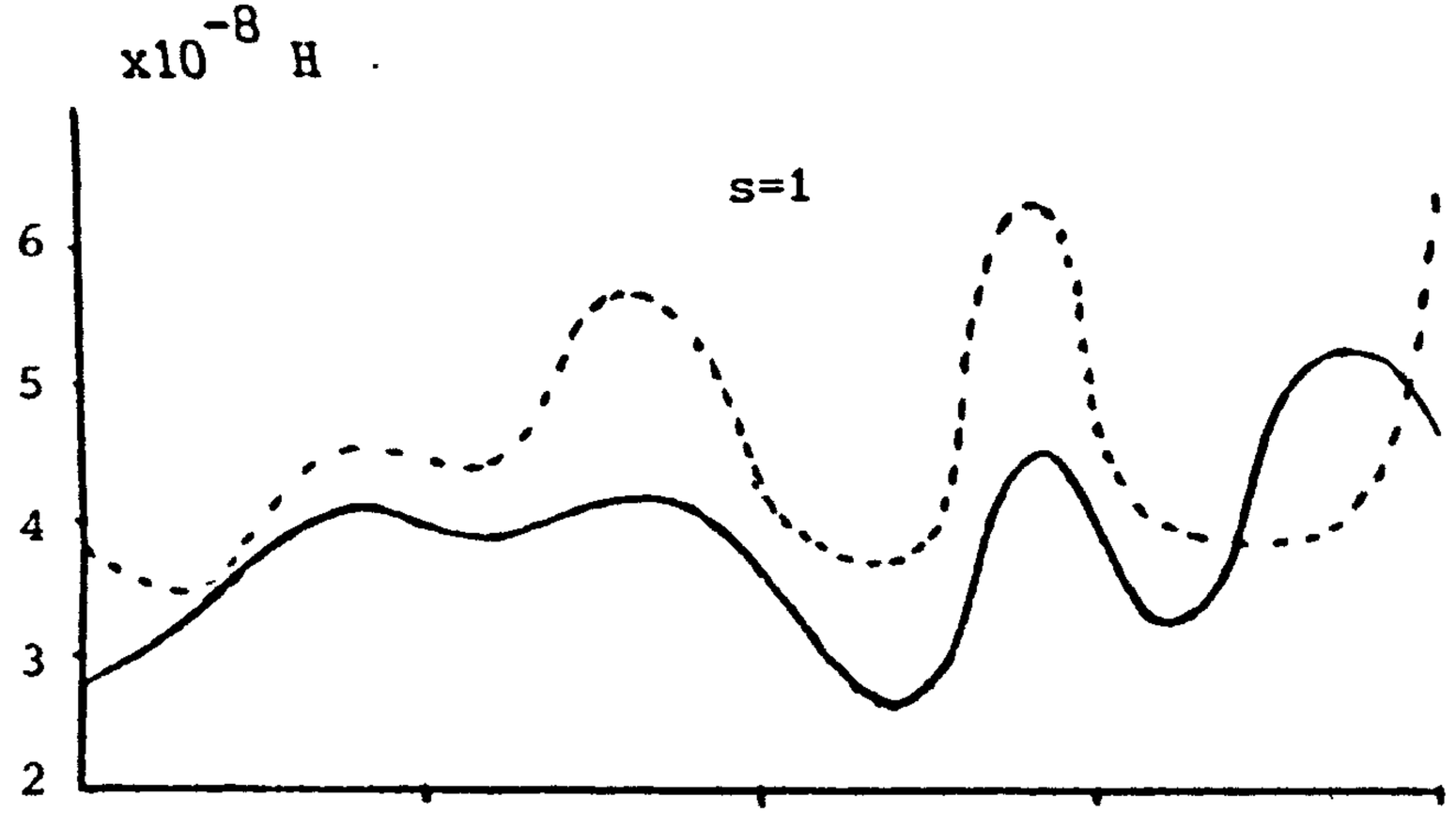

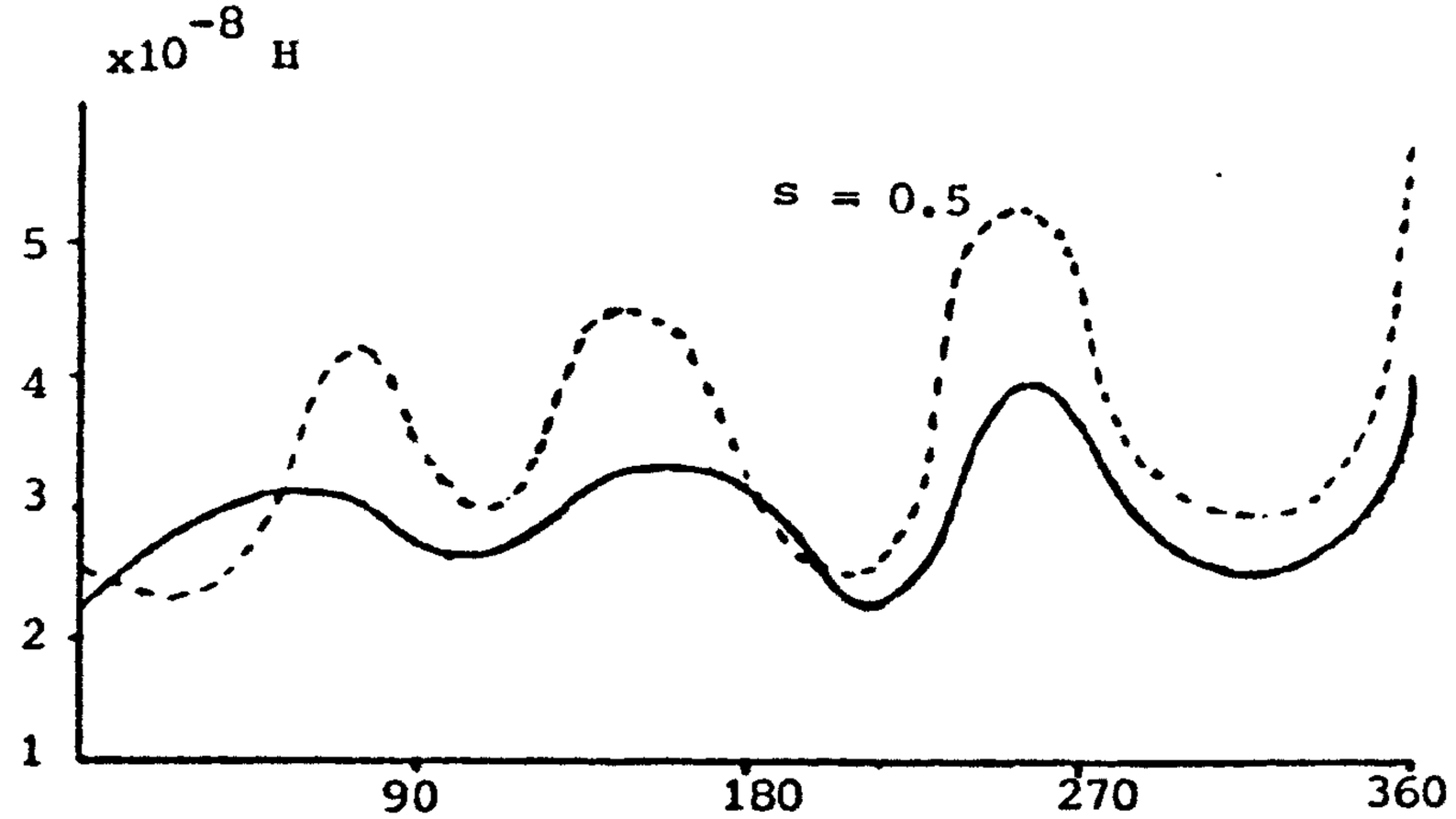

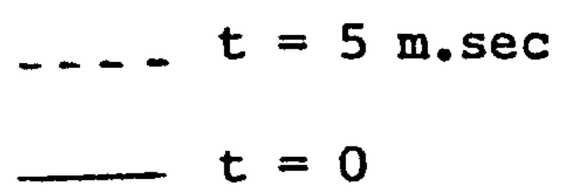

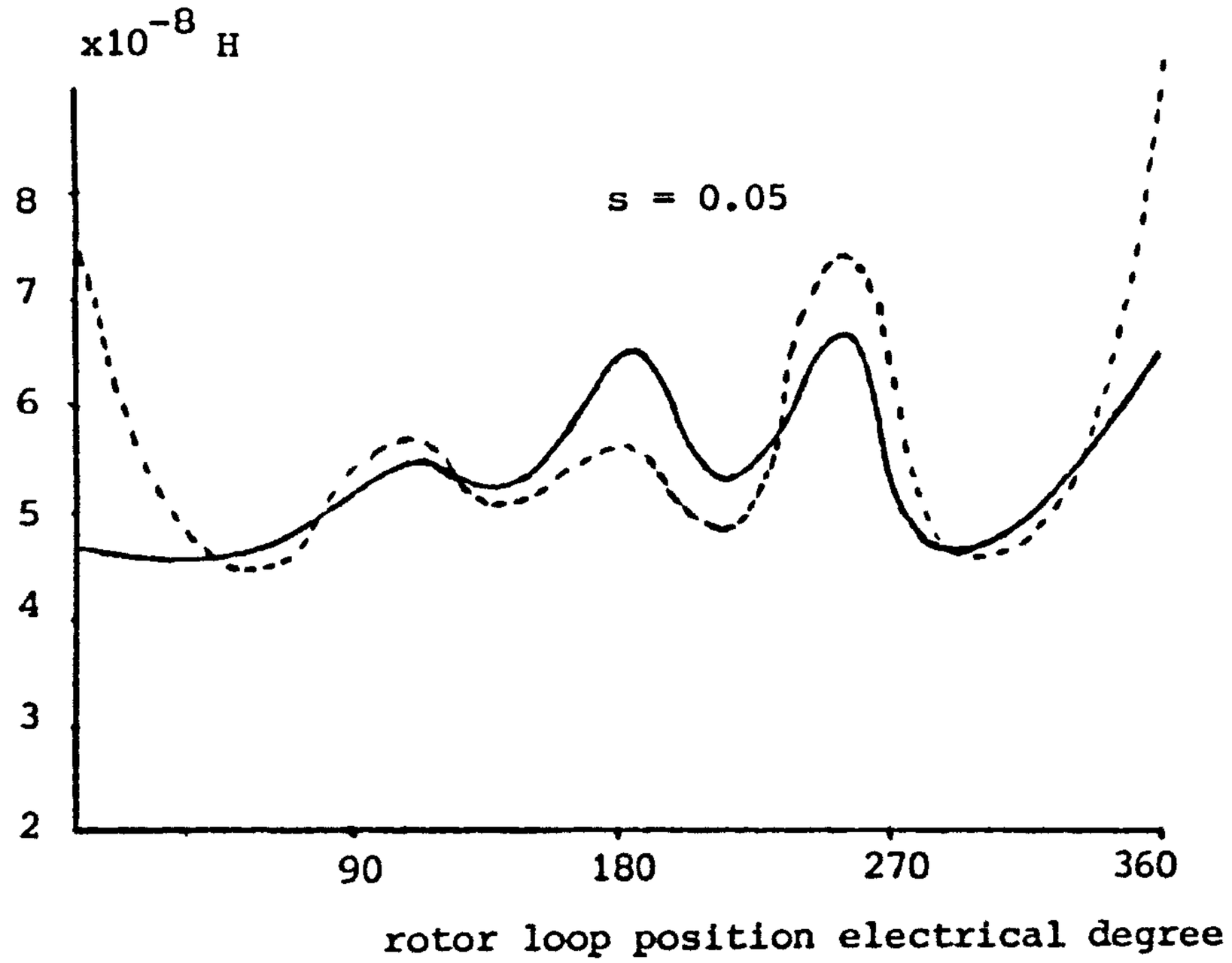

Figure 5.2.14 Mutual inductance between loop 1 & 4

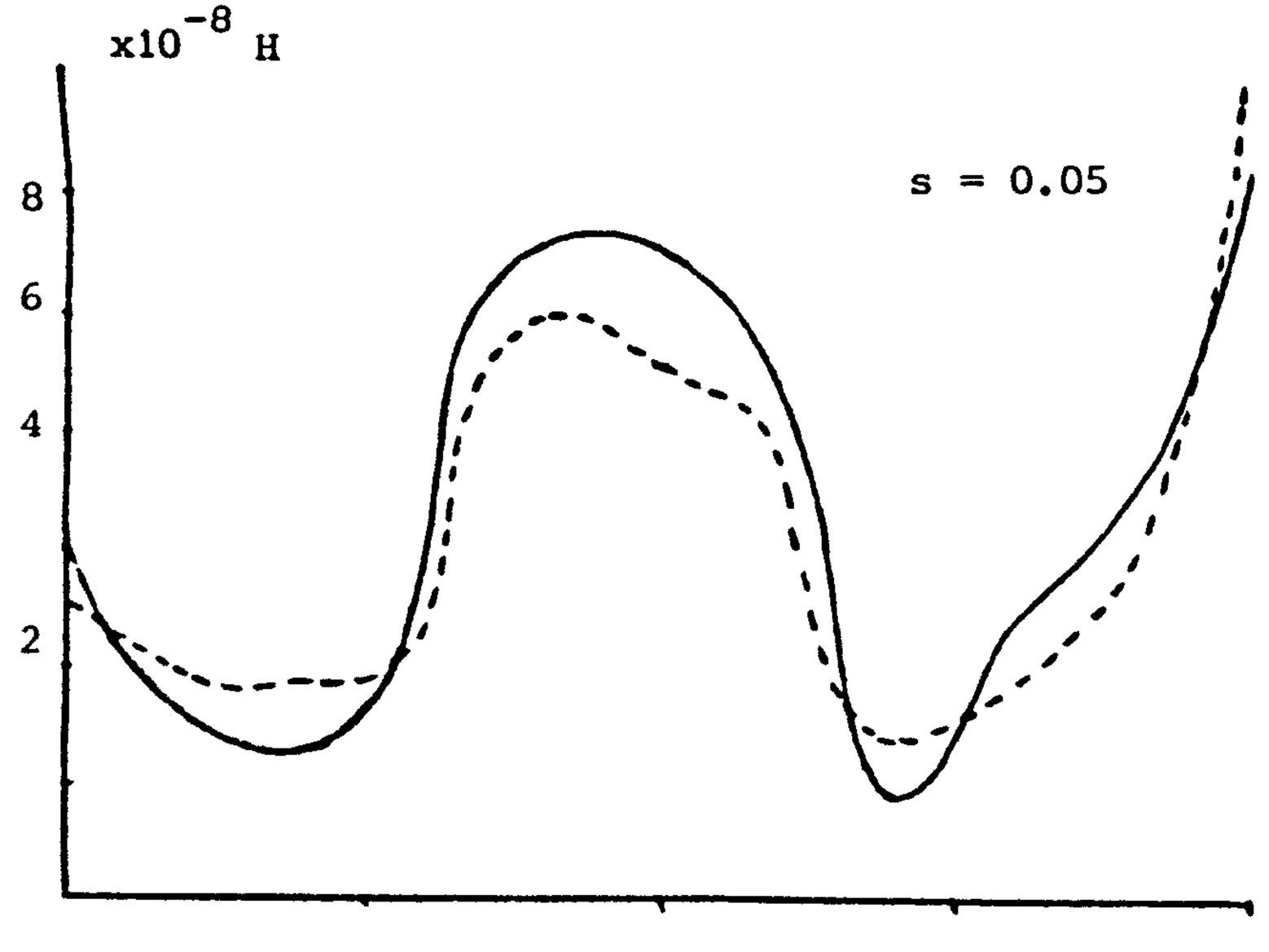

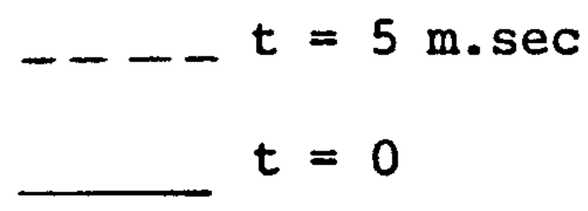

Figure 5.2.15 Mutual inductance between loop 1 & 5

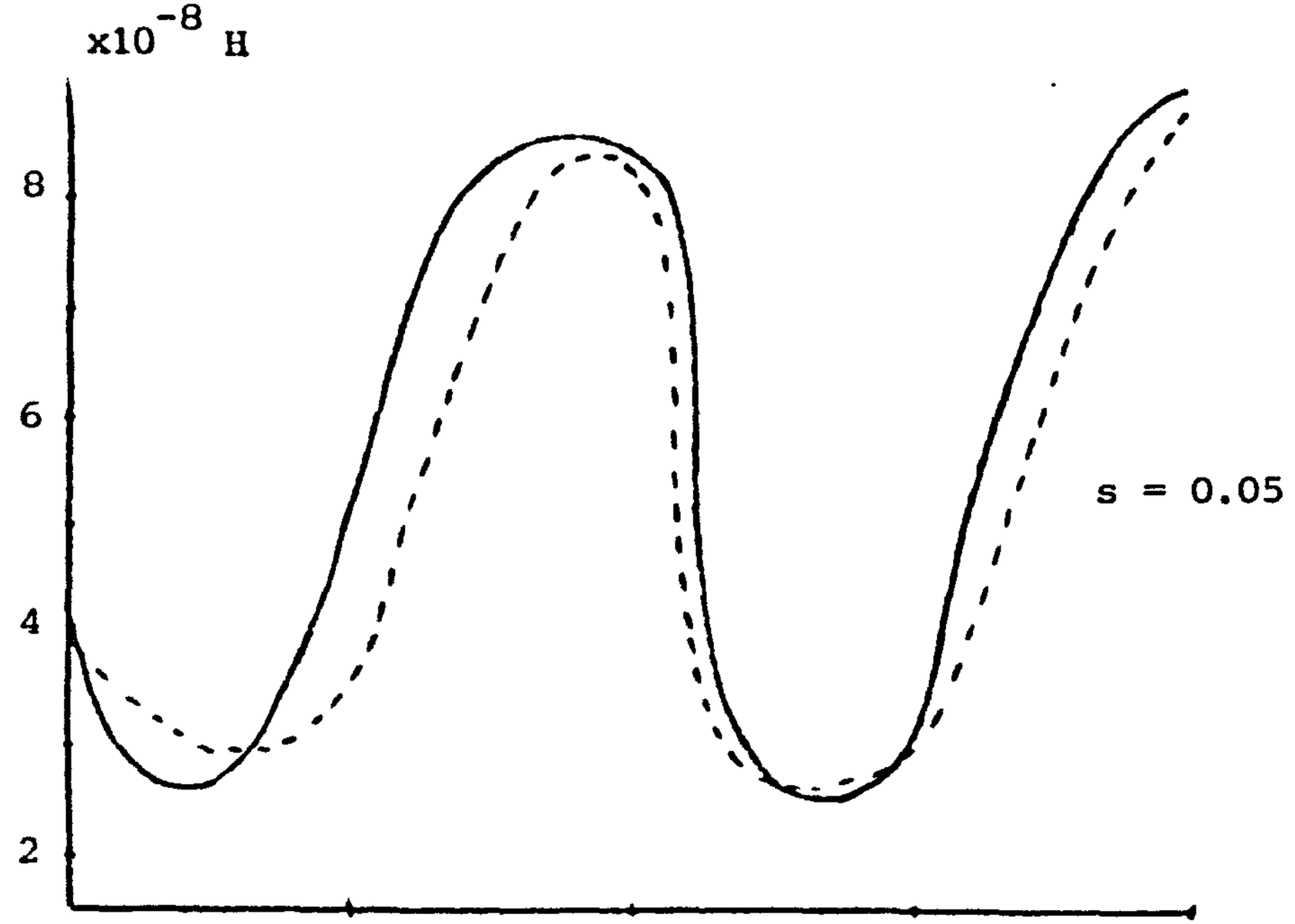

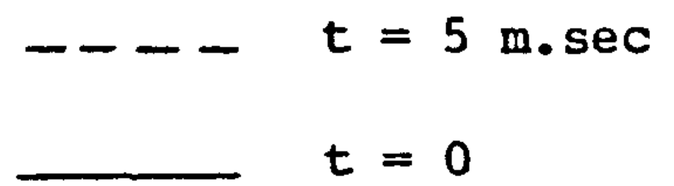

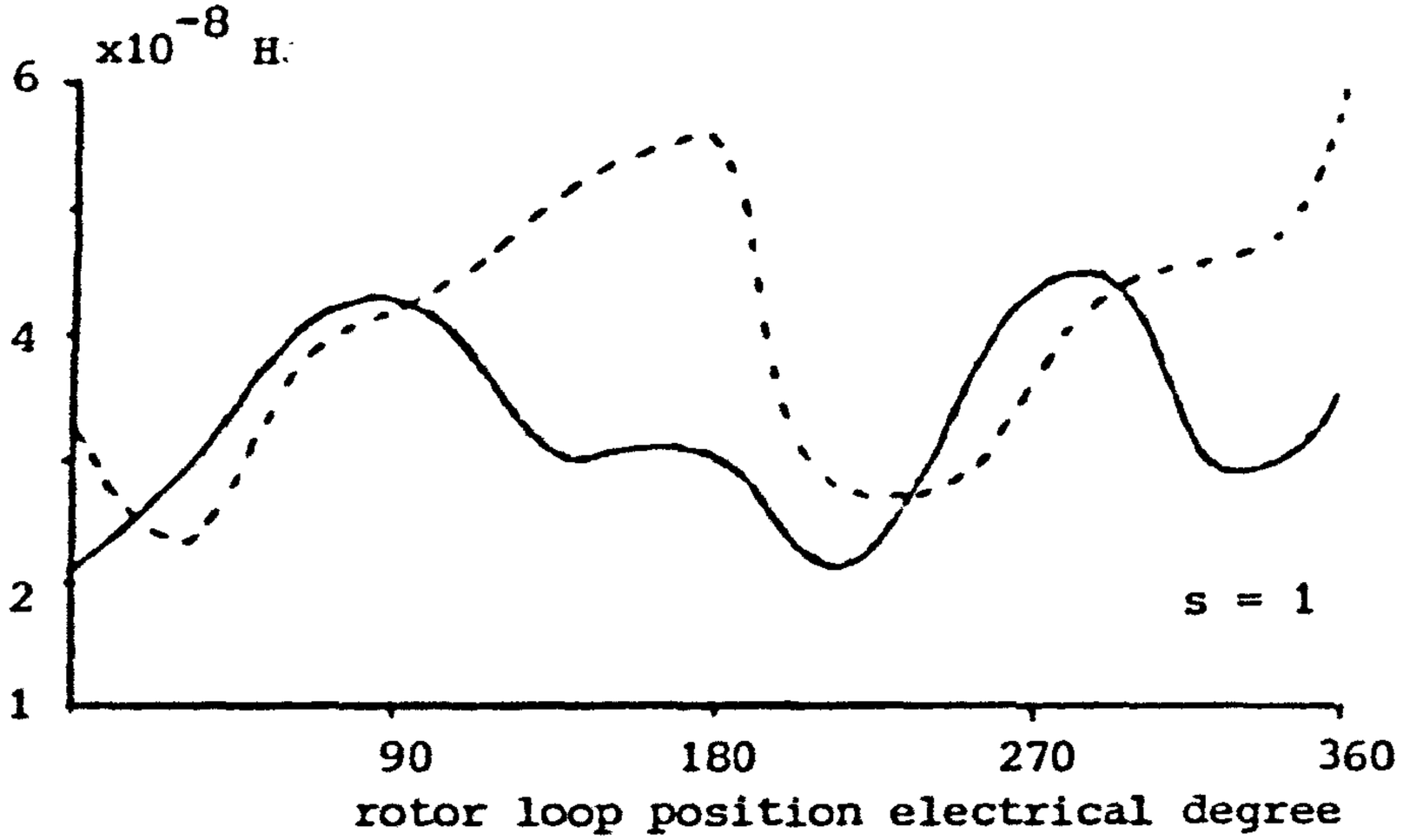

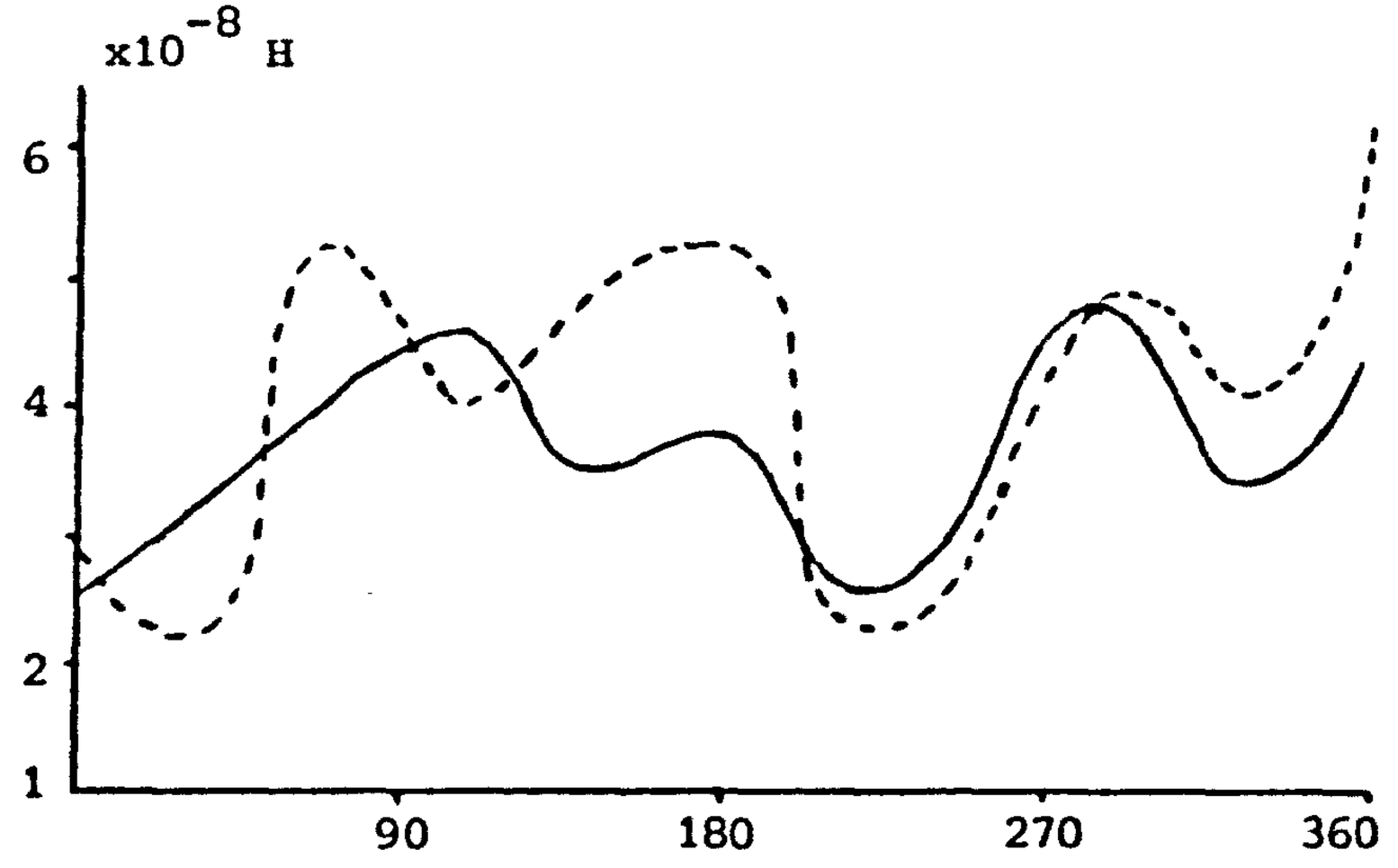

Figure 5.2.16 Mutual inductance between loop 1 & 6

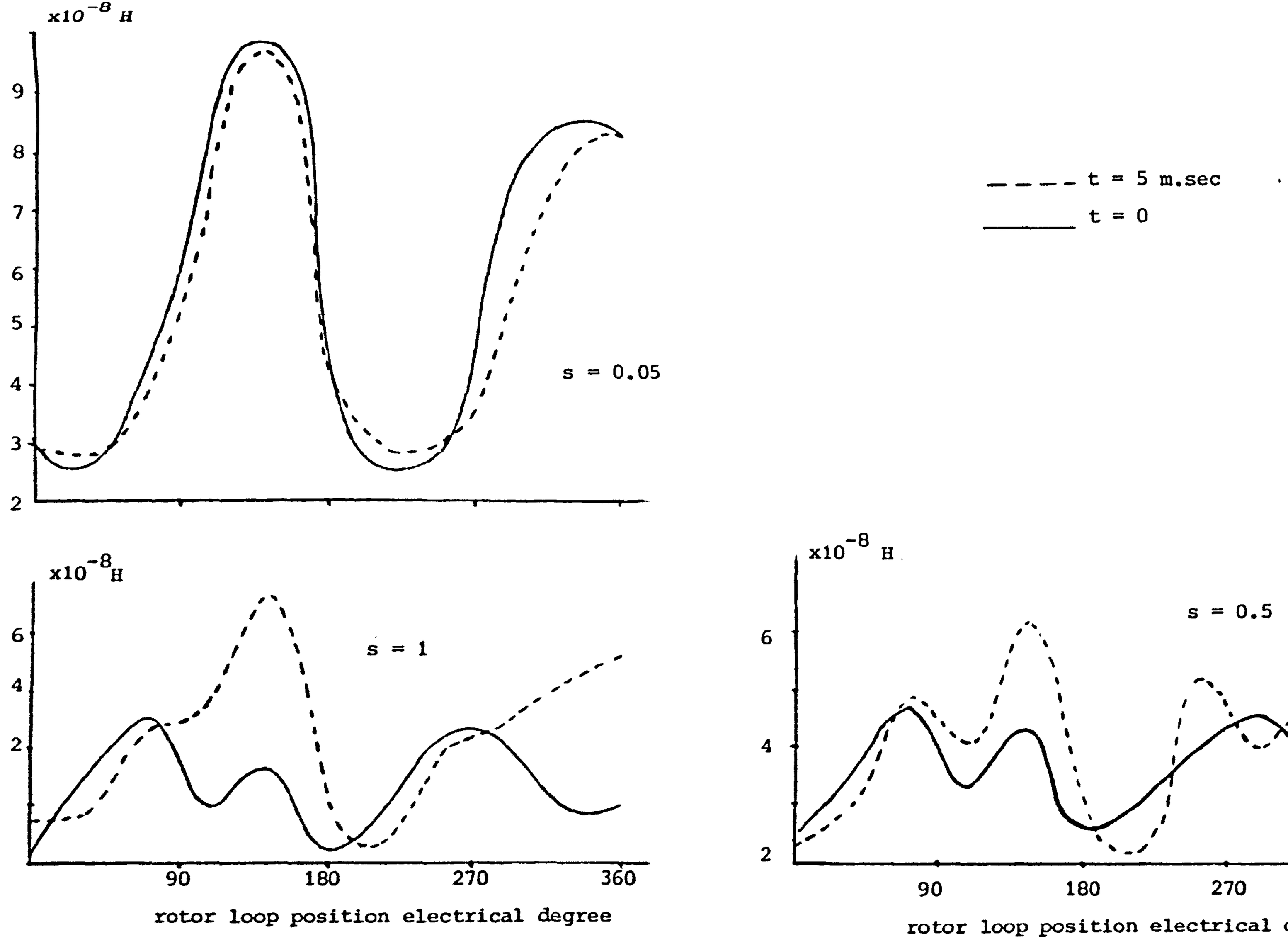

Figure 5.2.17 Mutual inductance between loop 1 & 7

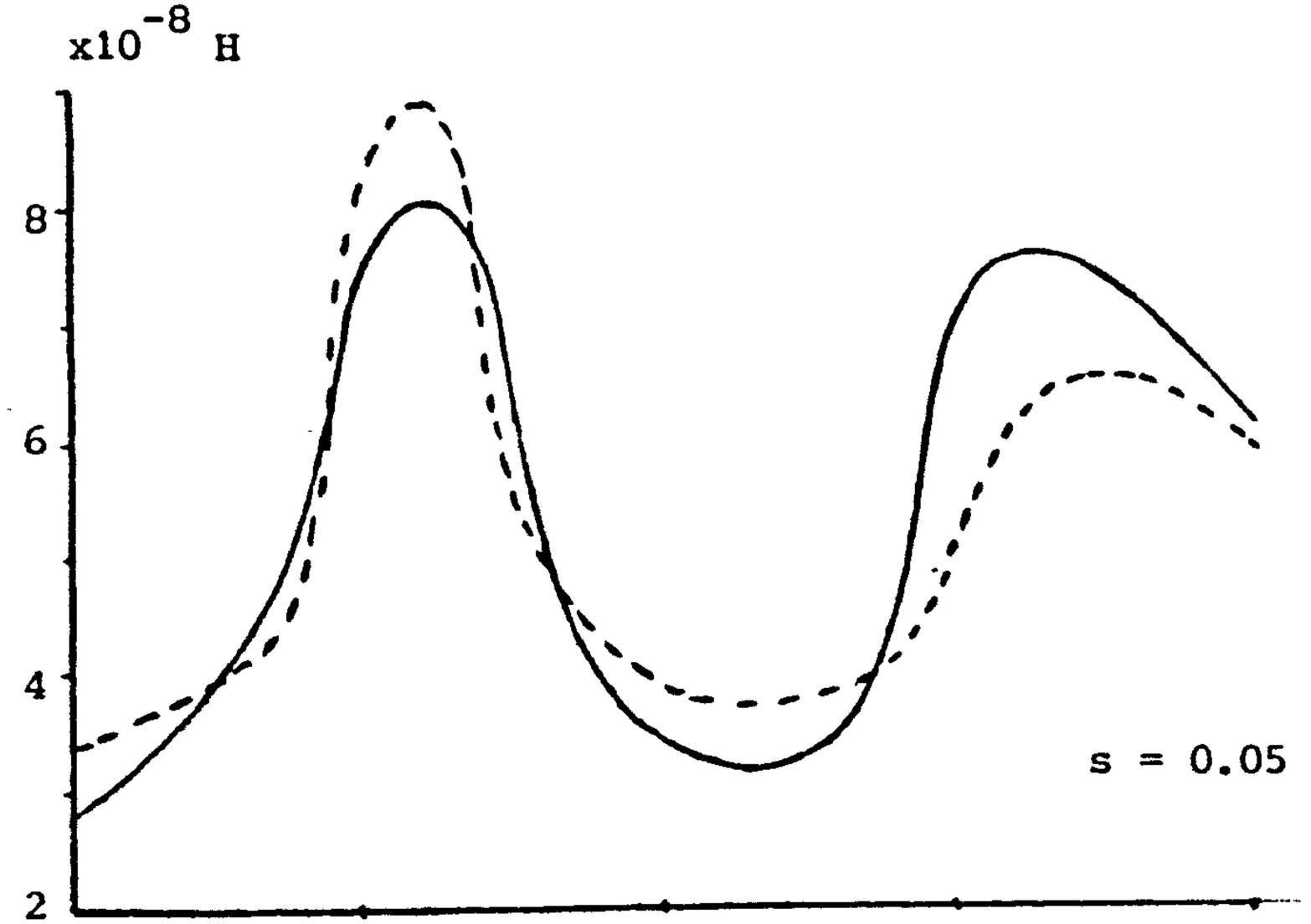

---- t = 5 m.sec
____ t = 0

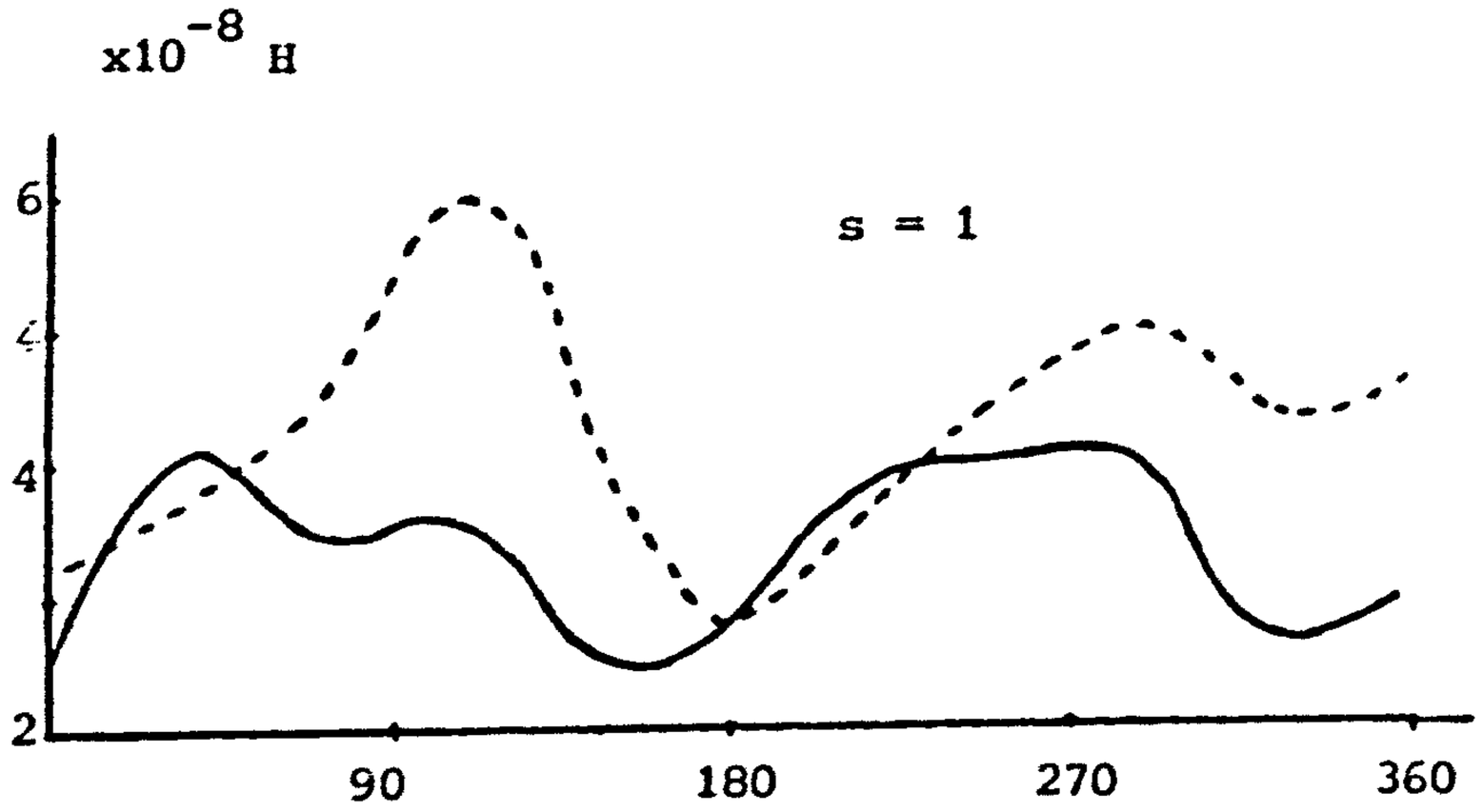

rotor loop position electrical degree

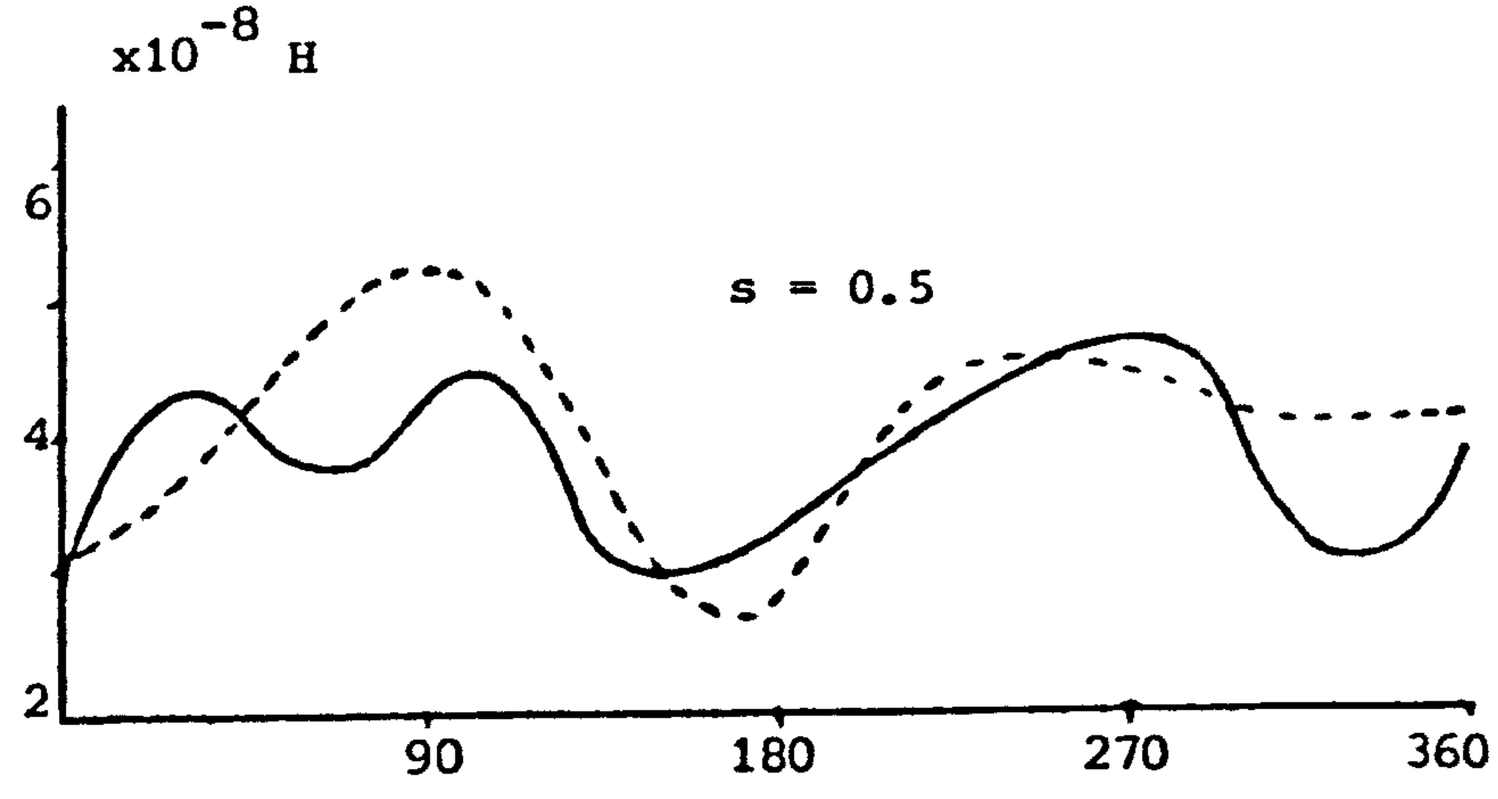

rotor loop position electrical degree

Figure 5.2.18 Mutual inductance between loop 1 & 8

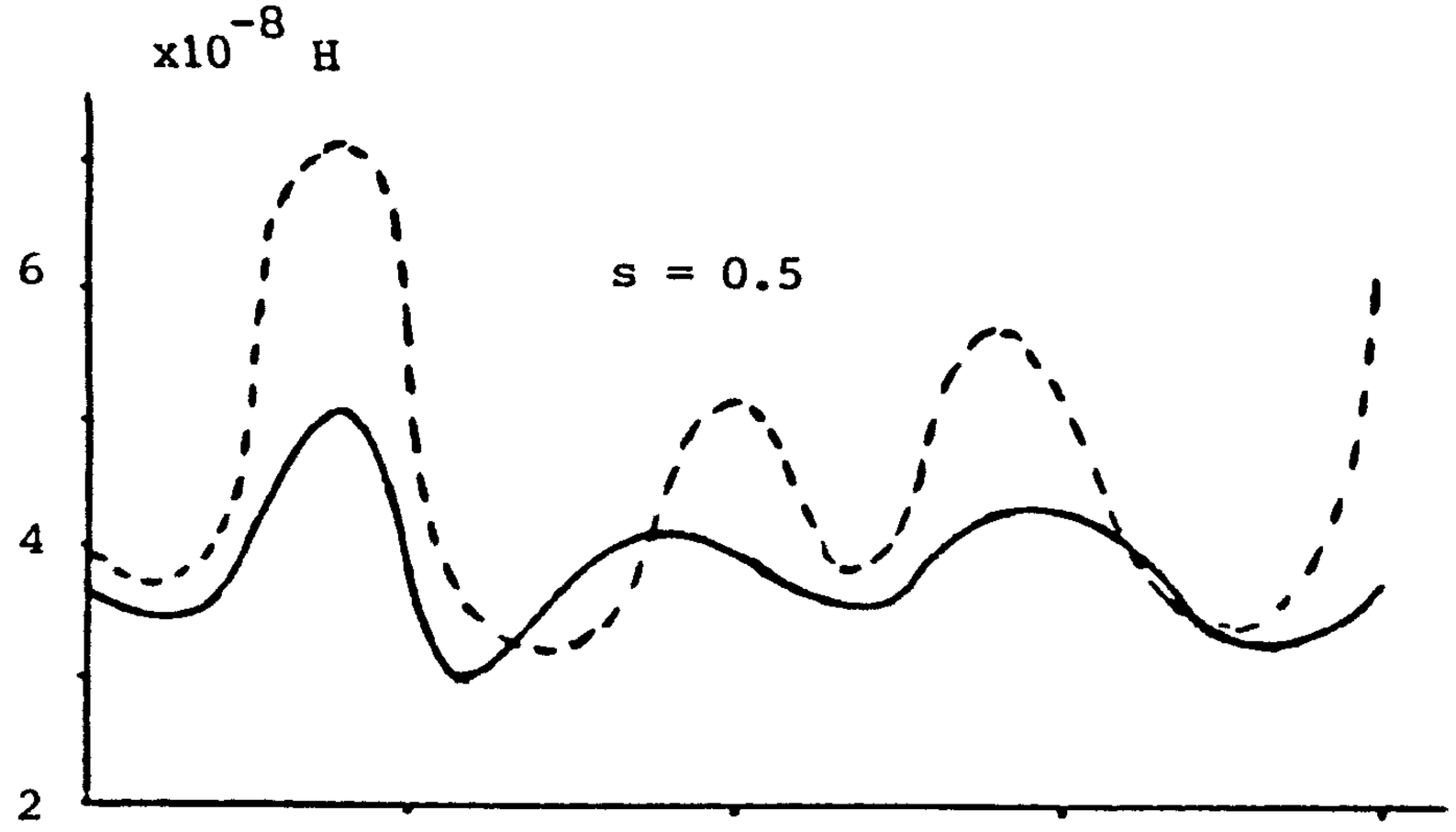

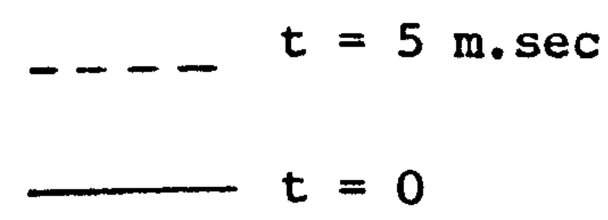

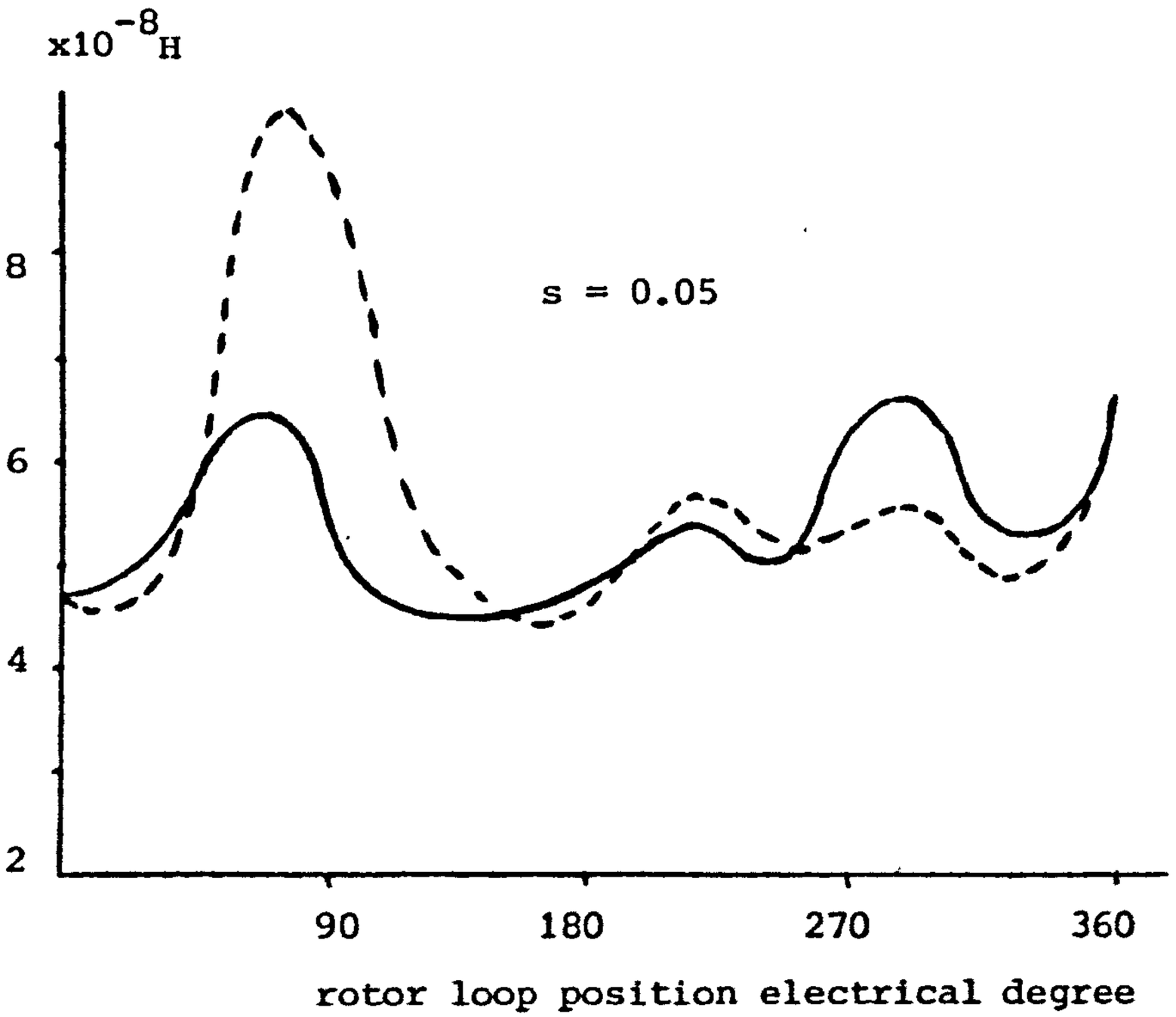

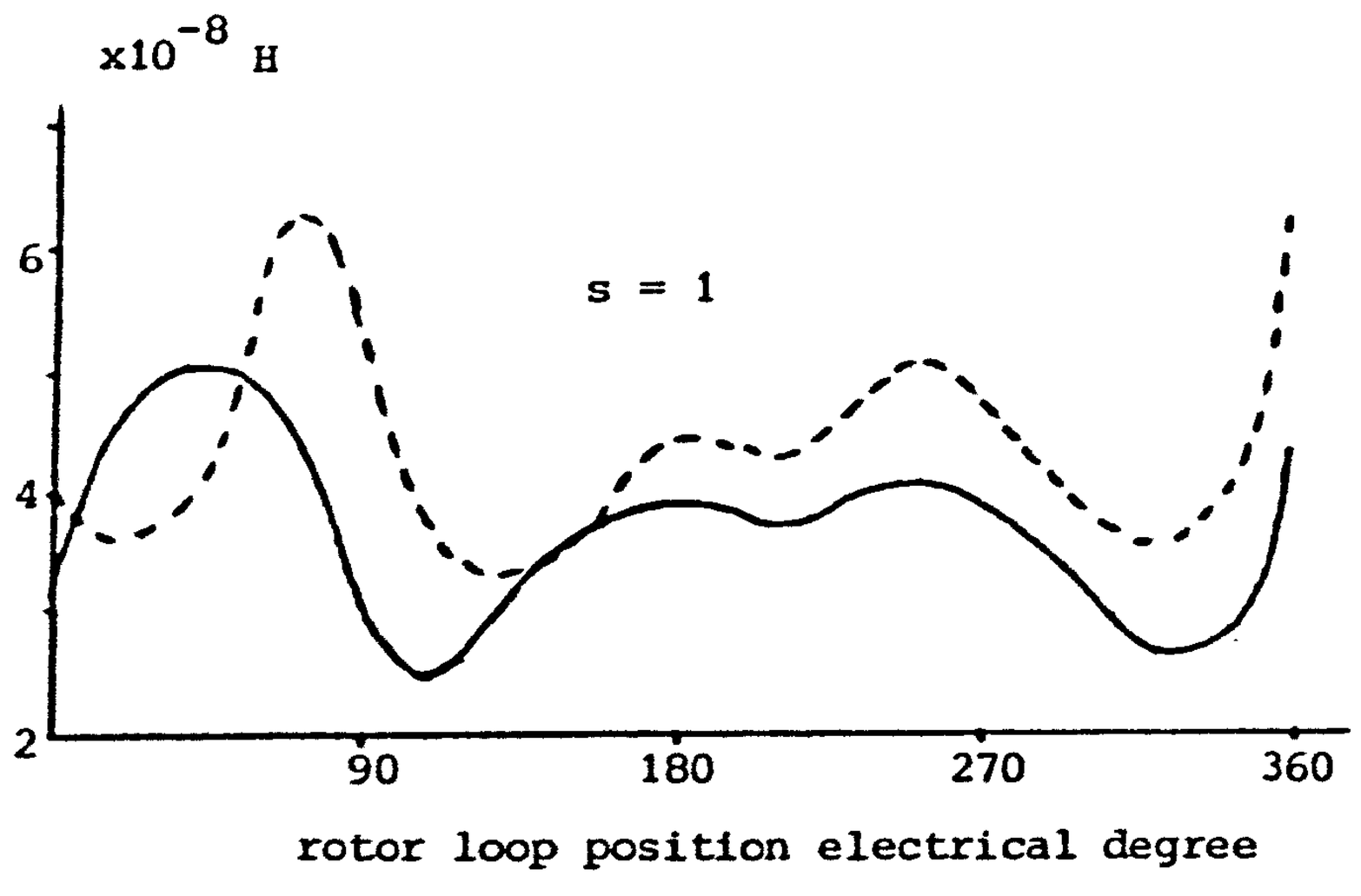

Figure 5.2.19 Mutual inductance between loop 1 & 9

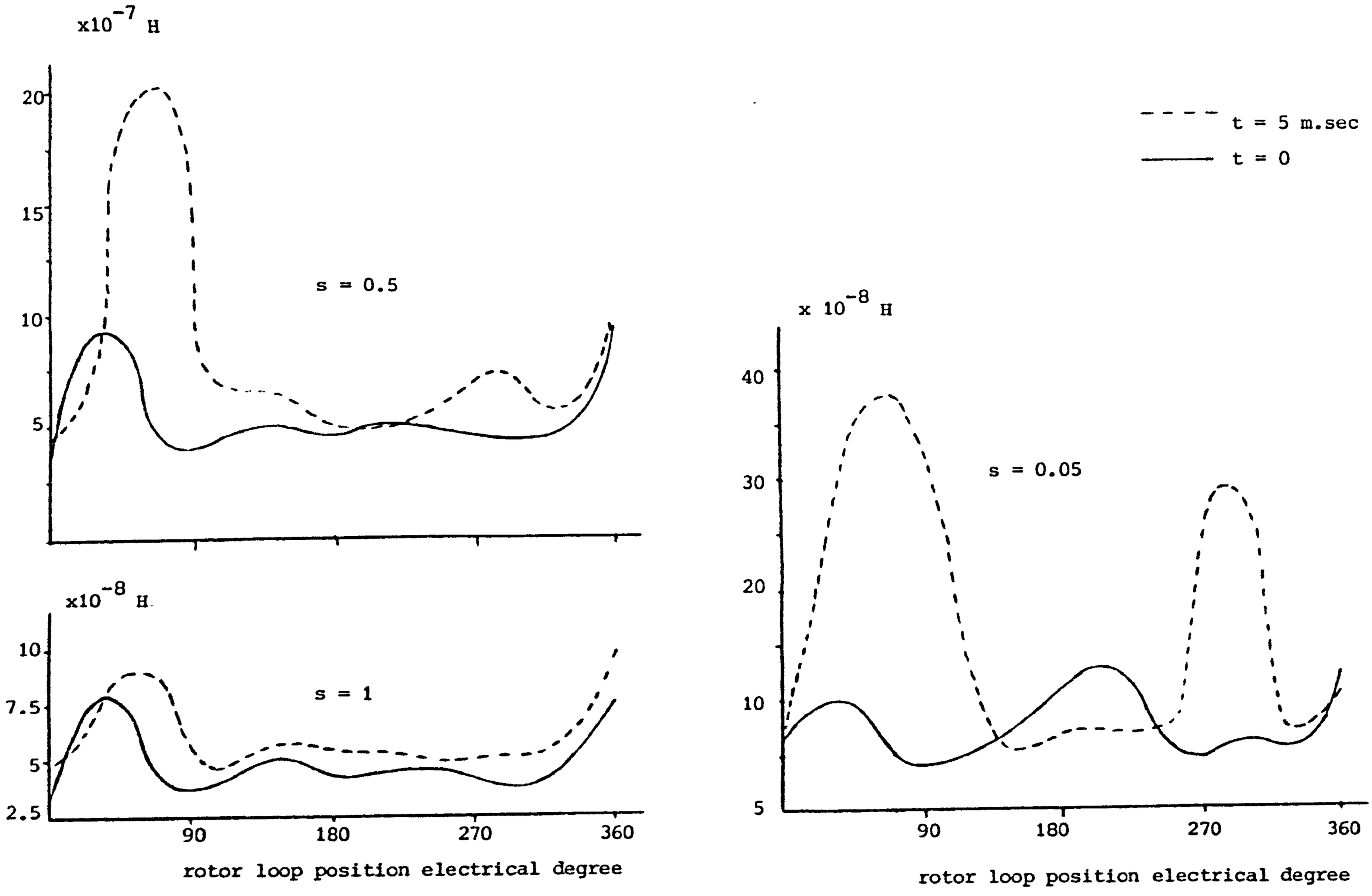

Figure 5.2.20 Mutual inductance between loop 1 & 10

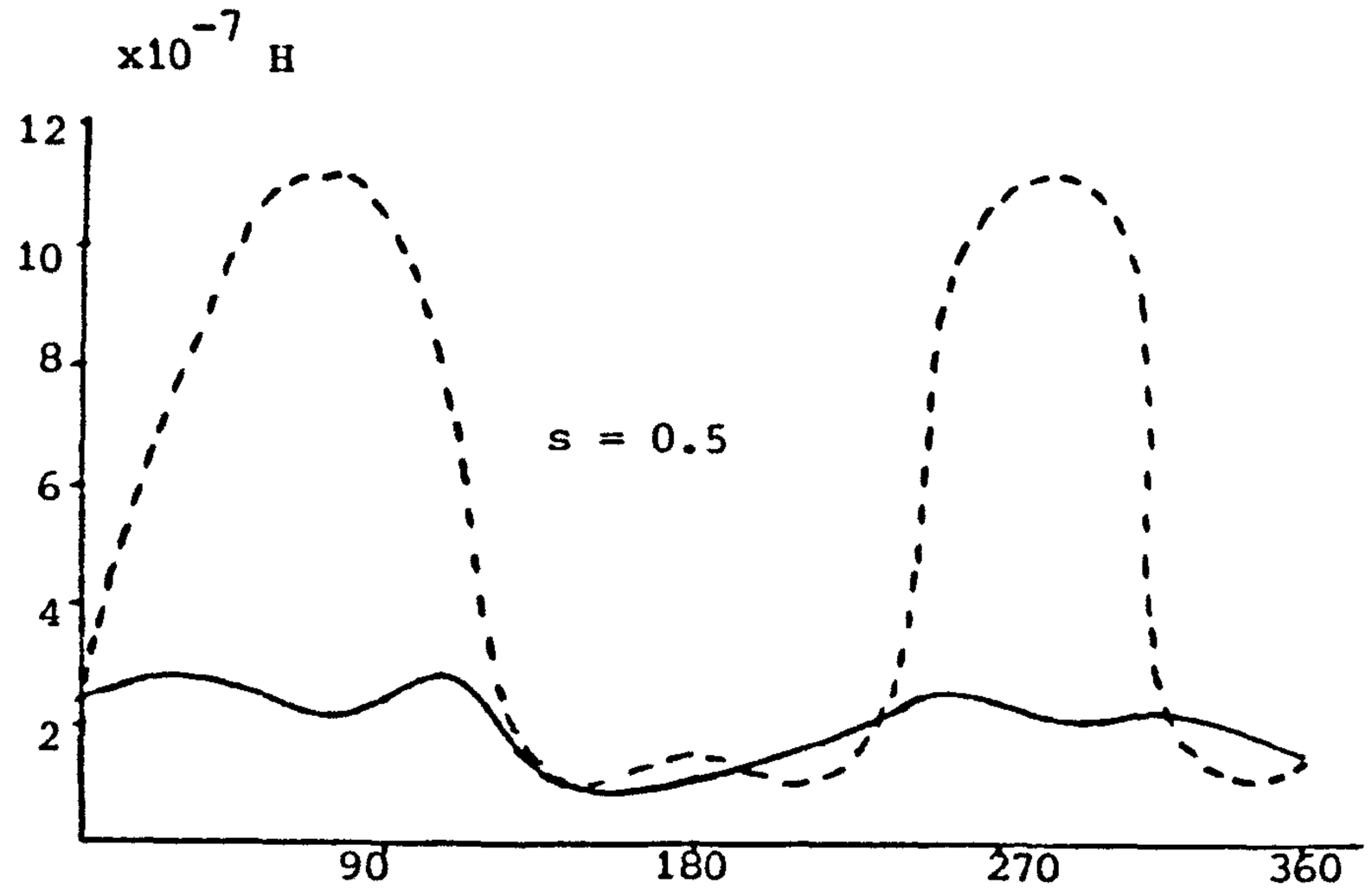

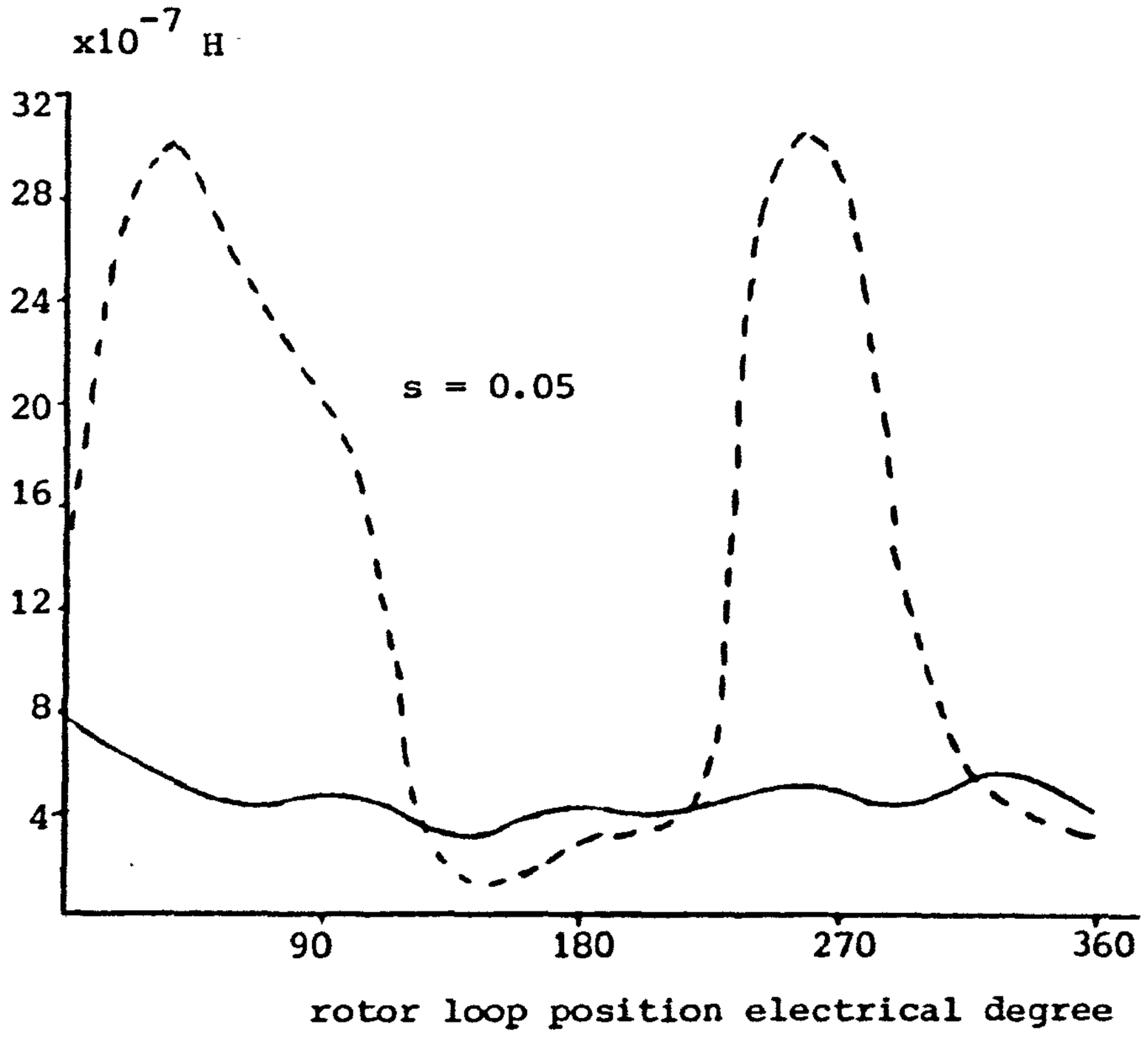

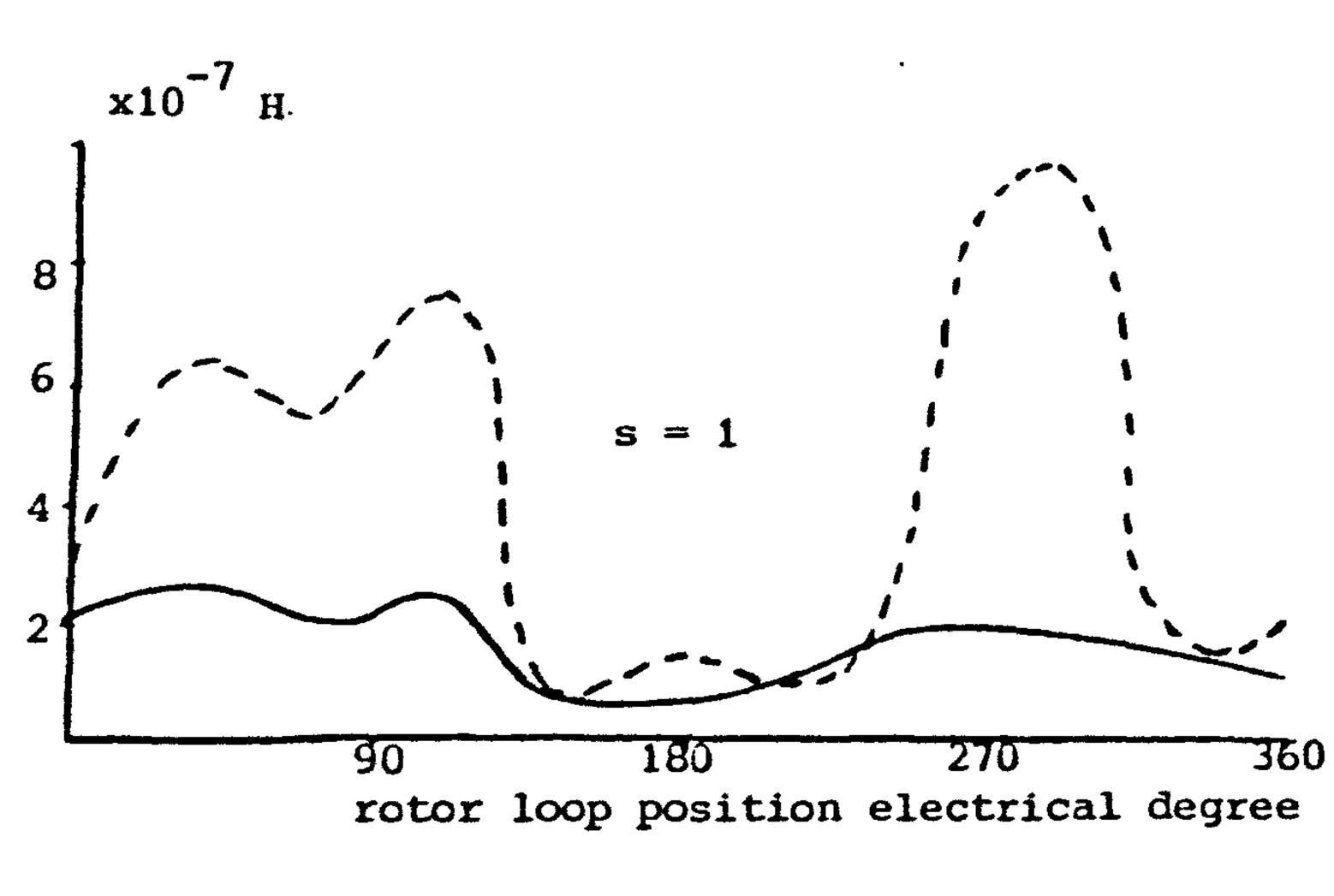

Figure 5.2.21 Mutual inductance between loop 1 & 11

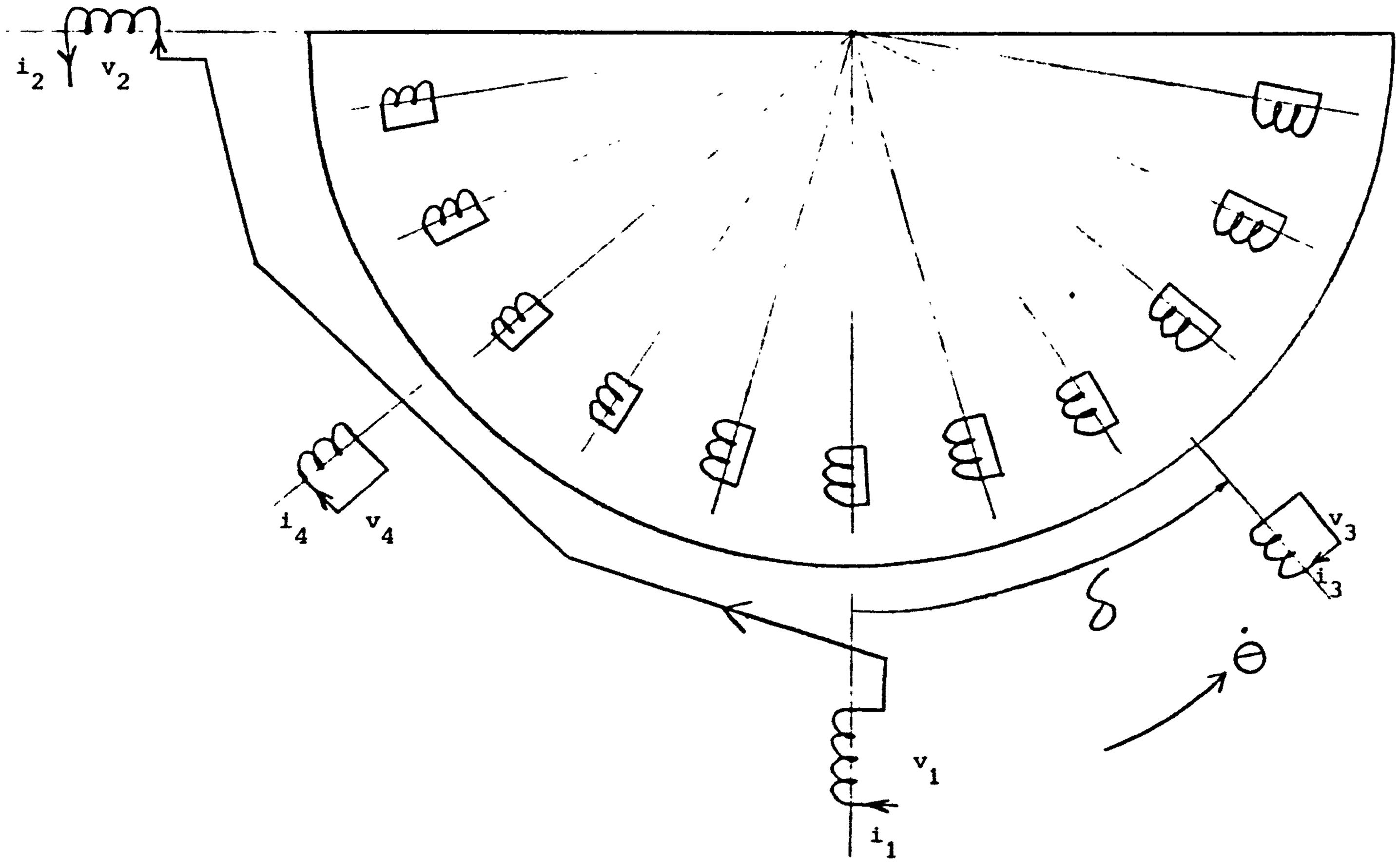

Figure 6.1

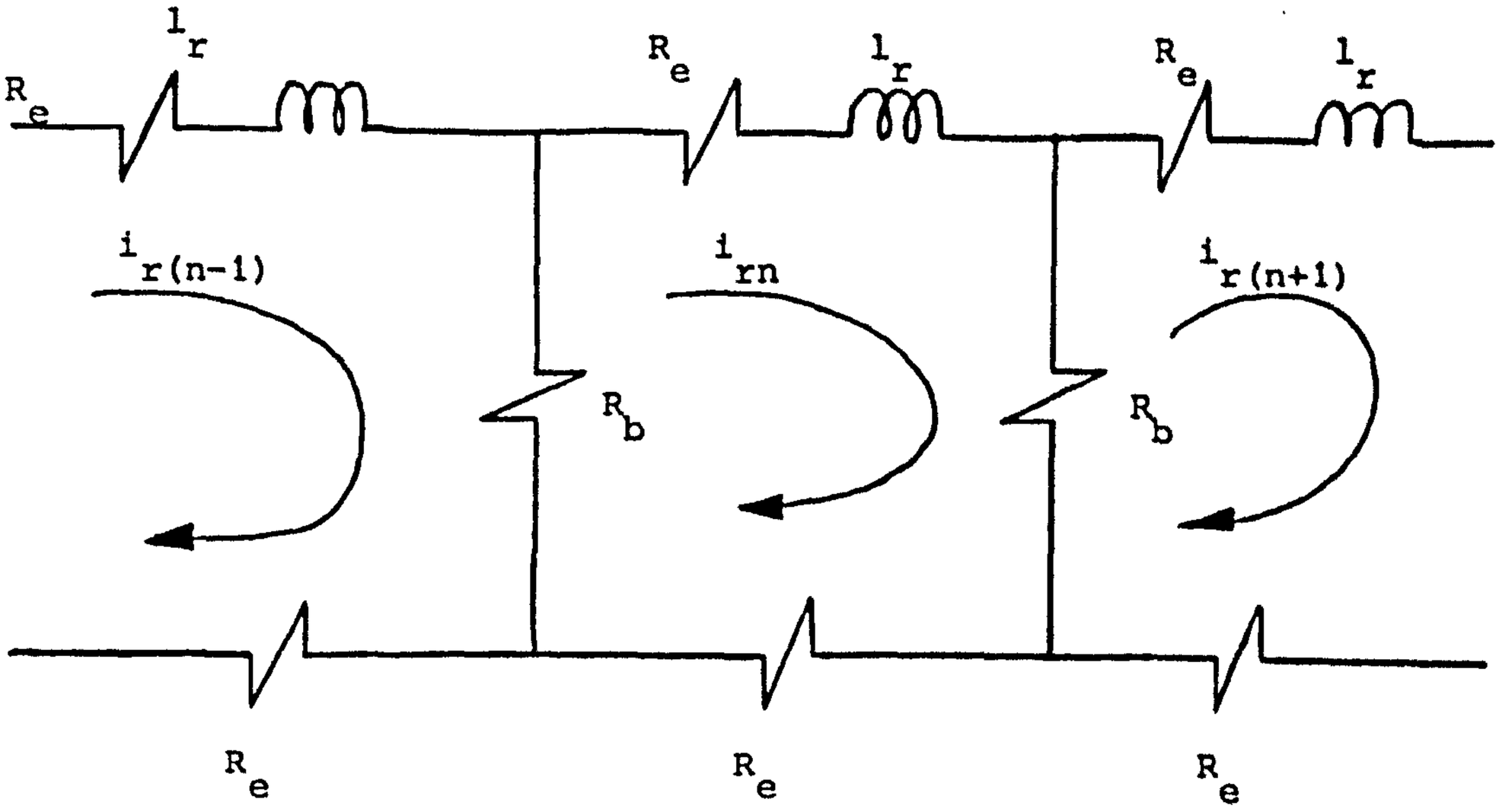

Figure 6.2 Rotor loops representation

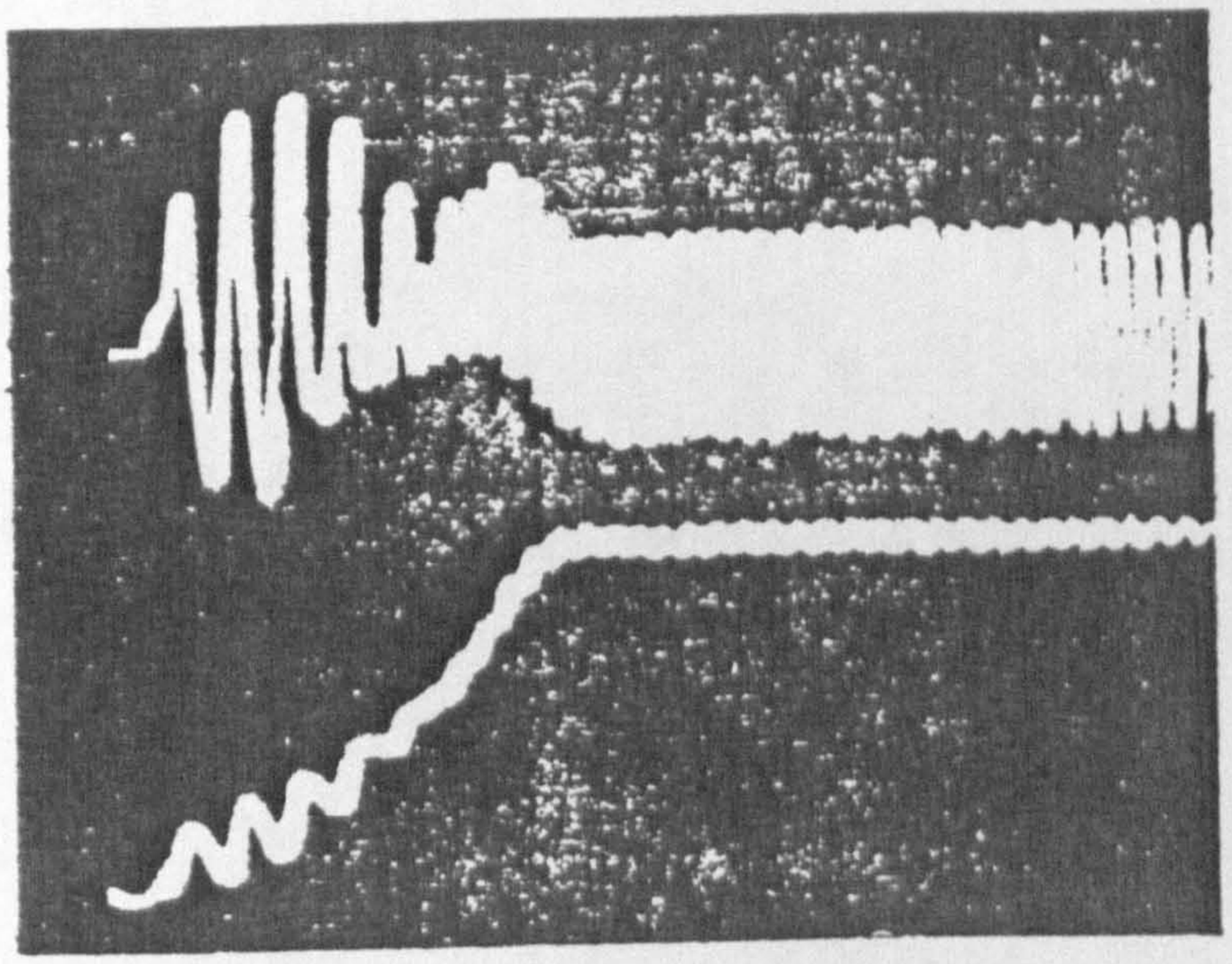

(a) Switching angle = 0°, initial speed = 0

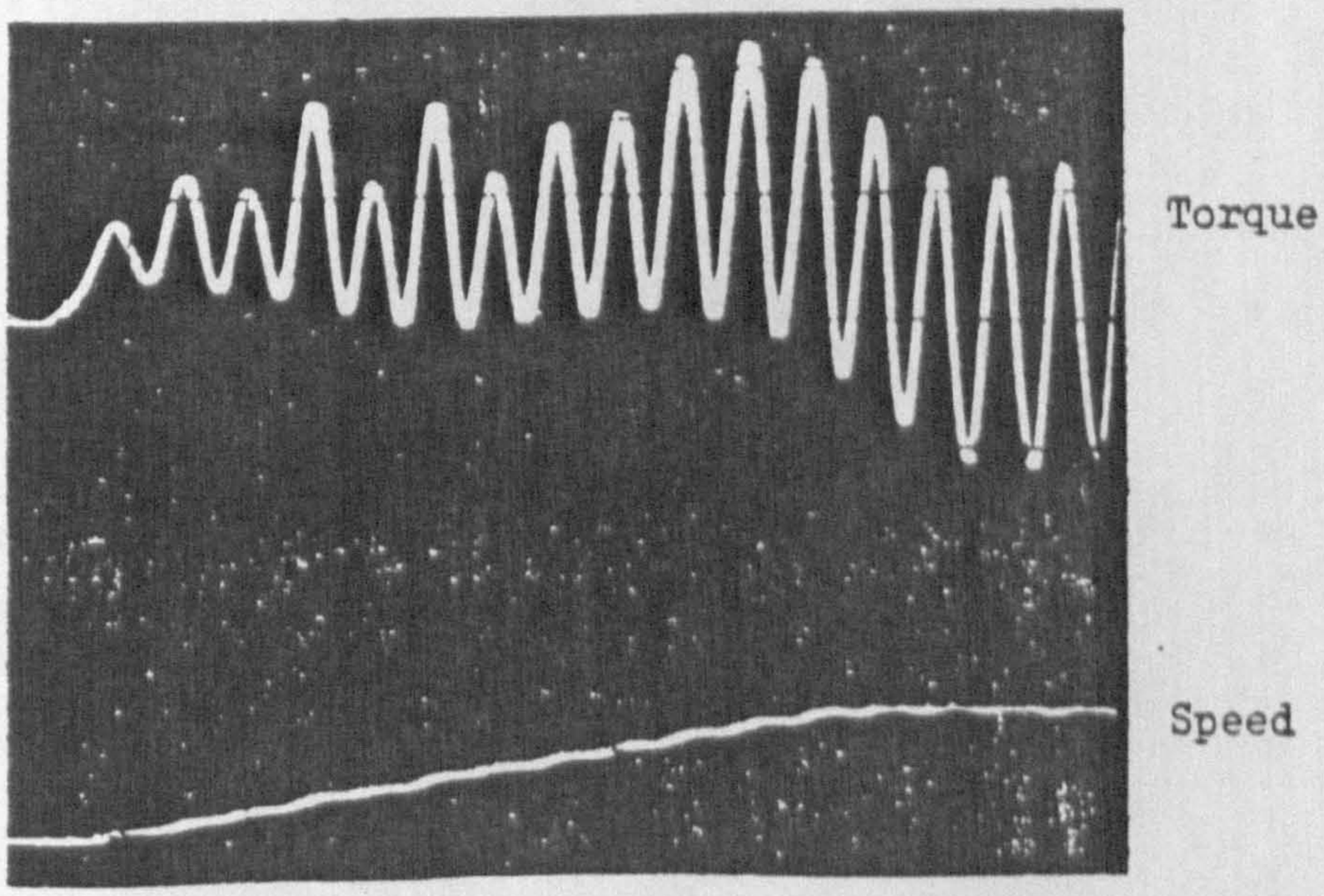

(b) Switching angle = 90°, initial speed = 0°

Figure 6.4 Recordings of torque-time and speed-time patterns

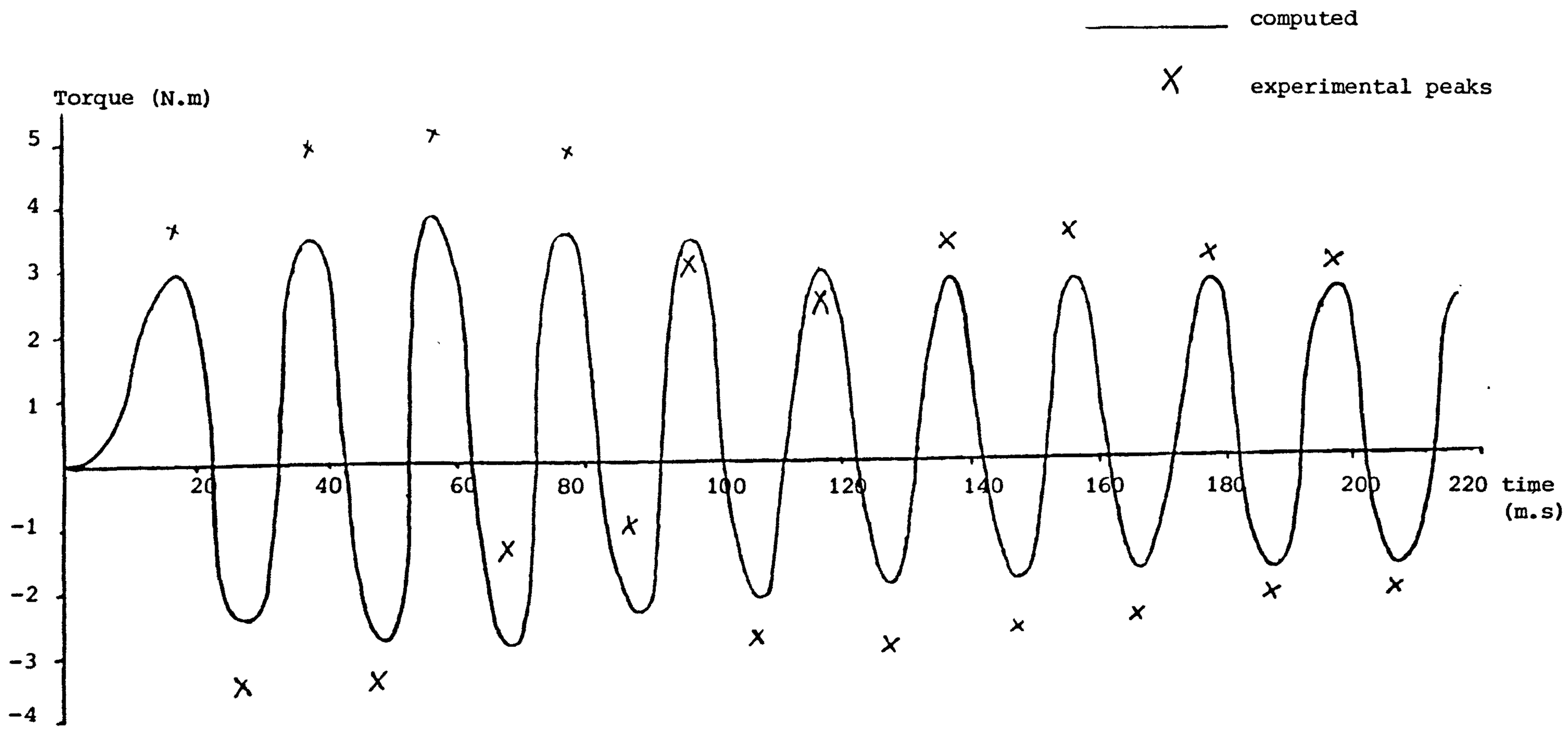

Figure 6.4c Transient torque-time patterns switching angle = 0

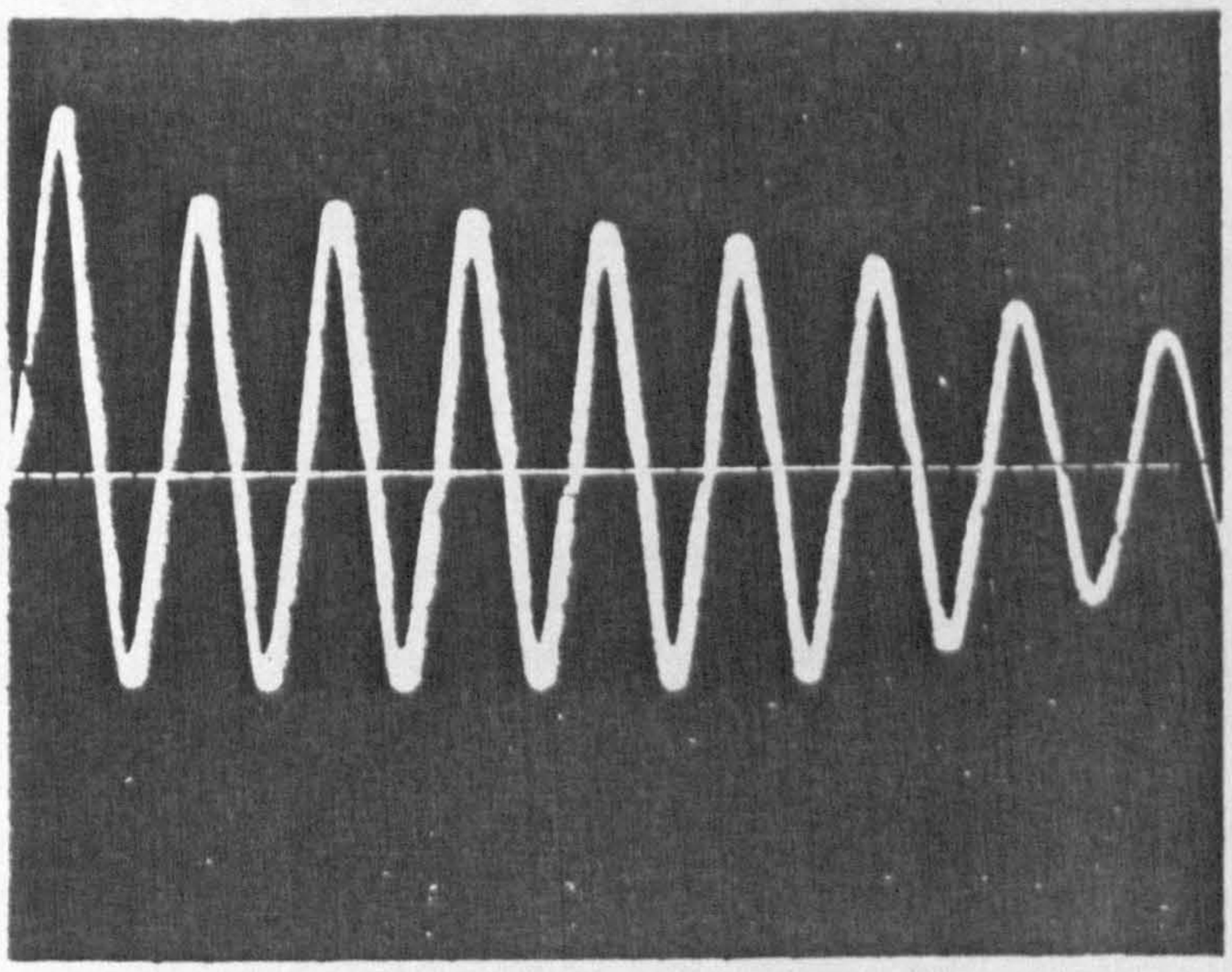

(a) Switching angle = 0°, initial speed = 0

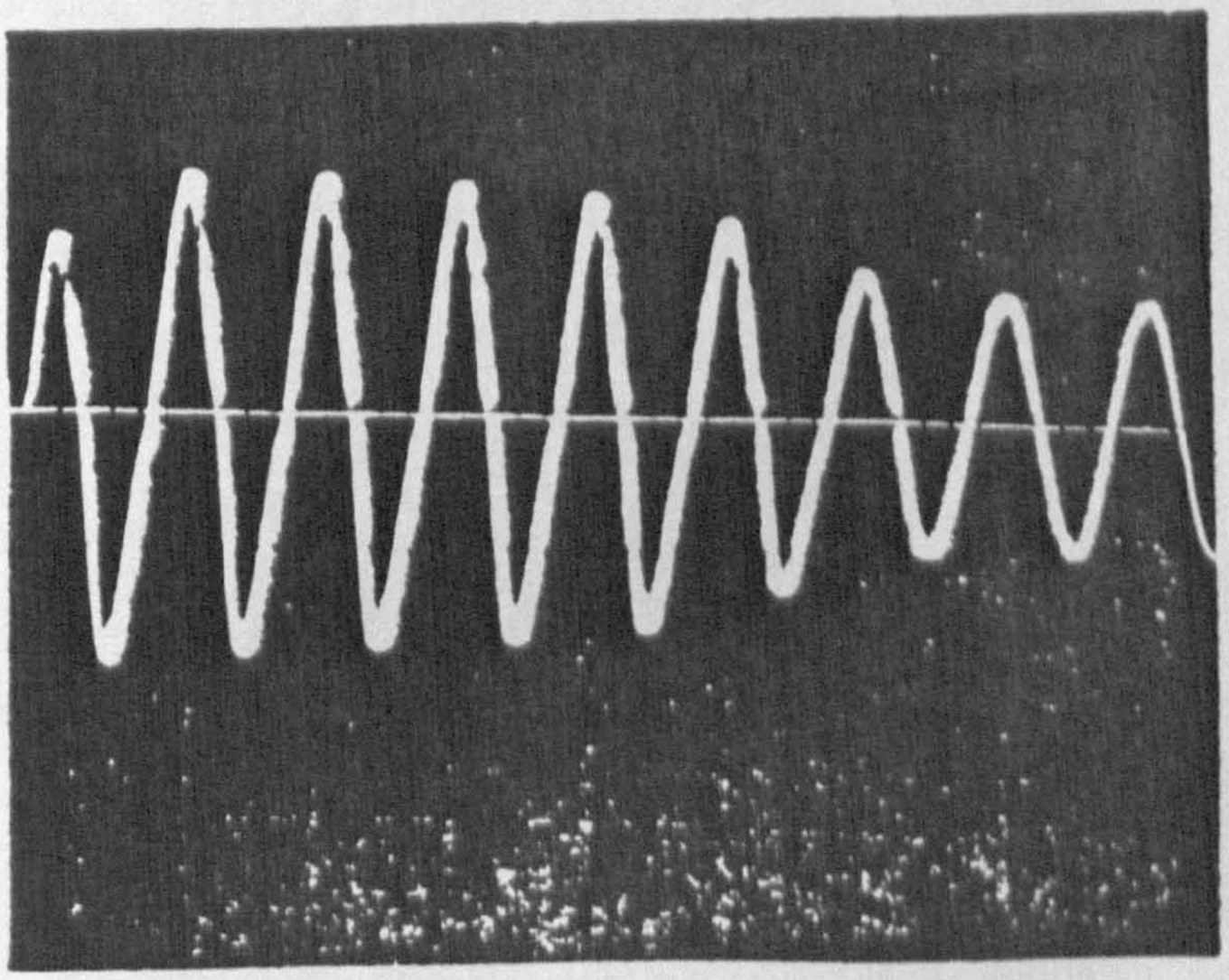

(b) Switching angle = 90°, initial speed = 0

Figure 6.5 Recordings of current-time patterns

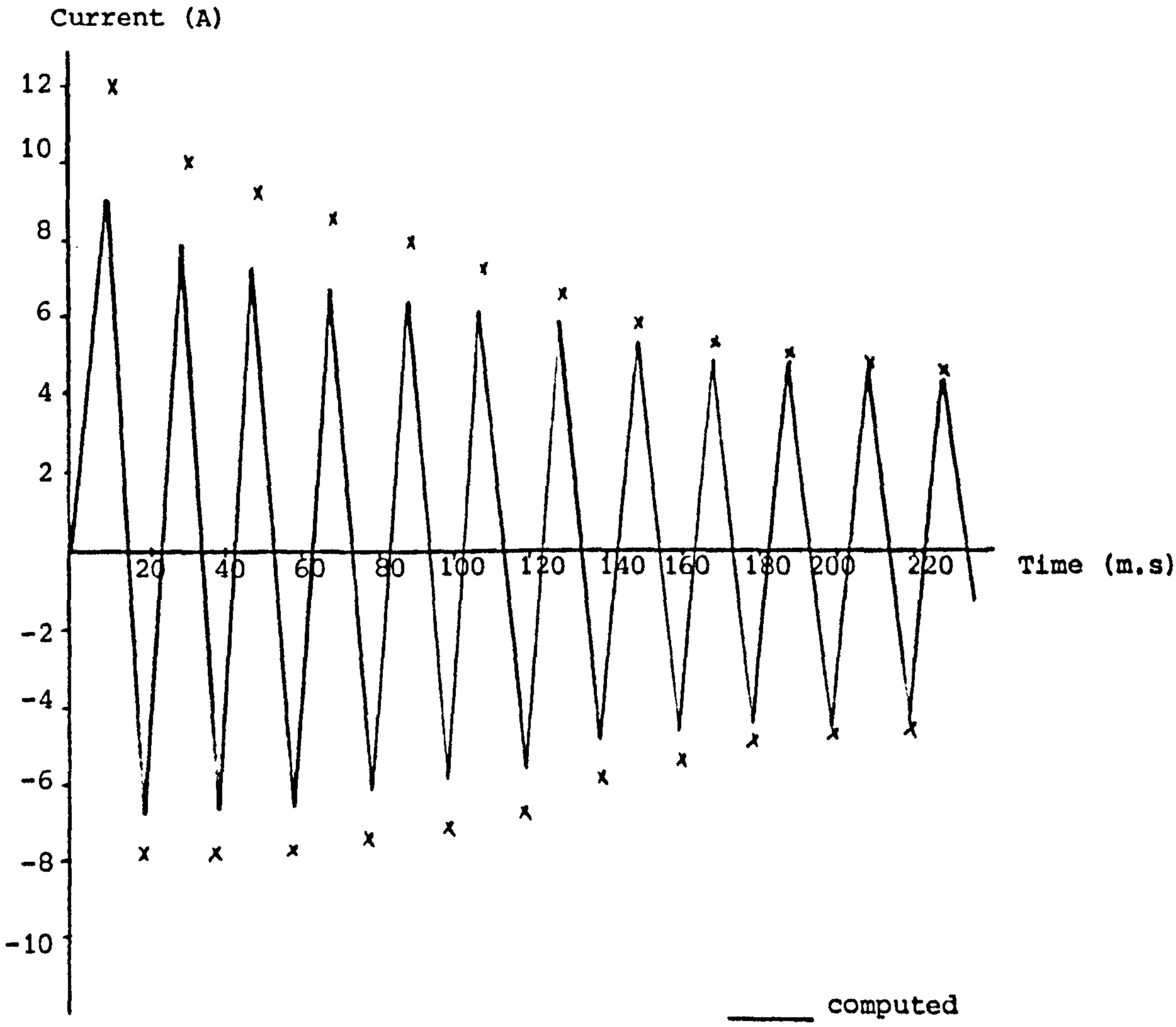

Figure 6.5c Transient current of main winding switching angle = 0

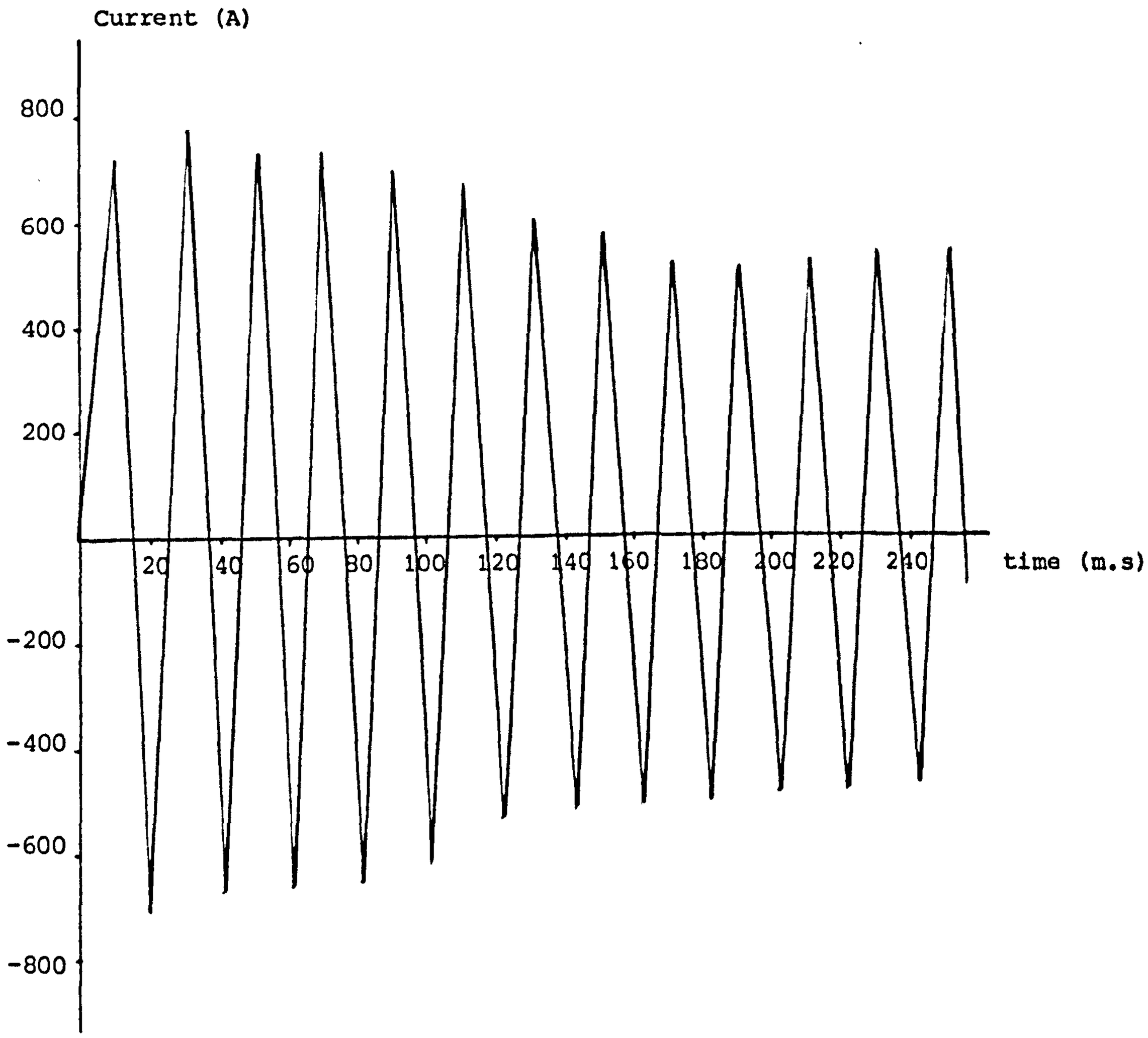

Figure 6.6 Transient current of shading ring switching ang = 0

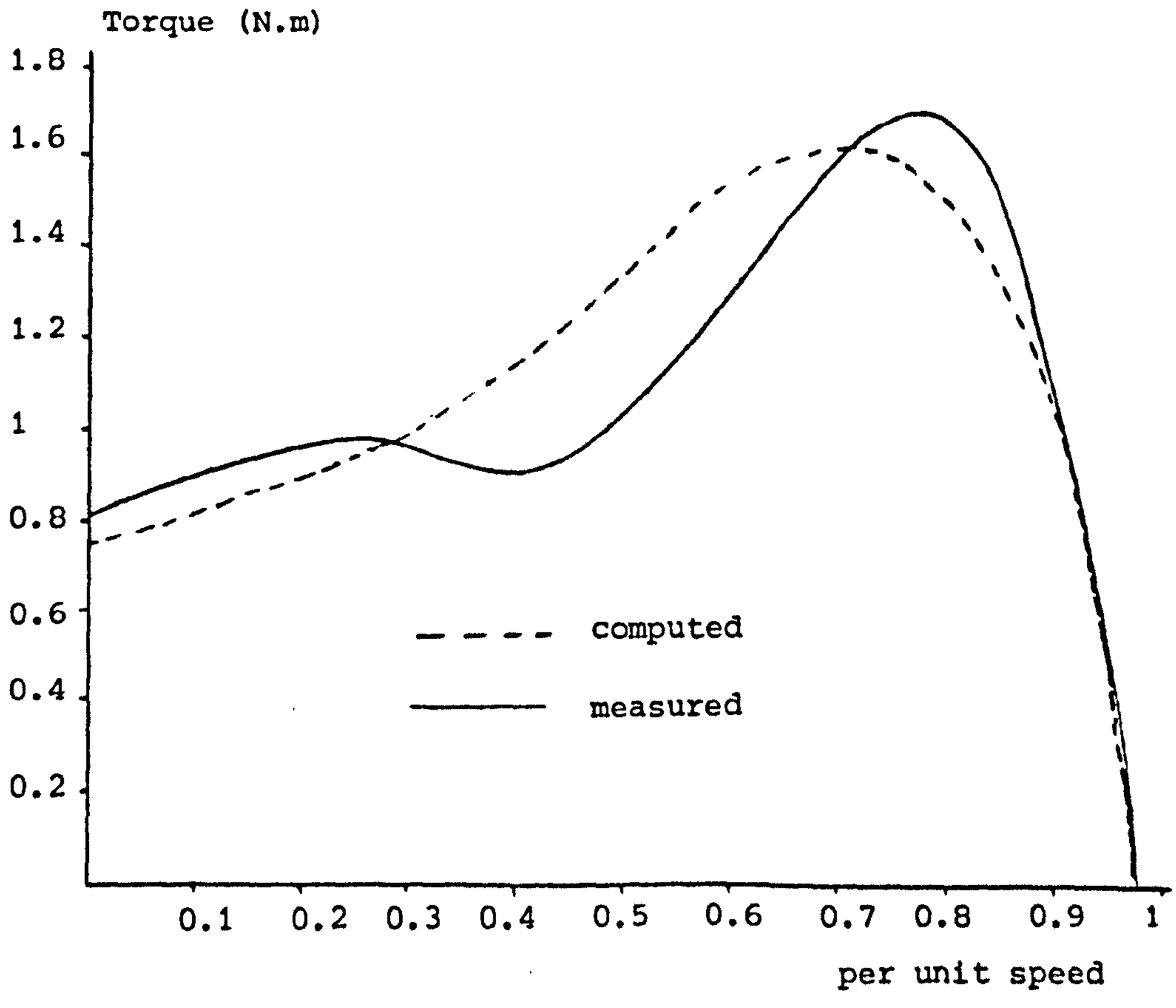

Figure 7.1 Torque/speed characteristics

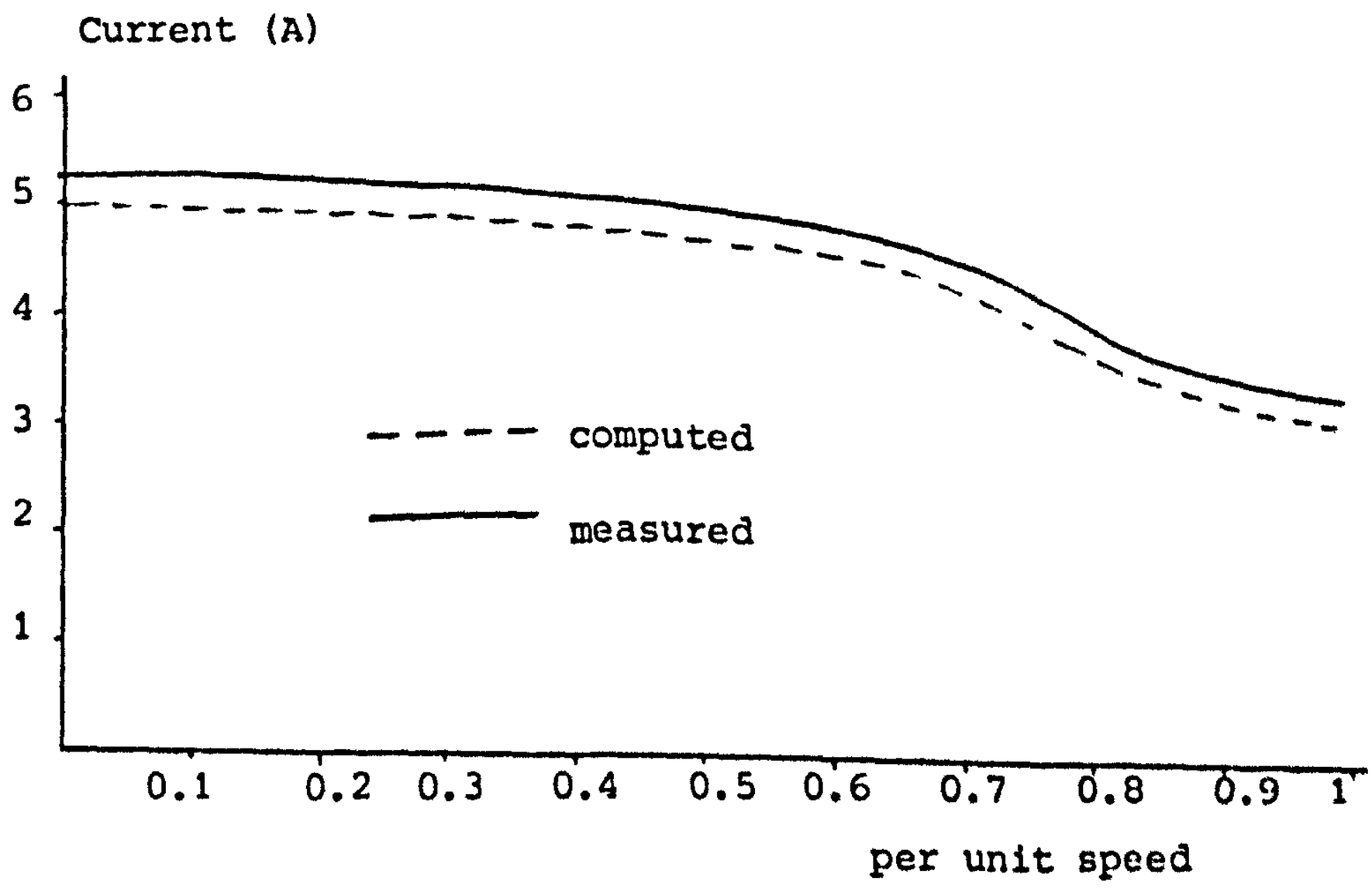

Figure 7.2 Current/speed characteristics